Pathological Consequences of a Chronic Hypoxic Response in Cone and Rod Photoreceptors and a Potential Gene Therapy

---

Dissertation

zur

Erlangung der naturwissenschaftlichen Doktorwürde
(Dr. sc. nat.)

vorgelegt der

Mathematisch-naturwissenschaftlichen Fakultät

der

Universität Zürich

von

Maya Barben

von
Thalwil ZH

Promotionskommission

Prof. Dr. Christian Grimm (Vorsitz)

PD Dr. Marijana Samardzija (Leitung der Dissertation)

Prof. Dr. Stephan Neuhauss

Prof. Dr. Melanie Greter

Zürich, 2017

SUMMARY

Retinal degenerations including age-related macular degeneration (AMD) have devastating consequences for patients. AMD primarily affects the cone-rich macular region of the retina that is responsible for central, high-acuity vision. With the rise in life expectancy, the prevalence of AMD continues to increase. Adequate treatment options are urgently needed, especially since available therapies are restricted to the less frequent neovascular form of the disease. The development of novel therapies, however, requires detailed understanding of disease mechanisms, a knowledge that is still limited in the case of AMD mostly due to the lack of suitable experimental models with a cone-rich macula.

Numerous factors have been proposed and/or validated to contribute to AMD disease development and progression. One such pathological factor might be reduced retinal oxygenation leading to local hypoxia. Age-related changes such as reduction of choroidal blood flow, accumulation of drusen and thickening of the Bruch's membrane may limit oxygen supply from the choroidal vasculature to photoreceptors and thereby activate a chronic hypoxic response. Hypoxia induces several cellular mechanisms orchestrated by hypoxia-inducible factors (HIFs). Considering the importance of high oxygen levels for normal photoreceptor metabolism it is highly likely that chronic hypoxia in senescent eyes might play an important role in AMD pathology.

In this work, we employed several mouse models to study cone degeneration and the contribution of hypoxia. First, we used *Rpe65^{R91W};Nrl$^{-/-}$* (*R91W;Nrl$^{-/-}$*) double-mutant mice to mimic the central cone-exclusive region of the human macula. *R91W;Nrl$^{-/-}$* mice express only cone photoreceptors in a functional, well-layered retina and can be used to study cone photoreceptor pathologies. To test the potential involvement of chronic hypoxia in AMD, we triggered a chronic hypoxia-like response in cone photoreceptors of *R91W;Nrl$^{-/-}$* and rod photoreceptors of wild-type mice. Then, to understand the mechanisms of cone degeneration, we analyzed retinal degenerative processes in the all-cone *R91W;Nrl$^{-/-}$* mouse model which was subjected to damaging blue light.

In the first part, we show that early stabilization of HIFs in cone photoreceptors of the all-cone retina led to subretinal neovascularization and cone degeneration, features that are central to a distinct form of AMD known as retinal angiomatous proliferation (RAP). Additionally, we present evidence that inactivation of *Hif1a* rescued the observed phenotype, which clearly identifies *Hif1a* as the pathological isoform. In the rod-dominant retina, long-term activation of the hypoxic response caused age-dependent retinal degeneration and retinal pigment epithelium defects, without inducing blood vessel growth into the subretinal space. Although photoreceptor degeneration was evident in both models, the progression of the degenerative process differed. While cones in the all-cone retina degenerated already at early time points, rod cell death in rod-dominant retinas was milder and progressed more slowly. To interfere with these hypoxia-related mechanisms that led to cell death,

we tested a gene therapy approach using adeno-associated virus (AAV)-mediated expression of anti-*Hif1a* shRNA. Our approach ameliorated the degenerative pathology and encourages further research to evaluate a potential translation of anti-*Hif1a* therapy to the clinics.

In the second part, we analyzed retinal degenerative processes in *R91W;Nrl*$^{-/-}$ mice which were exposed to blue light. Our data revealed essential differences between wild-type (rod-dominant retina) and *R91W;Nrl*$^{-/-}$ (all-cone retina) mice: the all-cone retina was more resistant to blue light damage in terms of photoreceptor degeneration. However, while in wild-type mice blue light damage affected the outer blood-retina barrier maintained by the retinal pigment epithelium, the inner blood-retinal barrier formed by tight junctions between retinal capillary endothelial cells was additionally impaired in *R91W;Nrl*$^{-/-}$ mice, resulting in vascular leakage and edema.

Investigating molecular pathways involved in retinal degeneration is essential to develop successful treatment approaches. This work contributes to the better understanding of the retinal response to chronic hypoxia-like conditions and toxic levels of light, two important features implicated in retinal degenerative diseases. Our findings support the concept that targeting HIFs might serve as a therapeutic strategy for hypoxia-mediated degenerative diseases.

ZUSAMMENFASSUNG

Sehbehinderungen und Erkrankungen der Netzhaut (Retina) beeinträchtigen die Lebensqualität der Betroffenen erheblich. Zu den häufigsten degenerativen Augenkrankheiten zählt die altersbedingte Makuladegeneration (AMD), bei welcher das Zentrum der Netzhaut, die sogenannte Makula, geschädigt wird. Das Absterben der dort in hoher Dichte vorkommenden Zapfen führt zu einer fortschreitenden Verschlechterung der zentralen Sehschärfe. Mit der steigenden Lebenserwartung wird die Anzahl der von AMD Betroffenen in Zukunft weiter zunehmen. Es werden deshalb dringend Behandlungsmöglichkeiten benötigt, zumal sich diese momentan auf die seltenere, feuchte Form der AMD beschränken. Im Gegensatz dazu steht für die trockene AMD bisher keine wirksame Therapie zur Verfügung. Die Erforschung der Ursachen und des Verlaufs der AMD gestaltet sich jedoch schwierig, da den meisten Tiermodellen eine Makula mit hoher Zapfendichte fehlt.

Zur Entstehung und zum Verlauf der AMD können zahlreiche Faktoren beitragen. Eine wichtige Rolle spielt möglicherweise auch ein Sauerstoffmangel (Hypoxie), der durch alterungsbedingte Prozesse entstehen kann. Im Laufe der Alterung kann die Sauerstoffzufuhr zu den Photorezeptoren durch den verminderten Blutfluss in der Choroidea (Aderhaut), die Zunahme der Ablagerungen unter der Netzhaut (sogenannte Drusen) und die Verdickung der Bruch-Membran eingeschränkt werden. Als Antwort auf den Sauerstoffmangel werden heterodimere hypoxie-induzierte Faktoren (HIF) aktiviert. In Anbetracht des hohen Sauerstoffbedarfs der Photorezeptoren für den Zellstoffwechsel kann eine chronisch aktivierte hypoxische Antwort eine wichtige Rolle bei der Pathogenese der AMD spielen.

In dieser Arbeit haben wir mit mehreren Mausmodellen Zapfendegenerationen und die Auswirkungen einer hypoxischen Antwort studiert. Hierfür haben wir *Rpe65*^{R91W}*;Nrl*$^{-/-}$ Mäuse (*R91W;Nrl*$^{-/-}$; "Zapfenmäuse"*)* analysiert, deren morphologisch normale Netzhaut ausschliesslich aus funktionstüchtigen Zapfen besteht und somit der Makula beim Menschen ähnlich ist. Diese Zapfenmaus ist ein ideales Modell, um die molekularen Mechanismen bei Zapfendegenerationen zu studieren. Um den Einfluss einer chronisch-hypoxischen Antwort zu analysieren, haben wir ausserdem lokale Hypoxie in zwei Mausmodellen simuliert. Einerseits haben wir die chronisch-hypoxische Zellantwort in den Stäbchen einer normalen, von Stäbchen dominierten Netzhaut und andererseits in den Zapfen der Zapfenmaus aktiviert. Um zusätzlich die Mechanismen der Zapfendegeneration besser zu verstehen, haben wir die durch Bestrahlung mit Licht im blauen Wellenlängenbereich ausgelöste Degeneration der Netzhaut in der Zapfenmaus studiert.

Im ersten Teil dieser Dissertation zeigen wir, dass die Aktivierung der hypoxischen Zellantwort in der Zapfenmaus zu subretinaler Neovaskularisation und Degeneration führte, und somit zu Merkmalen, die den zentralen Eigenschaften einer als retinale angiomatöse Proliferation (RAP) bezeichneten Form der feuchten AMD entsprechen. Ausserdem zeigen wir, dass die zusätzliche

Inaktivierung von *Hif1a* die Netzhaut vollständig schützte, womit wir in diesem Modell eindeutig *Hif1a* als pathologische Isoform identifizieren konnten. In der von Stäbchen dominierten Netzhaut verursachte die chronisch aktivierte Hypoxieantwort einen Verlust der Photorezeptoren sowie Veränderungen des retinalen Pigmentepithels, ohne subretinale Neovaskularisation anzuregen. Obwohl die Photorezeptoren in beiden Mausmodellen degenerierten, unterschied sich der Verlauf des degenerativen Prozesses. Während die Zapfen in der Zapfenmaus bereits früh starben, schritt der Verlust der Stäbchen in der von Stäbchen dominierten Netzhaut langsamer voran. Mittels Gentherapie haben wir versucht, den durch HIF1A ausgelösten Zelltod therapeutisch zu behandeln. Um *Hif1a* künstlich stillzulegen, haben wir eine shRNA-Sequenz in adeno-assoziierte Viren (AAV) verpackt und durch subretinale Injektionen in die Photorezeptoren eingeschleust. Dadurch konnten wir die Degeneration der Sehzellen vermindern. Weitere Untersuchungen mit dem Endziel einer möglichen klinischen Anwendung scheinen deshalb sinnvoll.

Im zweiten Teil haben wir mit dem Ziel, die Mechanismen der Zapfendegeneration besser zu verstehen, die durch Bestrahlung mit Licht im blauen Wellenlängenbereich ausgelöste Netzhautdegeneration in Wildtyp- und Zapfenmäusen studiert. Unsere Analysen zeigen deutliche Unterschiede zwischen den beiden Modellen: Die Netzhaut der Zapfenmaus scheint bezüglich der Degeneration resistenter zu sein. Während jedoch bei den Wildtypmäusen die äussere, durch das retinale Pigmentepithel gebildete Blut-Retina-Schranke geschädigt wurde, wurde bei den Zapfenmäusen auch die innere, durch die retinalen Endothelzellen gebildete Blut-Retina-Schranke beeinträchtigt. Aufgrund der undichten Blutgefässe kam es zu einer Flüssigkeitsansammlung, die eine Schwellung der Netzhaut verursachte (Netzhautödem).

Für die Entwicklung der therapeutischen Behandlungen ist es erforderlich, die molekularen Signalwege im Laufe der Degeneration zu kennen und zu verstehen. Diese Dissertation trägt zu einem besseren Verständnis der molekularen Auswirkungen einer chronisch aktivierten Hypoxieantwort und der Einwirkung von Licht auf Netzhautzellen bei, zwei wichtigen Faktoren im Zusammenhang mit degenerativen Netzhauterkrankungen. Unsere Forschungsergebnisse unterstützen insbesondere die Theorie, dass die gezielte Ausschaltung von *Hif1a* zur Behandlung der AMD und anderer mit einer hypoxischen Komponente assoziierten Netzhautdegenerationen in Betracht gezogen werden kann.

TABLE OF CONTENTS

1 INTRODUCTION

Our visual system is confronted with a large amount of different inputs – every second. Humans and non-human primates largely rely on sensory input by the visual system and any disturbance or malfunctioning of the visual system has devastating consequences for the patient's daily life. Over a broad range of light intensities, vision conveys signals about objects, their movements, speed and distance. Handling of this large amount of information is efficient both in terms of quantity and quality thanks to extensive parallel processing and sorting of visual data. Before the information is sent to the visual cortex in our brain, our eyes take the first step in visual processing at the level of the retina.

1.1 Retinal Structure and Function

1.1.1 Retina and retinal pigment epithelium

The retina is the innermost layer of the eye (Figure 1A) and is derived from the optic vesicle, an outpocketing of the diencephalon (Purves 2012). Upon light reception, the multilayered neuronal tissue processes the image and transmits electrical signals via the optic nerve to the brain. Six classes of cell types (photoreceptors, bipolar cells, horizontal cells, amacrine cells, Müller glia cells and ganglion cells) are structured into three layers, namely the outer nuclear layer (ONL), inner nuclear layer (INL) and the ganglion cell layer (GCL, Figure 1B,C). The ONL consists of two types of photoreceptors – the rods and cones – that are composed of membrane disks containing light-sensitive photopigments. Light absorption by the photopigments in the outer segments of the photoreceptors initiates a process called phototransduction (see 1.1.3). Signals are then transmitted from the photoreceptors to bipolar cells in the INL and to ganglion cells in the GCL. Synaptic contacts are made in the outer (photoreceptors and bipolar/horizontal cells) and inner plexiform layer (bipolar and ganglion/amacrine cells). The axons of ganglion cells form the optic nerve and transmit information to the visual centers in the brain (Purves 2012, Reid et al. 2013).

Horizontal cells establish lateral connections between photoreceptors and modulate the input to bipolar cells, while amacrine cells mediate lateral inhibition by interacting with bipolar and ganglion cells. Additionally, the retina has three glial cell types that support and protect retinal neurons: astrocytes, microglia and Müller cells. Astrocytes play important roles in neurovascular coupling and during development of the retinal vasculature (see 1.2.3; 1.3.1; (Kur et al. 2012)). Microglia cells are active sensors of the retinal microenvironment and are involved in immune defense (reviewed in (Karlstetter et al. 2015)). The main glial cells of the retina, Müller cells, provide metabolic support and protection of retinal neurons. Müller cell nuclei are located in the INL and their radial processes span the entire retina to mediate structural stabilization (Lewis et al. 1995, Reichenbach et al. 2013).

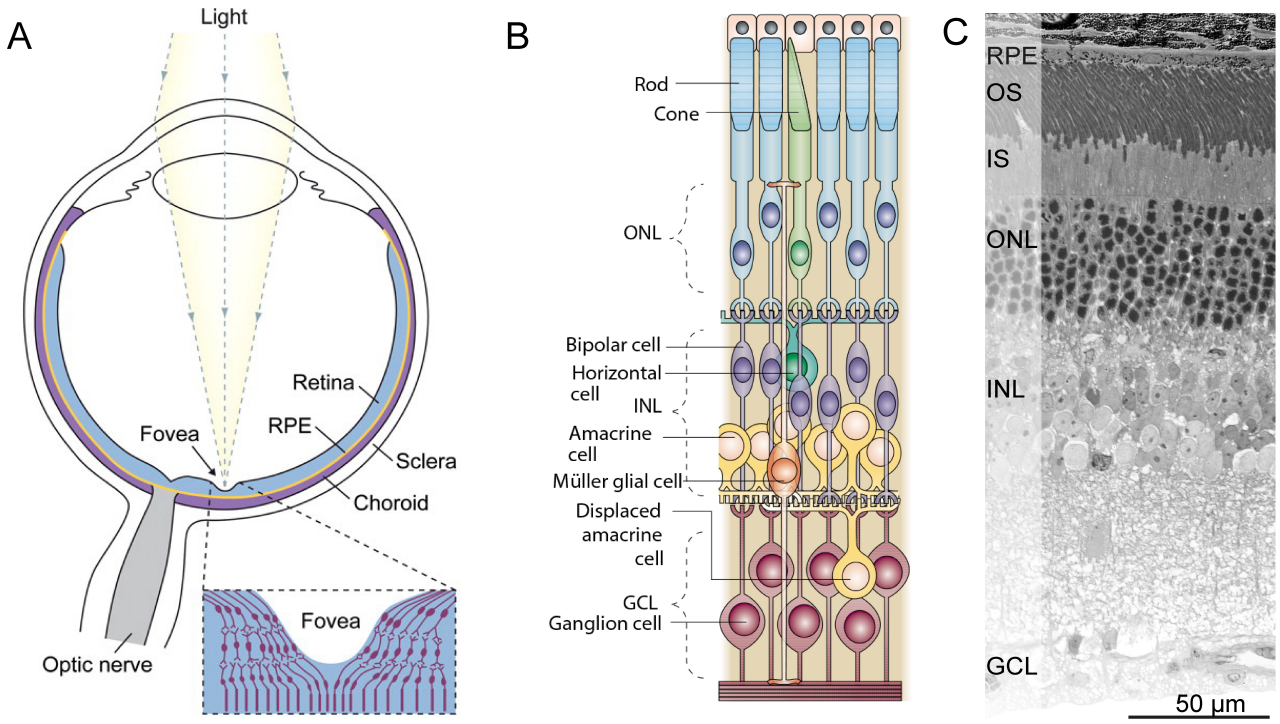

Figure 1. Structure of the eye and anatomy of the retina. (A) Diagram of the human eye. The retina forms the innermost layer, adjacent to the RPE. Enlarged box shows the central region of the macula called fovea, which has the highest visual acuity compared to other parts of the retina and is characteristic for humans and higher primates (i.e. haplorhines (Kirk et al. 2004)). (B) The different cell types of the retina are organized into three layers: ONL, INL and GCL. (C) Morphological section of the mouse retina. RPE: retinal pigment epithelium, OS: outer segments, IS: inner segments, ONL: outer nuclear layer, INL: inner nuclear layer, GCL: ganglion cell layer. Scale bar: 50 µm. Images in (A) and (B) adapted from (Dyer et al. 2001, Sung et al. 2010).

The retinal pigment epithelium (RPE) is a monolayer of cells located at the back of the eye between the photoreceptors and the choroidal blood vessels (see 1.2.1). The RPE fulfills diverse tasks to support photoreceptors and maintain visual function. For example, the RPE is essential for the regeneration of the visual chromophore 11-*cis* retinal, a photosensitive derivative of vitamin A (see 1.1.4). Beside its critical role in the visual cycle, the RPE ingests shed membrane disks of photoreceptors by circadian-regulated phagocytosis. This process called disk shedding is crucial for photoreceptor function, since outer segments have a limited life span and therefore require a constant renewal process. Additionally, the RPE establishes the outer blood-retinal barrier (BRB) through tight junctions between RPE cells, prevents reflection of light by absorbing scattered light through dark melanin granules and is involved in epithelial transport, spatial ion buffering, secretion and immune modulation (reviewed in (Strauss 2005)).

Interestingly, the vertebrate retina has an inverted design: light passes through all retinal layers before being captured by the photopigments in the photoreceptor outer segments. Although this seems counterintuitive, the chromophore provided by the RPE as well as the high oxygen and nutrient demand of the photoreceptors (see following sections) explain the need for close proximity to the choriocapillaris and the RPE (Kolb 2003).

1.1.2 Photoreceptors: rods and cones

The retina has two types of photoreceptors: rods and cones. Although they differ in size and shape, both have similar structures: outer segments with membrane disks containing light-sensitive photopigments, mitochondria-rich inner segments and cell bodies with synaptic terminals (Figure 2A). Photopigments consist of the visual chromophore 11-*cis* retinal and opsin, a protein component that determines the wavelength sensitivity. The visual pigment of rods, rhodopsin, has a peak sensitivity at ~500 nm (Berg et al. 2002). Opsin is synthetized in the rod inner segment, transported to the outer segment via vesicles and finally inserted into membranes of the rod outer segment (Papermaster et al. 1985). Several rods can contact the same rod bipolar cell. Consequently, the rod circuitry is highly convergent, but has a low spatial resolution. Due to this convergence, the rod system is specialized for sensitivity: a single photon of light may induce a functional response (Baylor et al. 1979).

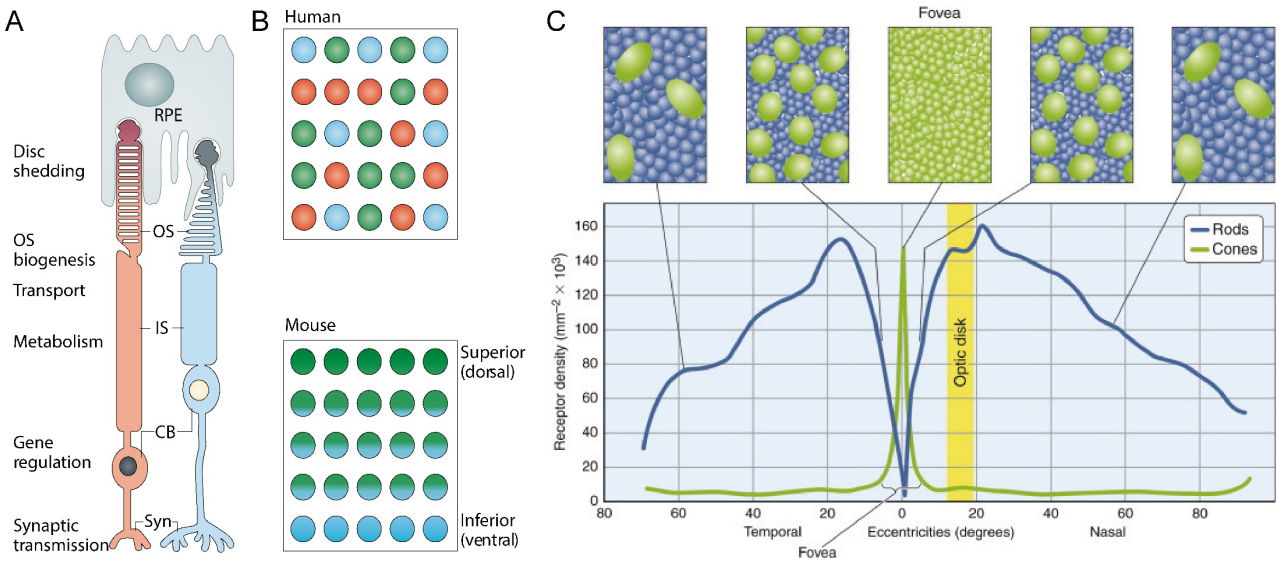

Figure 2. Two photoreceptor types: rods and cones. (A) Illustration of rod and cone structure including functions connected to different photoreceptor compartments. OS: outer segments, IS: inner segments, CB: cell body, Syn: synaptic terminals. (B) Distribution of cone photoreceptors in the human and mouse retina. S-, M- and L-opsin expressing cones in the human retina are organized in a mosaic-like pattern, whereas in mice the two cone types (S- and M-cones) are distributed along a dorso-ventral gradient. (C) Densities of rod and cone photoreceptors in the human retina. Cone density is highest in the fovea. Adapted from (Mustafi et al. 2009, Swaroop et al. 2010).

Whereas the highly light-sensitive rods function under dim light-conditions and allow night vision, cones mediate color perception and central, fine acuity vision. Even though rods outnumber cones by a ratio of 97:3, our vision largely depends on the cone system (Carter-Dawson et al. 1979, Swaroop et al. 2009). In the human retina, three different cone types expressing either S-, M- and L-opsin (peak sensitivity to short (blue), medium (green) and long (red) wavelength light, respectively), are arranged in a mosaic-like pattern (Roorda et al. 1999) (Figure 2B). In mice, S- and

M-opsin expressing cones are distributed along a dorso-ventral gradient and L-opsin cones are completely absent (Szel et al. 1992, Swaroop et al. 2010). In contrast to other animals like mice, humans and other higher primates (i.e. haplorhines (Kirk et al. 2004)) have a specialized central region called macula (Figure 2C). The central part of the macula, the fovea, primarily consists of cones and each cone is connected to only one bipolar and one ganglion cell. Thus, the cone system is far less convergent compared to rods and allows high-resolution vision, however at the expense of sensitivity (Sung et al. 2010, Purves 2012).

1.1.3 Phototransduction

The process by which photoreceptors absorb and convert light into electrical signals is called phototransduction. Typically, neurons respond to stimuli by depolarization of the cell membrane, leading to an action potential and release of neurotransmitters. In the retina, however, photon absorption by photopigments leads to hyperpolarization of photoreceptors, whereas dark-adapted photoreceptors are depolarized and have increased neurotransmitter release (Purves 2012). In the dark, cyclic guanosine monophosphate (cGMP) concentration is high and cGMP-gated ion channels are open, allowing sodium and calcium to enter the outer segment (Figure 3). Thereby the cell is depolarized and the neurotransmitter glutamate is released. In response to light, 11-*cis* retinal isomerizes to all-*trans* retinal. This activates the heterotrimeric G protein transducin, which is composed of α-, β-, and γ-subunits. On the α-subunit of transducin, guanosine diphosphate (GDP) is exchanged for guanosine triphosphate (GTP). As a consequence, the α-subunit dissociates and activates a phosphodiesterase (PDE) that hydrolyzes cGMP. Lower cytoplasmic concentration of cGMP leads to closure of cGMP-gated cation channels on the plasma membrane. Hence, photoreceptors hyperpolarize and release less of their neurotransmitter glutamate upon light stimulation (Arshavsky et al. 2002, Sung et al. 2010, Reid et al. 2013).

An important feature of phototransduction is the high degree of signal amplification, which is achieved on three levels: (1) conformational change of 11-*cis* to all-*trans* retinal activates many transducins; (2) every activated PDE subunit hydrolyzes many cGMP molecules; (3) numerous channels close in response to lower cGMP concentration (Burns et al. 2001).

Glutamate is the brain's major excitatory amino acid neurotransmitter (Deutch 2013). In the retina, however, glutamate released by photoreceptors elicits opposite responses on the two types of bipolar cells known as ON and OFF bipolar cells. While glutamate is inhibitory for ON bipolar cells which express a G protein-coupled metabotropic glutamate receptor (mGluR6), it has excitatory effects on OFF bipolar cells which express ionotropic receptors (kainate and α-amino-3-hydroxy-5-methyl-4-isoxazolepropionic acid (AMPA)). The mammalian retina consists of at least 13 types of cone bipolar cells and one type of rod bipolar cell (Ghosh et al. 2004, Wassle et al. 2009, Helmstaedter et al. 2013). Rod photoreceptors make connections with the ON rod bipolar cell only. In contrast, cone photoreceptors synapse with various types of ON and OFF cone bipolar cells

(reviewed in (Euler et al. 2014)). Signals are then further transmitted to either ON or OFF retinal ganglion cells and to the visual centers in the brain. ON and OFF pathways are important in terms of luminance contrast and light adaptation (Kuffler 1953, Reid et al. 2013).

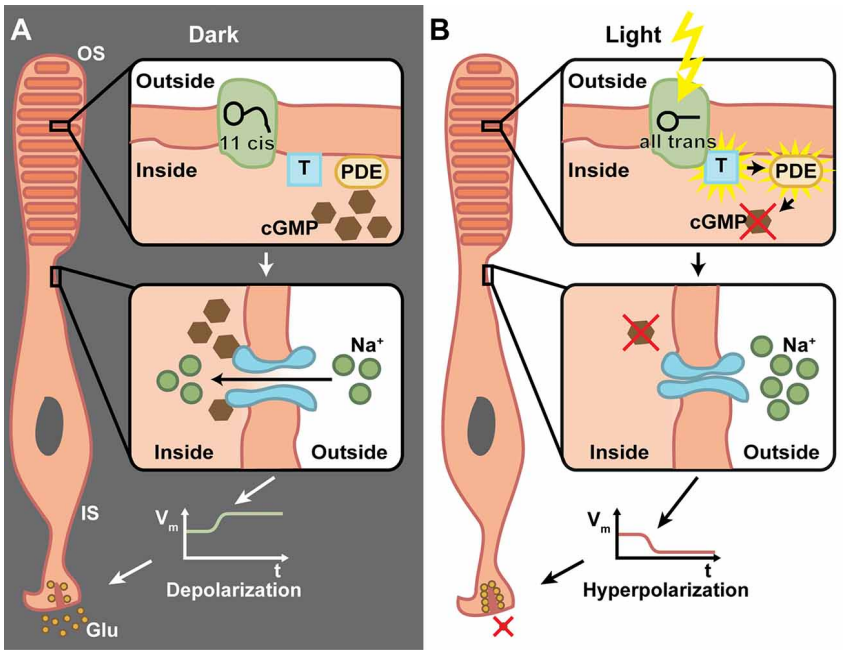

Figure 3. Phototransduction in vertebrate photoreceptors. (A) In darkness, open cGMP-gated ion channels lead to photoreceptor depolarization and release of the neurotransmitter glutamate. (B) Upon stimulation by light, 11-*cis* retinal changes its conformation to all-*trans* retinal. Transducin activates PDE, which lowers cGMP concentration and thereby leads to closure of cGMP-gated ion channels. Consequently, photoreceptors hyperpolarize and discontinue the release of glutamate. OS: outer segments, T: transducin, PDE: phosphodiesterase, cGMP: cyclic guanosine monophosphate, IS: inner segments, Glu: glutamate. From (Klapper et al. 2016).

Importantly, the proteins of the phototransduction cascade need to be returned to their inactivated state after light stimulation. Rhodopsin kinase (G protein-coupled receptor kinase 1, GRK1) phosphorylates activated rhodopsin and allows binding of arrestin, which blocks the interaction with transducin (Wilden et al. 1986, Kuhn et al. 1987). Guanylate cyclase, whose activity is regulated by Ca^{2+}-mediated inhibition, restores cGMP-levels and thereby permits reopening of cation channels (Kawamura et al. 1989).

1.1.4 The visual cycle

After intense stimulation, it can take around ten minutes until the visual sensitivity returns to baseline levels (Lamb et al. 2004). A significant amount of visual pigment is “bleached” and needs to be regenerated. The chromophore is recycled through a series of enzymatic steps called the visual cycle (Figure 4) (Baehr et al. 2003). First, all-*trans* retinal is transported from the intradiscal space to the cytosol of the rod outer segment, facilitated by ATP-binding cassette transporter 4 (ABCA4, also known as ATP-binding cassette transporter Retina (ABCR)). After modification from all-*trans* retinal to all-*trans* retinol by all-*trans* retinol dehydrogenase, it is removed from the photoreceptor

outer segments and transported to the RPE via the chaperone protein interphotoreceptor retinol binding protein (IRBP) (Strauss 2005). In the RPE, it binds to cellular retinol binding protein (CRBP) and is then esterified by lecithin retinol acyltransferase (LRAT) to all-*trans* retinyl ester. Subsequently, RPE65 (RPE-specific 65kDa protein) uses all-trans retinyl ester as a substrate to form 11-*cis* retinol (Redmond et al. 1998). 11-*cis* retinol dehydrogenase oxidizes 11-*cis* retinol to 11-*cis* retinal, which is supported by cellular retinaldehyde-binding protein (CRALBP). Subsequently, 11-*cis* retinal is transported back to photoreceptor outer segments, where it recombines with rod opsin (reviewed in (Strauss 2005, von Lintig et al. 2010, Kiser et al. 2014)).

In contrast to rods in which trans-*cis* isomerization of the chromophore takes place in the RPE, evidence suggests that cones additionally use a faster Müller cell-dependent alternative pathway for recycling of the chromophore (Mata et al. 2002, Schonthaler et al. 2007, Wang et al. 2011).

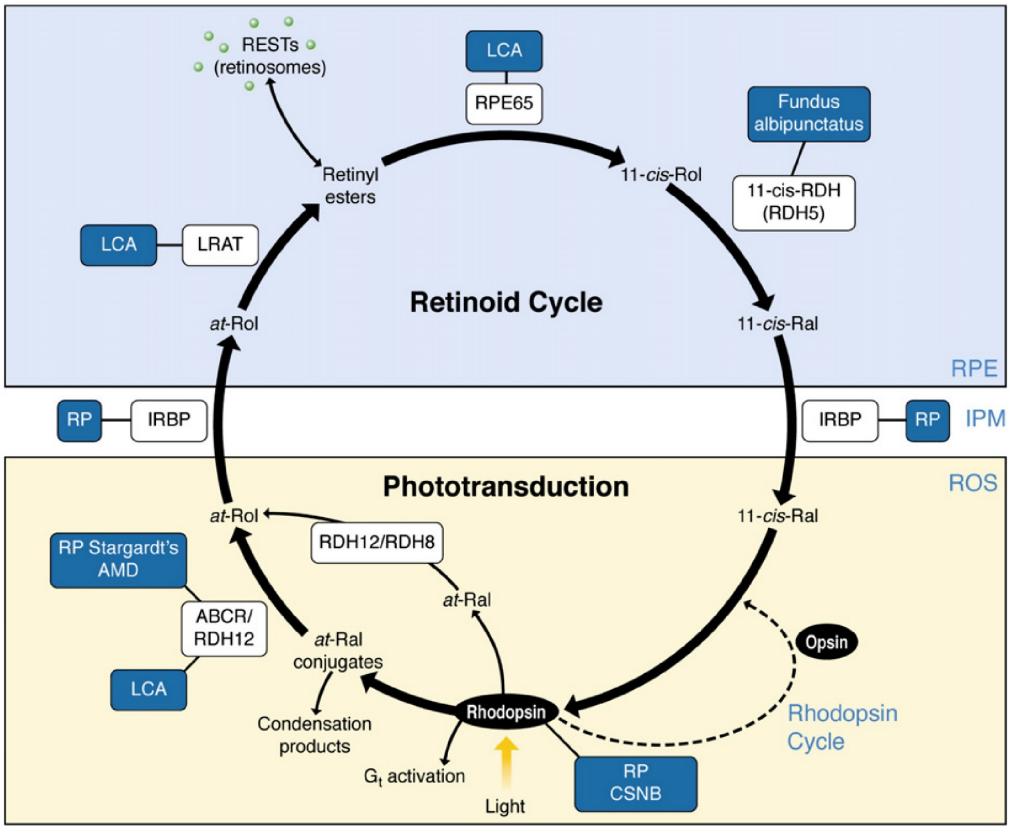

Figure 4. The visual cycle in rod photoreceptors and retinal diseases associated with mutations in key enzymes. Light stimulation converts 11-*cis* retinal to all-*trans* retinal and all-*trans* retinol in the photoreceptor outer segments. All-*trans* retinol is transported to the RPE, where it is converted to 11-*cis* retinal. After being transported back to the photoreceptor outer segments, it binds to rhodopsin. Several retinal diseases have been associated with mutations in visual cycle components (blue boxes). 11-*cis*-Rol: 11-*cis* retinol, 11-*cis*-Ral: 11-*cis* retinal, *at*-Ral: all-*trans* retinal, *at*-Rol: all-*trans* retinol, ABCR: ATP-binding cassette transporter Retina (also known as ABCA4), AMD: age-related macular degeneration, CSNB: congenital stationary night blindness, IPM: interphotoreceptor matrix, IRBP: interphotoreceptor retinol binding protein, LCA: Leber congenital amaurosis, LRAT: lecithin retinol acyltransferase, RDH: retinal dehydrogenase, ROS: rod outer segment, RP: retinitis pigmentosa, RPE: retinal pigment epithelium, RPE65: RPE-specific 65kDa protein. From (Kiser et al. 2012).

Mutations in visual cycle components may impair the regeneration of the visual chromophore and thus affect vision (reviewed in (Travis et al. 2007)). Several retinal disorders have been associated with mutations in key enzymes (indicated in Figure 4, blue boxes), such as Leber congenital amaurosis, age-related macular degeneration, congenital stationary night blindness, retinitis pigmentosa and Stargardt's disease. As outlined above, the isomerohydrolase RPE65 plays a key role in the regeneration of 11-*cis* retinal and is essential for rod and cone function (Redmond et al. 1998, Moiseyev et al. 2005, Wenzel et al. 2007). Mutations in human *RPE65* lead to severe retinal dysfunction and blindness, accounting for a significant percentage (11.4%) of early-onset retinal degenerations. Various diagnostic designations are used for patients suffering from *RPE65*-associated mutations, such as Leber congenital amaurosis type 2, early severe retinitis pigmentosa, autosomal recessive retinal dystrophy and early-onset severe retinal dystrophy (Thompson et al. 2000).

1.2 Oxygen Homeostasis in the Retina

As one of the most metabolically active tissues in the body, the retina – and especially the high-energy demanding photoreceptors – require appropriate oxygen levels to generate ATP (Niven et al. 2008, Okawa et al. 2008). In general, cells produce energy by oxidative phosphorylation in mitochondria and glycolysis in the cytosol, providing about 30 or 2 molecules of ATP per molecule glucose, respectively (Alberts et al. 2002). Whereas glutamate neurotransmission in the retina is mainly supported by glycolysis, phototransduction depends on oxidative metabolism (Ames et al. 1992, Xu et al. 2007).

1.2.1 Retinal vasculature

To ensure appropriate oxygen levels for normal retinal function, oxygen is delivered by two vascular systems: the retinal vasculature nourishes the inner retina and the choroidal vasculature at the basolateral side of the RPE supplies photoreceptors in the outer retina (Figure 5). Besides the different functions, the systems also differ in their properties. While the retinal vasculature has barrier properties and is part of the inner blood-retinal barrier, the choroidal vasculature has fenestrated capillaries (Saint-Geniez et al. 2004). Additionally, blood flow in the retinal vasculature is auto-regulated through the release of vasoactive substances in response to changes in oxygen levels (reviewed in (Pournaras et al. 2008)). The mature retinal vasculature consists of three vascular plexi: the superficial primary plexus spreads in the nerve fiber layer across the inner surface of the retina. The two other plexi – the intermediate and the deep plexus – are located in the inner and the outer plexiform layer where neuronal synaptic connections are made.

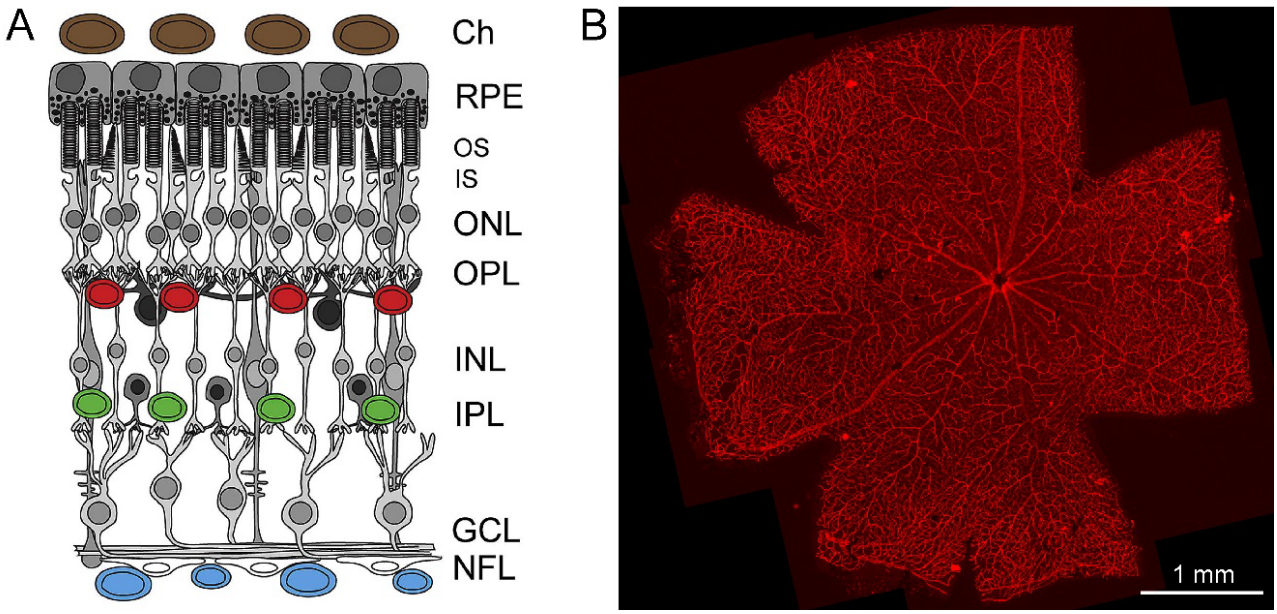

Figure 5. The vascular network in the mouse retina. (A) Schematic illustration of the three vascular plexi. The primary (blue), intermediate (green) and deep plexus (red) of the retinal vasculature. The choroidal vasculature (brown) is located at the basolateral side of the RPE. Ch: choroid, RPE: retinal pigment epithelium, OS: outer segments, IS: inner segments, ONL: outer nuclear layer, OPL: outer plexiform layer, INL: inner nuclear layer, IPL: inner plexiform layer, GCL: ganglion cell layer, NFL: nerve fiber layer (from (Caprara et al. 2012)). (B) Immunostaining of vessels stained with isolectin IB_4 on a retinal flat mount showing the superficial primary plexus (*BPCre;R91W;Nrl*$^{-/-}$*;Vhl*$^{f/f}$*;Hif1a*$^{f/f}$ mouse, see section results). Scale bar: 1 mm.

1.2.2 Hypoxia-inducible factors

The retina is highly vulnerable to any disturbances in oxygen saturation (Ames et al. 1992, Arjamaa et al. 2009). In response to reduced oxygen levels (hypoxia), regulatory systems in the body are activated, with hypoxia inducible factors (HIFs) playing a central role. In the retina, hypoxic conditions may occur due to different reasons (see following chapters: 1.2.3, 1.2.5).

HIF proteins are composed of an oxygen-labile α-subunit (HIFA) and a constitutively expressed β-subunit (aryl hydrocarbon receptor nuclear translocator (ARNT), alias HIF1B) (Wang et al. 2011). Each subunit contains a basic-helix-loop-helix (bHLH) and a Per/ARNT/Sim (PAS) domain (Wang et al. 1995) that mediate heterodimerization and DNA binding (Semenza 2004). Three structurally homologous α-chains were identified (Figure 6A): HIF1A (Semenza et al. 1992, Wang et al. 1995), HIF2A (alias, endothelial PAS domain protein 1 (EPAS1), (Ema et al. 1997, Flamme et al. 1997, Tian et al. 1997)) and HIF3A (Gu et al. 1998, Heidbreder et al. 2003).

In contrast to HIF1A that is ubiquitously expressed, HIF2A expression is more restricted. Hypoxic induction of HIF2A has been observed in brain, heart, lung, kidney, liver, pancreas, and intestine (Wiesener et al. 2003). While HIF1A and HIF2A have been studied extensively, the role of HIF3A is less well understood. Possibly, HIF3 modulates the hypoxic response by acting as a negative regulator of HIF1A function (Makino et al. 2001).

Both HIF1A and HIF2A can form a functional transcriptional complex with ARNT (HIF1B) (Tian et al. 1997). Three isoforms of HIF-β chains are known: ARNT (alias HIF1B), ARNT2, ARNT-like (ARNTL) (Hirose et al. 1996, Ikeda et al. 1997, Hogenesch et al. 1998, Hogenesch et al. 2000). Although they share homologous structures, not all isoforms promote responses to hypoxia. ARNT2 shares overlapping functions with ARNT (HIF1B) but is primarily involved in neural development (Keith et al. 2001). ARNTL, also known as brain and muscle ARNT-like protein 1 (BMAL1) (Ikeda et al. 1997), is an important regulator of circadian rhythm (Reppert et al. 2001).

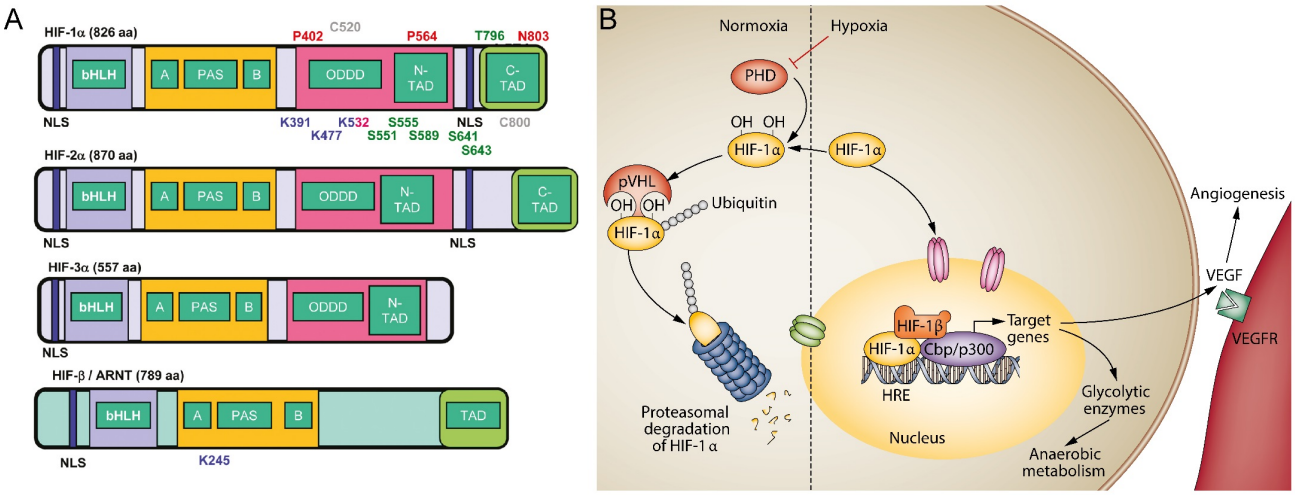

Figure 6. HIF isoforms and HIF pathway. (A) Illustration of the three HIFA subunits and HIF1B (alias, ARNT) structure. Specific domains on HIF1A, HIF2A and HIF3A mediate DNA binding, specificity and dimerization with HIF1B (bHLH/PAS), protein stability (ODDD/N-TAD), transcriptional activity (N-TAD/C-TAD) and nuclear localization (NLS). HIF1B lacks an ODDD and is thus not oxygen-dependently regulated. NLS: nuclear localization signal, bHLH: basic-helix-loop-helix, PAS: Per-ARNT-Sim motif, ODDD: oxygen-dependent degradation domain, N-TAD: N-terminal transactivation domain, C-TAD: C-terminal transactivation domain. (B) Under normoxic conditions, PHDs use oxygen to hydroxylate HIF1A on proline residues (Pro402 and Pro564). Subsequently, pVHL binds to HIF1A and recruits an ubiquitin E3 ligase. Consequently, HIF1A is degraded via the proteosomal pathway. Under hypoxic conditions, however, hydroxylation does not occur. HIF1A accumulates and enters the nucleus, where it dimerizes with HIF1B, interacts with co-activators Cbp/p300 and drives the transcription of target genes. PHD: prolyl hydroxylase, HIF-1α: hypoxia-inducible factor 1α, HIF-1β: hypoxia-inducible factor 1β (alias, ARNT), pVHL: von Hippel Lindau protein, HRE: hypoxia response element, VEGF: vascular endothelial growth factor. From (Krock et al. 2011, Maes et al. 2012).

Under normal oxygen levels (normoxia), HIFA is hydroxylated on proline residues (402 and 564 for HIF1A, 405 and 531 for HIF2A) by prolyl hydroxylases (PHDs). Three PHDs were identified in mammalian cells: PHD1, PHD2, PHD3 (Epstein et al. 2001). They contain Fe(II) in their active site and require 2-oxoglutarate (α-ketoglutarate) as a substrate as well as ascorbate as a cofactor. Proline hydroxylation promotes the interaction with the von-Hippel-Lindau (VHL) ubiquitin E3 ligase complex (Figure 6B), which leads to ubiquitination and degradation via the proteosomal pathway. Oxygen is rate-limiting for the enzymatic activity of hydroxylases. Thus, under conditions of reduced

oxygen availability (hypoxia), HIFA is less hydroxylated. Hence, HIFA proteins accumulate and enter the nucleus (Semenza 2004, Patel et al. 2008, Webb et al. 2009, Semenza 2011).

After translocation into the nucleus, HIF1A or HIF2A proteins dimerize with HIF1B and recruit co-activators, such as p300/CBP (CREB(cAMP-response element-binding protein)-binding protein) in the case of HIF1A (Arany et al. 1996, Semenza 2004). Other co-activators for HIF1A and HIF2A are summarized in (Loboda et al. 2010). Regulation of the interaction of HIFA with the co-activators p300/CBP is mediated by a second oxygen-sensitive hydroxylation event. Under normoxic conditions, factor inhibiting HIF1 (FIH) hydroxylates HIFA at an asparagine residue in the C-terminal transactivation domain (C-TAD) (Asn-803 for human HIF1A, Asn-851 for human HIF2A) and prevents the interaction with p300/CBP (Arany et al. 1996, Mahon et al. 2001, Lando et al. 2002, McNeill et al. 2002, Schofield et al. 2004). Under hypoxic conditions, however, hydroxylation is diminished. Consequently, HIF dimers and co-activators bind to hypoxia response elements (HREs) on HIF target gene promoters and drive the transcription of a multitude of target genes involved in angiogenesis, cell metabolism, survival, cytoskeletal structure and apoptosis (Semenza 2004).

HIF1A and HIF2A have both shared and unique transcriptional target genes: under hypoxia, HIF1A and HIF2A both stimulate expression of for example glucose transporter 1 (*Glut1*), adrenomedullin (*Adm*) and vascular endothelial growth factor (*Vegf*) (Hu et al. 2003). Glycolytic enzymes (such as lactate dehydrogenase A (*Ldha*)) and BCL2/adenovirus E1B interacting protein 3 (*Bnip3*) are targeted by HIF1A and erythropoietin (*Epo*) has been shown to be a HIF2A-target (Hu et al. 2003, Warnecke et al. 2004). HIF2A-target genes are more restricted and little is known about its targets in the retina. However, several candidate genes such as HtrA serine peptidase 1 (*Htra1*), tissue inhibitor of metallopreinase 3 (*Timp3*) and heme oxygenase (decycling) 1 (*Hmox1*) have been suggested to be HIF2A-regulated in rod photoreceptors (Kast et al. 2016).

1.2.3 Hypoxia during development of the retinal vasculature

During retinal development, photoreceptors are functional before the retinal vasculature has completely been formed (Graymore et al. 1959). Therefore, it has been proposed that the retina suffers from ‘physiological hypoxia’ which stimulates retinal angiogenesis (Chan-Ling et al. 1995).

Initially, an arterial network in the vitreous called hyaloid vasculature provides blood supply from the central hyaloid artery in the optic nerve to the retina and lens during early development (Saint-Geniez et al. 2004). The hyaloid vasculature usually regresses before or around birth, depending on the species. It is replaced by the retinal vasculature, which contains both arteries and veins (Fruttiger 2007). In the mouse retina, the primary plexus develops along a gradient from the center to the periphery and reaches the periphery at around postnatal day (PND) 8. At the same time, vessels start sprouting and penetrate the retina. They turn laterally when they reach the inner and outer boundary of the INL to first form the deep and consequently the intermediate plexus (Fruttiger 2007). The deep plexus in the retinal periphery is generated at around PND12, followed by the intermediate

plexus between PND12 and 15. By the end of the third postnatal week, all vascular plexi are fully mature (Stahl et al. 2010).

Hypoxia induces expression of *Vegf*, a potent angiogenic factor (Shweiki et al. 1992, Carmeliet 2003). It has been suggested that hypoxia-induced *Vegf* expression by astrocytes in the GCL regulates the formation of the primary plexus (Stone et al. 1995). Additionally, transient *Vegf* expression in the INL precedes the formation of the deep plexus (Stone et al. 1995). However, the study by Weidemann *et al.* shows that astrocyte-derived VEGF is not essential for primary plexus development (Weidemann et al. 2010). Although the role of VEGF (and other angiogenic factors) in formation of the primary plexus still needs to be clarified, the hypoxic response clearly plays a central role in retinal angiogenesis. Inactivation of *Vhl* in the retinal periphery during development leads to vessel growth into the ONL (Kurihara et al. 2010, Lange et al. 2011). Additionally, knockdown of *Hif1a* in the retinal periphery prevents the formation of the intermediate plexus (Caprara et al. 2011). Therefore, neurovascular crosstalk and a tight regulation of angiogenic factors such as VEGF (Okabe et al. 2014) seems to be essential to direct and guide appropriate retinal vascularization.

1.2.4 Hypoxia and retinal protection: hypoxic preconditioning

Besides being an important regulator of vascular development, hypoxia has also distinct roles in the adult retina. A period of acute hypoxia (6 hours) induces pro-survival factors and protects photoreceptors against light-induced degeneration in mice (Grimm et al. 2002). Additionally, hypoxic preconditioning has been shown to be protective in models for retinal ischemia (Whitlock et al. 2005, Zhu et al. 2007) and glaucoma (Zhu et al. 2013). Erythropoietin, an oxygen- and HIF2-regulated protein that stimulates the production of red blood cells, has been suggested as candidate factor mediating photoreceptor survival (Grimm et al. 2002). Interestingly, the protective response is neither HIF1- nor HIF2-dependent: rods lacking HIF1A, HIF2A or both factors are still protected against light-induced damage (Thiersch et al. 2009, Kast et al. 2016). Identification of the molecular mechanisms that activate these protective signaling events might further help in understanding neuroprotective pathways in the retina and other tissues.

1.2.5 Hypoxia and retinal diseases

In contrast to acute hypoxia that supports photoreceptor survival, long-term (chronic) hypoxia during aging may contribute to disease development. Photoreceptors receive their oxygen largely from the choroidal vasculature (see 1.2.1). During aging, reduced choroidal blood flow (Dallinger et al. 1998, Lam et al. 2003) and accumulation of extracellular deposits known as drusen (Grunwald et al. 2005) may impair oxygen supply to photoreceptors. Consequently, photoreceptors in the old human retina may suffer from reduced oxygen availability. Accumulating evidence proposes that chronic hypoxia may contribute to development and progression of degenerative diseases such as age-related macular degeneration (AMD). Choroidal ischemia in dry AMD (Ciulla et al. 1999, Coleman et al. 2013) suggests reduced oxygen transport from the choroid to the inner retina (Kim et al. 2013).

Decreased choroidal blood volume in AMD as well as the correlation of drusen density and decreased choroidal blood flow (Berenberg et al. 2012) support the hypothesis that hypoxia might play an important role in retinal pathologies by affecting hypoxic target genes involved in lipid handling, energy metabolism and cell survival.

Additionally, reduced tissue oxygenation may trigger neovascularization. As outlined above (see 1.2.3), hypoxic target genes modulate retinal angiogenesis. Increased concentration of VEGF stimulates vessel growth along the inner retinal surface and/or into the vitreous in retinal neovascular diseases, such as diabetic retinopathy (see 1.3.1), central retinal vein occlusion and retinopathy of prematurity (Aiello et al. 1994, Lashkari et al. 2000). Similarly, elevated VEGF levels cause pathological vessel growth from the choroid to the subretinal space in choroidal neovascular diseases (see 1.3.2). Hypoxia-related mechanisms may therefore be relevant for numerous retinal diseases in humans.

1.3 Macular Degenerations and Therapies

Loss of vision dramatically affects the patient's quality of life and represents a major burden for health and social systems (Chakravarthy et al. 2017). Global causes for blindness are cataract (i.e. clouding of the lens), glaucoma (i.e. vision loss due to damage to the optic nerve), age-related macular degeneration (AMD), corneal opacities, childhood blindness (a group of diseases occurring in childhood which, if left untreated, result in blindness), uncorrected refractive errors, trachoma (a bacterial infection) and diabetic retinopathy (DR) (Pascolini et al. 2012). Most of these causes, except AMD, are at least partially preventable or treatable, although access to care still strongly limits treatment in developing countries. In industrialized countries, AMD and other age-related diseases will become even more important with the increasing life expectancy of our population. With regard to the main projects of this thesis, I will briefly address DR and discuss AMD in more detail, since AMD is a major research focus in our lab.

1.3.1 Diabetic retinopathy (DR)

Chronically high blood sugar in patients suffering from diabetes may damage retinal blood vessels and lead to visual impairment known as DR. During disease progression, microaneurysms may leak blood into the retina and swelling of the retina known as macular edema may occur. As the disease progresses, dysfunctional blood vessels may cause vessel growth along the inner retina and into the vitreous. DR is separated into early, non-proliferative and proliferative DR. In contrast to non-proliferative DR, a hallmark of proliferative DR is neovascularization. Additionally, in advanced stages retinal detachment may affect visual acuity (reviewed in (Cheung et al. 2010, Antonetti et al. 2012); Figure 7).

Although improvements in glycemic control reduced the prevalence and incidence of DR (Klein et al. 2010), DR still affects up to 20% of patients after 30 years of disease, despite intensive insulin therapy (Nathan et al. 2009).

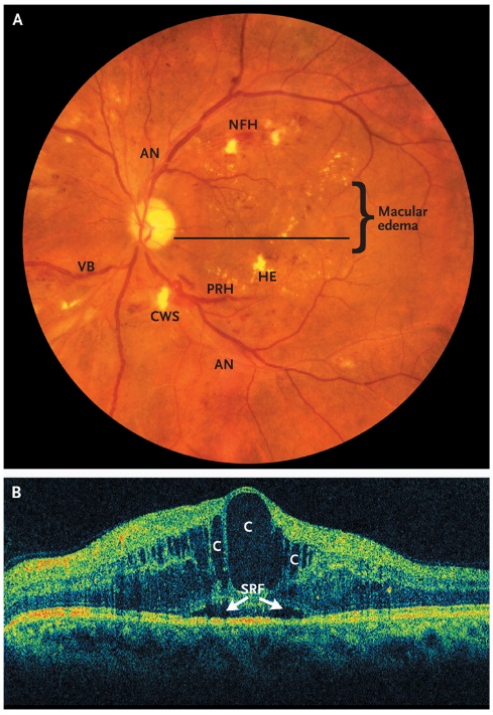

Figure 7. Diabetic Retinopathy: Clinical features and macular edema. (A) Proliferative DR with macular edema in a 57-year-old patient. AN: arteriolar narrowing, NFH: nerve-fiber hemorrhage, HE: hard exudates, CWS: cotton-wool spots, VB: venous beading, PRH: preretinal hemorrhage. (B) An optical coherence tomography (OCT) scan through the central fovea (marked with horizontal line in A) shows thickening and macular edema. C: cysts, SRF: subretinal fluid. Reproduced with permission from (Antonetti et al. 2012), Copyright Massachusetts Medical Society.

As outlined above, the molecular pathophysiology of DR is associated with a dysfunctional blood vessels and impaired BRB. VEGF-targeting therapies provide benefit for DR patients (Michaelides et al. 2010, Nguyen et al. 2010, Sultan et al. 2011), underlining a role for VEGF in vascular permeability and disease pathology. Several mouse models support the suggested key role of the neurovascular unit (i.e. neurons, glia cells and vasculature, Figure 8) in DR pathology. Loss of pericytes caused by platelet-derived growth factor (PDGF) ablation may cause retinopathy and mimics DR in mice (Enge et al. 2002). Additionally, inflammation including activation of microglial cells (Zeng et al. 2008) and increased levels of interleukin-1β and TNF-α (Schram et al. 2003, Demircan et al. 2006) contribute to disease development and progression. Further research focusing on the molecular changes may assist in understanding and treating DR pathology.

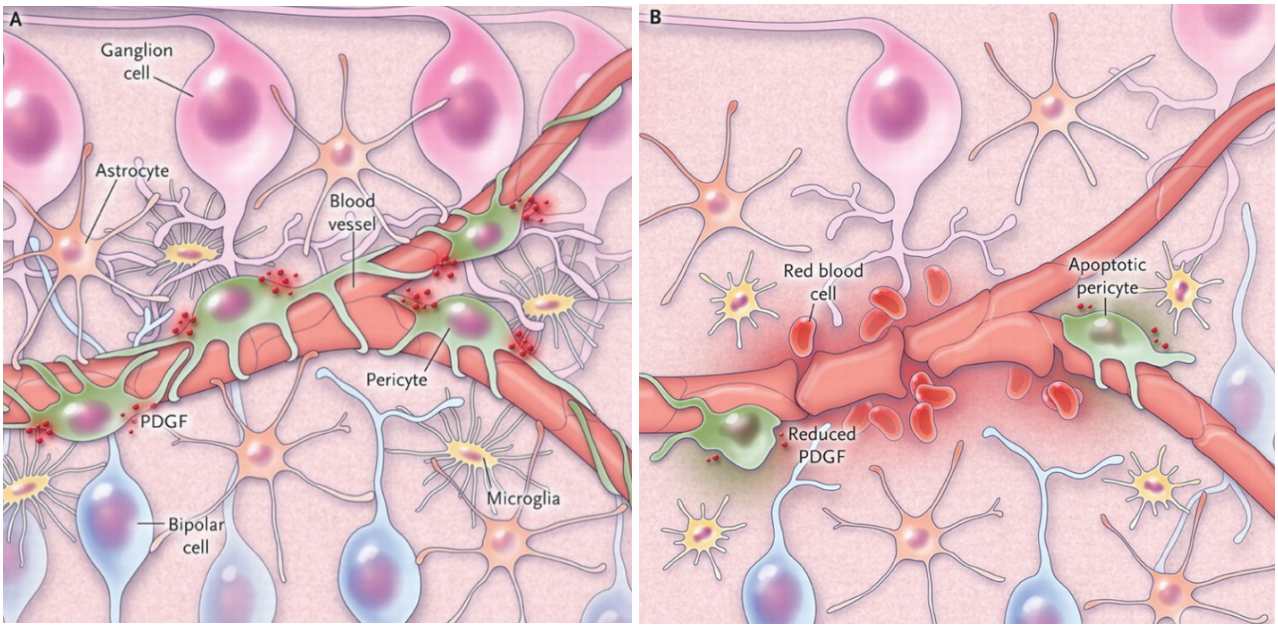

Figure 8. Dysfunction of the neurovascular unit in DR. (A) Neurovascular unit of the retina with pericytes, astrocytes and microglial cells. (B) In DR, increased levels of VEGF and inflammatory cytokines as well as the loss of PDGF signaling in pericytes impair the BRB and stimulate angiogenesis. PDGF: platelet-derived growth factor. Reproduced with permission from (Antonetti et al. 2012), Copyright Massachusetts Medical Society.

1.3.2 Age-related macular degeneration (AMD)

AMD is a highly prevalent blinding disease and a leading cause of visual impairment in the elderly population in industrialized nations (Klein et al. 1999, Buch et al. 2004, Wong et al. 2014). Due to the degeneration of photoreceptors and RPE in the macular region, patients lose the ability for central, high acuity vision (Green 1999, Swaroop et al. 2009). AMD is a multifactorial disease and numerous risk factors have been identified. Major genetic contributors include complement pathway genes (complement factor H (*CFH*) (Edwards et al. 2005, Hageman et al. 2005, Haines et al. 2005, Klein et al. 2005), complement 3 (*C3*) (Yates et al. 2007), complement factor B (*CFB*), complement component 2 (*C2*) (Gold et al. 2006)) and other genes such as age-related maculopathy susceptibility 2/HtrA serine peptidase 1 (*ARMS2/HTRA1*) (Rivera et al. 2005, Dewan et al. 2006). Additionally, many other candidate genes such as tissue inhibitor of metalloproteinase 3 (*TIMP3*) (Chen et al. 2010, Vierkotten et al. 2011, Ardeljan et al. 2013, Fritsche et al. 2016) and *SLC16A8* (Fritsche et al. 2016) have been related to AMD (Figure 9).

Besides genetic factors, numerous environmental risk factors have been reported. Elevated risk of AMD is associated with increasing age, cigarette smoking, cardiovascular disease, hypertension and obesity (Chakravarthy et al. 2010).

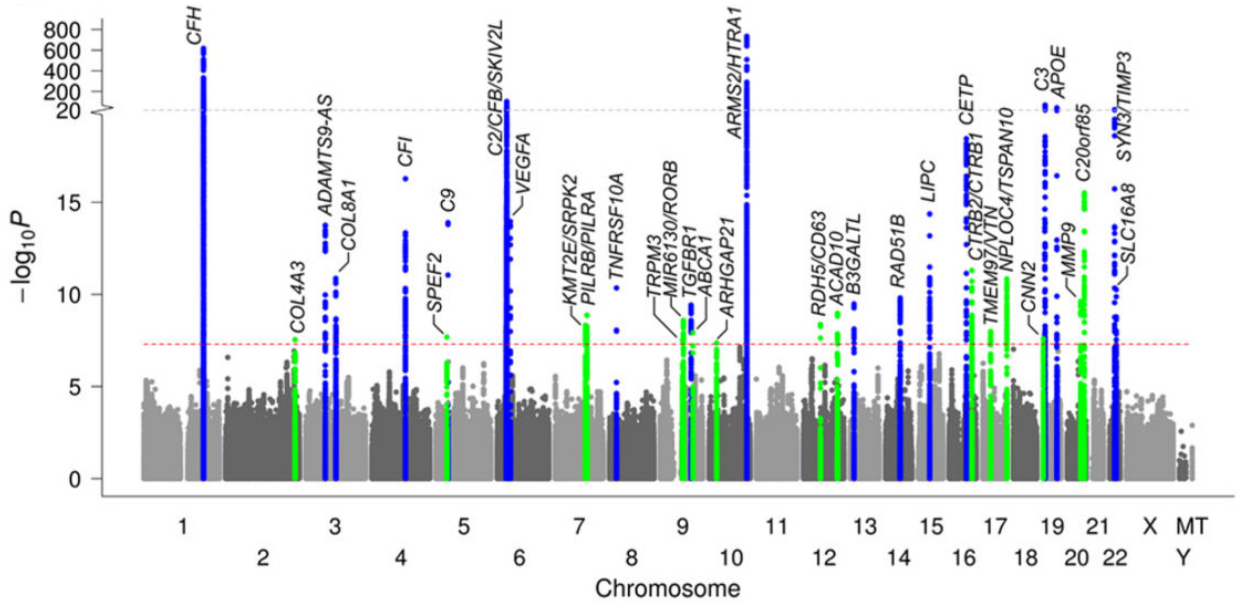

Figure 9. Genome-wide single variant association analysis in advanced AMD patients. Shown are novel (green) and known (blue) AMD loci. From (Fritsche et al. 2016).

Clinically, AMD is separated into early, intermediate and late AMD based on fundus inspection (Figure 10). Late AMD can further be divided into dry and neovascular (wet) AMD. Although the dry form of AMD is more frequent, neovascular AMD is responsible for the vast majority of cases of severe visual loss or blindness (Ferris et al. 1984, Ferris et al. 2013).

Apart from drusen (i.e. deposits between the basal lamina of the RPE and the Bruch's membrane), a hallmark of dry AMD is geographic atrophy, i.e. the cell death of photoreceptors and RPE within the macular region (Sarks 1976, Bird et al. 1995, Green 1999, Lim et al. 2012). Although drusen are part of the normal aging process (Sarks et al. 1999), excess amount and size of drusen may interfere with the functional photoreceptor/RPE unit. Similar to drusen, autofluorescent lipid and protein aggregates known as lipofuscin granules accumulate with increasing age in the RPE (Wing et al. 1978, Kennedy et al. 1995). Lipofuscin granules represent non-degraded debris from phagocytosed photoreceptor disks. A2E, a component of lipofuscin (Eldred 1995), inhibits the ATP-driven proton pump in lysosomes, leads to lysosomal dysfunction and thereby contributes to AMD pathogenesis (Bergmann et al. 2004). Thickness of the Bruch's membrane increases with age (Hogan et al. 1967, Ramrattan et al. 1994), which may affect fluid/nutrient transport (Starita et al. 1996) and initiate cell death of adjacent cells due to inappropriate cell adhesion known as anoikis (Gilmore 2005). As a consequence of the above mentioned factors, tissue hypoxia may occur, which has been implicated in the etiology of AMD (see 1.2.5 and (Remsch et al. 2000, Arjamaa et al. 2009, Sheridan et al. 2009, Boltz et al. 2010, Stefánsson et al. 2011, Kent 2014)).

In contrast to retinal neovascularization in DR where vessels grow along the inner retinal surface, new blood vessels in neovascular AMD grow from the choroid, penetrate the Bruch's membrane and extend into the subretinal space (Bressler et al. 1988, Spaide 2013). This process is known as

choroidal neovascularization (CNV). Retinal angiomatous proliferation (RAP), also known as deep retinal vascular anomalous complexes, represents an additional, distinct form of neovascular AMD (Yannuzzi et al. 2001). In contrast to the typical choroidal neovascular form of AMD, pathological vessels observed in RAP originate from the deep retinal plexus in the inner retina and extend into the photoreceptor layer and subretinal space (Hartnett et al. 1996, Yannuzzi et al. 2008). RAP accounts for 15-20% of neovascular AMD (Cohen et al. 2007, Massacesi et al. 2008).

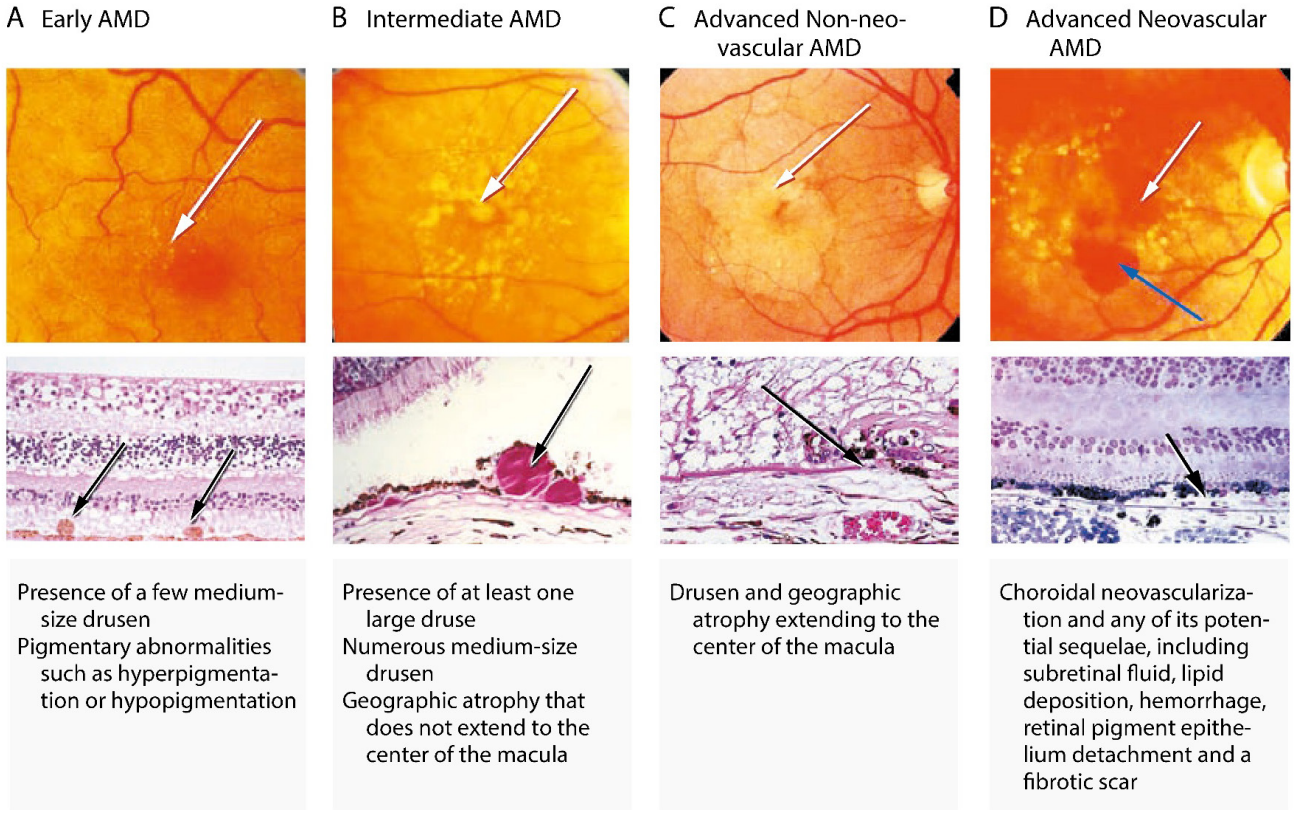

Figure 10. Fundus images and histology of different stages of AMD. Early AMD (A) with medium size drusen (arrows) and intermediate AMD (B) with large drusen (arrows) are shown. In advanced dry AMD (C), geographic atrophy (white arrow) with loss of Bruch's membrane (black arrow) is present. Advanced neovascular AMD (D) is characterized by subretinal hemorrhages (blue arrow) and choroidal neovascularization (white and black arrow). Shown are fundus (top) and histopathological images (middle) as well as a description of clinical features (bottom). Reproduced with permission from (Jager et al. 2008). Copyright Massachusetts Medical Society.

1.3.3 Current treatment of AMD

With an aging population, the number of people with age-related retinal diseases such as AMD is predicted to rise over the coming years. 196 million people are expected to suffer from AMD in 2020, increasing to 288 million in 2040 (Wong et al. 2014). These data highlight the urgent need for efficient therapeutic approaches. Current management of dry AMD includes cessation of smoking, maintenance of a healthy weight, regulation of blood pressure and antioxidant supplementation (vitamin C, E, beta-carotene, zinc oxide, cupric oxide). Such daily supplementation may reduce the

risk of progression from intermediate to advanced AMD (Age-Related Eye Disease Study Research 2001, Jager et al. 2008). In contrast to dry AMD, neovascular AMD can be treated by intravitreal anti-VEGF therapies (e.g. pegabtanib (Macugen) (Gragoudas et al. 2004), ranibizumab (Lucentis) (Rosenfeld et al. 2006), aflibercept (Eylea, VEGF trap-eye) (Holash et al. 2002, Heier et al. 2012), bevacizumab (avastin, off-label use (Maguire et al. 2016)). Although frequent intraocular injections may slow disease progression of neovascular AMD, no cure is available until now.

1.3.4 Stem cell therapy as a new therapeutic approach for degenerative diseases

New fields of research emerge and include, among others, stem cell transplantation and gene therapy. In advanced stages of retinal degeneration, stem cell therapy can replace lost photoreceptors and RPE. Several studies are ongoing (reviewed in (Scholl et al. 2016)) and first human studies of human embryonic stem cell(hESC)-derived RPE demonstrated not only feasibility but also challenges and risks. Studies by Dr. Schwartz and colleagues reported long-term safety in nine patients suffering from dry AMD and nine patients suffering from Stargardt's disease. In eight of 18 patients, visual acuity improved during the first year after surgery. Clearly, however, the low number of enrolled patients limits a conclusive interpretation of the results and subsequent clinical trials will be needed (Schwartz et al. 2015, Schwartz et al. 2016). Although no adverse events related to hESC-derived RPE cells were reported, some patients had adverse events due to surgical procedure and concomitant systemic immunosuppression (Schwartz et al. 2012, Schwartz et al. 2015, Song et al. 2015, Schwartz et al. 2016). Rejection and ethical concerns on using cells derived from human embryos favor the use of induced pluripotent stem cells (iPSCs), which can be derived from differentiated adult cells (Takahashi et al. 2006) and make the use of concomitant immunosuppressive therapy unnecessary. The first human trial on iPSCs that included only one patient was suspended in 2015 due to regulatory changes in Japan (Garber 2015), although the treatment was reported to be safe (Mandai et al. 2017). In this study, iPSCs were generated from skin fibroblasts, differentiated into an RPE cell sheet and transplanted in a patient with wet AMD (Mandai et al. 2017). Research focuses now on a change of strategy by using partially matched (human leukocyte antigen (HLA)-matched) allogenic iPSC-derived RPE cells, which is expected to tremendously reduce the cost and increase the number of patients that could be treated with the same therapy (Garber 2015).

1.3.5 Gene therapy for retinal disorders: adeno-associated viruses (AAV)

Another major research interest is gene therapy. The non-pathogenic, helper-dependent adeno-associated virus (AAV) has become the vector of choice in retinal gene therapy due to safety reasons and the availability of several serotypes conferring tropism to different tissues (Lisowski et al. 2015, Sengillo et al. 2016, Moore et al. 2017) and, most notably, different retinal cell types across species (Boye et al. 2013).

The wild-type AAV genome is about 4.7 kilobases long and consists of linear single-stranded DNA with two genes (replication (rep) and capsid (cap), Figure 11A) and two inverted terminal repeats (ITR) (Koczot et al. 1973). The four rep proteins (rep78, rep68, rep52, rep40) are required for the AAV life cycle and the three cap proteins (VP1, VP2, VP3) together assemble the icosahedral capsid. Upon binding to receptors on the outer cellular surface, the AAV enters the cell via endocytosis through clathrin-coated vesicles (reviewed in (Goncalves 2005, Kotterman et al. 2014, Samulski et al. 2014)).

To produce recombinant AAV for research purposes, different plasmids are co-transfected into AAV packaging cells: i) a pAAV-transgene plasmid (the gene of interest flanked by ITRs), and ii) packaging constructs (i.e. a plasmid with rep/cap and a helper plasmid (Figure 11B) (Samulski et al. 2014)). One of the most studied AAVs, AAV serotype 2, can be cross-packed into capsids of other serotypes (Rabinowitz et al. 2002). Capsid engineering can further increase flexibility and specificity of the AAV. It was discovered that phosphorylation of tyrosine residues on AAV capsids leads to ubiquitination and proteosomal degradation by the host cells (Zhong et al. 2008a, Zhong et al. 2008b). This finding prompted the development of tyrosine-to-phenylalanine mutated AAV capsids to escape host defense and increase target gene expression (Zhong et al. 2008b). Additionally, further efficiency increase can be achieved by using self-complementary AAVs, which have two complementary parts that anneal after uncoating without the need of prior DNA synthesis (McCarty 2008).

AAVs can be delivered to the retina by subretinal or intravitreal injections (Figure 11C). While intravitreal injections are only minimally invasive, subretinal injections deliver the vector between the photoreceptors and the RPE and thereby create a temporary retinal detachment. Currently, subretinal delivery is the method of choice to target cells of the outer retina but AAV variants are being engineered that allow efficient transduction of the outer retina via intravitreal injections, e.g. AAVs with tyrosine-to-phenylalanine mutations (Zhong et al. 2008b, Petrs-Silva et al. 2011, Kay et al. 2013) or AAV2-7m8 with a 10-amino acid peptide insertion (Dalkara et al. 2013, Khabou et al. 2016).

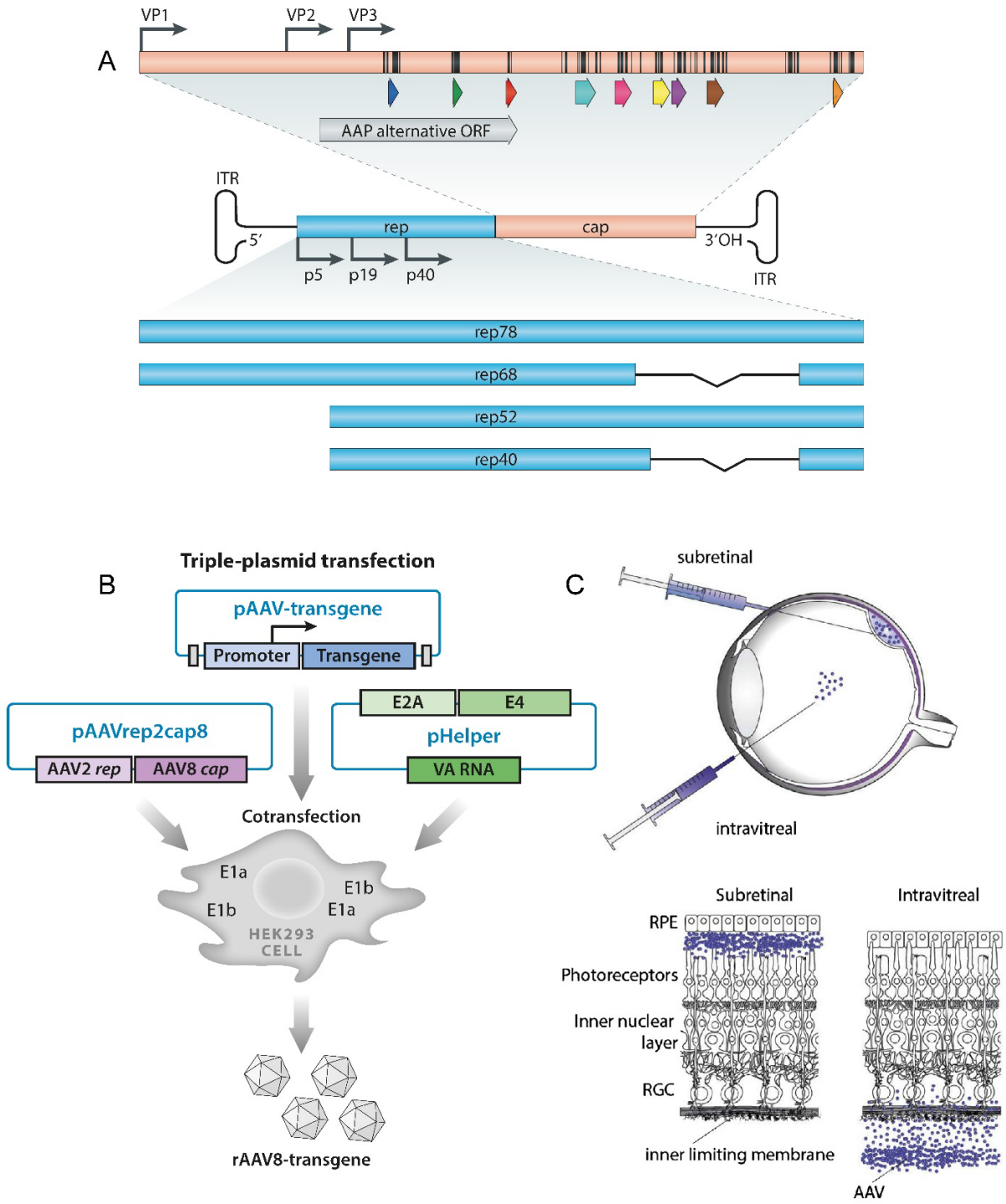

Figure 11. AAV biology and vector delivery routes. (A) The rep ORF encodes four non-structural proteins (rep78, rep68, rep52, rep40) needed for viral replication, transcriptional regulation, genome integration and virion assembly. The cap ORF encodes the structural proteins VP1, VP2 and VP3 and the assembly-activating protein (AAP, encoded by alternative ORF) that promotes capsid assembly (Sonntag et al. 2011). ORF: open reading frame. (B) rAAV production by triple-plasmid transfection. HEK293 cells (already expressing adenoviral genome fragments E1a/E1b) are co-transfected with a helper (pHelper, containing adenoviral helper genes E2A/E4/VA RNA), a rep/cap plasmid (pAAVrep2cap8) and the transgene plasmid (pAAV-transgene). (C) Schematic illustration of subretinal and intravitreal injections in the primate eye. RPE: retinal pigment epithelium, RGC: retinal ganglion cells. Adapted from (Dalkara et al. 2014, Kotterman et al. 2014, Samulski et al. 2014).

Gene therapy to treat retinal disorders is a major research topic, especially since the famous experiments with RPE65-associated Leber congenital amaurosis, an inherited congenital retinal dystrophy resulting in early vision loss. In these studies, an AAV serotype 2 expressing human RPE65 was injected subretinally to prove safety and efficacy (Bainbridge et al. 2008, Cideciyan et al. 2008, Maguire et al. 2008). Subsequent clinical studies confirmed these findings (Cideciyan 2010, Jacobson et al. 2012, Testa et al. 2013, Bainbridge et al. 2015, Weleber et al. 2016) and phase 3 (clinicaltrials.gov Identifier: NCT00999609) as well as phase 1 trials on optimized vectors are ongoing (NCT02781480).

For neovascular AMD, one of the earliest clinical trials using intraocular gene therapy involved intravitreal delivery of anti-angiogenic pigment epithelium-derived factor (PEDF) (NCT00109499). The phase I trial was generally safe but due to the lack of a randomized control group, no conclusions could be made regarding efficiency (Campochiaro et al. 2006).

Recent trials (NCT01024998, NCT01494805) used recombinant AAV2 expressing fms related tyrosine kinase 1 (sFLT1), a soluble form of VEGF receptor 1. sFLT1 is a potent antagonist of VEGF (Kendall et al. 1993) and it is important for photoreceptor avascular privilege (Luo et al. 2013). Studies in animals showed that AAV2-sFLT1 is well-tolerated and capable of long-term expression in cynomolgus monkeys (Maclachlan et al. 2011). In humans, both intravitreal (Heier et al. 2017) and subretinal (Rakoczy et al. 2015, Constable et al. 2016, Constable et al. 2017) delivery of AAV2-sFLT1 seemed to be safe. However, the results did not meet expectations in vision improvement, as both the control and gene therapy groups performed poor in terms of visual acuity (Constable et al. 2016, Moore et al. 2017) compared to standard anti-VEGF trials (MARINA (Rosenfeld et al. 2006) and ANCHOR (Brown et al. 2009)). Heier and colleagues suggested that pre-existing antibodies against AAV2 before treatment start may limit therapeutical benefit of intravitreal delivered AAV2-sFLT1 (Heier et al. 2017). However, more data to support this conclusion are needed. Recently, another anti-VEGF gene therapy approach has been initiated. This clinical trial uses an AAV8 vector expressing a monoclonal antibody fragment to bind and neutralize VEGF (NCT03066258).

In contrast to AAVs which have a limited packaging capacity (4.7 kilobases), lentiviral vectors have a larger capacity of up to 10 kilobases (Kumar et al. 2001). However, while recombinant AAVs mostly persist extra-chromosomally as episomes, lentiviruses integrate into the host genome with the potential for insertional mutagenesis (Kotterman et al. 2015, Moore et al. 2017). The only clinical trial using lentiviral vectors for visual disorders (Carvalho et al. 2015), NCT01301443, uses the non-primate-derived lentiviral Equine Infectious Anemia Virus (EIAV) vector (Mitrophanous et al. 1999, Wong et al. 2004) expressing endostatin and angiostatin (RetinoStat) to inhibit angiogenesis in advanced neovascular AMD. RetinoStat has been proven to be well-tolerated in non-human primates and rabbits (Binley et al. 2012). Although the clinical study demonstrated that subretinal injection of RetinoStat into humans is safe, data failed to prove a therapeutic benefit for the treatment of neovascular AMD (Campochiaro et al. 2017).

As outlined above, most AAV-based clinical trials have been initiated to treat neovascular AMD. For dry AMD, gene therapy is less advanced. Recently, a clinical trial using intravitreally delivered AAV2-sCD59 (AAVCAGsCD59, NCT03144999) has started. AAV2-sCD59 is believed to cause retinal cells to increase expression of a soluble form of CD59, which should inhibit the formation of the membrane attack complex, the final step of complement-mediated cell lysis (Cashman et al. 2011).

Future gene therapy approaches should consider combination therapies, use of improved vectors and targeting of broad antiangiogenic agents to further increase treatment success.

1.4 Mouse Models to Study Retinal Degeneration

To study retinal diseases, the choice of an adequate animal model is crucial. Due to the close evolutionary relationship, non-human primates would be best suited to study human diseases (Gwon 2008), but ethical and financial reasons as well as the available genetic tools favor the choice of mice as model organism.

1.4.1 Vision in mice

Similar to the human retina, the mouse retina is rod-dominant and consists of 97% rods and only 3% cones (Carter-Dawson et al. 1979). However, in contrast to humans and other higher primates, mice lack a cone-rich macula and have a low visual acuity (Prusky et al. 2004). Furthermore, mice are dichromats: they lack the L-opsin expressing cones (peak sensitivity to long wavelength, red light, see 1.1.2). However, the similarities (e.g. structure of the visual system) outnumber the differences (Huberman et al. 2011) and thus, the mouse has become the first choice for studying retinal degenerative diseases.

1.4.2 Models for induced retinal degeneration

Retinal degeneration is mostly studied by using genetically engineered mouse models (see 1.4.3) or by applying toxic stimuli. Photoreceptor damage can be induced by using chemical and physical stimuli, such as pharmacological agents (e.g. *N*-methyl-*N*-nitrosourea, MNU (Yuge et al. 1996, Nambu et al. 1997), digoxin (Hinshaw et al. 2016, Landfried et al. 2017)) or light exposure (Noell et al. 1966, Wenzel et al. 2005, Organisciak et al. 2010). Light is a natural stimulus that has been suggested to be a co-factor contributing to retinal diseases such as AMD (Taylor et al. 1990, Margrain et al. 2004). Upon light damage, photoreceptor apoptosis occurs in a relatively fast, synchronized process. The severity of damage can be modified by adjusting light intensities (Wenzel et al. 2005). The process of light-induced photoreceptor degeneration can be separated into four phases: induction, death signal transduction, execution and clearance (Wenzel et al. 2005). The peak of apoptosis is reached 36 hours after bright light exposure, and 10 days following light exposure almost no photoreceptors are left in the ONL (Wenzel et al. 2005). It has been shown that the process of light-induced retinal degeneration depends on the visual cycle and is mediated by

rhodopsin (Grimm et al. 2000). In addition to the described bright light exposure model, another model that uses continuous low light exposure and involves transducin-dependent apoptosis has been described (Hao et al. 2002).

1.4.3 Models for inherited retinal degeneration

Many genes that cause retinal degeneration have been identified (see section 1.4.4 and https://sph.uth.edu/retnet) and numerous mouse lines with naturally occurring mutations or genetically engineered mice have been described, e.g. retinal degeneration 1 (*rd1*), retinal degeneration 10 (*rd10*) and cone photoreceptor function loss 1 (*cpfl1*) (reviewed in (Chang et al. 2002, Samardzija et al. 2010)). Using these different models, researches aim to understand the particular genetic defect and its consequences. However, for non-monogenic diseases that have multifactorial causes such as AMD, generation of an appropriate mouse model is challenging.

1.4.4 Models for AMD

Although many mouse models for AMD exist, none can recapitulate all the different aspects of the disease (reviewed in (Rakoczy et al. 2006, Ramkumar et al. 2010, Pennesi et al. 2012)). Nevertheless, they help in understanding the pathological mechanisms and in developing treatment options.

Several mouse models have been described to study neovascular AMD including RAP (reviewed in (Grossniklaus et al. 2010)). In the model of laser-induced CNV, laser injury creates local breaks in the Bruch's membrane resulting in vessel recruitment from the choroid (Tobe et al. 1998b). In a transgenic mouse model with VEGF expression driven by the rhodopsin promoter (*rho/VEGF* mice), neovascularization originates in the deep plexus and extends into the photoreceptor layer/subretinal space, a phenotype that resembles RAP lesions (Okamoto et al. 1997, Tobe et al. 1998a, Ohno-Matsui et al. 2002). *Vldlr*$^{-/-}$ mice with a partial deletion of exon 5 of the very low density lipoprotein receptor (*Vldlr*) gene (Frykman et al. 1995) show a similar neovascular RAP-like phenotype due to increased VEGF levels (Heckenlively et al. 2003, Joyal et al. 2016).

To study non-vascular forms of macular degenerations, several models such as *Abcr*$^{-/-}$ (Weng et al. 1999) (Mata et al. 2000), *Elovl4*-mutant (Karan et al. 2005, Vasireddy et al. 2006) and *Timp3*$^{S156C/S156C}$ mice (Weber et al. 2002) are used, in which targeted genes were shown to play a key role in disease pathogenesis of AMD, Stargardt's disease and Sorsby's fundus dystrophy (an autosomal dominant, late-onset retinal dystrophy (Sorsby et al. 1949)), respectively. Certain murine models focus on the different pathways involved in pathology of dry AMD, e.g. inflammation and the complement pathway. In *Cfh*$^{-/-}$ mice with complement C3 accumulation, disorganized photoreceptor outer segments and RPE organelles were observed (Coffey et al. 2007). *Ccl2*$^{-/-}$ and *Ccr2*$^{-/-}$ mice that were generated to analyze the role of macrophage dysfunction were found to mimic some features of AMD (Ambati et al. 2003), including photoreceptor atrophy and accumulation of lipofuscin and

drusen-like deposits (later shown to be swollen macrophages (Luhmann et al. 2009)). Accumulation of microglia observed in *Cx3cr1*$^{-/-}$ mice has also been suggested to be a driving force in AMD (Combadiere et al. 2007). Increased levels of carboxyethylpyrrole (CEP)-adducted proteins in AMD patients (Crabb et al. 2002, Gu et al. 2003) and some features of AMD observed in CEP-immunized mice led to the hypothesis that oxidative damage could be an initiating event in AMD (Hollyfield et al. 2008, Hollyfield 2010). *Sod1*$^{-/-}$ mice with drusen-like deposits and thickening of Bruch's membrane (Imamura et al. 2006) and *Sod2* knockdown mice with RPE degeneration and atrophy of photoreceptors (Justilien et al. 2007) further underline the importance of oxidative stress in AMD disease development. Disturbances in cell metabolism were studied in *ApoE*$^{-/-}$ mice (Dithmar et al. 2000) and *APOE4/E2* transgenic mice on a high fat diet (Malek et al. 2005). Histological analyses showed thickening of Bruch's membrane, membrane-bound material and RPE changes. Additionally, hypoxia has been suggested to be involved in AMD pathogenesis (see 1.2.5), and a recent report shows degeneration of RPE cells in a chronic hypoxia-like model (Kurihara et al. 2016).

1.4.5 The all-cone *R91W;Nrl*$^{-/-}$ mouse

Wild-type mice have a rod-dominant retina (see 1.4.1; (Carter-Dawson et al. 1979)), which hinders the study of cone degeneration. In contrast, *Nrl*$^{-/-}$ knockout mice express only cone photoreceptors in their retinas (Mears et al. 2001). Neural retina leucine zipper (NRL) is a transcription factor required for rod photoreceptor development and plays an important role in rod homeostasis in the mature retina. In the absence of NRL, photoreceptor precursor cells follow the default pathway and become S-opsin expressing cones (Mears et al. 2001, Swaroop et al. 2010). However, disturbed cone layering with rosette formation in *Nrl*$^{-/-}$ mice impairs the analysis of cone degeneration. It has been shown that rosette formation in *Nrl*$^{-/-}$ is dependent on 11-*cis*-retinal (Wenzel et al. 2007, Kunchithapautham et al. 2009). However, combination of *Nrl*$^{-/-}$ and *Rpe65*$^{-/-}$ mice (RPE65 is essential for the regeneration of the visual chromophore 11-*cis*-retinal, see 1.1.4) results in *Rpe65*$^{-/-}$;*Nrl*$^{-/-}$ mice with complete chromophore absence and thus non-functional retinas (Feathers et al. 2008).

A mutation in *RPE65* (*RPE65*^{R91W}) has been identified in three consanguineous families with prevalent early-onset retinal dystrophy. Affected family members were homozygous for the mutation (Lorenz et al. 2000, El Matri et al. 2006). To model the disease and analyze the pathology, *Rpe65*^{R91W} knock-in mice were generated. In these mice, reduced amounts of the visual chromophore 11-*cis*-retinal and progressive loss of photoreceptor cells were observed (Samardzija et al. 2008). Under these conditions, rods and cones compete for 11-*cis*-retinal. Rods seem to take up the vast majority and consequently, cones suffer from chromophore deficiency. This leads to cone opsin mislocalization and cell death (Samardzija et al. 2009). Based on the hypothesis that reduced levels of 11-*cis*-retinal in *Rpe65*^{R91W} mice may still be high enough to support vision but prevent rosette formation, *Rpe65*^{R91W} mice were bred to *Nrl*$^{-/-}$ mice. Indeed, retinas of the resulting *Rpe65*^{R91W};*Nrl*$^{-/-}$ (*R91W;Nrl*$^{-/-}$) mice are functional and well-layered. Similar to *Nrl*$^{-/-}$ mice, *R91W;Nrl*$^{-/-}$ express predominantly blue-light sensitive S-cones (Mears et al. 2001, Samardzija et al. 2014). Retinas of

R91W;Nrl$^{-/-}$ mice are quite stable with only slow, age-related degeneration (Samardzija et al. 2014). Thus, *R91W;Nrl*$^{-/-}$ mice provide an ideal model to study cone-related mechanisms and cone degenerative diseases.

References

Age-Related Eye Disease Study Research G. (2001). A randomized, placebo-controlled, clinical trial of high-dose supplementation with vitamins C and E, beta carotene, and zinc for age-related macular degeneration and vision loss: AREDS report no. 8. *Arch Ophthalmol* **119**(10): 1417-1436.

Aiello L. P., Avery R. L., Arrigg P. G., Keyt B. A., Jampel H. D., Shah S. T., Pasquale L. R., Thieme H., Iwamoto M. A., Park J. E. and et al. (1994). Vascular endothelial growth factor in ocular fluid of patients with diabetic retinopathy and other retinal disorders. *N Engl J Med* **331**(22): 1480-1487.

Alberts B., Johnson A., Lewis J., Raff M., Roberts K. and Walter P. (2002). Molecular Biology of the Cell, Fourth Edition, Garland Science.

Ambati J., Anand A., Fernandez S., Sakurai E., Lynn B. C., Kuziel W. A., Rollins B. J. and Ambati B. K. (2003). An animal model of age-related macular degeneration in senescent Ccl-2- or Ccr-2-deficient mice. *Nat Med* **9**(11): 1390-1397.

Ames A., 3rd, Li Y. Y., Heher E. C. and Kimble C. R. (1992). Energy metabolism of rabbit retina as related to function: high cost of Na+ transport. *J Neurosci* **12**(3): 840-853.

Antonetti D. A., Klein R. and Gardner T. W. (2012). Diabetic retinopathy. *N Engl J Med* **366**(13): 1227-1239.

Arany Z., Huang L. E., Eckner R., Bhattacharya S., Jiang C., Goldberg M. A., Bunn H. F. and Livingston D. M. (1996). An essential role for p300/CBP in the cellular response to hypoxia. *Proc Natl Acad Sci U S A* **93**(23): 12969-12973.

Ardeljan D., Meyerle C. B., Agron E., Wang J. J., Mitchell P., Chew E. Y., Zhao J., Maminishkis A., Chan C. C. and Tuo J. (2013). Influence of TIMP3/SYN3 polymorphisms on the phenotypic presentation of age-related macular degeneration. *Eur J Hum Genet* **21**(10): 1152-1157.

Arjamaa O., Nikinmaa M., Salminen A. and Kaarniranta K. (2009). Regulatory role of HIF-1 a in the pathogenesis of age-related macular. *Ageing Research Reviews* **8**: 349-358.

Arshavsky V. Y., Lamb T. D. and Pugh E. N., Jr. (2002). G proteins and phototransduction. *Annu Rev Physiol* **64**: 153-187.

Baehr W., Wu S. M., Bird A. C. and Palczewski K. (2003). The retinoid cycle and retina disease. *Vision Res* **43**(28): 2957-2958.

Bainbridge J. W., Mehat M. S., Sundaram V., Robbie S. J., Barker S. E., Ripamonti C., Georgiadis A., Mowat F. M., Beattie S. G., Gardner P. J., Feathers K. L., Luong V. A., Yzer S., Balaggan K., Viswanathan A., de Ravel T. J., Casteels I., Holder G. E., Tyler N., Fitzke F. W., Weleber R. G., Nardini M., Moore A. T., Thompson D. A., Petersen-Jones S. M., Michaelides M., van den Born L. I., Stockman A., Smith A. J., Rubin G. and Ali R. R. (2015). Long-term effect of gene therapy on Leber's congenital amaurosis. *N Engl J Med* **372**(20): 1887-1897.

Bainbridge J. W., Smith A. J., Barker S. S., Robbie S., Henderson R., Balaggan K., Viswanathan A., Holder G. E., Stockman A., Tyler N., Petersen-Jones S., Bhattacharya S. S., Thrasher A. J., Fitzke F. W., Carter B. J., Rubin G. S., Moore A. T. and Ali R. R. (2008). Effect of gene therapy on visual function in Leber's congenital amaurosis. *N Engl J Med* **358**(21): 2231-2239.

Baylor D. A., Lamb T. D. and Yau K. W. (1979). Responses of retinal rods to single photons. *J Physiol* **288**: 613-634.

Berenberg T. L., Metelitsina T. I., Madow B., Dai Y., Ying G. S., Dupont J. C., Grunwald L., Brucker A. J. and Grunwald J. E. (2012). The association between drusen extent and foveolar choroidal blood flow in age-related macular degeneration. *Retina* **32**(1): 25-31.

Berg J. M., Tymoczko J. L. and Stryer L. (2002). Biochemistry, Fifth Edition, W.H. Freeman.

Bergmann M., Schutt F., Holz F. G. and Kopitz J. (2004). Inhibition of the ATP-driven proton pump in RPE lysosomes by the major lipofuscin fluorophore A2-E may contribute to the pathogenesis of age-related macular degeneration. *FASEB J* **18**(3): 562-564.

Binley K., Widdowson P. S., Kelleher M., de Belin J., Loader J., Ferrige G., Carlucci M., Esapa M., Chipchase D., Angell-Manning D., Ellis S., Mitrophanous K., Miskin J., Bantseev V., Nork T. M., Miller P. and Naylor S. (2012). Safety and biodistribution of an equine infectious anemia virus-based gene therapy, RetinoStat((R)), for age-related macular degeneration. *Hum Gene Ther* **23**(9): 980-991.

Bird A. C., Bressler N. M., Bressler S. B., Chisholm I. H., Coscas G., Davis M. D., de Jong P. T., Klaver C. C., Klein B. E., Klein R. and et al. (1995). An international classification and grading system for age-related maculopathy and age-related macular degeneration. The International ARM Epidemiological Study Group. *Surv Ophthalmol* **39**(5): 367-374.

Boltz A., Luksch A., Wimpissinger B., Maar N., Weigert G., Frantal S., Brannath W., Garhofer G., Ergun E., Stur M. and Schmetterer L. (2010). Choroidal blood flow and progression of age-related macular degeneration in the fellow eye in patients with unilateral choroidal neovascularization. *Invest Ophthalmol Vis Sci* **51**(8): 4220-4225.

Boye S. E., Boye S. L., Lewin A. S. and Hauswirth W. W. (2013). A comprehensive review of retinal gene therapy. *Mol Ther* **21**(3): 509-519.

Bressler N. M., Bressler S. B. and Fine S. L. (1988). Age-related macular degeneration. *Surv Ophthalmol* **32**(6): 375-413.

Brown D. M., Michels M., Kaiser P. K., Heier J. S., Sy J. P., Ianchulev T. and Group A. S. (2009). Ranibizumab versus verteporfin photodynamic therapy for neovascular age-related macular degeneration: Two-year results of the ANCHOR study. *Ophthalmology* **116**(1): 57-65 e55.

Buch H., Vinding T., La Cour M., Appleyard M., Jensen G. B. and Nielsen N. V. (2004). Prevalence and causes of visual impairment and blindness among 9980 Scandinavian adults: the Copenhagen City Eye Study. *Ophthalmology* **111**(1): 53-61.

Burns M. E. and Baylor D. A. (2001). Activation, deactivation, and adaptation in vertebrate photoreceptor cells. *Annu Rev Neurosci* **24**: 779-805.

Campochiaro P. A., Lauer A. K., Sohn E. H., Mir T. A., Naylor S., Anderton M. C., Kelleher M., Harrop R., Ellis S. and Mitrophanous K. A. (2017). Lentiviral Vector Gene Transfer of Endostatin/Angiostatin for Macular Degeneration (GEM) Study. *Hum Gene Ther* **28**(1): 99-111.

Campochiaro P. A., Nguyen Q. D., Shah S. M., Klein M. L., Holz E., Frank R. N., Saperstein D. A., Gupta A., Stout J. T., Macko J., DiBartolomeo R. and Wei L. L. (2006). Adenoviral vector-delivered pigment epithelium-derived factor for neovascular age-related macular degeneration: results of a phase I clinical trial. *Hum Gene Ther* **17**(2): 167-176.

Caprara C. and Grimm C. (2012). From oxygen to erythropoietin: relevance of hypoxia for retinal development, health and disease. *Prog Retin Eye Res* **31**(1): 89-119.

Caprara C., Thiersch M., Lange C., Joly S., Samardzija M. and Grimm C. (2011). HIF1A is essential for the development of the intermediate plexus of the retinal vasculature. *Invest Ophthalmol Vis Sci* **52**(5): 2109-2117.

Carmeliet P. (2003). Angiogenesis in health and disease. *Nat Med* **9**(6): 653-660.

Carter-Dawson L. D. and LaVail M. M. (1979). Rods and cones in the mouse retina. I. Structural analysis using light and electron microscopy. *J Comp Neurol* **188**(2): 245-262.

Carvalho L. S. and Vandenberghe L. H. (2015). Promising and delivering gene therapies for vision loss. *Vision Res* **111**(Pt B): 124-133.

Cashman S. M., Ramo K. and Kumar-Singh R. (2011). A non membrane-targeted human soluble CD59 attenuates choroidal neovascularization in a model of age related macular degeneration. *PLoS One* **6**(4): e19078.

Chakravarthy U., Biundo E., Saka R. O., Fasser C., Bourne R. and Little J. A. (2017). The Economic Impact of Blindness in Europe. *Ophthalmic Epidemiol* **24**(4): 239-247.

Chakravarthy U., Wong T. Y., Fletcher A., Piault E., Evans C., Zlateva G., Buggage R., Pleil A. and Mitchell P. (2010). Clinical risk factors for age-related macular degeneration: a systematic review and meta-analysis. *BMC Ophthalmol* **10**: 31.

Chan-Ling T., Gock B. and Stone J. (1995). The effect of oxygen on vasoformative cell division. Evidence that 'physiological hypoxia' is the stimulus for normal retinal vasculogenesis. *Invest Ophthalmol Vis Sci* **36**(7): 1201-1214.

Chang B., Hawes N. L., Hurd R. E., Davisson M. T., Nusinowitz S. and Heckenlively J. R. (2002). Retinal degeneration mutants in the mouse. *Vision Res* **42**(4): 517-525.

Chen W., Stambolian D., Edwards A. O., Branham K. E., Othman M., Jakobsdottir J., Tosakulwong N., Pericak-Vance M. A., Campochiaro P. A., Klein M. L., Tan P. L., Conley Y. P., Kanda A., Kopplin L., Li Y., Augustaitis K. J., Karoukis A. J., Scott W. K., Agarwal A., Kovach J. L., Schwartz S. G., Postel E. A., Brooks M., Baratz K. H., Brown W. L., Complications of Age-Related Macular Degeneration Prevention Trial Research G., Brucker A. J., Orlin A., Brown G., Ho A., Regillo C., Donoso L., Tian L., Kaderli B., Hadley D., Hagstrom S. A., Peachey N. S., Klein R., Klein B. E., Gotoh N., Yamashiro K., Ferris Iii F., Fagerness J. A., Reynolds R., Farrer L. A., Kim I. K., Miller J. W., Corton M., Carracedo A., Sanchez-Salorio M., Pugh E. W., Doheny K. F., Brion M., Deangelis M. M., Weeks D. E., Zack D. J., Chew E. Y., Heckenlively J. R., Yoshimura N., Iyengar S. K., Francis P. J., Katsanis N., Seddon J. M., Haines J. L., Gorin M. B., Abecasis G. R. and Swaroop A. (2010). Genetic variants near TIMP3 and high-density lipoprotein-associated loci influence susceptibility to age-related macular degeneration. *Proc Natl Acad Sci U S A* **107**(16): 7401-7406.

Cheung N., Mitchell P. and Wong T. Y. (2010). Diabetic retinopathy. *Lancet* **376**(9735): 124-136.

Cideciyan A. V. (2010). Leber congenital amaurosis due to RPE65 mutations and its treatment with gene therapy. *Prog Retin Eye Res* **29**(5): 398-427.

Cideciyan A. V., Aleman T. S., Boye S. L., Schwartz S. B., Kaushal S., Roman A. J., Pang J. J., Sumaroka A., Windsor E. A., Wilson J. M., Flotte T. R., Fishman G. A., Heon E., Stone E. M., Byrne B. J., Jacobson S. G. and Hauswirth W. W. (2008). Human gene therapy for RPE65 isomerase deficiency activates the retinoid cycle of vision but with slow rod kinetics. *Proc Natl Acad Sci U S A* **105**(39): 15112-15117.

Ciulla T. A., Harris A., Chung H. S., Danis R. P., Kagemann L., McNulty L., Pratt L. M. and Martin B. J. (1999). Color Doppler imaging discloses reduced ocular blood flow velocities in nonexudative age-related macular degeneration. *Am J Ophthalmol* **128**(1): 75-80.

Coffey P. J., Gias C., McDermott C. J., Lundh P., Pickering M. C., Sethi C., Bird A., Fitzke F. W., Maass A., Chen L. L., Holder G. E., Luthert P. J., Salt T. E., Moss S. E. and Greenwood J. (2007). Complement factor H deficiency in aged mice causes retinal abnormalities and visual dysfunction. *Proc Natl Acad Sci U S A* **104**(42): 16651-16656.

Cohen S. Y., Creuzot-Garcher C., Darmon J., Desmettre T., Korobelnik J. F., Levrat F., Quentel G., Palies S., Sanchez A., de Gendre A. S., Schluep H., Weber M. and Delcourt C. (2007). Types of choroidal neovascularisation in newly diagnosed exudative age-related macular degeneration. *Br J Ophthalmol* **91**(9): 1173-1176.

Coleman D. J., Silverman R. H., Rondeau M. J., Lloyd H. O., Khanifar A. A. and Chan R. V. (2013). Age-related macular degeneration: choroidal ischaemia? *Br J Ophthalmol* **97**(8): 1020-1023.

Combadiere C., Feumi C., Raoul W., Keller N., Rodero M., Pezard A., Lavalette S., Houssier M., Jonet L., Picard E., Debre P., Sirinyan M., Deterre P., Ferroukhi T., Cohen S. Y., Chauvaud D., Jeanny J. C., Chemtob S., Behar-Cohen F. and Sennlaub F. (2007). CX3CR1-dependent subretinal microglia cell accumulation is associated with cardinal features of age-related macular degeneration. *J Clin Invest* **117**(10): 2920-2928.

Constable I. J., Lai C. M., Magno A. L., French M. A., Barone S. B., Schwartz S. D., Blumenkranz M. S., Degli-Esposti M. A. and Rakoczy E. P. (2017). Gene Therapy in Neovascular Age-related Macular Degeneration: Three-Year Follow-up of a Phase 1 Randomized Dose Escalation Trial. *Am J Ophthalmol* **177**: 150-158.

Constable I. J., Pierce C. M., Lai C. M., Magno A. L., Degli-Esposti M. A., French M. A., McAllister I. L., Butler S., Barone S. B., Schwartz S. D., Blumenkranz M. S. and Rakoczy E. P. (2016). Phase 2a Randomized Clinical Trial: Safety and Post Hoc Analysis of Subretinal rAAV.sFLT-1 for Wet Age-related Macular Degeneration. *EBioMedicine* **14**: 168-175.

Crabb J. W., Miyagi M., Gu X., Shadrach K., West K. A., Sakaguchi H., Kamei M., Hasan A., Yan L., Rayborn M. E., Salomon R. G. and Hollyfield J. G. (2002). Drusen proteome analysis: an approach to the etiology of age-related macular degeneration. *Proc Natl Acad Sci U S A* **99**(23): 14682-14687.

Dalkara D., Byrne L. C., Klimczak R. R., Visel M., Yin L., Merigan W. H., Flannery J. G. and Schaffer D. V. (2013). In vivo-directed evolution of a new adeno-associated virus for therapeutic outer retinal gene delivery from the vitreous. *Sci Transl Med* **5**(189): 189ra176.

Dalkara D. and Sahel J. A. (2014). Gene therapy for inherited retinal degenerations. *C R Biol* **337**(3): 185-192.

Dallinger S., Findl O., Strenn K., Eichler H. G., Wolzt M. and Schmetterer L. (1998). Age dependence of choroidal blood flow. *J Am Geriatr Soc* **46**(4): 484-487.

Demircan N., Safran B. G., Soylu M., Ozcan A. A. and Sizmaz S. (2006). Determination of vitreous interleukin-1 (IL-1) and tumour necrosis factor (TNF) levels in proliferative diabetic retinopathy. *Eye* **20**(12): 1366-1369.

Deutch A. Y. (2013). Chapter 6 - Neurotransmitters A2 - Squire, Larry R. Fundamental Neuroscience (Fourth Edition). D. Berg, F. E. Bloom, S. d. Lac, A. Ghosh and N. C. Spitzer. San Diego, Academic Press**:** 117-138.

Dewan A., Liu M., Hartman S., Zhang S. S., Liu D. T., Zhao C., Tam P. O., Chan W. M., Lam D. S., Snyder M., Barnstable C., Pang C. P. and Hoh J. (2006). HTRA1 promoter polymorphism in wet age-related macular degeneration. *Science* **314**(5801): 989-992.

Dithmar S., Curcio C. A., Le N. A., Brown S. and Grossniklaus H. E. (2000). Ultrastructural changes in Bruch's membrane of apolipoprotein E-deficient mice. *Invest Ophthalmol Vis Sci* **41**(8): 2035-2042.

Dyer M. A. and Cepko C. L. (2001). Regulating proliferation during retinal development. *Nat Rev Neurosci* **2**(5): 333-342.

Edwards A. O., Ritter R., 3rd, Abel K. J., Manning A., Panhuysen C. and Farrer L. A. (2005). Complement factor H polymorphism and age-related macular degeneration. *Science* **308**(5720): 421-424.

El Matri L., Ambresin A., Schorderet D. F., Kawasaki A., Seeliger M. W., Wenzel A., Arsenijevic Y., Borruat F. X. and Munier F. L. (2006). Phenotype of three consanguineous Tunisian families with early-onset retinal degeneration caused by an R91W homozygous mutation in the RPE65 gene. *Graefes Arch Clin Exp Ophthalmol* **244**(9): 1104-1112.

Eldred G. E. (1995). Lipofuscin fluorophore inhibits lysosomal protein degradation and may cause early stages of macular degeneration. *Gerontology* **41 Suppl 2**: 15-28.

Ema M., Taya S., Yokotani N., Sogawa K., Matsuda Y. and Fujii-Kuriyama Y. (1997). A novel bHLH-PAS factor with close sequence similarity to hypoxia-inducible factor 1alpha regulates the VEGF expression and is potentially involved in lung and vascular development. *Proc Natl Acad Sci U S A* **94**(9): 4273-4278.

Enge M., Bjarnegard M., Gerhardt H., Gustafsson E., Kalen M., Asker N., Hammes H. P., Shani M., Fassler R. and Betsholtz C. (2002). Endothelium-specific platelet-derived growth factor-B ablation mimics diabetic retinopathy. *EMBO J* **21**(16): 4307-4316.

Epstein A. C., Gleadle J. M., McNeill L. A., Hewitson K. S., O'Rourke J., Mole D. R., Mukherji M., Metzen E., Wilson M. I., Dhanda A., Tian Y. M., Masson N., Hamilton D. L., Jaakkola P., Barstead R., Hodgkin J., Maxwell P. H., Pugh C. W., Schofield C. J. and Ratcliffe P. J. (2001). C. elegans EGL-9 and

mammalian homologs define a family of dioxygenases that regulate HIF by prolyl hydroxylation. *Cell* **107**(1): 43-54.

Euler T., Haverkamp S., Schubert T. and Baden T. (2014). Retinal bipolar cells: elementary building blocks of vision. *Nat Rev Neurosci* **15**(8): 507-519.

Feathers K. L., Lyubarsky A. L., Khan N. W., Teofilo K., Swaroop A., Williams D. S., Pugh E. N., Jr. and Thompson D. A. (2008). Nrl-knockout mice deficient in Rpe65 fail to synthesize 11-cis retinal and cone outer segments. *Invest Ophthalmol Vis Sci* **49**(3): 1126-1135.

Ferris F. L., 3rd, Fine S. L. and Hyman L. (1984). Age-related macular degeneration and blindness due to neovascular maculopathy. *Arch Ophthalmol* **102**(11): 1640-1642.

Ferris F. L., 3rd, Wilkinson C. P., Bird A., Chakravarthy U., Chew E., Csaky K., Sadda S. R. and Beckman Initiative for Macular Research Classification C. (2013). Clinical classification of age-related macular degeneration. *Ophthalmology* **120**(4): 844-851.

Flamme I., Frohlich T., von Reutern M., Kappel A., Damert A. and Risau W. (1997). HRF, a putative basic helix-loop-helix-PAS-domain transcription factor is closely related to hypoxia-inducible factor-1 alpha and developmentally expressed in blood vessels. *Mech Dev* **63**(1): 51-60.

Fritsche L. G., Igl W., Bailey J. N., Grassmann F., Sengupta S., Bragg-Gresham J. L., Burdon K. P., Hebbring S. J., Wen C., Gorski M., Kim I. K., Cho D., Zack D., Souied E., Scholl H. P., Bala E., Lee K. E., Hunter D. J., Sardell R. J., Mitchell P., Merriam J. E., Cipriani V., Hoffman J. D., Schick T., Lechanteur Y. T., Guymer R. H., Johnson M. P., Jiang Y., Stanton C. M., Buitendijk G. H., Zhan X., Kwong A. M., Boleda A., Brooks M., Gieser L., Ratnapriya R., Branham K. E., Foerster J. R., Heckenlively J. R., Othman M. I., Vote B. J., Liang H. H., Souzeau E., McAllister I. L., Isaacs T., Hall J., Lake S., Mackey D. A., Constable I. J., Craig J. E., Kitchner T. E., Yang Z., Su Z., Luo H., Chen D., Ouyang H., Flagg K., Lin D., Mao G., Ferreyra H., Stark K., von Strachwitz C. N., Wolf A., Brandl C., Rudolph G., Olden M., Morrison M. A., Morgan D. J., Schu M., Ahn J., Silvestri G., Tsironi E. E., Park K. H., Farrer L. A., Orlin A., Brucker A., Li M., Curcio C. A., Mohand-Said S., Sahel J. A., Audo I., Benchaboune M., Cree A. J., Rennie C. A., Goverdhan S. V., Grunin M., Hagbi-Levi S., Campochiaro P., Katsanis N., Holz F. G., Blond F., Blanche H., Deleuze J. F., Igo R. P., Jr., Truitt B., Peachey N. S., Meuer S. M., Myers C. E., Moore E. L., Klein R., Hauser M. A., Postel E. A., Courtenay M. D., Schwartz S. G., Kovach J. L., Scott W. K., Liew G., Tan A. G., Gopinath B., Merriam J. C., Smith R. T., Khan J. C., Shahid H., Moore A. T., McGrath J. A., Laux R., Brantley M. A., Jr., Agarwal A., Ersoy L., Caramoy A., Langmann T., Saksens N. T., de Jong E. K., Hoyng C. B., Cain M. S., Richardson A. J., Martin T. M., Blangero J., Weeks D. E., Dhillon B., van Duijn C. M., Doheny K. F., Romm J., Klaver C. C., Hayward C., Gorin M. B., Klein M. L., Baird P. N., den Hollander A. I., Fauser S., Yates J. R., Allikmets R., Wang J. J., Schaumberg D. A., Klein B. E., Hagstrom S. A., Chowers I., Lotery A. J., Leveillard T., Zhang K., Brilliant M. H., Hewitt A. W., Swaroop A., Chew E. Y., Pericak-Vance M. A., DeAngelis M., Stambolian D., Haines J. L., Iyengar S. K., Weber B. H., Abecasis G. R. and Heid I. M. (2016). A large genome-wide association study of age-related macular degeneration highlights contributions of rare and common variants. *Nat Genet* **48**(2): 134-143.

Fruttiger M. (2007). Development of the retinal vasculature. *Angiogenesis* **10**(2): 77-88.

Frykman P. K., Brown M. S., Yamamoto T., Goldstein J. L. and Herz J. (1995). Normal plasma lipoproteins and fertility in gene-targeted mice homozygous for a disruption in the gene encoding very low density lipoprotein receptor. *Proc Natl Acad Sci U S A* **92**(18): 8453-8457.

Garber K. (2015). RIKEN suspends first clinical trial involving induced pluripotent stem cells. *Nat Biotechnol* **33**(9): 890-891.

Ghosh K. K., Bujan S., Haverkamp S., Feigenspan A. and Wassle H. (2004). Types of bipolar cells in the mouse retina. *J Comp Neurol* **469**(1): 70-82.

Gilmore A. P. (2005). Anoikis. *Cell Death Differ* **12 Suppl 2**: 1473-1477.

Gold B., Merriam J. E., Zernant J., Hancox L. S., Taiber A. J., Gehrs K., Cramer K., Neel J., Bergeron J., Barile G. R., Smith R. T., Group A. M. D. G. C. S., Hageman G. S., Dean M. and Allikmets R. (2006). Variation in factor B (BF) and complement component 2 (C2) genes is associated with age-related macular degeneration. *Nat Genet* **38**(4): 458-462.

Goncalves M. A. (2005). Adeno-associated virus: from defective virus to effective vector. *Virol J* **2**: 43.

Gragoudas E. S., Adamis A. P., Cunningham E. T., Feinsod M., Guyer D. R. and Neova V. I. S. O. (2004). Pegaptanib for neovascular age-related macular degeneration. *New England Journal of Medicine* **351**(27): 2805-2816.

Graymore C. N., Tansley K. and Kerly M. (1959). Metabolism of the developing retina. 2. The effect of an inherited retinal degeneration on the development of glycolysis in the rat retina. *Biochem J* **72**: 459-461.

Green W. R. (1999). Histopathology of age-related macular degeneration. *Mol Vis* **5**: 27.

Grimm C., Wenzel A., Groszer M., Mayser H., Seeliger M., Samardzija M., Bauer C., Gassmann M. and Reme C. E. (2002). HIF-1-induced erythropoietin in the hypoxic retina protects against light-induced retinal degeneration. *Nat Med* **8**(7): 718-724.

Grimm C., Wenzel A., Hafezi F., Yu S., Redmond T. M. and Reme C. E. (2000). Protection of Rpe65-deficient mice identifies rhodopsin as a mediator of light-induced retinal degeneration. *Nature Genetics* **25**(1): 63-66.

Grossniklaus H. E., Kang S. J. and Berglin L. (2010). Animal models of choroidal and retinal neovascularization. *Prog Retin Eye Res* **29**(6): 500-519.

Grunwald J. E., Metelitsina T. I., Dupont J. C., Ying G. S. and Maguire M. G. (2005). Reduced foveolar choroidal blood flow in eyes with increasing AMD severity. *Invest Ophthalmol Vis Sci* **46**(3): 1033-1038.

Gu X., Meer S. G., Miyagi M., Rayborn M. E., Hollyfield J. G., Crabb J. W. and Salomon R. G. (2003). Carboxyethylpyrrole protein adducts and autoantibodies, biomarkers for age-related macular degeneration. *The Journal of biological chemistry* **278**: 42027-42035.

Gu Y. Z., Moran S. M., Hogenesch J. B., Wartman L. and Bradfield C. A. (1998). Molecular characterization and chromosomal localization of a third alpha-class hypoxia inducible factor subunit, HIF3alpha. *Gene Expr* **7**(3): 205-213.

Gwon A. (2008). Chapter 14 - The Primate in Cataract/IOL Surgery A2 - Tsonis, Panagiotis A. Animal Models in Eye Research. London, Academic Press**:** 205-208.

Hageman G. S., Anderson D. H., Johnson L. V., Hancox L. S., Taiber A. J., Hardisty L. I., Hageman J. L., Stockman H. A., Borchardt J. D., Gehrs K. M., Smith R. J., Silvestri G., Russell S. R., Klaver C. C., Barbazetto I., Chang S., Yannuzzi L. A., Barile G. R., Merriam J. C., Smith R. T., Olsh A. K., Bergeron J., Zernant J., Merriam J. E., Gold B., Dean M. and Allikmets R. (2005). A common haplotype in the complement regulatory gene factor H (HF1/CFH) predisposes individuals to age-related macular degeneration. *Proc Natl Acad Sci U S A* **102**(20): 7227-7232.

Haines J. L., Hauser M. A., Schmidt S., Scott W. K., Olson L. M., Gallins P., Spencer K. L., Kwan S. Y., Noureddine M., Gilbert J. R., Schnetz-Boutaud N., Agarwal A., Postel E. A. and Pericak-Vance M. A. (2005). Complement factor H variant increases the risk of age-related macular degeneration. *Science* **308**(5720): 419-421.

Hao W., Wenzel A., Obin M. S., Chen C. K., Brill E., Krasnoperova N. V., Eversole-Cire P., Kleyner Y., Taylor A., Simon M. I., Grimm C., Reme C. E. and Lem J. (2002). Evidence for two apoptotic pathways in light-induced retinal degeneration. *Nat Genet* **32**(2): 254-260.

Hartnett M. E., Weiter J. J., Staurenghi G. and Elsner A. E. (1996). Deep retinal vascular anomalous complexes in advanced age-related macular degeneration. *Ophthalmology* **103**(12): 2042-2053.

Heckenlively J. R., Hawes N. L., Friedlander M., Nusinowitz S., Hurd R., Davisson M. and Chang B. (2003). Mouse model of subretinal neovascularization with choroidal anastomosis. *Retina* **23**(4): 518-522.

Heidbreder M., Frohlich F., Johren O., Dendorfer A., Qadri F. and Dominiak P. (2003). Hypoxia rapidly activates HIF-3alpha mRNA expression. *FASEB J* **17**(11): 1541-1543.

Heier J. S., Brown D. M., Chong V., Korobelnik J. F., Kaiser P. K., Nguyen Q. D., Kirchhof B., Ho A., Ogura Y., Yancopoulos G. D., Stahl N., Vitti R., Berliner A. J., Soo Y., Anderesi M., Groetzbach G., Sommerauer B., Sandbrink R., Simader C., Schmidt-Erfurth U., View and Groups V. S. (2012). Intravitreal aflibercept (VEGF trap-eye) in wet age-related macular degeneration. *Ophthalmology* **119**(12): 2537-2548.

Heier J. S., Kherani S., Desai S., Dugel P., Kaushal S., Cheng S. H., Delacono C., Purvis A., Richards S., Le-Halpere A., Connelly J., Wadsworth S. C., Varona R., Buggage R., Scaria A. and Campochiaro P. A. (2017). Intravitreous injection of AAV2-sFLT01 in patients with advanced neovascular age-related macular degeneration: a phase 1, open-label trial. *Lancet* **390**(10089): 50-61.

Helmstaedter M., Briggman K. L., Turaga S. C., Jain V., Seung H. S. and Denk W. (2013). Connectomic reconstruction of the inner plexiform layer in the mouse retina. *Nature* **500**(7461): 168-174.

Hinshaw S. J., Ogbeifun O., Wandu W. S., Lyu C., Shi G., Li Y., Qian H. and Gery I. (2016). Digoxin Inhibits Induction of Experimental Autoimmune Uveitis in Mice, but Causes Severe Retinal Degeneration. *Invest Ophthalmol Vis Sci* **57**(3): 1441-1447.

Hirose K., Morita M., Ema M., Mimura J., Hamada H., Fujii H., Saijo Y., Gotoh O., Sogawa K. and Fujii-Kuriyama Y. (1996). cDNA cloning and tissue-specific expression of a novel basic helix-loop-helix/PAS factor (Arnt2) with close sequence similarity to the aryl hydrocarbon receptor nuclear translocator (Arnt). *Mol Cell Biol* **16**(4): 1706-1713.

Hogan M. J. and Alvarado J. (1967). Studies on the human macula. IV. Aging changes in Bruch's membrane. *Arch Ophthalmol* **77**(3): 410-420.

Hogenesch J. B., Gu Y. Z., Jain S. and Bradfield C. A. (1998). The basic-helix-loop-helix-PAS orphan MOP3 forms transcriptionally active complexes with circadian and hypoxia factors. *Proc Natl Acad Sci U S A* **95**(10): 5474-5479.

Hogenesch J. B., Gu Y. Z., Moran S. M., Shimomura K., Radcliffe L. A., Takahashi J. S. and Bradfield C. A. (2000). The basic helix-loop-helix-PAS protein MOP9 is a brain-specific heterodimeric partner of circadian and hypoxia factors. *J Neurosci* **20**(13): RC83.

Holash J., Davis S., Papadopoulos N., Croll S. D., Ho L., Russell M., Boland P., Leidich R., Hylton D., Burova E., Ioffe E., Huang T., Radziejewski C., Bailey K., Fandl J. P., Daly T., Wiegand S. J., Yancopoulos

G. D. and Rudge J. S. (2002). VEGF-Trap: a VEGF blocker with potent antitumor effects. *Proc Natl Acad Sci U S A* **99**(17): 11393-11398.

Hollyfield J. G. (2010). Age-related macular degeneration: the molecular link between oxidative damage, tissue-specific inflammation and outer retinal disease: the Proctor lecture. *Investigative ophthalmology & visual science* **51**: 1275-1281.

Hollyfield J. G., Bonilha V. L., Rayborn M. E., Yang X., Shadrach K. G., Lu L., Ufret R. L., Salomon R. G. and Perez V. L. (2008). Oxidative damage-induced inflammation initiates age-related macular degeneration. *Nature medicine* **14**: 194-198.

Hu C. J., Wang L. Y., Chodosh L. A., Keith B. and Simon M. C. (2003). Differential roles of hypoxia-inducible factor 1alpha (HIF-1alpha) and HIF-2alpha in hypoxic gene regulation. *Mol Cell Biol* **23**(24): 9361-9374.

Huberman A. D. and Niell C. M. (2011). What can mice tell us about how vision works? *Trends Neurosci* **34**(9): 464-473.

Ikeda M. and Nomura M. (1997). cDNA cloning and tissue-specific expression of a novel basic helix-loop-helix/PAS protein (BMAL1) and identification of alternatively spliced variants with alternative translation initiation site usage. *Biochem Biophys Res Commun* **233**(1): 258-264.

Imamura Y., Noda S., Hashizume K., Shinoda K., Yamaguchi M., Uchiyama S., Shimizu T., Mizushima Y., Shirasawa T. and Tsubota K. (2006). Drusen, choroidal neovascularization, and retinal pigment epithelium dysfunction in SOD1-deficient mice: a model of age-related macular degeneration. *Proc Natl Acad Sci U S A* **103**(30): 11282-11287.

Jacobson S. G., Cideciyan A. V., Ratnakaram R., Heon E., Schwartz S. B., Roman A. J., Peden M. C., Aleman T. S., Boye S. L., Sumaroka A., Conlon T. J., Calcedo R., Pang J. J., Erger K. E., Olivares M. B., Mullins C. L., Swider M., Kaushal S., Feuer W. J., Iannaccone A., Fishman G. A., Stone E. M., Byrne B. J. and Hauswirth W. W. (2012). Gene therapy for leber congenital amaurosis caused by RPE65 mutations: safety and efficacy in 15 children and adults followed up to 3 years. *Arch Ophthalmol* **130**(1): 9-24.

Jager R. D., Mieler W. F. and Miller J. W. (2008). Age-Related Macular Degeneration. *New England Journal of Medicine* **358**(24): 2606-2617.

Joyal J. S., Sun Y., Gantner M. L., Shao Z., Evans L. P., Saba N., Fredrick T., Burnim S., Kim J. S., Patel G., Juan A. M., Hurst C. G., Hatton C. J., Cui Z., Pierce K. A., Bherer P., Aguilar E., Powner M. B., Vevis K., Boisvert M., Fu Z., Levy E., Fruttiger M., Packard A., Rezende F. A., Maranda B., Sapieha P., Chen J., Friedlander M., Clish C. B. and Smith L. E. (2016). Retinal lipid and glucose metabolism dictates angiogenesis through the lipid sensor Ffar1. *Nat Med* **22**(4): 439-445.

Justilien V., Pang J. J., Renganathan K., Zhan X., Crabb J. W., Kim S. R., Sparrow J. R., Hauswirth W. W. and Lewin A. S. (2007). SOD2 knockdown mouse model of early AMD. *Invest Ophthalmol Vis Sci* **48**(10): 4407-4420.

Karan G., Lillo C., Yang Z., Cameron D. J., Locke K. G., Zhao Y., Thirumalaichary S., Li C., Birch D. G., Vollmer-Snarr H. R., Williams D. S. and Zhang K. (2005). Lipofuscin accumulation, abnormal electrophysiology, and photoreceptor degeneration in mutant ELOVL4 transgenic mice: a model for macular degeneration. *Proc Natl Acad Sci U S A* **102**(11): 4164-4169.

Karlstetter M., Scholz R., Rutar M., Wong W. T., Provis J. M. and Langmann T. (2015). Retinal microglia: just bystander or target for therapy? *Prog Retin Eye Res* **45**: 30-57.

Kast B., Schori C. and Grimm C. (2016). Hypoxic preconditioning protects photoreceptors against light damage independently of hypoxia inducible transcription factors in rods. *Exp Eye Res* **146**: 60-71.

Kawamura S. and Murakami M. (1989). Regulation of cGMP levels by guanylate cyclase in truncated frog rod outer segments. *J Gen Physiol* **94**(4): 649-668.

Kay C. N., Ryals R. C., Aslanidi G. V., Min S. H., Ruan Q., Sun J., Dyka F. M., Kasuga D., Ayala A. E., Van Vliet K., Agbandje-McKenna M., Hauswirth W. W., Boye S. L. and Boye S. E. (2013). Targeting photoreceptors via intravitreal delivery using novel, capsid-mutated AAV vectors. *PLoS One* **8**(4): e62097.

Keith B., Adelman D. M. and Simon M. C. (2001). Targeted mutation of the murine arylhydrocarbon receptor nuclear translocator 2 (Arnt2) gene reveals partial redundancy with Arnt. *Proc Natl Acad Sci U S A* **98**(12): 6692-6697.

Kendall R. L. and Thomas K. A. (1993). Inhibition of vascular endothelial cell growth factor activity by an endogenously encoded soluble receptor. *Proc Natl Acad Sci U S A* **90**(22): 10705-10709.

Kennedy C. J., Rakoczy P. E. and Constable I. J. (1995). Lipofuscin of the retinal pigment epithelium: a review. *Eye (Lond)* **9 (Pt 6)**: 763-771.

Kent D. L. (2014). Age-related macular degeneration: beyond anti-angiogenesis. *Mol Vis* **20**: 46-55.

Khabou H., Desrosiers M., Winckler C., Fouquet S., Auregan G., Bemelmans A. P., Sahel J. A. and Dalkara D. (2016). Insight into the mechanisms of enhanced retinal transduction by the engineered AAV2 capsid variant -7m8. *Biotechnol Bioeng* **113**(12): 2712-2724.

Kim J. H., Kim J. R., Kang S. W., Kim S. J. and Ha H. S. (2013). Thinner choroid and greater drusen extent in retinal angiomatous proliferation than in typical exudative age-related macular degeneration. *Am J Ophthalmol* **155**(4): 743-749, 749 e741-742.

Kirk E. C. and Kay R. F. (2004). The Evolution of High Visual Acuity in the Anthropoidea. Anthropoid Origins: New Visions. C. F. Ross and R. F. Kay. Boston, MA, Springer US**:** 539-602.

Kiser P. D., Golczak M., Maeda A. and Palczewski K. (2012). Key enzymes of the retinoid (visual) cycle in vertebrate retina. *Biochim Biophys Acta* **1821**(1): 137-151.

Kiser P. D., Golczak M. and Palczewski K. (2014). Chemistry of the Retinoid (Visual) Cycle. *Chemical Reviews* **114**(1): 194-232.

Klapper S. D., Swiersy A., Bamberg E. and Busskamp V. (2016). Biophysical Properties of Optogenetic Tools and Their Application for Vision Restoration Approaches. *Front Syst Neurosci* **10**: 74.

Klein R. and Klein B. E. (2010). Are individuals with diabetes seeing better?: a long-term epidemiological perspective. *Diabetes* **59**(8): 1853-1860.

Klein R., Klein B. E. and Cruickshanks K. J. (1999). The prevalence of age-related maculopathy by geographic region and ethnicity. *Prog Retin Eye Res* **18**(3): 371-389.

Klein R. J., Zeiss C., Chew E. Y., Tsai J. Y., Sackler R. S., Haynes C., Henning A. K., SanGiovanni J. P., Mane S. M., Mayne S. T., Bracken M. B., Ferris F. L., Ott J., Barnstable C. and Hoh J. (2005). Complement factor H polymorphism in age-related macular degeneration. *Science* **308**(5720): 385-389.

Koczot F. J., Carter B. J., Garon C. F. and Rose J. A. (1973). Self-complementarity of terminal sequences within plus or minus strands of adenovirus-associated virus DNA. *Proc Natl Acad Sci U S A* **70**(1): 215-219.

Kolb H. (2003). How the retina works. *American scientist* **91**(1): 28-35.

Kotterman M. A., Chalberg T. W. and Schaffer D. V. (2015). Viral Vectors for Gene Therapy: Translational and Clinical Outlook. *Annu Rev Biomed Eng* **17**: 63-89.

Kotterman M. A. and Schaffer D. V. (2014). Engineering adeno-associated viruses for clinical gene therapy. *Nat Rev Genet* **15**(7): 445-451.

Krock B. L., Skuli N. and Simon M. C. (2011). Hypoxia-induced angiogenesis: good and evil. *Genes Cancer* **2**(12): 1117-1133.

Kuffler S. W. (1953). Discharge patterns and functional organization of mammalian retina. *J Neurophysiol* **16**(1): 37-68.

Kuhn H. and Wilden U. (1987). Deactivation of photoactivated rhodopsin by rhodopsin-kinase and arrestin. *J Recept Res* **7**(1-4): 283-298.

Kumar M., Keller B., Makalou N. and Sutton R. E. (2001). Systematic determination of the packaging limit of lentiviral vectors. *Hum Gene Ther* **12**(15): 1893-1905.

Kunchithapautham K., Coughlin B., Crouch R. K. and Rohrer B. (2009). Cone outer segment morphology and cone function in the Rpe65-/- Nrl-/- mouse retina are amenable to retinoid replacement. *Invest Ophthalmol Vis Sci* **50**(10): 4858-4864.

Kur J., Newman E. A. and Chan-Ling T. (2012). Cellular and physiological mechanisms underlying blood flow regulation in the retina and choroid in health and disease. *Prog Retin Eye Res* **31**(5): 377-406.

Kurihara T., Kubota Y., Ozawa Y., Takubo K., Noda K., Simon M. C., Johnson R. S., Suematsu M., Tsubota K., Ishida S., Goda N., Suda T. and Okano H. (2010). von Hippel-Lindau protein regulates transition from the fetal to the adult circulatory system in retina. *Development* **137**(9): 1563-1571.

Kurihara T., Westenskow P. D., Gantner M. L., Usui Y., Schultz A., Bravo S., Aguilar E., Wittgrove C., Friedlander M. S., Paris L. P., Chew E., Siuzdak G. and Friedlander M. (2016). Hypoxia-induced metabolic stress in retinal pigment epithelial cells is sufficient to induce photoreceptor degeneration. *Elife* **5**.

Lam A. K., Chan S. T., Chan H. and Chan B. (2003). The effect of age on ocular blood supply determined by pulsatile ocular blood flow and color Doppler ultrasonography. *Optom Vis Sci* **80**(4): 305-311.

Lamb T. D. and Pugh E. N., Jr. (2004). Dark adaptation and the retinoid cycle of vision. *Prog Retin Eye Res* **23**(3): 307-380.

Landfried B., Samardzija M., Barben M., Schori C., Klee K., Storti F. and Grimm C. (2017). Digoxin-induced retinal degeneration depends on rhodopsin. *Cell Death Dis* **8**(3): e2670.

Lando D., Peet D. J., Gorman J. J., Whelan D. A., Whitelaw M. L. and Bruick R. K. (2002). FIH-1 is an asparaginyl hydroxylase enzyme that regulates the transcriptional activity of hypoxia-inducible factor. *Genes Dev* **16**(12): 1466-1471.

Lange C., Caprara C., Tanimoto N., Beck S., Huber G., Samardzija M., Seeliger M. and Grimm C. (2011). Retina-specific activation of a sustained hypoxia-like response leads to severe retinal degeneration and loss of vision. *Neurobiol Dis* **41**(1): 119-130.

Lashkari K., Hirose T., Yazdany J., McMeel J. W., Kazlauskas A. and Rahimi N. (2000). Vascular endothelial growth factor and hepatocyte growth factor levels are differentially elevated in patients with advanced retinopathy of prematurity. *Am J Pathol* **156**(4): 1337-1344.

Lewis G. P., Matsumoto B. and Fisher S. K. (1995). Changes in the organization and expression of cytoskeletal proteins during retinal degeneration induced by retinal detachment. *Invest Ophthalmol Vis Sci* **36**(12): 2404-2416.

Lim L. S., Mitchell P., Seddon J. M., Holz F. G. and Wong T. Y. (2012). Age-related macular degeneration. *Lancet* **379**(9827): 1728-1738.

Lisowski L., Tay S. S. and Alexander I. E. (2015). Adeno-associated virus serotypes for gene therapeutics. *Curr Opin Pharmacol* **24**: 59-67.

Loboda A., Jozkowicz A. and Dulak J. (2010). HIF-1 and HIF-2 transcription factors--similar but not identical. *Mol Cells* **29**(5): 435-442.

Lorenz B., Gyurus P., Preising M., Bremser D., Gu S., Andrassi M., Gerth C. and Gal A. (2000). Early-onset severe rod-cone dystrophy in young children with RPE65 mutations. *Invest Ophthalmol Vis Sci* **41**(9): 2735-2742.

Luhmann U. F., Robbie S., Munro P. M., Barker S. E., Duran Y., Luong V., Fitzke F. W., Bainbridge J. W., Ali R. R. and MacLaren R. E. (2009). The drusenlike phenotype in aging Ccl2-knockout mice is caused by an accelerated accumulation of swollen autofluorescent subretinal macrophages. *Invest Ophthalmol Vis Sci* **50**(12): 5934-5943.

Luo L., Uehara H., Zhang X., Das S. K., Olsen T., Holt D., Simonis J. M., Jackman K., Singh N., Miya T. R., Huang W., Ahmed F., Bastos-Carvalho A., Le Y. Z., Mamalis C., Chiodo V. A., Hauswirth W. W., Baffi J., Lacal P. M., Orecchia A., Ferrara N., Gao G., Young-Hee K., Fu Y., Owen L., Albuquerque R., Baehr W., Thomas K., Li D. Y., Chalam K. V., Shibuya M., Grisanti S., Wilson D. J., Ambati J. and Ambati B. K. (2013). Photoreceptor avascular privilege is shielded by soluble VEGF receptor-1. *Elife* **2**: e00324.

Maclachlan T. K., Lukason M., Collins M., Munger R., Isenberger E., Rogers C., Malatos S., Dufresne E., Morris J., Calcedo R., Veres G., Scaria A., Andrews L. and Wadsworth S. (2011). Preclinical safety evaluation of AAV2-sFLT01- a gene therapy for age-related macular degeneration. *Mol Ther* **19**(2): 326-334.

Maes C., Carmeliet G. and Schipani E. (2012). Hypoxia-driven pathways in bone development, regeneration and disease. *Nat Rev Rheumatol* **8**(6): 358-366.

Maguire A. M., Simonelli F., Pierce E. A., Pugh E. N., Jr., Mingozzi F., Bennicelli J., Banfi S., Marshall K. A., Testa F., Surace E. M., Rossi S., Lyubarsky A., Arruda V. R., Konkle B., Stone E., Sun J., Jacobs J., Dell'Osso L., Hertle R., Ma J. X., Redmond T. M., Zhu X., Hauck B., Zelenaia O., Shindler K. S., Maguire M. G., Wright J. F., Volpe N. J., McDonnell J. W., Auricchio A., High K. A. and Bennett J. (2008). Safety and efficacy of gene transfer for Leber's congenital amaurosis. *N Engl J Med* **358**(21): 2240-2248.

Maguire M. G., Martin D. F., Ying G. S., Jaffe G. J., Daniel E., Grunwald J. E., Toth C. A., Ferris F. L., 3rd and Fine S. L. (2016). Five-Year Outcomes with Anti-Vascular Endothelial Growth Factor Treatment of Neovascular Age-Related Macular Degeneration: The Comparison of Age-Related Macular Degeneration Treatments Trials. *Ophthalmology* **123**(8): 1751-1761.

Mahon P. C., Hirota K. and Semenza G. L. (2001). FIH-1: a novel protein that interacts with HIF-1alpha and VHL to mediate repression of HIF-1 transcriptional activity. *Genes Dev* **15**(20): 2675-2686.

Makino Y., Cao R., Svensson K., Bertilsson G., Asman M., Tanaka H., Cao Y., Berkenstam A. and Poellinger L. (2001). Inhibitory PAS domain protein is a negative regulator of hypoxia-inducible gene expression. *Nature* **414**(6863): 550-554.

Malek G., Johnson L. V., Mace B. E., Saloupis P., Schmechel D. E., Rickman D. W., Toth C. A., Sullivan P. M. and Bowes Rickman C. (2005). Apolipoprotein E allele-dependent pathogenesis: a model for age-related retinal degeneration. *Proc Natl Acad Sci U S A* **102**(33): 11900-11905.

Mandai M., Watanabe A., Kurimoto Y., Hirami Y., Morinaga C., Daimon T., Fujihara M., Akimaru H., Sakai N., Shibata Y., Terada M., Nomiya Y., Tanishima S., Nakamura M., Kamao H., Sugita S., Onishi A., Ito T., Fujita K., Kawamata S., Go M. J., Shinohara C., Hata K. I., Sawada M., Yamamoto M., Ohta S., Ohara Y., Yoshida K., Kuwahara J., Kitano Y., Amano N., Umekage M., Kitaoka F., Tanaka A., Okada C., Takasu N., Ogawa S., Yamanaka S. and Takahashi M. (2017). Autologous Induced Stem-Cell-Derived Retinal Cells for Macular Degeneration. *N Engl J Med* **376**(11): 1038-1046.

Margrain T. H., Boulton M., Marshall J. and Sliney D. H. (2004). Do blue light filters confer protection against age-related macular degeneration? *Prog Retin Eye Res* **23**(5): 523-531.

Massacesi A. L., Sacchi L., Bergamini F. and Bottoni F. (2008). The prevalence of retinal angiomatous proliferation in age-related macular degeneration with occult choroidal neovascularization. *Graefe's Archive for Clinical and Experimental Ophthalmology* **246**(1): 89-92.

Mata N. L., Radu R. A., Clemmons R. C. and Travis G. H. (2002). Isomerization and oxidation of vitamin a in cone-dominant retinas: a novel pathway for visual-pigment regeneration in daylight. *Neuron* **36**(1): 69-80.

Mata N. L., Weng J. and Travis G. H. (2000). Biosynthesis of a major lipofuscin fluorophore in mice and humans with ABCR-mediated retinal and macular degeneration. *Proc Natl Acad Sci U S A* **97**(13): 7154-7159.

McCarty D. M. (2008). Self-complementary AAV vectors; advances and applications. *Mol Ther* **16**(10): 1648-1656.

McNeill L. A., Hewitson K. S., Claridge T. D., Seibel J. F., Horsfall L. E. and Schofield C. J. (2002). Hypoxia-inducible factor asparaginyl hydroxylase (FIH-1) catalyses hydroxylation at the beta-carbon of asparagine-803. *Biochem J* **367**(Pt 3): 571-575.

Mears A. J., Kondo M., Swain P. K., Takada Y., Bush R. A., Saunders T. L., Sieving P. A. and Swaroop A. (2001). Nrl is required for rod photoreceptor development. *Nat Genet* **29**(4): 447-452.

Michaelides M., Kaines A., Hamilton R. D., Fraser-Bell S., Rajendram R., Quhill F., Boos C. J., Xing W., Egan C., Peto T., Bunce C., Leslie R. D. and Hykin P. G. (2010). A prospective randomized trial of intravitreal bevacizumab or laser therapy in the management of diabetic macular edema (BOLT study) 12-month data: report 2. *Ophthalmology* **117**(6): 1078-1086 e1072.

Mitrophanous K., Yoon S., Rohll J., Patil D., Wilkes F., Kim V., Kingsman S., Kingsman A. and Mazarakis N. (1999). Stable gene transfer to the nervous system using a non-primate lentiviral vector. *Gene Ther* **6**(11): 1808-1818.

Moiseyev G., Chen Y., Takahashi Y., Wu B. X. and Ma J. X. (2005). RPE65 is the isomerohydrolase in the retinoid visual cycle. *Proc Natl Acad Sci U S A* **102**(35): 12413-12418.

Moore N. A., Bracha P., Hussain R. M., Morral N. and Ciulla T. A. (2017). Gene therapy for age-related macular degeneration. *Expert Opin Biol Ther*: 1-10.

Mustafi D., Engel A. H. and Palczewski K. (2009). Structure of cone photoreceptors. *Prog Retin Eye Res* **28**(4): 289-302.

Nambu H., Yuge K., Nakajima M., Shikata N., Takahashi K., Miki H., Uyama M. and Tsubura A. (1997). Morphologic characteristics of N-methyl-N-nitrosourea-induced retinal degeneration in C57BL mice. *Pathol Int* **47**(6): 377-383.

Nathan D. M., Zinman B., Cleary P. A., Backlund J. Y., Genuth S., Miller R. and Orchard T. J. (2009). Modern-day clinical course of type 1 diabetes mellitus after 30 years' duration: the diabetes control and complications trial/epidemiology of diabetes interventions and complications and Pittsburgh epidemiology of diabetes complications experience (1983-2005). *Arch Intern Med* **169**(14): 1307-1316.

Nguyen Q. D., Shah S. M., Khwaja A. A., Channa R., Hatef E., Do D. V., Boyer D., Heier J. S., Abraham P., Thach A. B., Lit E. S., Foster B. S., Kruger E., Dugel P., Chang T., Das A., Ciulla T. A., Pollack J. S., Lim J. I., Eliott D., Campochiaro P. A. and Group R.-S. (2010). Two-year outcomes of the ranibizumab for edema of the mAcula in diabetes (READ-2) study. *Ophthalmology* **117**(11): 2146-2151.

Niven J. E. and Laughlin S. B. (2008). Energy limitation as a selective pressure on the evolution of sensory systems. *J Exp Biol* **211**(Pt 11): 1792-1804.

Noell W. K., Walker V. S., Kang B. S. and Berman S. (1966). Retinal damage by light in rats. *Invest Ophthalmol* **5**(5): 450-473.

Ohno-Matsui K., Hirose A., Yamamoto S., Saikia J., Okamoto N., Gehlbach P., Duh E. J., Hackett S., Chang M., Bok D., Zack D. J. and Campochiaro P. A. (2002). Inducible expression of vascular endothelial growth factor in adult mice causes severe proliferative retinopathy and retinal detachment. *Am J Pathol* **160**(2): 711-719.

Okabe K., Kobayashi S., Yamada T., Kurihara T., Tai-Nagara I., Miyamoto T., Mukouyama Y. S., Sato T. N., Suda T., Ema M. and Kubota Y. (2014). Neurons limit angiogenesis by titrating VEGF in retina. *Cell* **159**(3): 584-596.

Okamoto N., Tobe T., Hackett S. F., Ozaki H., Vinores M. A., LaRochelle W., Zack D. J. and Campochiaro P. A. (1997). Transgenic mice with increased expression of vascular endothelial growth factor in the retina: a new model of intraretinal and subretinal neovascularization. *Am J Pathol* **151**(1): 281-291.

Okawa H., Sampath A. P., Laughlin S. B. and Fain G. L. (2008). ATP consumption by mammalian rod photoreceptors in darkness and in light. *Curr Biol* **18**(24): 1917-1921.

Organisciak D. T. and Vaughan D. K. (2010). Retinal light damage: mechanisms and protection. *Prog Retin Eye Res* **29**(2): 113-134.

Papermaster D. S., Schneider B. G. and Besharse J. C. (1985). Vesicular transport of newly synthesized opsin from the Golgi apparatus toward the rod outer segment. Ultrastructural immunocytochemical and autoradiographic evidence in Xenopus retinas. *Invest Ophthalmol Vis Sci* **26**(10): 1386-1404.

Pascolini D. and Mariotti S. P. (2012). Global estimates of visual impairment: 2010. *Br J Ophthalmol* **96**(5): 614-618.

Patel S. A. and Simon M. C. (2008). Biology of hypoxia-inducible factor-2alpha in development and disease. *Cell Death Differ* **15**(4): 628-634.

Pennesi M. E., Neuringer M. and Courtney R. J. (2012). Animal models of age related macular degeneration. *Molecular Aspects of Medicine* **33**: 487-509.

Petrs-Silva H., Dinculescu A., Li Q., Deng W. T., Pang J. J., Min S. H., Chiodo V., Neeley A. W., Govindasamy L., Bennett A., Agbandje-McKenna M., Zhong L., Li B., Jayandharan G. R., Srivastava A., Lewin A. S. and Hauswirth W. W. (2011). Novel properties of tyrosine-mutant AAV2 vectors in the mouse retina. *Mol Ther* **19**(2): 293-301.

Pournaras C. J., Rungger-Brandle E., Riva C. E., Hardarson S. H. and Stefansson E. (2008). Regulation of retinal blood flow in health and disease. *Prog Retin Eye Res* **27**(3): 284-330.

Prusky G. T. and Douglas R. M. (2004). Characterization of mouse cortical spatial vision. *Vision Res* **44**(28): 3411-3418.

Purves D., Ed. (2012). Neuroscience. Sunderland, MA 01375 U.S.A, Sinauer Associates, Inc.

Rabinowitz J. E., Rolling F., Li C., Conrath H., Xiao W., Xiao X. and Samulski R. J. (2002). Cross-packaging of a single adeno-associated virus (AAV) type 2 vector genome into multiple AAV serotypes enables transduction with broad specificity. *J Virol* **76**(2): 791-801.

Rakoczy E. P., Lai C. M., Magno A. L., Wikstrom M. E., French M. A., Pierce C. M., Schwartz S. D., Blumenkranz M. S., Chalberg T. W., Degli-Esposti M. A. and Constable I. J. (2015). Gene therapy with recombinant adeno-associated vectors for neovascular age-related macular degeneration: 1 year follow-up of a phase 1 randomised clinical trial. *Lancet* **386**(10011): 2395-2403.

Rakoczy P. E., Yu M. J. T., Nusinowitz S., Chang B. and Heckenlively J. R. (2006). Mouse models of age-related macular degeneration. **82**: 741-752.

Ramkumar H. L., Zhang J. and Chan C. C. (2010). Retinal ultrastructure of murine models of dry age-related macular degeneration (AMD). *Prog Retin Eye Res* **29**(3): 169-190.

Ramrattan R. S., van der Schaft T. L., Mooy C. M., de Bruijn W. C., Mulder P. G. and de Jong P. T. (1994). Morphometric analysis of Bruch's membrane, the choriocapillaris, and the choroid in aging. *Invest Ophthalmol Vis Sci* **35**(6): 2857-2864.

Redmond T. M., Yu S., Lee E., Bok D., Hamasaki D., Chen N., Goletz P., Ma J. X., Crouch R. K. and Pfeifer K. (1998). Rpe65 is necessary for production of 11-cis-vitamin A in the retinal visual cycle. *Nat Genet* **20**(4): 344-351.

Reichenbach A. and Bringmann A. (2013). New functions of Muller cells. *Glia* **61**(5): 651-678.

Reid R. C. and Usrey W. M. (2013). Chapter 26 - Vision A2 - Squire, Larry R. Fundamental Neuroscience (Fourth Edition). D. Berg, F. E. Bloom, S. d. Lac, A. Ghosh and N. C. Spitzer. San Diego, Academic Press**:** 577-595.

Remsch H., Spraul C. W., Lang G. K. and Lang G. E. (2000). Changes of retinal capillary blood flow in age-related maculopathy. *Graefes Arch Clin Exp Ophthalmol* **238**(12): 960-964.

Reppert S. M. and Weaver D. R. (2001). Molecular analysis of mammalian circadian rhythms. *Annu Rev Physiol* **63**: 647-676.

Rivera A., Fisher S. A., Fritsche L. G., Keilhauer C. N., Lichtner P., Meitinger T. and Weber B. H. (2005). Hypothetical LOC387715 is a second major susceptibility gene for age-related macular degeneration, contributing independently of complement factor H to disease risk. *Hum Mol Genet* **14**(21): 3227-3236.

Roorda A. and Williams D. R. (1999). The arrangement of the three cone classes in the living human eye. *Nature* **397**(6719): 520-522.

Rosenfeld P. J., Brown D. M., Heier J. S., Boyer D. S., Kaiser P. K., Chung C. Y., Kim R. Y. and Group M. S. (2006). Ranibizumab for neovascular age-related macular degeneration. *N Engl J Med* **355**(14): 1419-1431.

Saint-Geniez M. and D'Amore P. A. (2004). Development and pathology of the hyaloid, choroidal and retinal vasculature. *Int J Dev Biol* **48**(8-9): 1045-1058.

Samardzija M., Caprara C., Heynen S. R., Willcox DeParis S., Meneau I., Traber G., Agca C., von Lintig J. and Grimm C. (2014). A mouse model for studying cone photoreceptor pathologies. *Invest Ophthalmol Vis Sci* **55**(8): 5304-5313.

Samardzija M., Neuhauss S. C. F., Joly S., Kurz-Levin M. and Grimm C. (2010). Animal Models for Retinal Degeneration. Animal Models for Retinal Diseases. I. H. Pang and A. F. Clark. Totowa, Humana Press Inc. **46:** 51-79.

Samardzija M., Tanimoto N., Kostic C., Beck S., Oberhauser V., Joly S., Thiersch M., Fahl E., Arsenijevic Y., von Lintig J., Wenzel A., Seeliger M. W. and Grimm C. (2009). In conditions of limited chromophore supply rods entrap 11-cis-retinal leading to loss of cone function and cell death. *Human Molecular Genetics* **18**(7): 1266-1275.

Samardzija M., von Lintig J., Tanimoto N., Oberhauser V., Thiersch M., Reme C. E., Seeliger M., Grimm C. and Wenzel A. (2008). R91W mutation in Rpe65 leads to milder early-onset retinal dystrophy due to the generation of low levels of 11-cis-retinal. *Hum Mol Genet* **17**(2): 281-292.

Samulski R. J. and Muzyczka N. (2014). AAV-Mediated Gene Therapy for Research and Therapeutic Purposes. *Annu Rev Virol* **1**(1): 427-451.

Sarks S. H. (1976). Ageing and degeneration in the macular region: a clinico-pathological study. *Br J Ophthalmol* **60**(5): 324-341.

Sarks S. H., Arnold J. J., Killingsworth M. C. and Sarks J. P. (1999). Early drusen formation in the normal and aging eye and their relation to age related maculopathy: a clinicopathological study. *Br J Ophthalmol* **83**(3): 358-368.

Schofield C. J. and Ratcliffe P. J. (2004). Oxygen sensing by HIF hydroxylases. *Nat Rev Mol Cell Biol* **5**(5): 343-354.

Scholl H. P., Strauss R. W., Singh M. S., Dalkara D., Roska B., Picaud S. and Sahel J. A. (2016). Emerging therapies for inherited retinal degeneration. *Sci Transl Med* **8**(368): 368rv366.

Schonthaler H. B., Lampert J. M., Isken A., Rinner O., Mader A., Gesemann M., Oberhauser V., Golczak M., Biehlmaier O., Palczewski K., Neuhauss S. C. and von Lintig J. (2007). Evidence for RPE65-independent vision in the cone-dominated zebrafish retina. *Eur J Neurosci* **26**(7): 1940-1949.

Schram M. T., Chaturvedi N., Schalkwijk C. G., Fuller J. H., Stehouwer C. D. A. and Complications E. P. (2003). Markers of inflammation are associated with microvascular complications and cardiovascular disease in Type 1 diabetes - the EURODIAB Prospective Complications study. *Diabetologia* **46**: A43-A43.

Schwartz S. D., Hubschman J. P., Heilwell G., Franco-Cardenas V., Pan C. K., Ostrick R. M., Mickunas E., Gay R., Klimanskaya I. and Lanza R. (2012). Embryonic stem cell trials for macular degeneration: a preliminary report. *Lancet* **379**(9817): 713-720.

Schwartz S. D., Regillo C. D., Lam B. L., Eliott D., Rosenfeld P. J., Gregori N. Z., Hubschman J. P., Davis J. L., Heilwell G., Spirn M., Maguire J., Gay R., Bateman J., Ostrick R. M., Morris D., Vincent M., Anglade E., Del Priore L. V. and Lanza R. (2015). Human embryonic stem cell-derived retinal pigment epithelium in patients with age-related macular degeneration and Stargardt's macular dystrophy: follow-up of two open-label phase 1/2 studies. *Lancet* **385**(9967): 509-516.

Schwartz S. D., Tan G., Hosseini H. and Nagiel A. (2016). Subretinal Transplantation of Embryonic Stem Cell-Derived Retinal Pigment Epithelium for the Treatment of Macular Degeneration: An Assessment at 4 Years. *Invest Ophthalmol Vis Sci* **57**(5): ORSFc1-9.

Semenza G. L. (2004). Hydroxylation of HIF-1: oxygen sensing at the molecular level. *Physiology (Bethesda)* **19**: 176-182.

Semenza G. L. (2011). Oxygen sensing, homeostasis, and disease. *N Engl J Med* **365**(6): 537-547.

Semenza G. L. and Wang G. L. (1992). A nuclear factor induced by hypoxia via de novo protein synthesis binds to the human erythropoietin gene enhancer at a site required for transcriptional activation. *Mol Cell Biol* **12**(12): 5447-5454.

Sengillo J. D., Justus S., Tsai Y. T., Cabral T. and Tsang S. H. (2016). Gene and cell-based therapies for inherited retinal disorders: An update. *Am J Med Genet C Semin Med Genet* **172**(4): 349-366.

Sheridan C. M., Pate S., Hiscott P., Wong D., Pattwell D. M. and Kent D. (2009). Expression of hypoxia-inducible factor-1alpha and -2alpha in human choroidal neovascular membranes. *Graefes Arch Clin Exp Ophthalmol* **247**(10): 1361-1367.

Shweiki D., Itin A., Soffer D. and Keshet E. (1992). Vascular endothelial growth factor induced by hypoxia may mediate hypoxia-initiated angiogenesis. *Nature* **359**(6398): 843-845.

Song W. K., Park K. M., Kim H. J., Lee J. H., Choi J., Chong S. Y., Shim S. H., Del Priore L. V. and Lanza R. (2015). Treatment of macular degeneration using embryonic stem cell-derived retinal pigment epithelium: preliminary results in Asian patients. *Stem Cell Reports* **4**(5): 860-872.

Sorsby A. and Mason M. E. (1949). A fundus dystrophy with unusual features. *Br J Ophthalmol* **33**(2): 67-97.

Spaide R. F. (2013). Clinical Manifestations of Choroidal Neovascularization in AMD. Age-related Macular Degeneration. F. G. Holz, D. Pauleikhoff, R. F. Spaide and A. C. Bird. Berlin, Heidelberg, Springer Berlin Heidelberg**:** 111-119.

Stahl A., Connor K. M., Sapieha P., Chen J., Dennison R. J., Krah N. M., Seaward M. R., Willett K. L., Aderman C. M., Guerin K. I., Hua J., Lofqvist C., Hellstrom A. and Smith L. E. (2010). The mouse retina as an angiogenesis model. *Invest Ophthalmol Vis Sci* **51**(6): 2813-2826.

Starita C., Hussain A. A., Pagliarini S. and Marshall J. (1996). Hydrodynamics of ageing Bruch's membrane: implications for macular disease. *Exp Eye Res* **62**(5): 565-572.

Stefánsson E., Geirsdóttir Á. and Sigurdsson H. (2011). Metabolic physiology in age related macular degeneration. *Progress in Retinal and Eye Research* **30**: 72-80.

Stone J., Itin A., Alon T., Pe'er J., Gnessin H., Chan-Ling T. and Keshet E. (1995). Development of retinal vasculature is mediated by hypoxia-induced vascular endothelial growth factor (VEGF) expression by neuroglia. *J Neurosci* **15**(7 Pt 1): 4738-4747.

Strauss O. (2005). The retinal pigment epithelium in visual function. *Physiol Rev* **85**(3): 845-881.

Sultan M. B., Zhou D., Loftus J., Dombi T., Ice K. S. and Macugen Study G. (2011). A phase 2/3, multicenter, randomized, double-masked, 2-year trial of pegaptanib sodium for the treatment of diabetic macular edema. *Ophthalmology* **118**(6): 1107-1118.

Sung C. H. and Chuang J. Z. (2010). The cell biology of vision. *J Cell Biol* **190**(6): 953-963.

Swaroop A., Chew E. Y., Rickman C. B. and Abecasis G. R. (2009). Unraveling a multifactorial late-onset disease: from genetic susceptibility to disease mechanisms for age-related macular degeneration. *Annu Rev Genomics Hum Genet* **10**: 19-43.

Swaroop A., Kim D. and Forrest D. (2010). Transcriptional regulation of photoreceptor development and homeostasis in the mammalian retina. *Nat Rev Neurosci* **11**(8): 563-576.

Szel A., Rohlich P., Caffe A. R., Juliusson B., Aguirre G. and Van Veen T. (1992). Unique topographic separation of two spectral classes of cones in the mouse retina. *J Comp Neurol* **325**(3): 327-342.

Takahashi K. and Yamanaka S. (2006). Induction of pluripotent stem cells from mouse embryonic and adult fibroblast cultures by defined factors. *Cell* **126**(4): 663-676.

Taylor H. R., Munoz B., West S., Bressler N. M., Bressler S. B. and Rosenthal F. S. (1990). Visible light and risk of age-related macular degeneration. *Trans Am Ophthalmol Soc* **88**: 163-173; discussion 173-168.

Testa F., Maguire A. M., Rossi S., Pierce E. A., Melillo P., Marshall K., Banfi S., Surace E. M., Sun J., Acerra C., Wright J. F., Wellman J., High K. A., Auricchio A., Bennett J. and Simonelli F. (2013). Three-year follow-up after unilateral subretinal delivery of adeno-associated virus in patients with Leber congenital Amaurosis type 2. *Ophthalmology* **120**(6): 1283-1291.

Thiersch M., Lange C., Joly S., Heynen S., Le Y. Z., Samardzija M. and Grimm C. (2009). Retinal neuroprotection by hypoxic preconditioning is independent of hypoxia-inducible factor-1 alpha expression in photoreceptors. *Eur J Neurosci* **29**(12): 2291-2302.

Thompson D. A., Gyurus P., Fleischer L. L., Bingham E. L., McHenry C. L., Apfelstedt-Sylla E., Zrenner E., Lorenz B., Richards J. E., Jacobson S. G., Sieving P. A. and Gal A. (2000). Genetics and phenotypes of RPE65 mutations in inherited retinal degeneration. *Invest Ophthalmol Vis Sci* **41**(13): 4293-4299.

Tian H., McKnight S. L. and Russell D. W. (1997). Endothelial PAS domain protein 1 (EPAS1), a transcription factor selectively expressed in endothelial cells. *Genes Dev* **11**(1): 72-82.

Tobe T., Okamoto N., Vinores M. A., Derevjanik N. L., Vinores S. A., Zack D. J. and Campochiaro P. A. (1998a). Evolution of neovascularization in mice with overexpression of vascular endothelial growth factor in photoreceptors. *Invest Ophthalmol Vis Sci* **39**(1): 180-188.

Tobe T., Ortega S., Luna J. D., Ozaki H., Okamoto N., Derevjanik N. L., Vinores S. A., Basilico C. and Campochiaro P. A. (1998b). Targeted disruption of the FGF2 gene does not prevent choroidal neovascularization in a murine model. *Am J Pathol* **153**(5): 1641-1646.

Travis G. H., Golczak M., Moise A. R. and Palczewski K. (2007). Diseases caused by defects in the visual cycle: retinoids as potential therapeutic agents. *Annu Rev Pharmacol Toxicol* **47**: 469-512.

Vasireddy V., Jablonski M. M., Mandal M. N., Raz-Prag D., Wang X. F., Nizol L., Iannaccone A., Musch D. C., Bush R. A., Salem N., Jr., Sieving P. A. and Ayyagari R. (2006). Elovl4 5-bp-deletion knock-in mice develop progressive photoreceptor degeneration. *Invest Ophthalmol Vis Sci* **47**(10): 4558-4568.

Vierkotten S., Muether P. S. and Fauser S. (2011). Overexpression of HTRA1 leads to ultrastructural changes in the elastic layer of Bruch's membrane via cleavage of extracellular matrix components. *PLoS One* **6**(8): e22959.

von Lintig J., Kiser P. D., Golczak M. and Palczewski K. (2010). The biochemical and structural basis for trans-to-cis isomerization of retinoids in the chemistry of vision. *Trends Biochem Sci* **35**(7): 400-410.

Wang G. L., Jiang B. H., Rue E. A. and Semenza G. L. (1995). Hypoxia-inducible factor 1 is a basic-helix-loop-helix-PAS heterodimer regulated by cellular O2 tension. *Proc Natl Acad Sci U S A* **92**(12): 5510-5514.

Wang J. S. and Kefalov V. J. (2011). The cone-specific visual cycle. *Prog Retin Eye Res* **30**(2): 115-128.

Warnecke C., Zaborowska Z., Kurreck J., Erdmann V. A., Frei U., Wiesener M. and Eckardt K. U. (2004). Differentiating the functional role of hypoxia-inducible factor (HIF)-1alpha and HIF-2alpha (EPAS-1) by the use of RNA interference: erythropoietin is a HIF-2alpha target gene in Hep3B and Kelly cells. *FASEB J* **18**(12): 1462-1464.

Wassle H., Puller C., Muller F. and Haverkamp S. (2009). Cone contacts, mosaics, and territories of bipolar cells in the mouse retina. *J Neurosci* **29**(1): 106-117.

Webb J. D., Coleman Æ. M. L. and Pugh C. W. (2009). Hypoxia, hypoxia-inducible factors (HIF), HIF hydroxylases and oxygen sensing. *Cell Mol Life Sci* **66**: 3539-3554.

Weber B. H., Lin B., White K., Kohler K., Soboleva G., Herterich S., Seeliger M. W., Jaissle G. B., Grimm C., Reme C., Wenzel A., Asan E. and Schrewe H. (2002). A mouse model for Sorsby fundus dystrophy. *Invest Ophthalmol Vis Sci* **43**(8): 2732-2740.

Weidemann A., Krohne T. U., Aguilar E., Kurihara T., Takeda N., Dorrell M. I., Simon M. C., Haase V. H., Friedlander M. and Johnson R. S. (2010). Astrocyte hypoxic response is essential for pathological but not developmental angiogenesis of the retina. *Glia* **58**(10): 1177-1185.

Weleber R. G., Pennesi M. E., Wilson D. J., Kaushal S., Erker L. R., Jensen L., McBride M. T., Flotte T. R., Humphries M., Calcedo R., Hauswirth W. W., Chulay J. D. and Stout J. T. (2016). Results at 2 Years after Gene Therapy for RPE65-Deficient Leber Congenital Amaurosis and Severe Early-Childhood-Onset Retinal Dystrophy. *Ophthalmology* **123**(7): 1606-1620.

Weng J., Mata N. L., Azarian S. M., Tzekov R. T., Birch D. G. and Travis G. H. (1999). Insights into the function of Rim protein in photoreceptors and etiology of Stargardt's disease from the phenotype in abcr knockout mice. *Cell* **98**(1): 13-23.

Wenzel A., Grimm C., Samardzija M. and Reme C. E. (2005). Molecular mechanisms of light-induced photoreceptor apoptosis and neuroprotection for retinal degeneration. *Prog Retin Eye Res* **24**(2): 275-306.

Wenzel A., von Lintig J., Oberhauser V., Tanimoto N., Grimm C. and Seeliger M. W. (2007). RPE65 is essential for the function of cone photoreceptors in NRL-deficient mice. *Invest Ophthalmol Vis Sci* **48**(2): 534-542.

Whitlock N. A., Agarwal N., Ma J. X. and Crosson C. E. (2005). Hsp27 upregulation by HIF-1 signaling offers protection against retinal ischemia in rats. *Invest Ophthalmol Vis Sci* **46**(3): 1092-1098.

Wiesener M. S., Jurgensen J. S., Rosenberger C., Scholze C. K., Horstrup J. H., Warnecke C., Mandriota S., Bechmann I., Frei U. A., Pugh C. W., Ratcliffe P. J., Bachmann S., Maxwell P. H. and Eckardt K. U. (2003). Widespread hypoxia-inducible expression of HIF-2alpha in distinct cell populations of different organs. *FASEB J* **17**(2): 271-273.

Wilden U., Hall S. W. and Kuhn H. (1986). Phosphodiesterase activation by photoexcited rhodopsin is quenched when rhodopsin is phosphorylated and binds the intrinsic 48-kDa protein of rod outer segments. *Proc Natl Acad Sci U S A* **83**(5): 1174-1178.

Wing G. L., Blanchard G. C. and Weiter J. J. (1978). The topography and age relationship of lipofuscin concentration in the retinal pigment epithelium. *Invest Ophthalmol Vis Sci* **17**(7): 601-607.

Wong L. F., Azzouz M., Walmsley L. E., Askham Z., Wilkes F. J., Mitrophanous K. A., Kingsman S. M. and Mazarakis N. D. (2004). Transduction patterns of pseudotyped lentiviral vectors in the nervous system. *Mol Ther* **9**(1): 101-111.

Wong W. L., Su X., Li X., Cheung C. M., Klein R., Cheng C. Y. and Wong T. Y. (2014). Global prevalence of age-related macular degeneration and disease burden projection for 2020 and 2040: a systematic review and meta-analysis. *Lancet Glob Health* **2**(2): e106-116.

Xu Y., Ola M. S., Berkich D. A., Gardner T. W., Barber A. J., Palmieri F., Hutson S. M. and LaNoue K. F. (2007). Energy sources for glutamate neurotransmission in the retina: absence of the aspartate/glutamate carrier produces reliance on glycolysis in glia. *J Neurochem* **101**(1): 120-131.

Yannuzzi L. A., Freund K. B. and Takahashi B. S. (2008). Review of retinal angiomatous proliferation or type 3 neovascularization. *Retina* **28**(3): 375-384.

Yannuzzi L. A., Negrao S., Iida T., Carvalho C., Rodriguez-Coleman H., Slakter J., Freund K. B., Sorenson J., Orlock D. and Borodoker N. (2001). Retinal angiomatous proliferation in age-related macular degeneration. *Retina* **21**(5): 416-434.

Yates J. R., Sepp T., Matharu B. K., Khan J. C., Thurlby D. A., Shahid H., Clayton D. G., Hayward C., Morgan J., Wright A. F., Armbrecht A. M., Dhillon B., Deary I. J., Redmond E., Bird A. C., Moore A. T. and Genetic Factors in A. M. D. S. G. (2007). Complement C3 variant and the risk of age-related macular degeneration. *N Engl J Med* **357**(6): 553-561.

Yuge K., Nambu H., Senzaki H., Nakao I., Miki H., Uyama M. and Tsubura A. (1996). N-methyl-N-nitrosourea-induced photoreceptor apoptosis in the mouse retina. *In Vivo* **10**(5): 483-488.

Zeng H. Y., Green W. R. and Tso M. O. (2008). Microglial activation in human diabetic retinopathy. *Arch Ophthalmol* **126**(2): 227-232.

Zhong L., Li B., Jayandharan G., Mah C. S., Govindasamy L., Agbandje-McKenna M., Herzog R. W., Weigel-Van Aken K. A., Hobbs J. A., Zolotukhin S., Muzyczka N. and Srivastava A. (2008a). Tyrosine-phosphorylation of AAV2 vectors and its consequences on viral intracellular trafficking and transgene expression. *Virology* **381**(2): 194-202.

Zhong L., Li B., Mah C. S., Govindasamy L., Agbandje-McKenna M., Cooper M., Herzog R. W., Zolotukhin I., Warrington K. H., Jr., Weigel-Van Aken K. A., Hobbs J. A., Zolotukhin S., Muzyczka N. and Srivastava A. (2008b). Next generation of adeno-associated virus 2 vectors: point mutations in tyrosines lead to high-efficiency transduction at lower doses. *Proc Natl Acad Sci U S A* **105**(22): 7827-7832.

Zhu Y., Zhang L. and Gidday J. M. (2013). Role of hypoxia-inducible factor-1alpha in preconditioning-induced protection of retinal ganglion cells in glaucoma. *Mol Vis* **19**: 2360-2372.

Zhu Y., Zhang Y., Ojwang B. A., Brantley M. A., Jr. and Gidday J. M. (2007). Long-term tolerance to retinal ischemia by repetitive hypoxic preconditioning: role of HIF-1alpha and heme oxygenase-1. *Invest Ophthalmol Vis Sci* **48**(4): 1735-1743.

2 AIMS OF THE THESIS

Patients suffering from cone degenerative diseases including age-related macular degeneration (AMD) lose the ability for central, high acuity vision. Despite the ongoing strong research efforts worldwide, our knowledge about the mechanisms leading to cone cell death is very limited – partially due to the lack of suitable animal models. *Rpe65^{R91W};Nrl$^{-/-}$* (*R91W;Nrl$^{-/-}$*) mice express only cone photoreceptors in a functional and well-layered retina and therefore provide a suitable model to investigate cone cell death (Samardzija et al. 2014). We used the all-cone *R91W;Nrl$^{-/-}$* mouse model to analyze the response of cones to hypoxia, an important feature of AMD. To further understand the underlying mechanisms of cone cell death, we analyzed retinal degenerative processes in *R91W;Nrl$^{-/-}$* mice which were exposed to damaging blue light.

I. The effects of a chronic hypoxia-like response on photoreceptors

Risk factors for cone degenerative diseases such as AMD are manifold and include age, gene mutations and environmental influences. Hypoxia activates regulatory systems in the body with hypoxia-inducible factors (HIFs) playing a central role (see 1.2.2). It has been shown previously that the knockdown of *Vhl* in rod photoreceptors (*OpsinCre;Vhl$^{f/f}$* = *rod$^{\Delta Vhl}$* mice) causes long-term HIF1A stabilization and slow, age-dependent retinal degeneration (Lange et al. 2011). Here, I employed the all-cone *R91W;Nrl$^{-/-}$* mice and aimed to specifically analyze the response of cones to hypoxia. To analyze the effect of a chronic activation of the molecular response to hypoxia, we generated mice lacking von Hippel Lindau (VHL) protein specifically in cones (*BPCre;R91W;Nrl$^{-/-}$;Vhl$^{f/f}$* = *cone$^{\Delta Vhl}$* mice).

- Characterization of *cone$^{\Delta Vhl}$* mice
  The main focus was to analyze all-cone mice with cone-specific *Vhl* ablation (*cone$^{\Delta Vhl}$*) and to investigate the influence of HIF1A on cone photoreceptors and retinal vasculature.

- Anti-*Hif1a* gene therapy in *rod$^{\Delta Vhl}$* mice
  We hypothesized that genetic inactivation of HIF1A could rescue the observed phenotype in *rod$^{\Delta Vhl}$* mice. Therefore, we tested a gene therapy approach using an AAV-mediated expression of an shRNA directed against *Hif1a* in photoreceptors.

II. Blue light-induced retinal degeneration in the all-cone *R91W;Nrl$^{-/-}$* mouse

Bright light exposure is a well-described model to induce degeneration in the rod-dominant wild-type mouse (Wenzel et al. 2005) and lifetime light exposure has been implicated as a co-factor in the etiology of AMD (Taylor et al. 1990, Margrain et al. 2004). Additionally, constant production of reactive oxygen species within photoreceptors upon light absorption may lead to substantial

molecular damage and microglia infiltration (Margrain et al. 2004, Joly et al. 2009). Due to the high resistance of cones to bright light-induced damage (Okano et al. 2012), we used blue light exposure as a model to study cone cell death in all-cone *R91W;Nrl*$^{-/-}$ mice. The aim of this part of the thesis was to analyze and compare mechanisms of retinal degeneration in all-cone *R91W;Nrl*$^{-/-}$ and rod-dominant wild-type (*129S6*) mice in response to toxic levels of blue light.

References

Joly S., Francke M., Ulbricht E., Beck S., Seeliger M., Hirrlinger P., Hirrlinger J., Lang K. S., Zinkernagel M., Odermatt B., Samardzija M., Reichenbach A., Grimm C. and Reme C. E. (2009). Cooperative phagocytes: resident microglia and bone marrow immigrants remove dead photoreceptors in retinal lesions. *Am J Pathol* **174**(6): 2310-2323.

Lange C., Heynen S. R., Tanimoto N., Thiersch M., Le Y. Z., Meneau I., Seeliger M. W., Samardzija M., Caprara C. and Grimm C. (2011). Normoxic activation of hypoxia-inducible factors in photoreceptors provides transient protection against light-induced retinal degeneration. *Invest Ophthalmol Vis Sci* **52**(8): 5872-5880.

Margrain T. H., Boulton M., Marshall J. and Sliney D. H. (2004). Do blue light filters confer protection against age-related macular degeneration? *Prog Retin Eye Res* **23**(5): 523-531.

Okano K., Maeda A., Chen Y., Chauhan V., Tang J., Palczewska G., Sakai T., Tsuneoka H., Palczewski K. and Maeda T. (2012). Retinal cone and rod photoreceptor cells exhibit differential susceptibility to light-induced damage. *J Neurochem* **121**(1): 146-156.

Samardzija M., Caprara C., Heynen S. R., Willcox DeParis S., Meneau I., Traber G., Agca C., von Lintig J. and Grimm C. (2014). A mouse model for studying cone photoreceptor pathologies. *Invest Ophthalmol Vis Sci* **55**(8): 5304-5313.

Taylor H. R., Munoz B., West S., Bressler N. M., Bressler S. B. and Rosenthal F. S. (1990). Visible light and risk of age-related macular degeneration. *Trans Am Ophthalmol Soc* **88**: 163-173; discussion 173-168.

Wenzel A., Grimm C., Samardzija M. and Reme C. E. (2005). Molecular mechanisms of light-induced photoreceptor apoptosis and neuroprotection for retinal degeneration. *Prog Retin Eye Res* **24**(2): 275-306.

3 RESULTS

3.1 Article 1: Targeting *Hif1a* rescues cone degeneration and prevents subretinal neovascularization in a model of chronic hypoxia

Maya Barben[1,2], Christian Schori[1,3], Marijana Samardzija[1,4] and Christian Grimm[1,2,3,4]

[1]Lab for Retinal Cell Biology, Dept. Ophthalmology, University Hospital Zurich, University of Zurich, Switzerland

[2]Neuroscience Center Zurich (ZNZ), University of Zurich, Switzerland

[3]Zurich Center for Integrative Human Physiology (ZIHP), University of Zurich, Switzerland

[4]Equal contribution

Status of the manuscript:

Submitted

Personal Contribution

Design and performance of research, data analysis and interpretation, manuscript writing.

Abstract

Degeneration of cone photoreceptors leads to loss of vision in patients suffering from age-related macular degeneration (AMD) and other cone dystrophies. Evidence implicates reduced tissue oxygenation in AMD pathology and suggests a role of the cellular response to hypoxia for disease onset and progression. To investigate the consequence of a chronic activation of the molecular response to hypoxia in cones, we ablated the von Hippel Lindau protein (VHL) specifically in cones of the all-cone *Rpe65*^{R91W}*;Nrl*$^{-/-}$ mouse. The resulting stabilization and activation of hypoxia-inducible factor 1A (HIF1A) led to increased expression of genes associated with hypoxia and retinal stress, as well as to severe cone degeneration and pathologic vessel growth, features that are central to AMD pathology. Additional deletion of *Hif1a* protected cone cells, prevented pathological vessel growth and preserved vision. Our results identify HIF1A as a potential therapeutic target to rescue hypoxia-related vision loss in patients.

Significance statement

Despite the identification of several risk factors for age-related macular degeneration (AMD), a therapy is still an unmet medical need. Chronic hypoxia has been postulated to be important in AMD etiology. It induces several cellular responses including the accumulation of hypoxia-inducible factors that control expression of a multitude of target genes. We demonstrate that a chronic hypoxia-like response triggered specifically in cone photoreceptors (*cone*$^{\Delta Vhl}$ mice) leads to severe cone degeneration and pathological vessel growth into the photoreceptor layer. The observed vision loss in *cone*$^{\Delta Vhl}$ mice is rescued by selective inactivation of *Hif1a* in *cone*$^{\Delta VhlHif1a}$ mice. Our findings provide evidence for a HIF1A-mediated mechanism and identify HIF1A as potential target for a therapeutic intervention in hypoxia-mediated cone degenerative diseases.

Introduction

Age-related macular degeneration (AMD) is the leading cause of visual impairment in the elderly population in industrialized nations (Klein et al. 1999, Buch et al. 2004, Wong et al. 2014). Due to the degeneration of photoreceptors in the cone-rich macula and/or the ingrowth of blood vessels, patients suffering from AMD lose central, high acuity vision (Green 1999, Swaroop et al. 2009, Spaide 2013). While there is no therapy available for geographic atrophy (dry AMD), the neovascular (wet) form of AMD is treated by vascular endothelial growth factor (VEGF)-targeting therapies to slow disease progression (Gragoudas et al. 2004, Rosenfeld et al. 2006, Maguire et al. 2016). Choroidal neovascularization (CNV) defines the classic form of neovascular AMD and is characterized by the ingrowth of blood vessels from the choroid to the subretinal space (Bressler et al. 1988, Spaide 2013). Retinal angiomatous proliferation (RAP) has been described as an additional, distinct form of neovascular AMD (Yannuzzi et al. 2001). In RAP, also known as deep retinal vascular anomalous complexes, vessels originate not from the choroid but from the deep retinal plexus in the inner retina and extend into the photoreceptor layer and the subretinal space (Hartnett et al. 1996, Yannuzzi et al. 2008).

AMD is a multifactorial disease. Besides genetic and environmental risk factors (Swaroop et al. 2009, Chakravarthy et al. 2010, Fritsche et al. 2016), tissue hypoxia and changes in retinal blood flow have been implicated in its etiology (Remsch et al. 2000, Arjamaa et al. 2009, Boltz et al. 2010, Stefánsson et al. 2011, Kent 2014). Oxygen supply to photoreceptors in the eyes of elderly people may be impaired due to an age-dependent reduction of choroidal blood flow (Dallinger et al. 1998, Lam et al. 2003) and accumulation of drusen (Grunwald et al. 2005). Choroidal ischemia in dry AMD (Ciulla et al. 1999, Coleman et al. 2013) and decreased choroidal blood volume in AMD (Berenberg et al. 2012) further support the hypothesis that hypoxia might be implicated in disease development and progression. The retina is considered as one of the most metabolically active tissues and is therefore highly vulnerable to changes in oxygen tension (Ames et al. 1992, Arjamaa et al. 2009). In conditions of reduced oxygen supply (hypoxia), molecular responses are activated with hypoxia-inducible factor 1 (HIF1) playing a key regulatory role for adapting the cell/tissue to the new condition. Heterodimeric HIF1 proteins are composed of an oxygen-labile α-subunit and a constitutively expressed β-subunit (Wang et al. 1995). Under normoxic conditions, HIF1A is hydroxylated by prolyl hydroxylase domain (PHD) proteins. This promotes the interaction with the von Hippel-Lindau (VHL) ubiquitin E3 ligase complex leading to ubiquitination and rapid degradation of hydroxylated HIF1A by proteasomes. Under hypoxic conditions, hydroxylation of HIF1A is reduced. Hence, HIF1A accumulates, enters the nucleus and drives transcription of a multitude of target genes (Jaakkola et al. 2001, Semenza 2004, Semenza 2011).

In this study, we investigated the consequences of a chronic hypoxia-like response triggered in cone photoreceptors to elucidate the mechanisms of cell death in cone degenerative diseases such as AMD. To this end, we used *Rpe65*^{R91W}*;Nrl*$^{-/-}$ (*R91W;Nrl*$^{-/-}$) double-mutant mice which express only

cone photoreceptors in a well-layered, functional retina (Samardzija et al. 2014). To induce the hypoxia-like response, we ablated the VHL protein specifically from cones using the Cre-loxP system. We analyzed the effects of the cone-specific activation of the hypoxic response and validated the contribution of HIF1A to the resulting retinal pathology.

Results

Cone-specific inactivation of Vhl increased HIF1A target gene expression and induced progressive cone degeneration

Photoreceptors in the all-cone *R91W;Nrl*$^{-/-}$ mouse are predominantly blue-light sensitive S-cones (Mears et al. 2001, Samardzija et al. 2014). Therefore, we used *BP-Cre* transgenic mice, which express functional *Cre* recombinase under the transcriptional control of the blue cone opsin promoter (BP, (Akimoto et al. 2004)) to delete floxed sequences from cones in the all-cone mice. *BPCre;R91W;Nrl*$^{-/-}$*;ZsGreen* reporter mice verified that *Cre* was almost exclusively active in the ONL and in the majority of cones, as green fluorescence was only occasionally detected in few cells of the inner retina (Figure 1A). We validated *Vhl* excision in the *BPCre;R91W;Nrl*$^{-/-}$*;Vhl*$^{f/f}$ (=*cone*$^{\Delta Vhl}$) mouse line by analyzing genomic DNA isolated from retinal tissues of 4-week-old *cone*$^{\Delta Vhl}$ mice. The detection of a PCR product corresponding to the excised fragment suggested a successful *Cre*-mediated deletion of *Vhl* in retinas of *cone*$^{\Delta Vhl}$ but not of *ctrl* mice (=*R91W;Nrl*$^{-/-}$*;Vhl*$^{f/f}$, Figure 1B). Genomic deletion of *Vhl* led to the accumulation of HIF1A protein (Figure 1C) and to increased transcript levels of known hypoxic target genes such as adrenomedullin (*Adm*), egl-9 family hypoxia-inducible factor 1 (*Egln1*, also known as *Phd2*), glucose transporter 1 (*Glut1*) and BCL2/adenovirus E1B 19-kDa interacting protein 3 (*Bnip3*) in normoxic *cone*$^{\Delta Vhl}$ mice (Figure 1D, Table 2 for details on statistics). This suggested that cells, presumably cones, activated a hypoxia-like response in retinas of *cone*$^{\Delta Vhl}$ mice.

We observed an age-dependent decline in HIF1A protein levels and hypoxia target gene expression in *cone*$^{\Delta Vhl}$ mice (Figure 1C, D). This prompted us to analyze retinal function and morphology. B-wave amplitudes and photopic ERGs were not significantly different between *cone*$^{\Delta Vhl}$ mice and *ctrl* mice at 6 weeks of age (Figure 2A). However, the amplitudes were strongly reduced in 12-week-old *cone*$^{\Delta Vhl}$ mice as compared to age-matched *ctrl* mice (Figure 2B, Table 2 for details on statistics). This indicated an age-dependent loss of function potentially due to retinal degeneration. Indeed, we observed severe, progressive thinning of the outer nuclear layer (ONL) in *cone*$^{\Delta Vhl}$ mice with most cones lost at 26 weeks of age (Figure 3A, B). Additionally, partial loss of the retinal pigment epithelium (RPE) and strong perturbations in the inner nuclear layer (INL) were detected in older *cone*$^{\Delta Vhl}$ mice (Figure 3A, 12we *cone*$^{\Delta Vhl}$). In contrast, the *ctrl* mice showed only a slow age-related ONL thinning, as reported for the parental *R91W;Nrl*$^{-/-}$ mouse line before (Samardzija et al. 2014).

To gain insight into cellular mechanisms leading to cone degeneration, we analyzed expression of specific genes during aging in *cone$^{\Delta Vhl}$* and *ctrl* mice (Figure 3C, Table 2 for details on statistics). Caspase 1 (*Casp1*), a gene involved in retinal degeneration, was upregulated in *cone$^{\Delta Vhl}$* mice at 8 weeks and peaked at 12 weeks of age. Expression of the stress signaling gene glial fibrillary acidic protein (*Gfap*) was upregulated in *cone$^{\Delta Vhl}$* mice already at 4 weeks and remained elevated throughout the observation period. Interestingly, we observed increased expression of tissue inhibitor of metalloproteinase 3 (*Timp3*) during the aging process, a gene associated with age-related macular degeneration (Vierkotten et al. 2011, Ardeljan et al. 2013). Similarly, expression of vascular endothelial growth factor (*Vegf*), a hypoxic response gene that is involved in neovascularization in wet AMD, was strongly increased in *cone$^{\Delta Vhl}$* mice at 4 and 6 weeks of age.

Subretinal neovascularization and vascular leakage in cone$^{\Delta Vhl}$ mice

Increased transcription of *Timp3* is potentially associated with a higher risk to develop neovascular AMD (Ardeljan et al. 2013) and hypoxia-regulated genes such as *Vegf* contribute to retinal and choroidal neovascularization (reviewed in (Campochiaro 2015)). Therefore, we analyzed the vascular network of *cone$^{\Delta Vhl}$* mice. All three vascular plexi were detected at 4 weeks of age (Figure 4A, B, C). However, we observed vessels extending from the deep plexus into the normally avascular ONL in central retinas of *cone$^{\Delta Vhl}$* mice (Figure 4A, arrowheads). Vessels reached the RPE but did not cross Bruch's membrane (Figure 4D, E), as we never observed retinal-choroidal anastomoses. This suggests that abnormal vessels originated from the retinal vasculature and not from the choroid. Interestingly, abnormal vessel growth was characteristic for the central but not for the peripheral retina (Figure 4B). To evaluate the integrity of retinal vessels we performed fluorescein angiography. Signs of leakage were observed in *cone$^{\Delta Vhl}$* mice (Figure 4F, G). Detailed analysis by immunofluorescent staining on retinal cross-sections revealed strong albumin (ALB) immunoreactivity in the ONL, RPE and inner plexiform layer (IPL) in *cone$^{\Delta Vhl}$* mice, as opposed to the signal detected in *ctrl* mice that was confined to retinal vessels. The choroid with its extensive vasculature was also strongly positive for ALB in both types of mice (Figure 4H, I). Microglia/macrophages detected by IBA1 staining were found within the photoreceptor and subretinal layer in *cone$^{\Delta Vhl}$* but not *ctrl* mice (Figure 4J, K).

Early vascular defects in cone$^{\Delta Vhl}$ mice

S-opsin expression starts shortly before birth in mice (Roberts et al. 2006, Swaroop et al. 2010) and we observed *Cre*-activity in *BPCre;R91W;Nrl$^{-/-}$;ZsGreen* reporter mice as early as at postnatal day (PND) 1 (data not shown). The primary plexus in mice develops along a central-to-peripheral gradient and reaches the periphery around PND8-10 (Fruttiger 2007). Vessels sprout from the primary plexus into the retina and turn laterally when they reach the outer and inner boundaries of the INL to first form the deep plexus and subsequently the intermediate plexus (Fruttiger 2007). To determine the onset of neovascularization in *cone$^{\Delta Vhl}$* mice we stained retinal flat mounts with

isolectin at PND7 and PND11. Using 3D-reconstruction of blood vessels, no difference in early vessel formation was detected between *cone$^{\Delta Vhl}$* and *ctrl* mice at PND7 (Figure 5A). However, at PND11, before formation of the intermediate plexus, vessels growing from the deep plexus into the ONL were observed in *cone$^{\Delta Vhl}$* mice (Figure 5B).

Formation of the deep plexus is preceded by *Vegf* expression in the INL (Stone et al. 1995). We analyzed gene expression levels in *cone$^{\Delta Vhl}$*, *ctrl* and *129S6* (*wt,* rod-dominant retina) mice to test for different regulation of genes involved in angiogenesis and vessel guidance during and after the process of vessel formation (PND7, 14 and 28, Figure 5C, Table 2 for details on statistics). *Vegf* mRNA was not elevated at PND7, slightly increased by 1.3-fold at PND14 and significantly increased at PND28 (2-fold) in *cone$^{\Delta Vhl}$* mice compared to controls. Fibroblast growth factor 2 (*Fgf2*), a potent angiogenic factor that has been shown to be involved in retinal stress (Baird et al. 1985, Joly et al. 2008, Lange et al. 2011a), was upregulated at PND28, at a time when developmental vascularization is completed. Recently, protective effects of semaphorin 3F (*Sema3f*) against subretinal neovascularization have been demonstrated (Sun et al. 2017). *Sema3f* gene expression levels in all-cone mice did not differ between *ctrl* and *cone$^{\Delta Vhl}$* mice (Figure 5C). Platelet derived growth factor, B polypeptide (*Pdgfb*) was upregulated in *cone$^{\Delta Vhl}$* mice at PND28 compared to *ctrl* and *wt* mice. *Pdgfb* expression by endothelial cells is essential for pericyte recruitment and is increased under hypoxia (Lindahl et al. 1997, Lindblom et al. 2003, Betsholtz 2004, Campochiaro 2013). Expression levels of von Willebrand factor (*vWf*), a marker for endothelial cells, was not increased and we did also not detect differences in expression of *Pdgfb* receptor (*Pdgfrb*).

HIF1 is responsible for pathological vessel growth and progressive cone degeneration in cone$^{\Delta Vhl}$ mice

We hypothesized that stabilized HIF1A, and not other *Vhl* targets, might promote retinal degeneration and neovascularization in *cone$^{\Delta Vhl}$* mice. Therefore, we additionally deleted *Hif1a* in cone photoreceptors (*BPCre;R91W;Nrl$^{-/-}$;Vhl$^{f/f}$;Hif1a$^{f/f}$=cone$^{\Delta VhlHif1a}$*). After we confirmed the presence of deletion alleles for both *Hif1a* and *Vhl* in genomic DNA of *cone$^{\Delta VhlHif1a}$* retinas (not shown) we determined retinal function. At 12 weeks of age, photopic ERG traces and b-wave amplitudes were similar in *cone$^{\Delta VhlHif1a}$* and *ctrl* (*R91W;Nrl$^{-/-}$;Vhl$^{f/f}$;Hif1a$^{f/f}$*) mice (Figure 6A, B) indicating no functional loss upon *Hif1a* inactivation in *cone$^{\Delta Vhl}$* mice. Similarly, retinal morphology (Figure 6C) and ONL thickness (Figure 6D) of *cone$^{\Delta VhlHif1a}$* mice was comparable to *ctrl* mice, whereas the thickness of the ONL in *cone$^{\Delta Vhl}$* mice was prominently reduced (same data as in Figure 3B) at 12 weeks of age.

Hif1a deletion also prevented pathological neovascularization into the ONL but had no effect on the developmental formation of the three vascular plexi (Figure 6E). No induction of the expression of hypoxic target genes such as *Adm*, *Egln1*, *Vegf* and *Timp3* were detected in *cone$^{\Delta VhlHif1a}$* mice, confirming that HIF1 was the responsible HIF isoform for regulating their expression in cones (Figure

6F). Altogether, these data indicate HIF1 as the causative factor for retinal degeneration and pathological vessel growth in *cone*$^{\Delta Vhl}$ mice.

Discussion

Previously, it has been demonstrated that the knockdown of *Vhl* in rod cells causes HIF1A stabilization under normoxic conditions (Lange et al. 2011b). Here, we particularly investigated the effects of a chronic hypoxia-like response in cone photoreceptors. We show that ablation of *Vhl* in cones resulted in a chronic hypoxia-like situation with accumulation of HIF1A and induction of HIF1A target genes. This led to pathological vessel growth into the photoreceptor layer, reduced retinal function and severe, progressive cone degeneration. These consequences resemble some of the features of AMD pathology, particularly of a subset of neovascular AMD known as RAP. In human patients, HIF1A and HIF2A were detected in macrophages and endothelial cells of neovascular membranes associated with AMD (Inoue et al. 2007). Additionally, the correlation of drusen density and decreased choroidal blood flow (Berenberg et al. 2012) as well as choroidal ischemia in AMD patients (Ciulla et al. 1999, Grunwald et al. 2005, Coleman et al. 2013) suggest reduced oxygen transport from the choroid to the inner retina (Kim et al. 2013). Therefore, tissue hypoxia and HIFs might play an important role in disease development and/or progression.

Expression of numerous genes involved in metabolism, stress, cell survival and angiogenesis was increased in *cone*$^{\Delta Vhl}$ mice (Figures 1D, 3C, 5C), as was *Timp3* (Figure 3C). TIMP3 is an important regulator of extracellular matrix (ECM) remodeling through inhibition of matrix metalloproteases and has been suggested to be a senescence-related protein (Kamei et al. 1999) that is potentially regulated by HIF2 in rods (Kast et al. 2016). Importantly, TIMP3 inhibits angiogenesis by interacting with VEGF (Qi et al. 2003) and is relevant for Bruch's membrane integrity (Kamei et al. 1999, Macgregor et al. 2009). Furthermore, mutations in *Timp3* have been associated with Sorsby's fundus dystrophy, an autosomal dominant maculopathy with submacular choroidal neovascularization (Weber et al. 1994, Lin et al. 2006). We can only speculate about the reasons for elevated *Timp3* during the aging process in *cone*$^{\Delta Vhl}$ mice but it seems plausible that retinas of *cone*$^{\Delta Vhl}$ mice require extensive ECM remodeling due to progressive cone degeneration (Figure 3).

We detected early and prominent vascular defects with abnormal vessel growth into the ONL, subretinal space and RPE layer in *cone*$^{\Delta Vhl}$ mice. Increased VEGF levels in transgenic mice expressing *Vegf* under the transcriptional control of the rhodopsin promoter (*rho/VEGF* mice) were shown to cause subretinal neovascularization (Okamoto et al. 1997, Ohno-Matsui et al. 2002, Ida et al. 2003). In our model, *Vegf* was not upregulated at PND14, at a time when vessels had already started growing into the ONL (Figure 5). However, transient *Vegf* expression in the INL regulates the formation of the deep plexus during development (Stone et al. 1995), i.e. already minor changes in the local *Vegf* concentration gradient, which are not detectable by RT-PCR, may misguide retinal

vessels in *cone*$^{\Delta Vhl}$ mice. To date, it remains unclear which pro-angiogenic factor(s) are responsible for the observed neovascularization. Nonetheless, our findings demonstrate that this is a *Hif1a*-mediated mechanism, as additional deletion of *Hif1a* fully rescued the vascular defects (Figure 6).

Interestingly, cone-specific deletion of *Hif1a* did not affect formation of the three vascular plexi (Figure 6E), while it has been shown that knockdown of *Hif1a* in most cells of the retinal periphery prevented formation of the intermediate plexus (Caprara et al. 2011). Thus, our results suggest that *Hif1a* expression in cones, as opposed to other cells presumably in the INL, is not essential for the development of the intermediate plexus.

Our data do not define whether cone degeneration in *cone*$^{\Delta Vhl}$ mice is due to the effects of the chronic intrinsic activation of the hypoxic response or to early development of vascular defects. Another mouse model shows, however, that a chronic hypoxia-like response in rods leads to slow photoreceptor degeneration in the absence of reported vascular defects (*rod*$^{\Delta Vhl}$ mice (Lange et al. 2011b)). This suggests that the long-term activation of HIF1 may reduce cell survival by an intrinsic mechanism. During hypoxia, HIF1 regulates mitochondrial respiration and thus metabolic adaptation towards glycolysis (Semenza 2007) leading to reduced energy (ATP) levels and potentially starvation. It has been shown that starvation of cones may lead to cone cell death (Punzo et al. 2009). Furthermore, it has been suggested that cones might be more sensitive to reduced oxygen and nutrient levels compared to rods, for reasons not fully understood (Punzo et al. 2012, Kurihara et al. 2016). This could possibly explain the progressive degeneration and the accelerated phenotype in *cone*$^{\Delta Vhl}$ compared to *rod*$^{\Delta Vhl}$ mice.

It might also be possible, however, that photoreceptor degeneration is secondary to the early pathological vascular defects. Inactivation of *Vhl* in the retinal periphery during development leads to vessel growth into the ONL and severe retinal degeneration (Kurihara et al. 2010, Lange et al. 2011a). Whereas the retinal periphery was strongly degenerated at 10 weeks of age, photoreceptor loss in the normal vascularized central retina was less pronounced (Lange et al. 2011a). We observed microglia activation and impaired function of the blood-retina-barrier in *cone*$^{\Delta Vhl}$ mice, as shown by IBA1 and ALB staining, respectively (Figure 4H-K). It seems likely that retinal hemorrhages exacerbate cone photoreceptor degeneration in our model, as suggested for other models (Zhao et al. 2011, Geiger et al. 2015). Photoreceptor degeneration was also observed in very low density lipoprotein receptor knockout mice (*Vldlr*$^{-/-}$; (Frykman et al. 1995)) where early retinal neovascularization causes vessels to extend from the deep plexus into the subretinal space (Heckenlively et al. 2003, Hu et al. 2008). Interestingly, it has been suggested that the *Vldlr*$^{-/-}$ phenotype is linked to HIF1A. Joyal and colleagues proposed that starved *Vldlr*$^{-/-}$ photoreceptors have reduced amounts of the Krebs cycle metabolite α-ketoglutarate, which decreases PHD activity and thus promotes stabilization of HIF1A. Consequently, *Vegf* is secreted, leading to RAP-like neovascularization (Joyal et al. 2016). We hypothesize that the combination of early vascular defects and the activation of a chronic hypoxia-like response, which affects expression of genes involved in

cellular metabolism and retinal stress, leads to the progressive cone degeneration observed in *cone*$^{\Delta Vhl}$ mice.

Our findings identify HIF1 in cones as the factor causing cone degeneration, pathological neovascularization and loss of function. Similarly, chronic activation of the hypoxic response in rods resulted in an HIF1- and age-dependent retinal degeneration (Barben et al., submitted). Whereas this provides strong evidence that activation of HIF1 in rod and cone photoreceptors leads to retinal degeneration, the activation of HIF2 but not of HIF1 is responsible for metabolic stress in RPE upon RPE-specific *Vhl* inactivation (Kurihara et al. 2016). Thus, our data and data published by others suggest cell type-specific roles for HIF1A and HIF2A in retinal pathology.

In conclusion, *cone*$^{\Delta Vhl}$ mice serve as a model to study HIF1A-mediated degeneration and angiogenesis. Additionally, evidence shows that HIF1A can be safely inactivated in cones (see above), rods (Kast et al., 2016; Barben et al, submitted) and RPE (Kurihara et al. 2016) suggesting that targeting HIF transcription factors in photoreceptors and RPE may provide a potential therapeutic approach to rescue hypoxia-mediated retinal degeneration in patients and an alternative to anti-VEGF agents.

Material and Methods

Mice

All experimental procedures were performed according to 'The Association for Research in Vision and Ophthalmology' statement on animal use in ophthalmic and vision research and the regulation of the veterinary authorities of Zurich, Switzerland. *Rpe65^{R91W};Nrl$^{-/-}$* mice were generated by crossing *Rpe65^{R91W}* (Samardzija et al. 2008) to *Nrl$^{-/-}$* mice (Mears et al. 2001), and were described recently (Samardzija et al. 2014). *BPCre;R91W;Nrl$^{-/-}$;Vhl$^{f/f}$* (=*cone$^{\Delta Vhl}$*) mice were generated by breeding *Rpe65^{R91W};Nrl$^{-/-}$* mice to *Vhl$^{f/f}$* mice (Haase et al. 2001) and mice expressing the *Cre* recombinase under the transcriptional control of the blue cone opsin (BP) promoter (Akimoto et al. 2004). To generate *BPCre;R91W;Nrl$^{-/-}$;Vhl$^{f/f}$;Hif1a$^{f/f}$* (=*cone$^{\Delta VhlHif1a}$*) mice, *BPCre;R91W;Nrl$^{-/-}$;Vhl$^{f/f}$* were bred to *Hif1a$^{f/f}$* mice (Ryan et al. 2000). *R91W;Nrl$^{-/-}$;Vhl$^{f/f}$* and *R91W;Nrl$^{-/-}$;Vhl$^{f/f}$;Hif1a$^{f/f}$* littermates without *Cre* recombinase served as respective control mice (=*ctrl*). Genotyping was performed by PCR using DNA isolated from ear clips and primer pairs as described previously (Lange et al. 2011b, Kast et al. 2016). Presence of *BPCre* was tested using the following primer pair: forward (5'-GGACATGTTCAGGGATCGCCAGGCG-3') and reverse (5'-GCATAACCAGTGAAACAGCATTGCTG-3'). The amplification reaction resulted in a 268 bp fragment in the presence of the transgene. To test for deletion of floxed sequences, genomic DNA was isolated from retinal tissues and tested by PCR using appropriate primer pairs as described (Lange et al. 2011b, Kast et al. 2016). *129S6* (Taconic, Ejby, Denmark) mice were used as wild-type controls. To test expression of the *Cre* recombinase *BPCre;R91W;Nrl$^{-/-}$* mice were bred to a ZsGreen reporter line (*Ai6* mice, *Gt(ROSA)26Sor$^{tm6(CAG-ZsGreen1)Hze}$*, (Madisen et al. 2010)). Mice of both sexes were used for experiments and were housed at the animal facility of the University Zurich under a 14 h : 10 h light/dark cycle with lights on at 6 am and lights off at 8 pm. Food and water was provided *ad libitum*.

Morphology/quantification

To evaluate retinal morphology, eyes were enucleated and fixed in 2.5% glutaraldehyde in cacodylate buffer (pH 7.2, 0.1 M), according to the previously described procedure (Heynen et al. 2011). By cutting through the optic nerve head, nasal and temporal halves of the eyecups were separated and embedded in epon plastic. Semi-thin cross sections (0.5 µm) were counterstained with toluidine blue and analyzed by light microscopy (Axioplan; Zeiss, Jena, Germany). Thickness of the outer nuclear layer was measured at indicated distances from the optic nerve head using the Adobe Photoshop CS6 ruler tool (Adobe Systems, Inc., San Jose, CA, USA) on reconstructed retinal panorama images.

Immunofluorescence

After euthanasia, eyes were marked nasally, enucleated and fixed in 4% paraformaldehyde (PFA) in phosphate buffer for 1 h at 4°C. Cornea and lens were removed and the dissected eyecups postfixed for 2 h in 4% PFA. After immersion in 30% sucrose (in PBS 0.1 M) the eyecups were embedded in tissue freezing medium (O.C.T., Leica Biosystems Nussloch GmbH, Nussloch, Germany), frozen in a 2-methylbutane bath cooled by liquid nitrogen and stored at -80°C. Cryosections (12 µm) were blocked (3% normal goat serum (Sigma-Aldrich, St. Louis, MO, USA), 0.3% Triton X-100 (Sigma) in PBS) and incubated with the following primary antibodies overnight at 4°C: Isolectin GS-IB_4-Alexa594 from *Griffonia simplicifolia* (1:300, I21413; Thermo Fisher Scientific, Waltham, MA, USA), rabbit anti-allograft inflammatory factor 1 (alias IBA1, 1:1000, 019-19741; Wako, Neuss, Germany), rabbit anti-albumin (ALB, 1:500, RARaAlb; Nordic Immunology, Tilburg, Netherlands). Sections were washed with PBS, incubated with secondary antibodies (Cy3-labeled, Jackson ImmunoResearch Laboratories, Westgrove, PA, USA) for 1 h at room temperature (RT), counterstained with DAPI (4',6-Diamidine-2'-phenylindole dihydrochloride, Roche, Basel, Switzerland) and analyzed by fluorescence microscopy (Axioplan; Zeiss).

Analysis of retinal vasculature in whole mounted retinas

Eyes were isolated and incubated for 5 to 10 minutes in 2% PFA in PBS as described recently (Caprara et al. 2011). After removal of cornea and lens, the retina was dissected and flat-mounted in PBS. After postfixation in 4% PFA for 1 h at RT, flat-mounts were blocked (3% normal goat serum, 0.3% Triton X-100 in PBS, 1 h) and incubated with isolectin GS-IB_4-Alexa594 (1:300, Thermo Fisher Scientific) at 4°C overnight. Retinas were washed in PBS, mounted on glass slides and analyzed by fluorescence microscopy (Axioplan/ApoTome; Zeiss). Blood vessels were reconstructed in three dimensions using Imaris software (Versions 7.7.2/8.3.0, Bitplane AG, Zurich, Switzerland). For better recognition and distinction of the vascular plexi, the z-value of the z-stacks was increased five times.

RNA isolation and semi-quantitative real-time PCR

Retinas were isolated through a slit in the cornea, frozen in liquid nitrogen and stored at -80°C. RNA was extracted using an RNA isolation kit (RNeasy; Qiagen, Hilden, Germany) including a DNAse treatment. 1 µg of RNA, oligo (dT) and M-MLV reverse transcriptase (Promega, Fitchburg, WI, USA) were used to prepare cDNA. To analyze gene expression by real-time PCR, 10 ng of cDNA template was amplified using a PCR polymerase ready mix (LightCycler 480 SYBR Green I Master, Roche Diagnostics, Rotkreuz, Switzerland), specific primer pairs (Table 1) and a thermocycler (LightCycler 480, Roche Diagnostics). Expression levels were normalized to β-actin (*Actb*) and relative expression was calculated using the comparative threshold cycle method ($\Delta\Delta C_T$) of the LightCycler480 software (Roche Diagnostics). At least 3 mice per strain and time point were used.

Protein isolation and Western blotting

Proteins were isolated by homogenizing the retinas in ice-cold Tris-HCl (100 mM, pH 7.5) using ultrasound at 4°C. Protein concentrations were determined spectrophotometrically by using Bradford reagent (Bio-Rad, Hercules, CA, USA). SDS-PAGE and Western blotting were performed as described (Heynen et al. 2011) and proteins detected by rabbit anti-HIF1A (1:2000, NB100-479, Novus Biologicals, Littleton, CO, USA) and mouse anti-β-actin (1:10'000, A5441, Sigma-Aldrich) antibodies. HRP-conjugated secondary antibodies were applied for 1 h at RT and signals were visualized using Western lightning chemiluminescence reagent (PerkinElmer, Waltham, MA, USA) and X-ray films.

Electroretinography (ERG)

Mice were dark-adapted overnight and pupils were dilated under dim red light with 1% cyclogyl (Alcon Switzerland SA, Rotkreuz, Switzerland) and 5% neosynephrin-POS (Ursapharm Schweiz GmbH, Roggwil, Switzerland) 30 minutes prior to recording. Mice were anesthetized with a subcutaneous injection of ketamine (85 mg/kg, Pfizer PFE Switzerland GmbH, Zurich, Switzerland) and xylazine (Rompun 2%, 4mg/kg, Bayer, Leverkusen, Germany). To keep the cornea moist, a drop of mydriaticum dispersa (Omnivision AG, Neuhausen, Switzerland) was applied to each eye. Low background illumination for 5 min was used for light adaptation. Electroretinograms were recorded simultaneously from both eyes as described (Samardzija et al. 2014). Flashes of 8 different light intensities ranging from -10 to 25 dB (0.25–790.5694 cd*s/m^2) were applied under photopic conditions. 10 responses were averaged per light intensity. Traces from n≥4 mice were averaged for each light intensity.

Fundus imaging and fluorescein angiography

Fundus photographs were taken with a Micron IV system (Phoenix Research Labs, Pleasanton, CA, USA). The pupils were dilated and the mice were anesthetized as described above. Methocel 2% (Omnivision) was applied to lubricate the eyes. Fluorescein images were captured 1-5 minutes after intraperitoneal injection of 20 µL of 2% fluorescein solution (Akorn, Lake Forest, IL, USA).

Experimental Design and Statistical Analysis

Two-way ANOVA with Šídák's multiple comparison test was performed using GraphPad Prism (version 7.02, GraphPad Software, San Diego, CA, USA) for statistical analysis of gene expression levels and ERG traces. All data are shown as means ± SD. Details of statistical analyses are shown in Table 2.

References

Akimoto M., Filippova E., Gage P. J., Zhu X., Craft C. M. and Swaroop A. (2004). Transgenic mice expressing Cre-recombinase specifically in M- or S-cone photoreceptors. *Invest Ophthalmol Vis Sci* **45**(1): 42-47.

Ames A., 3rd, Li Y. Y., Heher E. C. and Kimble C. R. (1992). Energy metabolism of rabbit retina as related to function: high cost of Na+ transport. *J Neurosci* **12**(3): 840-853.

Ardeljan D., Meyerle C. B., Agron E., Wang J. J., Mitchell P., Chew E. Y., Zhao J., Maminishkis A., Chan C. C. and Tuo J. (2013). Influence of TIMP3/SYN3 polymorphisms on the phenotypic presentation of age-related macular degeneration. *Eur J Hum Genet* **21**(10): 1152-1157.

Arjamaa O., Nikinmaa M., Salminen A. and Kaarniranta K. (2009). Regulatory role of HIF-1 a in the pathogenesis of age-related macular. *Ageing Research Reviews* **8**: 349-358.

Baird A., Esch F., Gospodarowicz D. and Guillemin R. (1985). Retina- and eye-derived endothelial cell growth factors: partial molecular characterization and identity with acidic and basic fibroblast growth factors. *Biochemistry* **24**(27): 7855-7860.

Berenberg T. L., Metelitsina T. I., Madow B., Dai Y., Ying G. S., Dupont J. C., Grunwald L., Brucker A. J. and Grunwald J. E. (2012). The association between drusen extent and foveolar choroidal blood flow in age-related macular degeneration. *Retina* **32**(1): 25-31.

Betsholtz C. (2004). Insight into the physiological functions of PDGF through genetic studies in mice. *Cytokine Growth Factor Rev* **15**(4): 215-228.

Boltz A., Luksch A., Wimpissinger B., Maar N., Weigert G., Frantal S., Brannath W., Garhofer G., Ergun E., Stur M. and Schmetterer L. (2010). Choroidal blood flow and progression of age-related macular degeneration in the fellow eye in patients with unilateral choroidal neovascularization. *Invest Ophthalmol Vis Sci* **51**(8): 4220-4225.

Bressler N. M., Bressler S. B. and Fine S. L. (1988). Age-related macular degeneration. *Surv Ophthalmol* **32**(6): 375-413.

Buch H., Vinding T., La Cour M., Appleyard M., Jensen G. B. and Nielsen N. V. (2004). Prevalence and causes of visual impairment and blindness among 9980 Scandinavian adults: the Copenhagen City Eye Study. *Ophthalmology* **111**(1): 53-61.

Campochiaro P. A. (2013). Ocular neovascularization. *J Mol Med (Berl)* **91**(3): 311-321.

Campochiaro P. A. (2015). Molecular pathogenesis of retinal and choroidal vascular diseases. *Prog Retin Eye Res* **49**: 67-81.

Caprara C., Thiersch M., Lange C., Joly S., Samardzija M. and Grimm C. (2011). HIF1A is essential for the development of the intermediate plexus of the retinal vasculature. *Invest Ophthalmol Vis Sci* **52**(5): 2109-2117.

Chakravarthy U., Wong T. Y., Fletcher A., Piault E., Evans C., Zlateva G., Buggage R., Pleil A. and Mitchell P. (2010). Clinical risk factors for age-related macular degeneration: a systematic review and meta-analysis. *BMC Ophthalmol* **10**: 31.

Ciulla T. A., Harris A., Chung H. S., Danis R. P., Kagemann L., McNulty L., Pratt L. M. and Martin B. J. (1999). Color Doppler imaging discloses reduced ocular blood flow velocities in nonexudative age-related macular degeneration. *Am J Ophthalmol* **128**(1): 75-80.

Coleman D. J., Silverman R. H., Rondeau M. J., Lloyd H. O., Khanifar A. A. and Chan R. V. (2013). Age-related macular degeneration: choroidal ischaemia? *Br J Ophthalmol* **97**(8): 1020-1023.

Dallinger S., Findl O., Strenn K., Eichler H. G., Wolzt M. and Schmetterer L. (1998). Age dependence of choroidal blood flow. *J Am Geriatr Soc* **46**(4): 484-487.

Fritsche L. G., Igl W., Bailey J. N., Grassmann F., Sengupta S., Bragg-Gresham J. L., Burdon K. P., Hebbring S. J., Wen C., Gorski M., Kim I. K., Cho D., Zack D., Souied E., Scholl H. P., Bala E., Lee K. E., Hunter D. J., Sardell R. J., Mitchell P., Merriam J. E., Cipriani V., Hoffman J. D., Schick T., Lechanteur Y. T., Guymer R. H., Johnson M. P., Jiang Y., Stanton C. M., Buitendijk G. H., Zhan X., Kwong A. M., Boleda A., Brooks M., Gieser L., Ratnapriya R., Branham K. E., Foerster J. R., Heckenlively J. R., Othman M. I., Vote B. J., Liang H. H., Souzeau E., McAllister I. L., Isaacs T., Hall J., Lake S., Mackey D. A., Constable I. J., Craig J. E., Kitchner T. E., Yang Z., Su Z., Luo H., Chen D., Ouyang H., Flagg K., Lin D., Mao G., Ferreyra H., Stark K., von Strachwitz C. N., Wolf A., Brandl C., Rudolph G., Olden M., Morrison M. A., Morgan D. J., Schu M., Ahn J., Silvestri G., Tsironi E. E., Park K. H., Farrer L. A., Orlin A., Brucker A., Li M., Curcio C. A., Mohand-Said S., Sahel J. A., Audo I., Benchaboune M., Cree A. J., Rennie C. A., Goverdhan S. V., Grunin M., Hagbi-Levi S., Campochiaro P., Katsanis N., Holz F. G., Blond F., Blanche H., Deleuze J. F., Igo R. P., Jr., Truitt B., Peachey N. S., Meuer S. M., Myers C. E., Moore E. L., Klein R., Hauser M. A., Postel E. A., Courtenay M. D., Schwartz S. G., Kovach J. L., Scott W. K., Liew G., Tan A. G., Gopinath B., Merriam J. C., Smith R. T., Khan J. C., Shahid H., Moore A. T., McGrath J. A., Laux R., Brantley M. A., Jr., Agarwal A., Ersoy L., Caramoy A., Langmann T., Saksens N. T., de Jong E. K., Hoyng C. B., Cain M. S., Richardson A. J., Martin T. M., Blangero J., Weeks D. E., Dhillon B., van Duijn C. M., Doheny K. F., Romm J., Klaver C. C., Hayward C., Gorin M. B., Klein M. L., Baird P. N., den Hollander A. I., Fauser S., Yates J. R., Allikmets R., Wang J. J.,

Schaumberg D. A., Klein B. E., Hagstrom S. A., Chowers I., Lotery A. J., Leveillard T., Zhang K., Brilliant M. H., Hewitt A. W., Swaroop A., Chew E. Y., Pericak-Vance M. A., DeAngelis M., Stambolian D., Haines J. L., Iyengar S. K., Weber B. H., Abecasis G. R. and Heid I. M. (2016). A large genome-wide association study of age-related macular degeneration highlights contributions of rare and common variants. *Nat Genet* **48**(2): 134-143.

Fruttiger M. (2007). Development of the retinal vasculature. *Angiogenesis* **10**(2): 77-88.

Frykman P. K., Brown M. S., Yamamoto T., Goldstein J. L. and Herz J. (1995). Normal plasma lipoproteins and fertility in gene-targeted mice homozygous for a disruption in the gene encoding very low density lipoprotein receptor. *Proc Natl Acad Sci U S A* **92**(18): 8453-8457.

Geiger P., Barben M., Grimm C. and Samardzija M. (2015). Blue light-induced retinal lesions, intraretinal vascular leakage and edema formation in the all-cone mouse retina. *Cell Death Dis* **6**: e1985.

Gragoudas E. S., Adamis A. P., Cunningham E. T., Feinsod M., Guyer D. R. and Neova V. I. S. O. (2004). Pegaptanib for neovascular age-related macular degeneration. *New England Journal of Medicine* **351**(27): 2805-2816.

Green W. R. (1999). Histopathology of age-related macular degeneration. *Mol Vis* **5**: 27.

Grunwald J. E., Metelitsina T. I., Dupont J. C., Ying G. S. and Maguire M. G. (2005). Reduced foveolar choroidal blood flow in eyes with increasing AMD severity. *Invest Ophthalmol Vis Sci* **46**(3): 1033-1038.

Haase V. H., Glickman J. N., Socolovsky M. and Jaenisch R. (2001). Vascular tumors in livers with targeted inactivation of the von Hippel-Lindau tumor suppressor. *Proc Natl Acad Sci U S A* **98**(4): 1583-1588.

Hartnett M. E., Weiter J. J., Staurenghi G. and Elsner A. E. (1996). Deep retinal vascular anomalous complexes in advanced age-related macular degeneration. *Ophthalmology* **103**(12): 2042-2053.

Heckenlively J. R., Hawes N. L., Friedlander M., Nusinowitz S., Hurd R., Davisson M. and Chang B. (2003). Mouse model of subretinal neovascularization with choroidal anastomosis. *Retina* **23**(4): 518-522.

Heynen S. R., Tanimoto N., Joly S., Seeliger M. W., Samardzija M. and Grimm C. (2011). Retinal degeneration modulates intracellular localization of CDC42 in photoreceptors. *Mol Vis* **17**: 2934-2946.

Hu W., Jiang A., Liang J., Meng H., Chang B., Gao H. and Qiao X. (2008). Expression of VLDLR in the retina and evolution of subretinal neovascularization in the knockout mouse model's retinal angiomatous proliferation. *Invest Ophthalmol Vis Sci* **49**(1): 407-415.

Ida H., Tobe T., Nambu H., Matsumura M., Uyama M. and Campochiaro P. A. (2003). RPE cells modulate subretinal neovascularization, but do not cause regression in mice with sustained expression of VEGF. *Invest Ophthalmol Vis Sci* **44**(12): 5430-5437.

Inoue Y., Yanagi Y., Matsuura K., Takahashi H., Tamaki Y. and Araie M. (2007). Expression of hypoxia-inducible factor 1alpha and 2alpha in choroidal neovascular membranes associated with age-related macular degeneration. *Br J Ophthalmol* **91**(12): 1720-1721.

Jaakkola P., Mole D. R., Tian Y. M., Wilson M. I., Gielbert J., Gaskell S. J., von Kriegsheim A., Hebestreit H. F., Mukherji M., Schofield C. J., Maxwell P. H., Pugh C. W. and Ratcliffe P. J. (2001). Targeting of HIF-alpha to the von Hippel-Lindau ubiquitylation complex by O2-regulated prolyl hydroxylation. *Science* **292**(5516): 468-472.

Joly S., Lange C., Thiersch M., Samardzija M. and Grimm C. (2008). Leukemia inhibitory factor extends the lifespan of injured photoreceptors in vivo. *J Neurosci* **28**(51): 13765-13774.

Joyal J. S., Sun Y., Gantner M. L., Shao Z., Evans L. P., Saba N., Fredrick T., Burnim S., Kim J. S., Patel G., Juan A. M., Hurst C. G., Hatton C. J., Cui Z., Pierce K. A., Bherer P., Aguilar E., Powner M. B., Vevis K., Boisvert M., Fu Z., Levy E., Fruttiger M., Packard A., Rezende F. A., Maranda B., Sapieha P., Chen J., Friedlander M., Clish C. B. and Smith L. E. (2016). Retinal lipid and glucose metabolism dictates angiogenesis through the lipid sensor Ffar1. *Nat Med* **22**(4): 439-445.

Kamei M. and Hollyfield J. G. (1999). TIMP-3 in Bruch's membrane: changes during aging and in age-related macular degeneration. *Invest Ophthalmol Vis Sci* **40**(10): 2367-2375.

Kast B., Schori C. and Grimm C. (2016). Hypoxic preconditioning protects photoreceptors against light damage independently of hypoxia inducible transcription factors in rods. *Exp Eye Res* **146**: 60-71.

Kent D. L. (2014). Age-related macular degeneration: beyond anti-angiogenesis. *Mol Vis* **20**: 46-55.

Kim J. H., Kim J. R., Kang S. W., Kim S. J. and Ha H. S. (2013). Thinner choroid and greater drusen extent in retinal angiomatous proliferation than in typical exudative age-related macular degeneration. *Am J Ophthalmol* **155**(4): 743-749, 749 e741-742.

Klein R., Klein B. E. and Cruickshanks K. J. (1999). The prevalence of age-related maculopathy by geographic region and ethnicity. *Prog Retin Eye Res* **18**(3): 371-389.

Kurihara T., Kubota Y., Ozawa Y., Takubo K., Noda K., Simon M. C., Johnson R. S., Suematsu M., Tsubota K., Ishida S., Goda N., Suda T. and Okano H. (2010). von Hippel-Lindau protein regulates transition from the fetal to the adult circulatory system in retina. *Development* **137**(9): 1563-1571.

Kurihara T., Westenskow P. D., Gantner M. L., Usui Y., Schultz A., Bravo S., Aguilar E., Wittgrove C., Friedlander M. S., Paris L. P., Chew E., Siuzdak G. and Friedlander M. (2016). Hypoxia-induced metabolic stress in retinal pigment epithelial cells is sufficient to induce photoreceptor degeneration. *Elife* **5**.

Lam A. K., Chan S. T., Chan H. and Chan B. (2003). The effect of age on ocular blood supply determined by pulsatile ocular blood flow and color Doppler ultrasonography. *Optom Vis Sci* **80**(4): 305-311.

Lange C., Caprara C., Tanimoto N., Beck S., Huber G., Samardzija M., Seeliger M. and Grimm C. (2011a). Retina-specific activation of a sustained hypoxia-like response leads to severe retinal degeneration and loss of vision. *Neurobiol Dis* **41**(1): 119-130.

Lange C., Heynen S. R., Tanimoto N., Thiersch M., Le Y. Z., Meneau I., Seeliger M. W., Samardzija M., Caprara C. and Grimm C. (2011b). Normoxic activation of hypoxia-inducible factors in photoreceptors provides transient protection against light-induced retinal degeneration. *Invest Ophthalmol Vis Sci* **52**(8): 5872-5880.

Lin R. J., Blumenkranz M. S., Binkley J., Wu K. and Vollrath D. (2006). A novel His158Arg mutation in TIMP3 causes a late-onset form of Sorsby fundus dystrophy. *Am J Ophthalmol* **142**(5): 839-848.

Lindahl P., Johansson B. R., Leveen P. and Betsholtz C. (1997). Pericyte loss and microaneurysm formation in PDGF-B-deficient mice. *Science* **277**(5323): 242-245.

Lindblom P., Gerhardt H., Liebner S., Abramsson A., Enge M., Hellstrom M., Backstrom G., Fredriksson S., Landegren U., Nystrom H. C., Bergstrom G., Dejana E., Ostman A., Lindahl P. and Betsholtz C. (2003). Endothelial PDGF-B retention is required for proper investment of pericytes in the microvessel wall. *Genes Dev* **17**(15): 1835-1840.

Macgregor A. M., Eberhart C. G., Fraig M., Lu J. and Halushka M. K. (2009). Tissue inhibitor of matrix metalloproteinase-3 levels in the extracellular matrix of lung, kidney, and eye increase with age. *J Histochem Cytochem* **57**(3): 207-213.

Madisen L., Zwingman T. A., Sunkin S. M., Oh S. W., Zariwala H. A., Gu H., Ng L. L., Palmiter R. D., Hawrylycz M. J., Jones A. R., Lein E. S. and Zeng H. (2010). A robust and high-throughput Cre reporting and characterization system for the whole mouse brain. *Nat Neurosci* **13**(1): 133-140.

Maguire M. G., Martin D. F., Ying G. S., Jaffe G. J., Daniel E., Grunwald J. E., Toth C. A., Ferris F. L., 3rd and Fine S. L. (2016). Five-Year Outcomes with Anti-Vascular Endothelial Growth Factor Treatment of Neovascular Age-Related Macular Degeneration: The Comparison of Age-Related Macular Degeneration Treatments Trials. *Ophthalmology* **123**(8): 1751-1761.

Mears A. J., Kondo M., Swain P. K., Takada Y., Bush R. A., Saunders T. L., Sieving P. A. and Swaroop A. (2001). Nrl is required for rod photoreceptor development. *Nat Genet* **29**(4): 447-452.

Ohno-Matsui K., Hirose A., Yamamoto S., Saikia J., Okamoto N., Gehlbach P., Duh E. J., Hackett S., Chang M., Bok D., Zack D. J. and Campochiaro P. A. (2002). Inducible expression of vascular endothelial growth factor in adult mice causes severe proliferative retinopathy and retinal detachment. *Am J Pathol* **160**(2): 711-719.

Okamoto N., Tobe T., Hackett S. F., Ozaki H., Vinores M. A., LaRochelle W., Zack D. J. and Campochiaro P. A. (1997). Transgenic mice with increased expression of vascular endothelial growth factor in the retina: a new model of intraretinal and subretinal neovascularization. *Am J Pathol* **151**(1): 281-291.

Punzo C., Kornacker K. and Cepko C. L. (2009). Stimulation of the insulin/mTOR pathway delays cone death in a mouse model of retinitis pigmentosa. *Nat Neurosci* **12**(1): 44-52.

Punzo C., Xiong W. and Cepko C. L. (2012). Loss of daylight vision in retinal degeneration: are oxidative stress and metabolic dysregulation to blame? *J Biol Chem* **287**(3): 1642-1648.

Qi J. H., Ebrahem Q., Moore N., Murphy G., Claesson-Welsh L., Bond M., Baker A. and Anand-Apte B. (2003). A novel function for tissue inhibitor of metalloproteinases-3 (TIMP3): inhibition of angiogenesis by blockage of VEGF binding to VEGF receptor-2. *Nat Med* **9**(4): 407-415.

Remsch H., Spraul C. W., Lang G. K. and Lang G. E. (2000). Changes of retinal capillary blood flow in age-related maculopathy. *Graefes Arch Clin Exp Ophthalmol* **238**(12): 960-964.

Roberts M. R., Srinivas M., Forrest D., Morreale de Escobar G. and Reh T. A. (2006). Making the gradient: thyroid hormone regulates cone opsin expression in the developing mouse retina. *Proc Natl Acad Sci U S A* **103**(16): 6218-6223.

Rosenfeld P. J., Brown D. M., Heier J. S., Boyer D. S., Kaiser P. K., Chung C. Y., Kim R. Y. and Group M. S. (2006). Ranibizumab for neovascular age-related macular degeneration. *N Engl J Med* **355**(14): 1419-1431.

Ryan H. E., Poloni M., McNulty W., Elson D., Gassmann M., Arbeit J. M. and Johnson R. S. (2000). Hypoxia-inducible factor-1alpha is a positive factor in solid tumor growth. *Cancer Res* **60**(15): 4010-4015.

Samardzija M., Caprara C., Heynen S. R., Willcox DeParis S., Meneau I., Traber G., Agca C., von Lintig J. and Grimm C. (2014). A mouse model for studying cone photoreceptor pathologies. *Invest Ophthalmol Vis Sci* **55**(8): 5304-5313.

Samardzija M., von Lintig J., Tanimoto N., Oberhauser V., Thiersch M., Reme C. E., Seeliger M., Grimm C. and Wenzel A. (2008). R91W mutation in Rpe65 leads to milder early-onset retinal dystrophy due to the generation of low levels of 11-cis-retinal. *Hum Mol Genet* **17**(2): 281-292.

Semenza G. L. (2004). Hydroxylation of HIF-1: oxygen sensing at the molecular level. *Physiology (Bethesda)* **19**: 176-182.

Semenza G. L. (2007). Oxygen-dependent regulation of mitochondrial respiration by hypoxia-inducible factor 1. *Biochem J* **405**(1): 1-9.

Semenza G. L. (2011). Oxygen sensing, homeostasis, and disease. *N Engl J Med* **365**(6): 537-547.

Spaide R. F. (2013). Clinical Manifestations of Choroidal Neovascularization in AMD. Age-related Macular Degeneration. F. G. Holz, D. Pauleikhoff, R. F. Spaide and A. C. Bird. Berlin, Heidelberg, Springer Berlin Heidelberg**:** 111-119.

Stefánsson E., Geirsdóttir Á. and Sigurdsson H. (2011). Metabolic physiology in age related macular degeneration. *Progress in Retinal and Eye Research* **30**: 72-80.

Stone J., Itin A., Alon T., Pe'er J., Gnessin H., Chan-Ling T. and Keshet E. (1995). Development of retinal vasculature is mediated by hypoxia-induced vascular endothelial growth factor (VEGF) expression by neuroglia. *J Neurosci* **15**(7 Pt 1): 4738-4747.

Sun Y., Liegl R., Gong Y., Buhler A., Cakir B., Meng S. S., Burnim S. B., Liu C. H., Reuer T., Zhang P., Walz J. M., Ludwig F., Lange C., Agostini H., Bohringer D., Schlunck G., Smith L. E. H. and Stahl A. (2017). Sema3f Protects Against Subretinal Neovascularization In Vivo. *EBioMedicine* **18**: 281-287.

Swaroop A., Chew E. Y., Rickman C. B. and Abecasis G. R. (2009). Unraveling a multifactorial late-onset disease: from genetic susceptibility to disease mechanisms for age-related macular degeneration. *Annual review of genomics and human genetics* **10**: 19-43.

Swaroop A., Kim D. and Forrest D. (2010). Transcriptional regulation of photoreceptor development and homeostasis in the mammalian retina. *Nat Rev Neurosci* **11**(8): 563-576.

Vierkotten S., Muether P. S. and Fauser S. (2011). Overexpression of HTRA1 leads to ultrastructural changes in the elastic layer of Bruch's membrane via cleavage of extracellular matrix components. *PLoS One* **6**(8): e22959.

Wang G. L., Jiang B. H., Rue E. A. and Semenza G. L. (1995). Hypoxia-inducible factor 1 is a basic-helix-loop-helix-PAS heterodimer regulated by cellular O2 tension. *Proc Natl Acad Sci U S A* **92**(12): 5510-5514.

Weber B. H., Vogt G., Pruett R. C., Stohr H. and Felbor U. (1994). Mutations in the tissue inhibitor of metalloproteinases-3 (TIMP3) in patients with Sorsby's fundus dystrophy. *Nat Genet* **8**(4): 352-356.

Wong W. L., Su X., Li X., Cheung C. M., Klein R., Cheng C. Y. and Wong T. Y. (2014). Global prevalence of age-related macular degeneration and disease burden projection for 2020 and 2040: a systematic review and meta-analysis. *Lancet Glob Health* **2**(2): e106-116.

Yannuzzi L. A., Freund K. B. and Takahashi B. S. (2008). Review of retinal angiomatous proliferation or type 3 neovascularization. *Retina* **28**(3): 375-384.

Yannuzzi L. A., Negrao S., Iida T., Carvalho C., Rodriguez-Coleman H., Slakter J., Freund K. B., Sorenson J., Orlock D. and Borodoker N. (2001). Retinal angiomatous proliferation in age-related macular degeneration. *Retina* **21**(5): 416-434.

Zhao L., Ma W., Fariss R. N. and Wong W. T. (2011). Minocycline attenuates photoreceptor degeneration in a mouse model of subretinal hemorrhage microglial: inhibition as a potential therapeutic strategy. *Am J Pathol* **179**(3): 1265-1277.

Figure 1

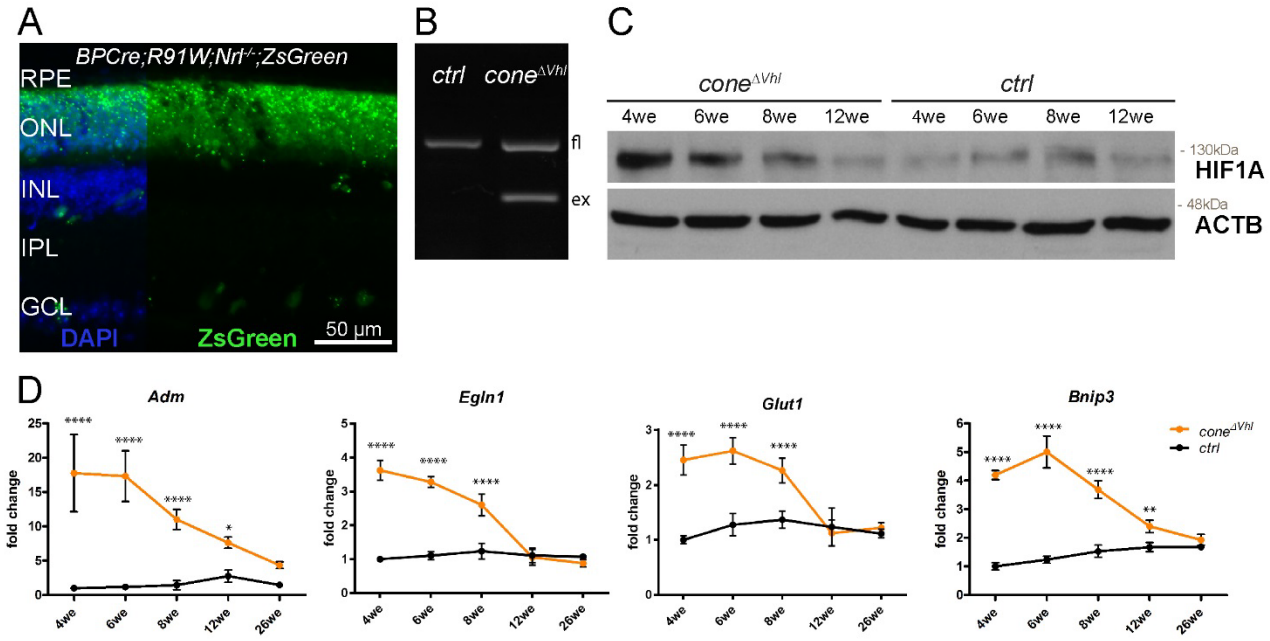

Figure 1. Knockdown of *Vhl* in cones of the all-cone mouse (*cone*$^{\Delta Vhl}$). (**A**) Expression of *Cre* recombinase in *BPCre;R91W;Nrl*$^{-/-}$*;ZsGreen* mice. Green fluorescence (ZsGreen) indicates *Cre* activity. RPE: retinal pigment epithelium, ONL: outer nuclear layer, INL: inner nuclear layer, IPL: inner plexiform layer, GCL: ganglion cell layer. Scale bar 50 µm. (**B**) PCR of genomic DNA from retinas of 4-week-old ctrl and *cone*$^{\Delta Vhl}$ mice. Floxed *Vhl* (fl) is detected at 460 bp and *Cre*-mediated excision (ex) results in a 260 bp fragment. (**C**) Western blot analysis of HIF1A in 4, 6, 8 and 12-week-old *cone*$^{\Delta Vhl}$ and *ctrl* (littermates without *Cre* recombinase) mice. ACTB served as loading control. (**D**) Relative expression of hypoxic target genes in retinas of *ctrl* (black) and *cone*$^{\Delta Vhl}$ (orange) mice. Expression levels were normalized to beta-actin (*Actb*) and calculated relatively to 4-week-old *ctrl* mice, which were set to 1. Shown are means ± SD. Two-way ANOVA with Šídák's multiple comparison test was used for statistical analysis (*Adm*: ****p<0.0001, *p=0.0306; *Egln1*: ****p<0.0001; *Glut1*: ****p<0.0001; *Bnip3*: ****p<0.0001, **p=0.0043; n≥3 per time point, Table 2 for details on ANOVA). *Adm*: Adrenomedullin, *Egln1*: egl-9 family hypoxia-inducible factor 1, *Glut1*: Glucose transporter 1, *Bnip3*: BCL2/adenovirus E1B interacting protein 3. *Cre*-negative littermates were used as *ctrl* mice in all experiments unless otherwise indicated.

Figure 2

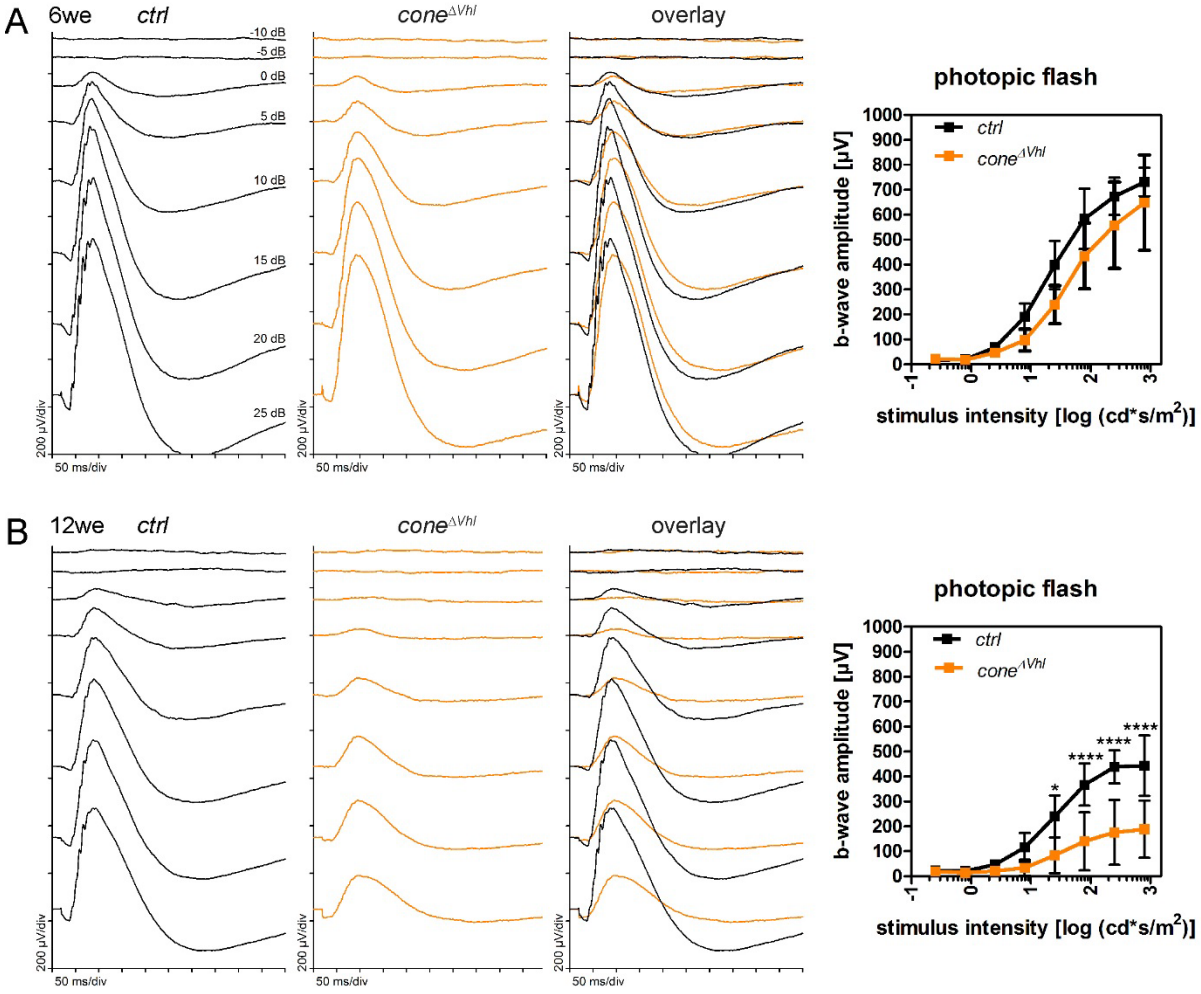

Figure 2. Reduced retinal function in aged *cone*$^{\Delta Vhl}$ mice. (**A**) Averaged traces of single-flash photopic ERGs and b-wave amplitudes showed no significant differences in *cone*$^{\Delta Vhl}$ mice (orange) compared to *ctrl* mice (black) at 6 weeks of age. (**B**) At 12 weeks of age, photopic b-wave amplitudes were strongly reduced in *cone*$^{\Delta Vhl}$ mice (orange) as compared to *ctrl* mice (black). b-wave amplitudes are shown as means ± SD. Two-way ANOVA with Šídák's multiple comparison test was used for statistical analysis (6we *ctrl* and *cone*$^{\Delta Vhl}$ n=5, 12we *ctrl* n=6 and *cone*$^{\Delta Vhl}$ n=4, *p=0.0115, ****p<0.0001, Table 2 for details on ANOVA).

Figure 3

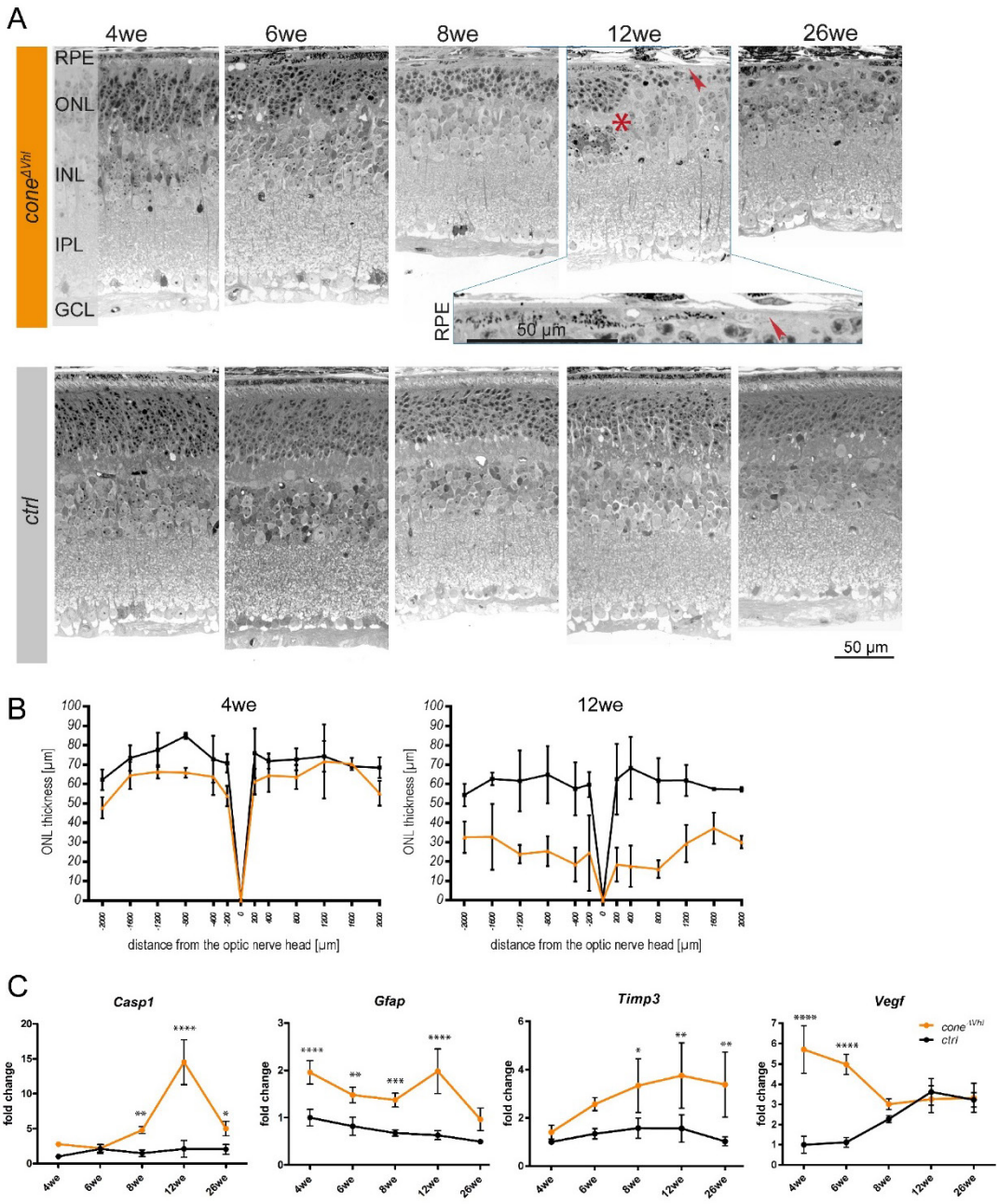

Figure 3. Progressive cone degeneration in *cone*$^{\Delta Vhl}$ mice. (**A**) Inactivation of *Vhl* in cones led to progressive retinal degeneration (upper panels) as compared to *ctrl* mice (lower panels). *Cone*$^{\Delta Vhl}$ mice displayed disturbed layering with reorganization of the INL (asterisk, 12we *cone*$^{\Delta Vhl}$), severe loss of the ONL and partial loss of the RPE (arrowhead, 12we *cone*$^{\Delta Vhl}$, inset) at 12 and 26 weeks of age. Abbreviations as in Figure 1. Scale bar 50 µm. (**B**) Line chart of ONL thickness in *cone*$^{\Delta Vhl}$ mice (orange) as compared to *ctrl* mice (black) at 4 and 12 weeks of age. n≥3. (**C**) Relative expression levels of genes involved in stress signaling and degeneration. Expression levels were normalized to *Actb* and calculated relatively to 4-week-old *ctrl* mice, which were set to 1. Shown are means ± SD. Two-way ANOVA with Šídák's multiple comparison test was used for statistical analysis (*Casp1*: **p=0.0026, ****p<0.0001, *p=0.0244, *Gfap*: ****p<0.0001, **p=0.0035, ***p=0.0004, ****p<0.0001, *Timp3*: *p=0.0235, **p=0.0036, **p=0.0035, *Vegf*: ****p<0.0001, n≥3 per time point, Table 2 for details on ANOVA). *Casp1*: caspase 1, *Gfap*: glial fibrillary acidic protein, *Timp3*: tissue inhibitor of metalloproteinase 3, *Vegf*: vascular endothelial growth factor.

Figure 4

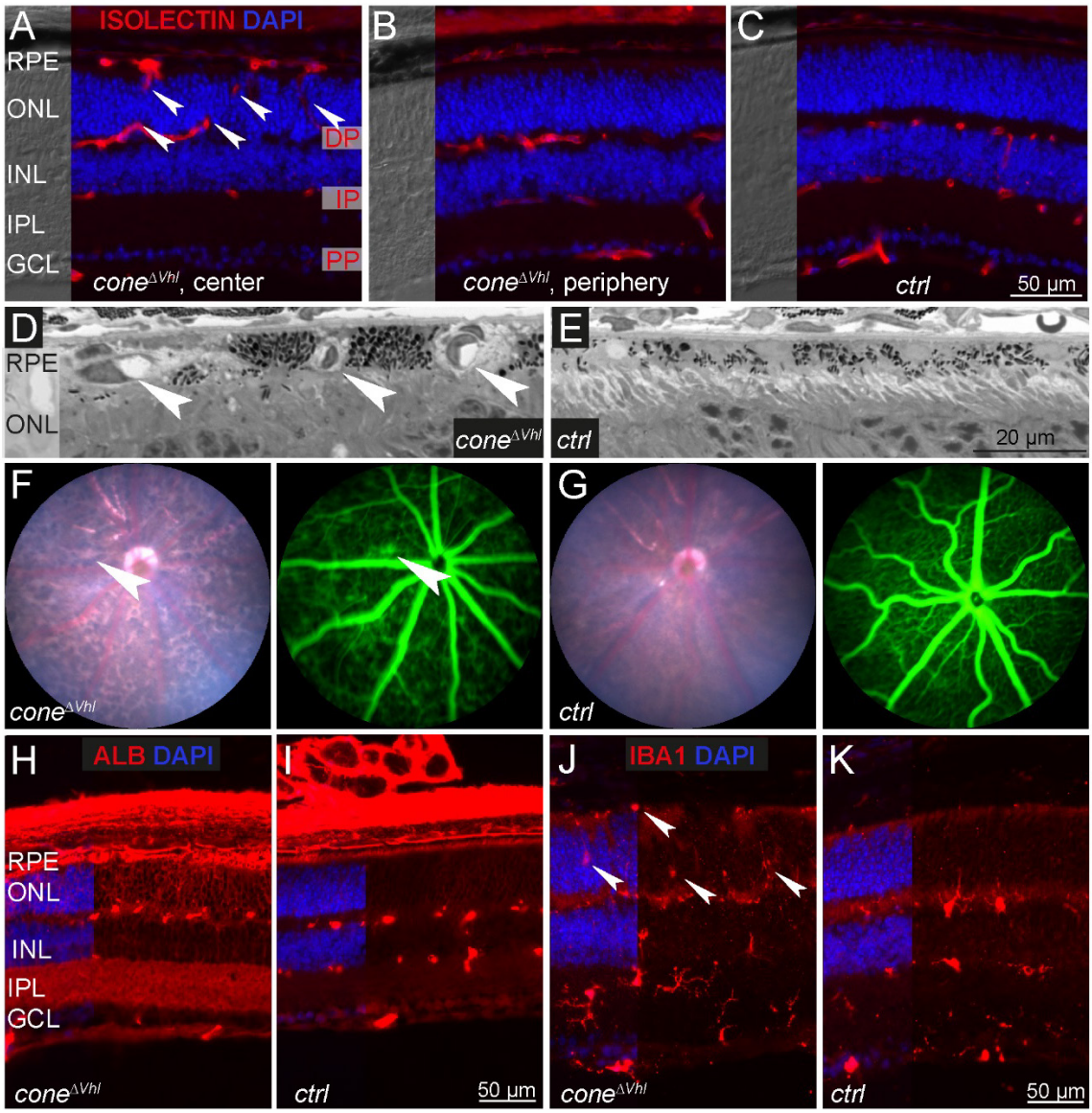

Figure 4. Subretinal neovascularization in *cone*$^{\Delta Vhl}$ mice. (**A-C**) Immunostaining of cross-sections of the central (A) and peripheral (B) retina of 4-week-old *cone*$^{\Delta Vhl}$ and age-matched *ctrl* mice (C, central retina) with isolectin. Arrowheads indicate vessels extending from the deep plexus into the ONL in central retinas of *cone*$^{\Delta Vhl}$ mice. DP: deep plexus, IP: intermediate plexus, PP: primary plexus. Scale bar 50 µm. (**D, E**) Light microscopy of 4-week-old *cone*$^{\Delta Vhl}$ and *ctrl* mice. Neovessels (arrowheads) reached the RPE, but did not cross Bruch's membrane. Scale bar 20 µm. (**F, G**) Fundus imaging and fluorescein angiography of *cone*$^{\Delta Vhl}$ mice and *ctrl* mice at 4 weeks of age. Signs of leakage (arrowhead) were detected in *cone*$^{\Delta Vhl}$ mice. (**H-K**) Retinal cross-sections of *ctrl* (**H, J**) and *cone*$^{\Delta Vhl}$ mice (**I, K**) were stained with antibodies against ALB (**H, I**) and IBA1 (**J, K**) at 4 weeks of age. Microglia/macrophages were found within the photoreceptor layer and RPE in *cone*$^{\Delta Vhl}$ mice (arrowheads). Scale bar 50 µm. Abbreviations as in Figure 1.

Figure 5

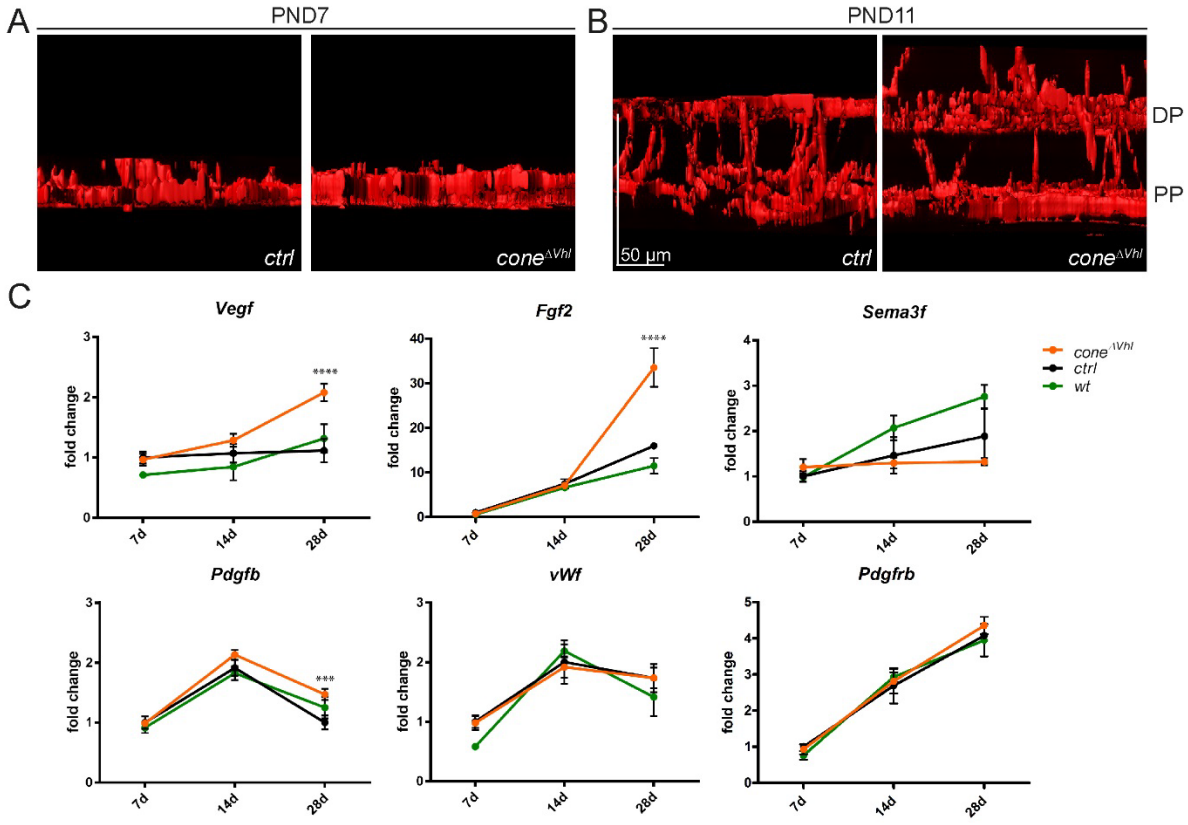

Figure 5. Pathological vessel growth starts around PND11 in *cone*$^{\Delta Vhl}$ mice. (**A, B**) 3D-reconstruction of blood vessels stained with isolectin on retinal flat mounts of *ctrl* (left) and *cone*$^{\Delta Vhl}$ (right) mice at PND7 (A) and PND 11 (B). At PND11, vessels extended from the deep plexus towards the ONL. The intermediate plexus has not yet been formed in both *ctrl* and *cone*$^{\Delta Vhl}$ mice. For better recognition and distinction the z-value of the z-stacks was increased five times. DP: deep plexus, PP: primary plexus. Scale bar 50 µm. (**C**) Relative expression levels of angiogenic genes in retinas of *cone*$^{\Delta Vhl}$ (orange), *ctrl* (black) and *wt* (green) mice at indicated time points. Expression levels were normalized to *Actb* and compared to *ctrl* mice at PND7, which were set to 1. Shown are means ± SD. Two-way ANOVA with Šídák's multiple comparison test was used for statistical analysis comparing *ctrl* with *cone*$^{\Delta Vhl}$ mice (*Vegf*: ****p<0.0001, *Fgf2*: ****p<0.0001, *Pdgfb*: ***p=0.0009, n=3 per time point, Table 2 for details on ANOVA). *Vegf*: vascular endothelial growth factor, *Fgf2*: fibroblast growth factor 2, *Sema3f*: semaphorin 3F, *Pdgfb*: platelet derived growth factor, B polypeptide, *vWf*: von Willebrand factor, *Pdgfrb*: platelet derived growth factor receptor, beta polypeptide.

Figure 6

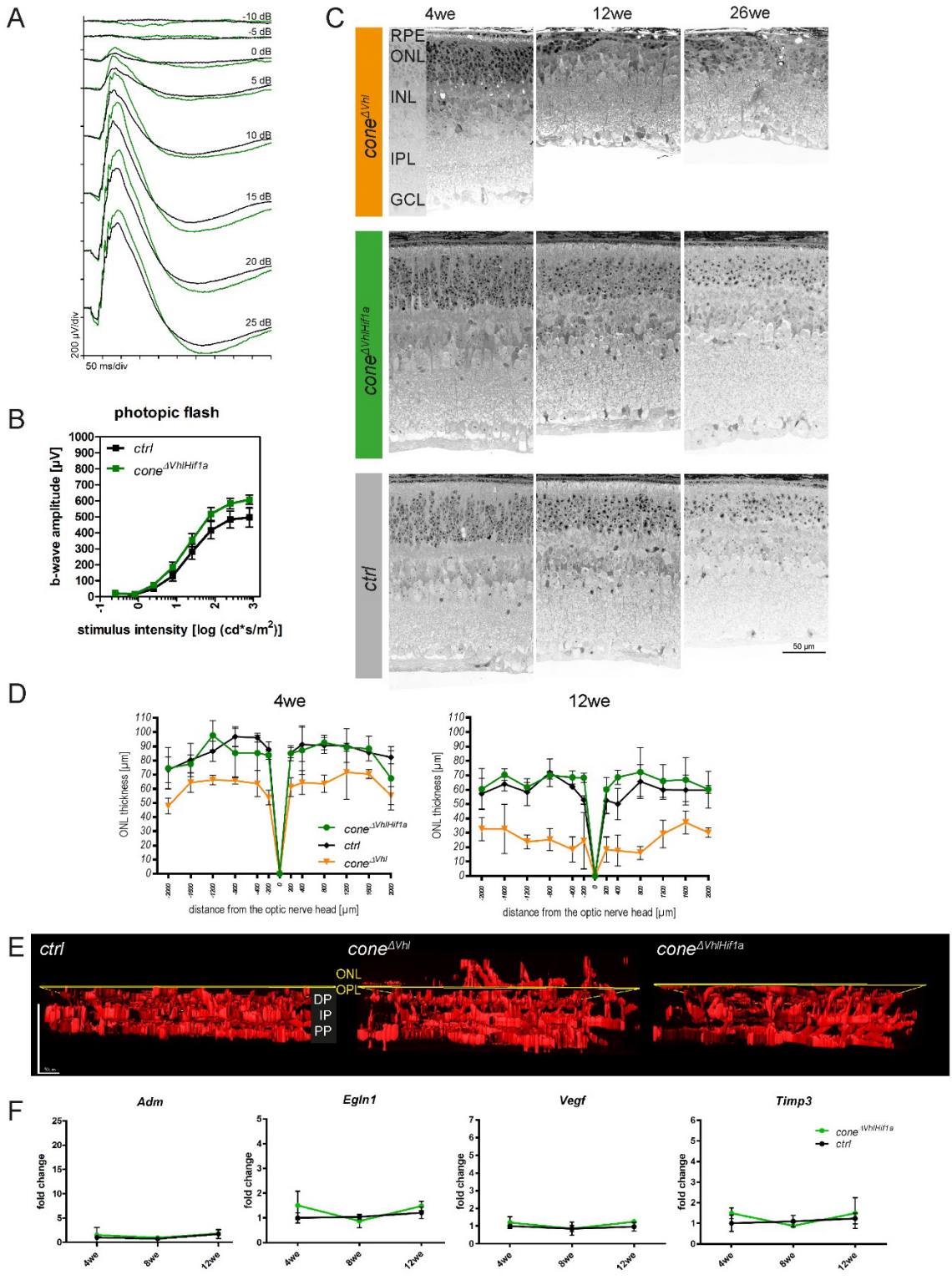

Figure 6. Combined deletion of *Hif1a* and *Vhl* (*cone*$^{\Delta VhlHif1a}$) rescues the defects in retinal function, morphology and vasculature observed in *cone*$^{\Delta Vhl}$ mice. (**A, B**) Average single-flash photopic ERGs and b-wave amplitudes showed no significant differences in *cone*$^{\Delta VhlHif1a}$ mice (green) compared to *ctrl* mice (*R91W;Nrl*$^{-/-}$*;Vhl*$^{f/f}$; *Hif1a*$^{f/f}$, black) at 12 weeks of age. n=4 per group. b-wave amplitudes are shown as means ± SD. (**C, D**) Light microscopy analysis and measurement of the ONL thickness in *cone*$^{\Delta VhlHif1a}$ (green), *ctrl* mice (*R91W;Nrl*$^{-/-}$*;Vhl*$^{f/f}$; *Hif1a*$^{f/f}$, black) and *cone*$^{\Delta Vhl}$ mice (orange, as shown in Figure 3B) at indicated time points. Abbreviations as in Figure 1. Scale bar 50 µm. (**E**) 3D-

reconstruction of blood vessels stained with isolectin on retinal flat mounts of *ctrl* (left), *cone*$^{\Delta Vhl}$ (middle) and *cone*$^{\Delta VhlHif1a}$ mice (right). Inactivation of *Hif1a* (*cone*$^{\Delta VhlHif1a}$) rescued the pathological neovascularization. Analysis at 4 weeks of age, n=3. For better recognition and distinction the z-value of the z-stacks was increased five times. The yellow line indicates the border between the outer plexiform layer (OPL) and the ONL. DP: deep plexus, IP: intermediate plexus, PP: primary plexus. (**F**) Relative gene expression of hypoxic target genes in *cone*$^{\Delta VhlHif1a}$ mice (green) and *ctrl* mice (*R91W;Nrl*$^{-/-}$*;Vhl*$^{f/f}$; *Hif1a*$^{f/f}$, black) at 4we, 8we and 12we as indicated. Abbreviations as in Figure 1 and 3. Expression levels were normalized to *Actb* and compared to 4-week-old *ctrl* mice, which were set to 1. Shown are means ± SD. n≥3 per time point. Scale bar 50 µm.

Table 1. Primers used for real-time PCR

Gene	Forward (5'-3')	Reverse (5'-3')	Product (bp)
Actb	CAACGGCTCCGGCATGTGC	CTCTTGCTCTGGGCCTCG	153
Adm	TCCTGGTTTCTCGGCTTCTC	ATTCTGTGGCGATGCTCTGA	133
Bnip3	CCTGTCGCAGTTGGGTTC	GAAGTGCAGTTCTACCCAGGAG	93
Casp1	GGCAGGAATTCTGGAGCTTCAA	GTCAGTCCTGGAAATGTGCC	138
Fgf2	TGTGTCTATCAAGGGAGTGTGTGC	ACCAACTGGAGTATTTCCGTGACCG	158
Gfap	CCACCAAACTGGCTGATGTCTAC	TTCTCTCCAAATCCACACGAGC	240
Glut1	CAGTGTATCCTGTTGCCCTTCTG	GCCGACCCTCTTCTTTCATCTC	151
Pdgfb	GCTGCTGCAATAACCGCAAT	GTGGTCCTCCAAGGTCACTG	131
Pdgfrb	CTTGCCCTTCAAAGTGGTGG	CCAGGTGGAGTCGTAAGGC	199
Egln1	GCAGCATGGACGACCTGAT	CAACGTGACGGACATAGCCT	123
Sema3f	CGTCGCGCACAGGATTA	GGAAAATGGCTGCATCGGTA	166
Timp3	GCCTCAAGCTAGAAGTCAACAAA	TGTACATCTTGCCTTCATACACG	69
Vegf	ACTTGTGTTGGGAGGAGGATGTC	AATGGGTTTGTCGTGTTTCTGG	171
vWF	CCCTGGACAACTTGACAGCAG	ACAAGCAGGCAGATCTCATACC	192

Table 2. Statistical analyses: Two-way ANOVA

Figure	Number of mice	Experiment	*F*-values	*P*-value
1D	4we: n=3, 6we: n=3, 8we: n=4, 12we: *ctrl* n=4; *cone*$^{\Delta Vhl}$ n=3, 26we: n=3	*Adm*	*Interaction: F* (4, 23) = 14.63	*P*<0.0001
			Strain: F (1, 23) = 183.2	*P*<0.0001
		Egln1	*Interaction: F* (4, 23) = 60.19	*P*<0.0001
			Strain: F (1, 23) = 259.4	*P*<0.0001
		Glut1	*Interaction: F* (4, 23) = 17.28	*P*<0.0001
			Strain: F (1, 23) = 92.58	*P*<0.0001
		Bnip3	*Interaction: F* (4, 23) = 61.1	*P*<0.0001
			Strain: F (1, 23) = 535	*P*<0.0001
2B	*ctrl* n=6, *cone*$^{\Delta Vhl}$ n=4	12we	*Interaction: F* (7, 64) = 5.76	*P*<0.0001
			Strain: *F* (1, 64) = 59.33	*P*<0.0001
3C	4we: n=3, 6we: n=3, 8we: *ctrl* n=4; *cone*$^{\Delta Vhl}$ n=4 and n=3 for *Timp3*, 12we: *ctrl* n=4; *cone*$^{\Delta Vhl}$ n=3, 26we: n=3	*Casp1*	*Interaction: F* (4, 23) = 27.6	*P*<0.0001
			Strain: F (1, 23) = 100.9	*P*<0.0001
		Gfap	*Interaction: F* (4, 23) = 4.392	*P*=0.0088
			Strain: F (1, 23) = 130	*P*<0.0001
		Timp3	*Interaction: F* (4, 22) = 1.846	*P*=0.1561
			Strain: F (1, 22) = 37.12	*P*<0.0001
		Vegf	*Interaction: F* (4, 23) = 26.52	*P*<0.0001
			Strain: F (1, 23) = 81.18	*P*<0.0001
5C	n=3	*Vegf*	*Interaction: F* (4, 18) = 6.041	*P*=0.0029
			Strain: F (2, 18) = 17.4	*P*<0.0001
		Fgf2	*Interaction: F* (4, 18) = 19.52	*P*<0.0001
			Strain: F (2, 18) = 20.16	*P*<0.0001
		Pdgfb	*Interaction: F* (4, 18) = 3.333	*P*=0.0329
			Strain: F (2, 18) = 8.26	*P*=0.0028

3.2 Article 2: *Hif1a* inactivation rescues photoreceptor degeneration induced by a chronic hypoxia-like stress

*__Maya Barben__[1,2], *Divya Ail[1,3], Federica Storti[1], Katrin Klee[1,4], Christian Schori[1,4], Marijana Samardzija[1], Stelios Michalakis[5], Martin Biel[5], Isabelle Meneau[6], Frank Blaser[6], Daniel Barthelmes[6,7], Christian Grimm[1,2,4]

[1]Lab for Retinal Cell Biology, Department of Ophthalmology, University of Zürich, Zürich, Switzerland

[2]Neuroscience Center Zurich (ZNZ), University of Zürich, Zürich, Switzerland

[3]Present address: Paris-Saclay Institute of Neuroscience, CNRS, Univ. Paris-Sud, Université Paris-Saclay, Orsay, France

[4]Center for Integrative Human Physiology (ZIHP), University of Zürich, Zürich, Switzerland

[5]Munich Center for Integrated Protein Science at the Department of Pharmacy, Center for Drug Research, Ludwig-Maximilians-Universität München, Munich, Germany

[6]Dept. Ophthalmology, University Hospital Zürich, Zürich, Switzerland

[7]Save Sight Institute, The University of Sydney, Sydney, Australia

* These authors contributed equally to the work.

Status of the manuscript:

Submitted

Personal Contribution

Cell culture experiments (siRNA, shRNA), AAV-mediated rescue, interpretation of the results, manuscript editing.

Abstract

Reduced choroidal blood flow and tissue changes in the ageing human eye impairs oxygen delivery to photoreceptors and the retinal pigment epithelium. As a consequence, mild but chronic hypoxia may develop and disturb cell metabolism, function and ultimately survival, potentially contributing to retinal pathologies such as age-related macular degeneration (AMD). Here, we show that several hypoxia-inducible genes were expressed at higher levels in the aged human retina suggesting increased activity of hypoxia-inducible transcription factors (HIFs) during the physiological ageing process. To model chronically elevated HIF activity and investigate ensuing consequences for photoreceptors, we generated mice lacking von Hippel Lindau (VHL) protein in rods. This activated HIF transcription factors and led to a slowly progressing retinal degeneration in the ageing mouse retina. Importantly, this process depended on HIF1 but not on HIF2. A gene therapy approach using AAV-mediated RNA interference through an anti-*Hif1a* shRNA significantly mitigated the degeneration suggesting a potential intervention strategy that may be applicable to human patients.

Introduction

Several blinding conditions of the retina are characterized by the progressive loss of photoreceptors and retinal pigment epithelium (RPE) cells. Underlying causes are manifold and include gene mutations, age-related tissue changes, systemic alterations and environmental factors. A relevant condition that can lead to retinal pathology is hypoxia. Reduced tissue oxygenation is causative for the production of vascular endothelial growth factor (VEGF), a main factor involved in the development of diabetic macular edema and neovascularization in age-related macular degeneration (AMD) (Caprara and Grimm, 2012; Simó et al., 2014; Campochiaro, 2015). However, tissue hypoxia may also be of significance for retinal pathologies not associated with abnormal vessel growth such as the highly prevalent non-exudative form of AMD (Arjamaa et al., 2009; Feigl, 2009; Stefánsson et al., 2011). Reduced choroidal blood flow in the ageing eye (Dallinger et al., 1998; Lam et al., 2003) and in the foveolar region of AMD patients (Grunwald et al., 2005), choroidal ischemia in dry AMD (Ciulla et al., 1999; Grunwald et al., 2005; Coleman et al., 2013) and the correlation between drusen accumulation and decreased choroidal blood volume in AMD (Berenberg et al., 2012) has led to the hypothesis that reduced oxygen availability to retinal cells might be a significant factor that contributes – likely together with other factors – to disease development and progression (Arjamaa et al., 2009; Kent, 2014). Since both rods and cones have an extraordinarily high demand for energy (Okawa et al., 2008), their function and survival might be especially sensitive to reduced tissue oxygenation.

Hypoxia-inducible transcription factors (HIFs) are the major regulators of the cellular response to reduced oxygen levels (Webb et al., 2009). They are composed of a constitutively expressed β–(HIFB) and an oxygen-labile α–subunit (HIFA). In the presence of O_2, prolyl hydroxylases hydroxylate the α–subunit that is then recognized by the von Hippel Lindau (VHL) protein complex. An E3 ligase in this complex adds ubiquitins to the hydroxylated HIFAs targeting them for rapid proteasomal degradation. In hypoxia, HIFAs are less hydroxylated, escape recognition by VHL, ubiquitination and degradation, and can thus function as transcription factors (Maxwell et al., 1999; Jaakkola et al., 2001). Probably the most prominent HIF target genes are *VEGF* and erythropoietin (*EPO*). Both play eminent roles in the response to hypoxia and are key factors for neovascularization and the increase in haematocrit, respectively. Although HIF1 and HIF2 share several common targets, they may also have their own set of genes for specific regulation (Loboda et al., 2010).

Inactivation of VHL prevents degradation of HIF-alpha subunits and leads to increased HIF1 and HIF2 activity. It is an experimental way to model a major part of the molecular response to hypoxia in normoxic conditions. When the *Vhl* gene is inactivated in retinal cells already during development, a severe vessel phenotype develops and the retina degenerates (Kurihara et al., 2010; Lange et al., 2011a). Recently, Kurihara and colleagues inactivated *Vhl* also in the RPE and showed that the ensuing molecular response in these cells leads to severe alterations in RPE morphology and metabolism causing cell death (Kurihara et al., 2016). This phenotype was rescued by the

additional inactivation of *Hif2a* suggesting that HIF2 may be responsible for RPE degeneration in conditions of reduced tissue oxygenation. The importance of a tightly controlled VHL/HIF system within the retina is further underlined by the observation that a rod-specific inactivation of *Vhl* after postnatal development leads to a late onset and age-dependent loss of photoreceptors and retinal function (Lange et al., 2011b). Here, we show that the ageing human retina may indeed experience increased hypoxic stress. We also identify HIF1 as the factor being responsible for photoreceptor degeneration in a model of chronic hypoxia-like conditions and demonstrate that AAV-mediated expression of an shRNA targeting *Hif1a* mitigates the degenerative phenotype.

Results

Increased expression of hypoxia-related genes in the aged human retina

Reduced choroidal blood flow and tissue changes may reduce oxygen availability for photoreceptors in the aged neuronal retina (see introduction). To test this hypothesis, we analysed expression of hypoxia-related genes in the central and peripheral retina from 10 human donors between the age of 17 and 92 years without diagnosed retinal pathology (Table 1). The central retina samples included the macular region whereas peripheral tissue was isolated from the mid periphery of the nasal retina. Although post-mortem times differed considerably (Table 1), Ct-values of the housekeeping genes glyceraldehyde 3-phosphate dehydrogenase (*GAPDH*), ribosomal protein L28 (*RPL28*) and beta-actin (*ACTB*) were relatively similar in the samples (Fig. 1A,B). Expression levels of genes of interest, however, varied strongly between donor eyes. Although R^2 values were low (not shown), linear regression indicated a tendency of an age-dependent increased expression of the classic hypoxia-regulated HIF-target genes adrenomedullin (*ADM*), *VEGFA* and to a lower extent also of pyruvate dehydrogenase kinase 1 (*PDK1*) and glucose transporter type 1 (*GLUT1*) in both the central and the peripheral retina (Fig. 1C,D). In contrast, rod and cone-specific genes involved in phototransduction including rhodopsin (*RHO*), G protein subunit alpha transducin 2 (cone transducin, *GNAT2*) and rod phosphodiesterase 6A (*PDE6A*) showed the opposite trend and seemed to be expressed at reduced levels in the aged retina. The only exception was cone phosphodiesterase 6C (*PDE6C*) in the central retina that followed expression of the reference gene *RPL28* (Fig. 1E,F). Thus, the aged human retina may upregulate expression of hypoxia-related factors and reduce expression of photoreceptor-specific genes. Given that photoreceptors receive their oxygen largely from the choroidal blood with its reduced flow in older eyes, it is plausible to assume that photoreceptors contribute to the upregulation of hypoxia-induced HIF target genes in response to a mild but chronic hypoxia that may develop during ageing.

Rod photoreceptor degeneration induced by a chronic hypoxia-like response is controlled by HIF1

To model a state of chronically activated HIF transcription factors in photoreceptors as it may be found in the aged human retina, we inactivated *Vhl* in adult rods using the opsin-Cre mouse (LMOPC1; (Le et al., 2006)). We have chosen rods as target cells because they are among the first cells to die in AMD (Curcio et al., 1996). The additional rod-specific inactivation of *Hif1a* and/or *Hif2a* allowed to test the contribution of each transcription factor to the phenotype. Opsin-Cre-mediated excision of floxed sequences occurs postnatally in about 50% of rods and reaches its maximal extent at around 6 weeks of age (Le et al., 2006; Lange et al., 2011a). Genomic excision was verified by PCR (Fig. 2A) and normoxic stabilization of HIF1A and HIF2A confirmed in retinas of 11 weeks old $rod^{\Delta Vhl}$ mice by Western blotting (Fig. 2B) as reported earlier (Lange et al., 2011b). Additional inactivation of *Hif1a* and/or *Hif2a* resulted in increased levels of only HIF2A in $rod^{\Delta Vhl;Hif1a}$ or of HIF1A in $rod^{\Delta Vhl;Hif2a}$, or in unchanged levels of both HIFA transcription factors in $rod^{\Delta Vhl;Hif1a;Hif2a}$ mice (Fig. 2B). Rod-specific inactivation of *Vhl* ($rod^{\Delta Vhl}$) resulted in a late onset and slowly progressing retinal degeneration reaching its maximal extent (loss of about 50% of photoreceptors) around 6 months of age. Since only about 50% of rods express Cre (Le et al., 2006; Lange et al., 2011a), it is likely that surviving photoreceptors were without Cre and may thus not have activated HIF transcription factors. Although an earlier cohort of $rod^{\Delta Vhl}$ mice showed no functional loss or degeneration at 17 weeks of age (Lange et al., 2011b), we detected photoreceptor degeneration already at 4 months in the cohort presented here (Fig. 3). The reason for the slightly accelerated degeneration is unclear, but may be based on changed environmental conditions in the new animal facility of the University of Zurich with a prolonged light period (14 h instead of 12 h) and slightly increased light levels. Importantly, however, the new cohort also showed a slowly progressing, age-dependent photoreceptor degeneration similar to the cohort used before. The degenerative phenotype of $rod^{\Delta Vhl}$ mice was completely rescued by the additional inactivation of *Hif1a* or of *Hif1a* and *Hif2a* together, but not of *Hif2a* alone. This was also reflected by the retinal stress marker glial fibrillary acidic protein (GFAP) that was elevated in $rod^{\Delta Vhl}$ and $rod^{\Delta Vhl;Hif2a}$ retinas that were prone to degeneration, but remained at basal levels when *Hif1a* was inactivated (see below, Fig. 7). Surprisingly, $rod^{\Delta Vhl}$ mice showed also an RPE phenotype, albeit with variable severity and only in isolated areas. Fundus imaging detected few pale flecks that appeared in the OCT scans as thick, hyperreflective regions in or close to the RPE layer at 4 months of age (Fig. 4A). Unevenly distributed fundus flecks that correspond to hyperreflective OCT signals close to the RPE are also described for human retinal degenerative diseases such as Stargardt dystrophy (Sparrow et al., 2015). Thus, even in the presence of causative gene mutations for instance in *ABCA4*, degeneration of retinal cells and fundus appearance may not always be uniform across the retina. Cross sections of $rod^{\Delta Vhl}$ retinas showed that the RPE was thicker and multi-layered in focused regions that may correspond to the flecks detected by fundus imaging and OCT. RPE cells appeared more heavily pigmented, partially vesiculated and enlarged (Fig. 4B,C). This was confirmed in flatmounts where phalloidin staining indicated that some RPE cells had a less regular shape and contact to an unusually high number of neighbouring cells (Fig.

4D). Photoreceptors below affected RPE regions seemed less viable as many pyknotic nuclei were detectable in the ONL (Fig. 4B, arrows). Since this RPE phenotype was never observed in $rod^{\Delta Vhl;Hif1a}$ mice we conclude that chronic activation of HIF1 in rods not only caused cell death *in cis* but also affected neighbouring RPE cells in some parts of the retina.

The tissue phenotype was mirrored by retinal function. At 6 months of age, $rod^{\Delta Vhl}$ and $rod^{\Delta Vhl;Hif2a}$ mice had significantly reduced scotopic a- and b-wave amplitudes at higher flash intensities compared to their respective control littermates. Mice lacking *Hif1a* in addition to *Vhl* ($rod^{\Delta Vhl;Hif1a}$ and $rod^{\Delta Vhl;Hif1a;Hif2a}$ mice), however, retained normal function (Fig. 5). This is of significance since it shows that adult photoreceptors do not require HIF1 for function or survival. Although *Vhl* inactivation was rod-specific, the cone-driven photopic b-wave amplitudes at higher light intensities were also reduced in $rod^{\Delta Vhl}$ mice suggesting that loss of VHL in rods affected cone function or survival. Interestingly, the reduction in cone-driven ERG responses was prevented by the additional inactivation of *Hif1a* and/or *Hif2a* (Fig. S1). The reason for this is unclear but may point to mechanisms in rods that can affect cone function in a HIF1- and HIF2-dependent manner. However, this needs further testing.

The transcriptomic response

Increased expression of the HIF1 targets *Adm*, *Vegf*, *Glut1*, *Pdk1* and Egl-9 family hypoxia inducible factor 1 (*Egln1*) in $rod^{\Delta Vhl}$ and $rod^{\Delta Vhl;Hif2a}$ mice at 11 weeks of age verified that HIF1 was transcriptionally active (Fig. 6). Normal expression levels of these genes in $rod^{\Delta Vhl;Hif1a}$ and $rod^{\Delta Vhl;Hif1a;Hif2a}$ mice confirmed their dependency on HIF1. Expression of these HIF1-target genes was less increased at 6 months, probably because most rods lacking *Vhl* have already degenerated at this age (Fig. 3). BCL2 interacting protein 3 (*Bnip3*), caspase-1 (*Casp1*), leukemia inhibitory factor (*Lif*), endothelin-2 (*Edn2*), fibroblast growth factor-2 (*Fgf2*), signal transducer and activator of transcription-3 (*Stat3*) and *Gfap* are upregulated in the degenerating retina and connected to cell death or cell survival (Guo et al., 2001; Samardzija et al., 2006a; Samardzija et al., 2006b; Joly et al., 2008). These genes were activated exclusively in the degenerating retinas of $rod^{\Delta Vhl}$ (Lange et al., 2011b) and $rod^{\Delta Vhl;Hif2a}$ mice. It is noteworthy that *LIF* and to a lesser extent also *EDN2* and *CASP1* showed a trend of increased expression in the aged human retina (Fig. 8) pointing to a stress response that is more likely to be activated in the senescent retina.

It is important to note that in addition to HIF1A and HIF2A also levels of pSTAT3 were increased in $rod^{\Delta Vhl}$ and $rod^{\Delta Vhl;Hif2a}$ mice (Fig. 7). It has been reported that HIF1 may cooperate with STAT3 to regulate HIF1-specific gene expression (Pawlus et al., 2013). It has also been shown that HIF1 increases STAT3 activity through decreasing the levels of suppressor of cytokine signalling 3 (SOCS3) (Yokogami et al., 2013) and that constitutively active STAT3 directly interacts with the C-

terminal domain of HIF1A (Jung et al., 2008). Thus, regulation of individual genes in *rod*$^{\Delta Vhl}$ and *rod*$^{\Delta Vhl;Hif2a}$ mice may be attributable to HIF1, STAT3 or to both transcription factors.

To detect novel genes that were differentially regulated by chronically active HIF in rods, we determined the retinal transcriptomes of *rod*$^{\Delta Vhl}$, *rod*$^{\Delta Vhl;Hif1a}$ and of *Vhl*$^{flox/flox}$*;Hif1a*$^{flox/flox}$ controls at 11 weeks of age. Tables S1-S3 show the top 20 up- and downregulated genes of the individual comparisons. Table S1 lists genes that may be regulated by HIF1, HIF2 or STAT3, or by a combination of those, Table S2 shows genes that may be controlled by HIF1, STAT3 or by both of them, and genes in Table S3 may be regulated mostly by HIF2. Complete gene lists are available on request. Venn-diagrams summarized overlaps between the individual comparisons (Fig. S2). For a detailed description of the transcriptomic data, see the supplemental information.

Among the top 20 upregulated genes in *rod*$^{\Delta Vhl}$ mice were *Adm* and *Edn2* that were already verified by real-time PCR in Figure 6, and many genes with less well known function. Among those, we verified the expression pattern of lysyl oxidase like 4 (*Loxl4*), ladinin 1 (*Lad1*) and smoothelin like 2 (*Smtnl2*) by real-time PCR (Fig. 6) establishing them as HIF-responsive genes in mouse rods.

Gene expression in the human retina

The gene expression pattern in the mouse retina may also be relevant to understand ageing processes in human eyes. *LIF* that was strongly induced in the stressed (degenerating) mouse retina (Fig. 6) was also expressed at higher levels in the aged central and peripheral human retina. *EDN2*, another gene of the LIF-signalling pathway in mice (Joly et al., 2008), also showed a slight tendency of an age-dependent increase in expression both in the central and peripheral human retina. Similarly, *CASP1*, a proinflammatory protein (Sun and Scott, 2016) that has been implicated in inflammasome-triggered pyroptosis (Miao et al., 2011) revealed a trend of increased expression in aged human retinas (Fig. 8A,B) providing some evidence of potential inflammatory processes in the old eye.

Although *LAD1* was detected in only 5 out of 10 samples of the central retina and in 8 out of 9 samples of the peripheral retina, it showed a clear tendency of increased expression with age. Expression of *LOXL4* and *SMTNL2* was also detected, but expression of these genes followed a similar trend as observed for *RPL28* and was thus without apparent regulation during ageing (Fig. 8C,D). *LAD1* encodes an anchoring filament protein that has been associated with basement membranes (Klobučar et al., 2016). Its function in rods has not been determined but as a HIF1 target gene, *LAD1* might be involved in a structural adaptation to reduced oxygen levels. The HIF target *LOXL4* encodes a lysyl oxidase-like protein that has been implicated in collagen remodelling and metastasis formation in cancer (Semenza, 2012). Its expression in the retina has not yet been described but it might be involved in extracellular matrix remodelling during hypoxic periods. Even less is known about *SMTNL2* and its function, except that it may be a target gene of c-Jun N-terminal

kinase (Gordon et al., 2013). It will be of interest to localize these proteins in the normal and hypoxic retina and to elucidate their functions.

Anti-Hif1a gene therapy

Our genetic experiments showed that chronically active HIF1 was responsible for retinal degeneration in *rod*$^{\Delta Vhl}$ mice (Fig. 3). To establish a therapeutic approach aiming at the reduction of toxic HIF1 levels in photoreceptors, we used RNA interference through the AAV-mediated expression of an shRNA against *Hif1a*. A scrambled sequence served as control. Test of the shRNA and corresponding siRNA in NIH3T3 cells showed a highly efficient downregulation of HIF1A whereas STAT3 was not affected (Fig. 9A). AAV2/8(Y733F) viral particles carrying the *sh-Hif1a* or a scrambled sequence (*sh-ctrl*) as well as an *Egfp* expression cassette were injected into the subretinal space of *rod*$^{\Delta Vhl}$ mice at 5 weeks of age. *sh-Hif1a* and *Egfp* expression was driven by the ubiquitous U6 and CMV promoters, respectively (Fig. S3). Fundus fluorescence imaging at 6 months of age showed widespread expression of EGFP in both *sh-ctrl* and *sh-Hif1a* injected mice (Fig. 9B). The EGFP-positive retinal areas were surprisingly large in most injected mice. Possibly, retinal damage inflicted by the injection allowed the virus to diffuse and reach cells also peripheral to the injection site. OCT scans suggested that retinal architecture and layering in the ONL was more regular in retinas of *sh-Hif1a* injected eyes. Dorsoventral sections showed widespread expression of EGFP that was predominantly localized in the ONL and RPE (Fig. 9C). Treatment with *sh-Hif1a* resulted in a significantly increased ONL thickness that was most pronounced in the ventral retina and the dorsal retina close to the optic nerve head (Fig. 9D, E). These data strongly support the hypothesis that an *anti-Hif1a* approach may be developed as a therapy to protect photoreceptors in a situation of chronic tissue hypoxia.

Discussion

Tissue hypoxia is relevant for many pathologies that affect the retinal and choroidal vasculature in diseases such as diabetic retinopathy and neovascular AMD. The HIF-regulated growth factor VEGF for example is central for the development of choroidal neovascularization and anti-VEGF therapies show great benefit for patients suffering from wet AMD. However, chronic hypoxia may also slowly develop in the normal retina during ageing as indicated by the increased expression of HIF target genes in retinas of older donors (Fig. 1). Since chronic HIF activity led to age-dependent photoreceptor degeneration in mice, we and others hypothesize that chronically increased HIF activity in aged human retinas may be involved in AMD pathogenesis in at least some patients (Arjamaa et al., 2009; Kent, 2014). The hypothesis, however, does not imply that elevated HIF activity is toxic *per se* but that it may be one of several factors that contribute to multifactorial pathologies found in diseases such as dry AMD. Thus, reducing HIF levels may be a potential

strategy to eliminate one of the disease-contributing factors. This may lessen the burden for cells and potentially result in delaying or even preventing onset and/or progression of the disease.

Earlier we showed that a short 6-hour period of acute systemic hypoxic preconditioning activates HIF transcription factors in the retina and induces a response that protects photoreceptors (Grimm et al., 2002). This protective response depends either on HIF-independent mechanisms or on HIF activity in cells other than photoreceptors (Thiersch et al., 2009; Kast et al., 2016). Also, after mice are released from acute hypoxia retinal HIF1A returns to basal levels in less than one hour allowing the cells to quickly recover and re-establish a normoxic gene expression profile (Grimm et al., 2002; Thiersch et al., 2008). This is in contrast to the degeneration-inducing chronic activation of HIF1 in rods. Here, increased HIF1 activity over weeks or months may induce lasting changes in the cellular metabolism, which may lead to deficits such as reduced energy production and finally to cell death. Indeed, increased expression of *Pdk1* and *Glut1* in $rod^{\Delta Vhl}$ mice indicated a metabolic shift that may have resulted in reduced oxidative phosphorylation and thus reduced production of ATP in rods. If long-lasting, such a shift may curtail metabolic support and weaken the cells ability to survive periods of stress. Gene expression profiling revealed that HIF1-induced degeneration in $rod^{\Delta Vhl}$ mice followed similar signalling mechanisms as detected in other models of retinal degeneration. This included activation of the *Lif* - *Edn2* - *Fgf2* pathway (Samardzija et al., 2006a; Joly et al., 2008; Bürgi et al., 2009) with a late increase in *Casp1* expression (Samardzija et al., 2006b). In addition, we detected a variety of differentially expressed HIF1 target genes in retinas of $rod^{\Delta Vhl}$ mice, even before the onset of extensive degeneration. Among those, *LAD1, LOXL4* and *SMTNL2* were also detected in the human retina, with *LAD1* showing a tendency of increased expression with age.

The individual or combined genetic inactivation of the two HIFA transcription factors clearly showed that chronic activation of intrinsic HIF1 but not of HIF2 caused rod cells to die. This is of relevance and in marked contrast to RPE cells where chronically active HIF2, but not HIF1, leads to RPE loss (Kurihara et al., 2016). Intriguingly, the changes in cellular metabolism resulting from chronically active HIF1 in rods or HIF2 in RPE not only caused cell death *in cis* but also affected neighbouring cells (Fig. 4 and (Kurihara et al., 2016)) either through secreted factors, accumulation of toxic debris from degenerated cells or reduced metabolic support. The differential toxicity of chronically active HIF1 and HIF2 for rods and RPE, respectively, may reflect the highly divergent function of these two cell types and indicates that different aspects of the hypoxic response can be toxic. These might be altered lipid handling for RPE cells (Kurihara et al., 2016) and affected energy metabolism (see above) or other factors for rods.

Although it will be important to define the individual processes and hypoxia-related mechanisms that lead to HIF1-dependent cell death of rods and to HIF2-dependent degeneration of RPE cells, their detailed knowledge might not be essential to establish and test therapeutic approaches. Our genetic experiments showed that inactivation of *Hif1a* at the beginning of the hypoxic response rescued photoreceptor cells. Patients, however, may seek medical advice only

once pathological processes are ongoing. Thus, it is important to establish an interventional therapy. We tested RNA interference through the AAV-based delivery of an sh-RNA against *Hif1a* and showed that this may be an applicable strategy to protect photoreceptors in conditions of chronic HIF activity. However, from our data and data published by Kurihara and colleagues (Kurihara et al., 2016) it seems clear that a therapy targeting solely *Hif1a* in photoreceptors will not be sufficient for patients. Since reduced choroidal blood flow in the ageing eye causes tissue hypoxia affecting photoreceptors as well as the RPE, a combination therapy that targets both cell types and both *HIF1* and *HIF2* transcription factors may be needed. For the success of such a therapy it is mandatory that inactivation of HIF1 and HIF2 in adult photoreceptors and RPE does not lead to toxic effects. We recently showed that *Hif1a* and *Hif2a* can be safely inactivated in adult rods (Kast et al., 2016). Similarly, inactivation of *Hif1* alone in RPE cells had no obvious consequences (Lin et al., 2012) and we have collected preliminary evidence that simultaneous inactivation of both *Hif1a* and *Hif2a* did not adversely affect RPE function or survival (not shown). This is further supported by the normal appearance of the retina and RPE in mice lacking *Vhl*, *Hif1a* and *Hif2a* in the RPE (Kurihara et al., 2016). However, since a beneficial effect of *Hif1a* in retinal detachment has been suggested (Shelby et al., 2015), it may be advisable not to inhibit HIF completely but to merely reduce its expression or activity. In conclusion, our data show that a chronic activation of HIF transcription factors in photoreceptors induces retinal degeneration in a HIF1-dependent manner. Since several hypoxia-related genes may be expressed at higher levels in the retina of older donors, hypoxia-related mechanism may be relevant in the ageing human retina and may contribute to retinal diseases such as AMD. As HIF transcription factors do not seem essential for adult photoreceptors and RPE, anti-HIF therapies may prove beneficial for patients.

Material and Methods

Mice, genotyping and excision of floxed sequences

All mice were maintained as breeding colonies at the Laboratory Animal Services Center (LASC) of the University of Zurich in a 14 h : 10 h light-dark cycle with lights on a 6 am and lights off at 8 pm. Mice had access to food and water *ad libitum*. Average light intensity at cage levels was 60 -150 lux, depending on the position in the rack.

Vhl$^{flox/flox}$ (Haase et al., 2001), *Hif1a*$^{flox/flox}$ (Ryan et al., 2000), *Hif2a*$^{flox/flox}$ (Gruber et al., 2007) and OpsinCre (LMOPC1; (Le et al., 2006)) mice were intercrossed to obtain *rod*$^{\Delta Vhl}$ (*Vhl*$^{flox/flox}$*;OpsinCre*), *rod*$^{\Delta Vhl;Hif1a}$ (*Vhl*$^{flox/flox}$*;Hif1a*$^{flox/flox}$*; OpsinCre*), *rod*$^{\Delta Vhl;Hif2a}$ (*Vhl*$^{flox/flox}$*; Hif2a*$^{flox/flox}$*;OpsinCre*) and *rod*$^{\Delta Vhl;Hif1a;Hif2a}$ (*Vhl*$^{flox/flox}$*; Hif1a*$^{flox/flox}$*;Hif2a*$^{flox/flox}$*;OpsinCre*) mice. Breeding pairs were always heterozygous for *OpsinCre* and pups without *OpsinCre* served as littermate controls. Rod-specific *Cre* expression in *OpsinCre* mice starts around postnatal day 7 and increases up to 6 weeks of age (Le et al., 2006). All mice were homozygous for the *Rpe65*$_{450Leu}$ variant (Danciger et al., 2000). Genotyping was performed by conventional PCR using DNA isolated from ear clips and primer pairs as specified in Table 2. To detect alleles carrying CRE-mediated deletions of the floxed sequences, genomic DNA was isolated from retinal tissue and amplified by PCR using the primer pairs shown in Table 3. All PCR products were run on agarose gels and visualized using ethidium bromide.

Human retina samples

Peripheral nasal retina and central retina including the macula were isolated and frozen separately. RNA was isolated using the RNeasy kit (Qiagen, Hilden, Germany). cDNA synthesis and real-time PCR were performed as described for the mouse samples (see below) using human-specific primer pairs (Table 4).

Western blotting

Isolated retinas were sonicated in 200 µl of 100 mM Tris/HCl (pH 8,0). After centrifugation (1000 x g; 3 min) protein concentrations were determined in the supernatants using Bradford reagent (BioRad, Hercules, CA, USA). Standard SDS-PAGE and Western blotting were performed using the following primary antibodies: rabbit anti-HIF1A (1:2,000 – 1:4,000, NB100-479, Novus Biologicals, Cambridge, UK); rabbit anti-HIF2A (1:1,000, PAB12124, Abnova, Aachen, Germany); rabbit anti-pSTAT3$_{Tyr705}$ (1:500, #913L, Cell Signaling Technology, Danvers, MA, USA); rabbit anti-STAT3 (1:1,000, D3Z2G, Cell Signaling Technology); mouse anti-GFAP (1:1,000, G3893-Clone G-A-5, Sigma, Buchs, Switzerland); mouse anti-ACTB (1:10,000, A5441, Sigma). Primary antibodies were

diluted in 5% non-fat blocking milk (BioRad, Cressier, Switzerland) in TBST, added to the membrane and incubated over night at 4°C with gentle agitation. Appropriate HRP-conjugated secondary antibodies were added and signals detected using the Western lightning chemiluminescence reagent (PerkinElmer, Waltham, MA, USA). Signals were analysed using X-ray films.

Morphology, RPE flatmounts and immunofluorescence

Eyes were marked at the dorsal limbus, enucleated, fixed in glutaraldehyde (2.5% in cacodylate buffer) for 12 – 24 h at 4°C, trimmed, post-fixed in 1% osmium tetroxide and embedded in Epon 812 as described (Samardzija et al., 2006a). Tempero-nasal cross-sections of 0.5 µm were cut through the optic nerve head, stained with toluidine blue and analysed by light microscopy (Zeiss, Axioplan, Jena, Germany). RPE flatmounts were prepared and stained as described elsewhere (Oczos et al., 2014). Briefly, eyes were enucleated and incubated in 2% paraformaldehyde for 5 min. After removal of cornea and lens and incubation in phosphate buffer containing 140 mM NaCl and 2.7 mM KCl for 20 min, the detached retina was gently removed and the eyecup prepared for flat mounting by making four incisions. The resulting clover-leafed eyecup was post-fixed in 4% PFA for 1 hour. Alexa Fluor 488-phalloidin (1:100, A12379, Thermo Fischer Scientific, Waltham, MA, USA) was applied for 2 hours and nuclei stained with DAPI for 30 minutes. Flatmounts were analysed using a fluorescent microscope (Axioplan 2, Zeiss, Switzerland).

Electroretinography, fundus imaging and OCT

Pupils of dark-adapted mice were dilated with Cyclogyl 1% (Alcon Pharmaceuticals, Fribourg, Switzerland) and Neosynephrine 5% (Ursapharm Schweiz GmbH, Roggwil, Switzerland). Mice were anesthetized by a subcutaneous injection of ketamine (85 mg/kg, Parke-Davis, Berlin, Germany) and xylazine (4 mg/kg, Bayer AG, Leverkusen, Germany). A drop of atropin 0.5% (Thea Pharma, Schaffhausen, Switzerland) was applied to each cornea just prior to placing gold ring electrodes onto each cornea. Recordings were done with an LKC UTAS Bigshot unit (LKC Technologies, Inc. Gaithersburg, MD, USA) using flash intensities from -50 db (0.000025 cd*s/m^2) to 15 db (79 cd*s/m^2) for scotopic and from -10 db (25 cd*s/m^2) to 25 db (790 cd*s/m^2) for photopic responses. Before photopic responses were recorded, mice were light-adapted for 5 minutes. Ten recordings were averaged per light intensity.

For fundus imaging and OCT scans, pupils were dilated and mice anesthetized as described above. A drop of 2% methocel (OmniVision AG, Neuhausen, Switzerland) was applied to keep eyes moist. Fundus images and OCT scans were acquired using the Micron IV system (Phoenix Research Labs, Pleasanton, CA, USA) as described (Geiger et al., 2015).

RNA isolation, gene chip analysis and semi-quantitative real-time PCR

Total RNA was purified from retinas using RNA isolation kits (RNeasy, Qiagen, Hilden, Germany; Machery-Nagel, Düren, Germany) according to the manufacturer's instructions with an on-column DNAse treatment to digest residual genomic DNA. RNA concentrations were measured using a Nanodrop spectrophotometer (Thermo Fisher Scientific). The retinal transcriptomes of 11 weeks old *rod$^{\Delta Vhl}$, rod$^{\Delta Vhl;Hif1a}$, and Vhl$^{flox/flox}$;Hif1a$^{flox/flox}$* (controls, ctrl) mice were determined at the Functional Genomics Center of the University of Zurich using 'Agilent Mouse 4x44k V2' gene chips. RNA isolates from 4 individual mice per genotype were analysed.

For real-time PCR, cDNA was prepared from total RNA using oligo(dT) and M-MLV reverse transcriptase (Promega, Dübendorf, Switzerland). 10 ng cDNA was amplified in a LightCycler480 instrument with SYBR Green I master mix (Roche Diagnostics). Primer pairs (Table 4) avoided known SNPs and were designed to span large intronic regions. Levels were normalized to *Actb* as reference gene and relative expression was calculated using the comparative threshold cycle method ($\Delta\Delta C_T$). At least 3 mice per strain were used for each time point and strain. Deletion strains were compared to their respective control strain, which expression was set to 1 for each time point.

siRNA and shRNA-mediated gene silencing in NIH3T3 cells

NIH3T3 cells (ATCC® CRL-1658™) were plated on 6-well plates and grown in DMEM + 10% heat-inactivated fetal bovine serum (FBS, Gibco, Thermo Fisher Scientific) and 1% penicillin-streptomycin (Gibco) at 37°C and 5% CO_2 for 24 h. Cells were transfected with 80 pmol anti-*Hif1a* siRNA (5'-GUGGAUAGCGAUAUGGUCAUU-3') using lipofectamine RNAiMAX (Invitrogen, Thermo Fisher Scientific) and Opti-MEM (Gibco). A scrambled sequence (AllStars negative control siRNA; Qiagen) served as control. 24 h after transfection, cells were or were not exposed to hypoxia (0.2% O_2, 5% CO_2) at 37°C for 6 hours. After washing with pre-warmed PBS, cells were collected with sample buffer and Western blotting was performed as described above.

To test the efficiency of the corresponding anti-*Hif1a* shRNA, we used lentivirus-pseudotyped particles that were produced using HEK293T cells (ATCC® CRL-3216). Briefly, cells were plated in 75 cm^2 culture flasks and co-transfected with anti-*Hif1a* shRNA or non-target shRNA (Sigma) using the Vira-Power lentiviral expression vector system and lipofectamine 3000 (Invitrogen, Thermo Fisher Scientific). The following day, the medium was replaced with fresh medium containing 10% FBS and 1% penicillin-streptomycin. The supernatant was collected 72 h post transfection, centrifuged to pellet large particles and debris, and filtered through a 0.45 µm filter (Merck&Cie, Schaffhausen, Switzerland). The filtrate was used to transduce NIH3T3 cells with lentiviral particles containing *sh-Hif1a* or *sh-ctrl* and 6 µg/mL polybrene, followed by selection with 2 µg/mL puromycin. To test *shHif1a*-mediated downregulation of HIF1A in hypoxia, cells were exposed to 0.2% O_2 for 6

h and harvested immediately thereafter. Protein homogenates were used for Western blotting as described above.

AAV–mediated shRNA expression and analysis

pAAV2.1-U6-*shHif1a*-CMV-EGFP ($3x10^{11}$ vector genomes (vg)/µL) and pAAV2.1-U6-sh-*control*-CMV-EGFP ($3x10^{10}$ vg/µL) (Fig. S3) were packaged as AAV2/8Y733F and produced as described recently (Becirovic et al., 2016). For subretinal injections, the pupils were dilated and mice were anesthetized as described above. Viscotears (Bausch & Lomb Swiss AG, Zug, Switzerland) were applied to keep the eyes moist. $1.5x10^{10}$ total vg were injected into the subretinal space using the NanoFil Intraocular Injection Kit (WPI, Berlin, Germany). To visualize and control the injection, we added a small amount of fluorescein (0.1 mg/mL, Akorn Inc., IL, USA) to the AAV solution. Mice were injected at 5 weeks of age and analysed at 6 months of age. After euthanasia, eyes were marked nasally, enucleated and fixed in 4% paraformaldehyde for 1 h at 4°C as described (Heynen et al., 2011). Dorsoventral cryosections (12 µm) were cut, counterstained with DAPI (4',6-Diamidine-2'-phenylindole dihydrochloride, Roche, Basel, Switzerland) and analysed by fluorescence microscopy (Axioplan; Zeiss, Jena, Germany). The thickness of the outer nuclear layer was measured at indicated distances from the optic nerve head using the Adobe Photoshop CS6 ruler tool (Adobe Systems, Inc., San Jose, CA, USA). Areas of tissue that was damaged due to injections were excluded from measurements. The average ONL thickness, excluding the optic nerve head, was calculated and compared (Lewin et al., 1998) after treatment with *sh-Hif1a (*115 measurements) and *sh-ctrl* (99 measurements) viruses.

Statistical analysis

a- and b-wave amplitudes of ERG recordings were tested using 2-way ANOVA with Sidak's multiple comparison test. Gene expression in deletion strains was compared to their respective control strains at each time point individually and evaluated by Student's t-test (GraphPad Prism, San Diego, CA, USA). Student's t-test was also used to compare the overall ONL thickness of *sh-Hif1a* and *sh-crl* treated mice. *P*-values < 0.05 were considered to show significant differences. Linear regression of gene expression in human samples was calculated using Prism software (GraphPad).

Study approval

Mouse experiments were performed in accordance with the regulations of the Veterinary Authority of Zurich (ZH109/2013; ZH219/2012; ZH216/2015; ZH141/2016) and with the statement

of ‘The Association for Research in Vision and Ophthalmology’ for the use of animals in research. Human retinas were collected from donor eyes that were enucleated post-mortem at the University Hospital Zurich, Switzerland. Collection of retinas was approved by the ethics committee of Zurich, Switzerland (KEK-ZH-Nr: 2015-0489) and adhered to the tenets of the Declaration of Helsinki.

Acknowledgements

The authors thank Andrea Gubler, Cornelia Imsand and Sarah Nötzli for excellent technical support, Prof. Ian Frew (University Medical Center Freiburg, Germany) for advice on the *Hif1a* siRNA sequence and Prof. Roland Wenger (University of Zürich, Switzerland) for providing lentiviral vectors. Supported by the Swiss National Science Foundation (SNF #31003A_133043 and 31003A_173008).

Author contributions:

MB: siRNA, shRNA, AAV-mediated rescue, contribution to most experiments, manuscript editing

DA: chip experiments and analysis, contribution to most experiments, draft of an early manuscript version

FS: human retina samples: RNA and real-time PCR

KK: fundus imaging, OCT, morphology

CS: transcriptomic analysis, tables

MS: analysis of data, discussion, manuscript editing

SM: cloning of shRNA, generation of AAV

MB: discussion of data, providing AAV

IM: human eye sampling

FB: human eye sampling

DB: discussion of data, development of hypothesis

CG: ERG recordings, morphology, data analysis, manuscript

References

Arjamaa, O., M. Nikinmaa, A. Salminen, and K. Kaarniranta. 2009. Regulatory role of HIF-1alpha in the pathogenesis of age-related macular degeneration (AMD). *Ageing Res Rev*. 8:349-358. doi:10.1016/j.arr.2009.06.002.

Becirovic, E., S. Böhm, O.N. Nguyen, L.M. Riedmayr, V. Hammelmann, C. Schön, E.S. Butz, C. Wahl-Schott, M. Biel, and S. Michalakis. 2016. AAV Vectors for FRET-Based Analysis of Protein-Protein Interactions in Photoreceptor Outer Segments. *Front Neurosci*. 10:356. doi:10.3389/fnins.2016.00356.

Berenberg, T.L., T.I. Metelitsina, B. Madow, Y. Dai, G.S. Ying, J.C. Dupont, L. Grunwald, A.J. Brucker, and J.E. Grunwald. 2012. The association between drusen extent and foveolar choroidal blood flow in age-related macular degeneration. *Retina*. 32:25-31. doi:10.1097/IAE.0b013e3182150483.

Bürgi, S., M. Samardzija, and C. Grimm. 2009. Endogenous leukemia inhibitory factor protects photoreceptor cells against light-induced degeneration. *Mol Vis*. 15:1631-1637

Campochiaro, P.A. 2015. Molecular pathogenesis of retinal and choroidal vascular diseases. *Prog Retin Eye Res*. 49:67-81. doi:10.1016/j.preteyeres.2015.06.002.

Caprara, C., and C. Grimm. 2012. From oxygen to erythropoietin: relevance of hypoxia for retinal development, health and disease. *Prog Retin Eye Res*. 31:89-119. doi:10.1016/j.preteyeres.2011.11.003.

Ciulla, T.A., A. Harris, H.S. Chung, R.P. Danis, L. Kagemann, L. McNulty, L.M. Pratt, and B.J. Martin. 1999. Color Doppler imaging discloses reduced ocular blood flow velocities in nonexudative age-related macular degeneration. *Am J Ophthalmol*. 128:75-80

Coleman, D.J., R.H. Silverman, M.J. Rondeau, H.O. Lloyd, A.A. Khanifar, and R.V. Chan. 2013. Age-related macular degeneration: choroidal ischaemia. *Br J Ophthalmol*. 97:1020-1023. doi:10.1136/bjophthalmol-2013-303143.

Curcio, C.A., N.E. Medeiros, and C.L. Millican. 1996. Photoreceptor loss in age-related macular degeneration. *Invest Ophthalmol Vis Sci*. 37:1236-1249

Dallinger, S., O. Findl, K. Strenn, H.G. Eichler, M. Wolzt, and L. Schmetterer. 1998. Age dependence of choroidal blood flow. *J Am Geriatr Soc*. 46:484-487

Danciger, M., M.T. Matthes, D. Yasamura, N.B. Akhmedov, T. Rickabaugh, S. Gentleman, T.M. Redmond, M.M. La Vail, and D.B. Farber. 2000. A QTL on distal chromosome 3 that influences the severity of light-induced damage to mouse photoreceptors. *Mamm Genome*. 11:422-427

Feigl, B. 2009. Age-related maculopathy - linking aetiology and pathophysiological changes to the ischaemia hypothesis. *Prog Retin Eye Res*. 28:63-86. doi:10.1016/j.preteyeres.2008.11.004.

Geiger, P., M. Barben, C. Grimm, and M. Samardzija. 2015. Blue light-induced retinal lesions, intraretinal vascular leakage and edema formation in the all-cone mouse retina. *Cell Death Dis*. 6:e1985. doi:10.1038/cddis.2015.333.

Gordon, E.A., T.C. Whisenant, M. Zeller, R.M. Kaake, W.M. Gordon, P. Krotee, V. Patel, L. Huang, P. Baldi, and L. Bardwell. 2013. Combining docking site and phosphosite predictions to find new substrates: identification of smoothelin-like-2 (SMTNL2) as a c-Jun N-terminal kinase (JNK) substrate. *Cell Signal*. 25:2518-2529. doi:10.1016/j.cellsig.2013.08.004.

Grimm, C., A. Wenzel, M. Groszer, H. Mayser, M. Seeliger, M. Samardzija, C. Bauer, M. Gassmann, and C.E. Remé. 2002. HIF-1-induced erythropoietin in the hypoxic retina protects against light-induced retinal degeneration. *Nat Med*. 8:718-724. doi:10.1038/nm723.

Gruber, M., C.J. Hu, R.S. Johnson, E.J. Brown, B. Keith, and M.C. Simon. 2007. Acute postnatal ablation of Hif-2alpha results in anemia. *Proc Natl Acad Sci U S A*. 104:2301-2306. doi:10.1073/pnas.0608382104.

Grunwald, J.E., T.I. Metelitsina, J.C. Dupont, G.S. Ying, and M.G. Maguire. 2005. Reduced foveolar choroidal blood flow in eyes with increasing AMD severity. *Invest Ophthalmol Vis Sci*. 46:1033-1038. doi:10.1167/iovs.04-1050.

Guo, K., G. Searfoss, D. Krolikowski, M. Pagnoni, C. Franks, K. Clark, K.T. Yu, M. Jaye, and Y. Ivashchenko. 2001. Hypoxia induces the expression of the pro-apoptotic gene BNIP3. *Cell Death Differ*. 8:367-376. doi:10.1038/sj.cdd.4400810.

Haase, V.H., J.N. Glickman, M. Socolovsky, and R. Jaenisch. 2001. Vascular tumors in livers with targeted inactivation of the von Hippel-Lindau tumor suppressor. *Proc Natl Acad Sci U S A*. 98:1583-1588

Heynen, S.R., N. Tanimoto, S. Joly, M.W. Seeliger, M. Samardzija, and C. Grimm. 2011. Retinal degeneration modulates intracellular localization of CDC42 in photoreceptors. *Mol Vis*. 17:2934-2946

Jaakkola, P., D.R. Mole, Y.M. Tian, M.I. Wilson, J. Gielbert, S.J. Gaskell, A. von Kriegsheim, H.F. Hebestreit, M. Mukherji, C.J. Schofield, P.H. Maxwell, C.W. Pugh, and P.J. Ratcliffe. 2001. Targeting of HIF-alpha to the von Hippel-Lindau ubiquitylation complex by O2-regulated prolyl hydroxylation. *Science*. 292:468-472. doi:10.1126/science.1059796.

Joly, S., C. Lange, M. Thiersch, M. Samardzija, and C. Grimm. 2008. Leukemia inhibitory factor extends the lifespan of injured photoreceptors in vivo. *J Neurosci*. 28:13765-13774. doi:10.1523/JNEUROSCI.5114-08.2008.

Jung, J.E., H.S. Kim, C.S. Lee, Y.J. Shin, Y.N. Kim, G.H. Kang, T.Y. Kim, Y.S. Juhnn, S.J. Kim, J.W. Park,

S.K. Ye, and M.H. Chung. 2008. STAT3 inhibits the degradation of HIF-1alpha by pVHL-mediated ubiquitination. *Exp Mol Med*. 40:479-485. doi:10.3858/emm.2008.40.5.479.

Kast, B., C. Schori, and C. Grimm. 2016. Hypoxic preconditioning protects photoreceptors against light damage independently of hypoxia inducible transcription factors in rods. *Exp Eye Res*. 146:60-71. doi:10.1016/j.exer.2015.12.008.

Kent, D.L. 2014. Age-related macular degeneration: beyond anti-angiogenesis. *Mol Vis*. 20:46-55

Klobučar, M., M. Sedić, P. Gehrig, J. Grossmann, M. Bilić, L. Kovač-Bilić, K. Pavelić, and S. Kraljević Pavelić. 2016. Basement membrane protein ladinin-1 and the MIF-CD44-β1 integrin signaling axis are implicated in laryngeal cancer metastasis. *Biochim Biophys Acta*. 1862:1938-1954. doi:10.1016/j.bbadis.2016.07.014.

Kurihara, T., Y. Kubota, Y. Ozawa, K. Takubo, K. Noda, M.C. Simon, R.S. Johnson, M. Suematsu, K. Tsubota, S. Ishida, N. Goda, T. Suda, and H. Okano. 2010. von Hippel-Lindau protein regulates transition from the fetal to the adult circulatory system in retina. *Development*. 137:1563-1571. doi:10.1242/dev.049015.

Kurihara, T., P.D. Westenskow, M.L. Gantner, Y. Usui, A. Schultz, S. Bravo, E. Aguilar, C. Wittgrove, M.S. Friedlander, L.P. Paris, E. Chew, G. Siuzdak, and M. Friedlander. 2016. Hypoxia-induced metabolic stress in retinal pigment epithelial cells is sufficient to induce photoreceptor degeneration. *Elife*. 510.7554/eLife.14319.

Lam, A.K., S.T. Chan, H. Chan, and B. Chan. 2003. The effect of age on ocular blood supply determined by pulsatile ocular blood flow and color Doppler ultrasonography. *Optom Vis Sci*. 80:305-311

Lange, C., C. Caprara, N. Tanimoto, S. Beck, G. Huber, M. Samardzija, M. Seeliger, and C. Grimm. 2011a. Retina-specific activation of a sustained hypoxia-like response leads to severe retinal degeneration and loss of vision. *Neurobiol Dis*. 41:119-130. doi:10.1016/j.nbd.2010.08.028.

Lange, C., S.R. Heynen, N. Tanimoto, M. Thiersch, Y.Z. Le, I. Meneau, M.W. Seeliger, M. Samardzija, C. Caprara, and C. Grimm. 2011b. Normoxic activation of hypoxia-inducible factors in photoreceptors provides transient protection against light-induced retinal degeneration. *Invest Ophthalmol Vis Sci*. 52:5872-5880. doi:10.1167/iovs.11-7204.

Le, Y.Z., L. Zheng, W. Zheng, J.D. Ash, M.P. Agbaga, M. Zhu, and R.E. Anderson. 2006. Mouse opsin promoter-directed Cre recombinase expression in transgenic mice. *Mol Vis*. 12:389-398

Lewin, A.S., K.A. Drenser, W.W. Hauswirth, S. Nishikawa, D. Yasumura, J.G. Flannery, and M.M. LaVail. 1998. Ribozyme rescue of photoreceptor cells in a transgenic rat model of autosomal dominant retinitis pigmentosa. *Nat Med*. 4:967-971

Lin, M., Y. Hu, Y. Chen, K.K. Zhou, J. Jin, M. Zhu, Y.Z. Le, J. Ge, and J.X. Ma. 2012. Impacts of hypoxia-inducible factor-1 knockout in the retinal pigment epithelium on choroidal neovascularization. *Invest Ophthalmol Vis Sci*. 53:6197-6206. doi:10.1167/iovs.11-8936.

Loboda, A., A. Jozkowicz, and J. Dulak. 2010. HIF-1 and HIF-2 transcription factors--similar but not identical. *Mol Cells*. 29:435-442. doi:10.1007/s10059-010-0067-2.

Maxwell, P.H., M.S. Wiesener, G.W. Chang, S.C. Clifford, E.C. Vaux, M.E. Cockman, C.C. Wykoff, C.W. Pugh, E.R. Maher, and P.J. Ratcliffe. 1999. The tumour suppressor protein VHL targets hypoxia-inducible factors for oxygen-dependent proteolysis. *Nature*. 399:271-275. doi:10.1038/20459.

Miao, E.A., J.V. Rajan, and A. Aderem. 2011. Caspase-1-induced pyroptotic cell death. *Immunol Rev*. 243:206-214. doi:10.1111/j.1600-065X.2011.01044.x.

Oczos, J., I. Sutter, B. Kloeckener-Gruissem, W. Berger, M. Riwanto, K. Rentsch, T. Hornemann, A. von Eckardstein, and C. Grimm. 2014. Lack of paraoxonase 1 alters phospholipid composition, but not morphology and function of the mouse retina. *Invest Ophthalmol Vis Sci*. 55:4714-4727. doi:10.1167/iovs.14-14332.

Okawa, H., A.P. Sampath, S.B. Laughlin, and G.L. Fain. 2008. ATP consumption by mammalian rod photoreceptors in darkness and in light. *Curr Biol*. 18:1917-1921. doi:10.1016/j.cub.2008.10.029.

Pawlus, M.R., L. Wang, A. Murakami, G. Dai, and C.J. Hu. 2013. STAT3 or USF2 contributes to HIF target gene specificity. *PLoS One*. 8:e72358. doi:10.1371/journal.pone.0072358.

Ryan, H.E., M. Poloni, W. McNulty, D. Elson, M. Gassmann, J.M. Arbeit, and R.S. Johnson. 2000. Hypoxia-inducible factor-1alpha is a positive factor in solid tumor growth. *Cancer Res*. 60:4010-4015

Samardzija, M., A. Wenzel, S. Aufenberg, M. Thiersch, C. Remé, and C. Grimm. 2006a. Differential role of Jak-STAT signaling in retinal degenerations. *FASEB J*. 20:2411-2413. doi:10.1096/fj.06-5895fje.

Samardzija, M., A. Wenzel, M. Thiersch, R. Frigg, C. Remé, and C. Grimm. 2006b. Caspase-1 ablation protects photoreceptors in a model of autosomal dominant retinitis pigmentosa. *Invest Ophthalmol Vis Sci*. 47:5181-5190. doi:10.1167/iovs.06-0556.

Semenza, G.L. 2012. Molecular mechanisms mediating metastasis of hypoxic breast cancer cells. *Trends Mol Med*. 18:534-543. doi:10.1016/j.molmed.2012.08.001.

Shelby, S.J., P.S. Angadi, Q.D. Zheng, J. Yao, L. Jia, and D.N. Zacks. 2015. Hypoxia inducible factor 1α contributes to regulation of autophagy in retinal detachment. *Exp Eye Res*. 137:84-93. doi:10.1016/j.exer.2015.06.016.

Simó, R., J.M. Sundstrom, and D.A. Antonetti. 2014. Ocular Anti-VEGF therapy for diabetic retinopathy: the role of VEGF in the pathogenesis of diabetic retinopathy. *Diabetes Care*. 37:893-899. doi:10.2337/dc13-

2002.
Sparrow, J.R., M. Marsiglia, R. Allikmets, S. Tsang, W. Lee, T. Duncker, and J. Zernant. 2015. Flecks in Recessive Stargardt Disease: Short-Wavelength Autofluorescence, Near-Infrared Autofluorescence, and Optical Coherence Tomography. *Invest Ophthalmol Vis Sci*. 56:5029-5039. doi:10.1167/iovs.15-16763.
Stefánsson, E., A. Geirsdóttir, and H. Sigurdsson. 2011. Metabolic physiology in age related macular degeneration. *Prog Retin Eye Res*. 30:72-80. doi:10.1016/j.preteyeres.2010.09.003.
Sun, Q., and M.J. Scott. 2016. Caspase-1 as a multifunctional inflammatory mediator: noncytokine maturation roles. *J Leukoc Biol*. 100:961-967. doi:10.1189/jlb.3MR0516-224R.
Thiersch, M., C. Lange, S. Joly, S. Heynen, Y.Z. Le, M. Samardzija, and C. Grimm. 2009. Retinal neuroprotection by hypoxic preconditioning is independent of hypoxia-inducible factor-1 alpha expression in photoreceptors. *Eur J Neurosci*. 29:2291-2302. doi:10.1111/j.1460-9568.2009.06781.x.
Thiersch, M., W. Raffelsberger, R. Frigg, M. Samardzija, A. Wenzel, O. Poch, and C. Grimm. 2008. Analysis of the retinal gene expression profile after hypoxic preconditioning identifies candidate genes for neuroprotection. *BMC Genomics*. 9:73. doi:10.1186/1471-2164-9-73.
Webb, J.D., M.L. Coleman, and C.W. Pugh. 2009. Hypoxia, hypoxia-inducible factors (HIF), HIF hydroxylases and oxygen sensing. *Cell Mol Life Sci*. 66:3539-3554. doi:10.1007/s00018-009-0147-7.
Yokogami, K., S. Yamashita, and H. Takeshima. 2013. Hypoxia-induced decreases in SOCS3 increase STAT3 activation and upregulate VEGF gene expression. *Brain Tumor Pathol*. 30:135-143. doi:10.1007/s10014-012-0122-0.

Figure 1

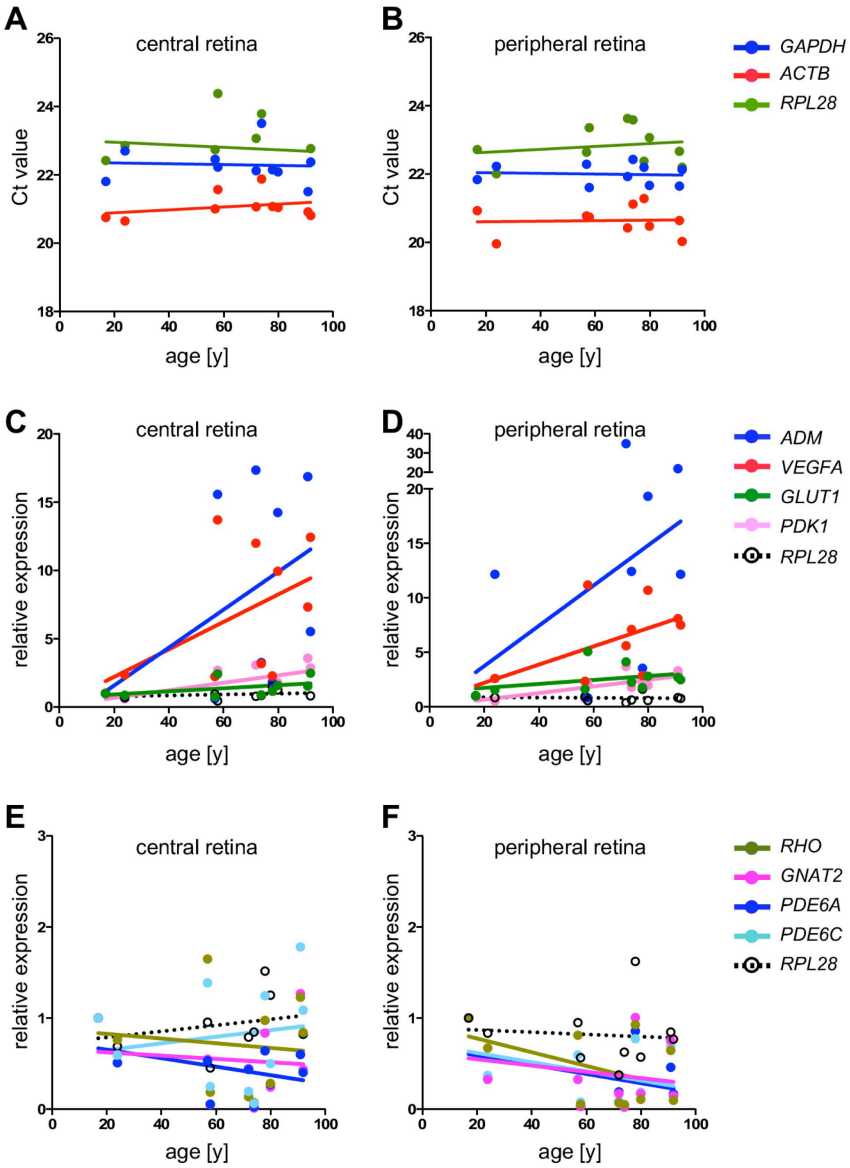

Fig 1. Expression of HIF controlled genes in the human retina.

A,B) Ct-values of housekeeping genes *GAPDH, RPL28* and *ACTB* in the central and peripheral retina of 10 donor eyes. 10 ng cDNA were used as template. **C,D)** Expression of HIF regulated genes in the central and peripheral retina of 10 donor eyes relative to the expression level in a 17 year old donor. **E,F)** Expression of rod- and cone-specific genes in the central and peripheral retina of 10 donor eyes relative to the expression level in a 17 year old donor. Expression of genes was normalized to *ACTB* and the housekeeping gene *RPL28* served as control (C-F). Dots: individual values. Lines: linear regression through all values. Note the tendency of hypoxia-regulated genes to be expressed at higher levels and photoreceptor-specific genes to be expressed at lower levels in aged human retinas.

Figure 2

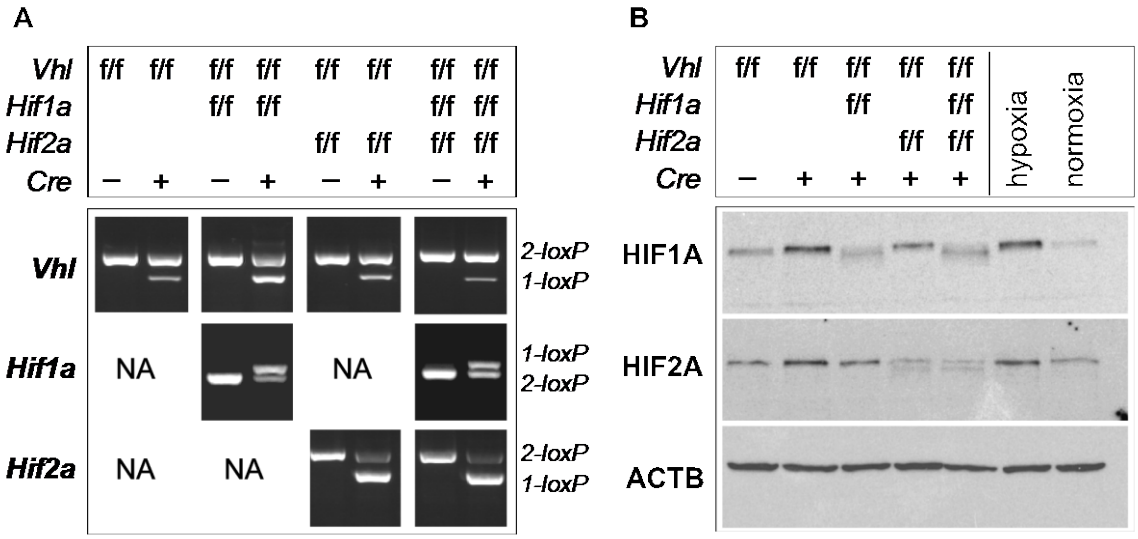

Fig 2. Characterization of mouse strains.

A) Cre-positive (+) and Cre-negative (-) strains carrying floxed (f/f) alleles of *Vhl*, *Hif1a* and *Hif2a* were tested for excision of floxed sequences from genomic DNA of the retina by conventional PCR. *2-loxP*: not excised; *1-loxP*: excised; NA: not applicable. Note that genomic DNA was isolated from total retina that included cells without CRE expression. Thus, the 2-*loxP* band was expected in all samples. **B)** Western blots for HIF1A and HIF2A in retinal homogenates of strains with genotypes as indicated. ACTB was used as control. Mice were 10-11 weeks of age. Retinal homogenates of wild type mice exposed to 6 h of hypoxia (7% O_2) were used as positive controls. Homogenates of normoxic wild type mice served as negative controls. *N* = 3.

Figure 3

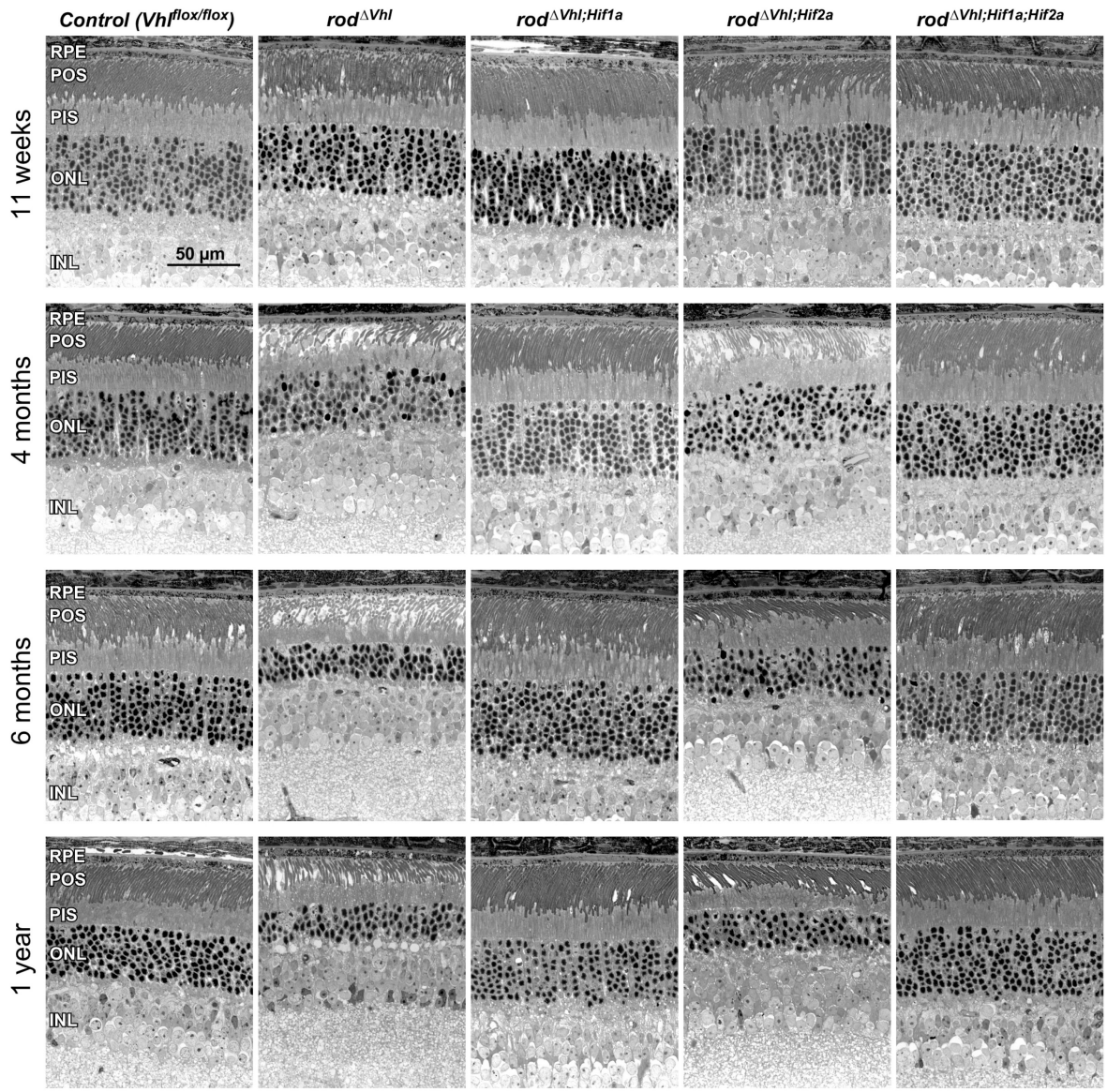

Fig 3. Retinal morphology of mice with chronically activated HIF transcription factors in rods.

Retinal morphology was tested at 11 weeks, 4 months, 6 months and 1 year of age as indicated. Cre-negative *Vhl*$^{flox/flox}$ mice served as controls. RPE: retinal pigment epithelium; POS: photoreceptor outer segments; PIS: photoreceptor inner segments; ONL: outer nuclear layer; INL: inner nuclear layer. Scale bar: 50 µm. $N \geq 3$.

Figure 4

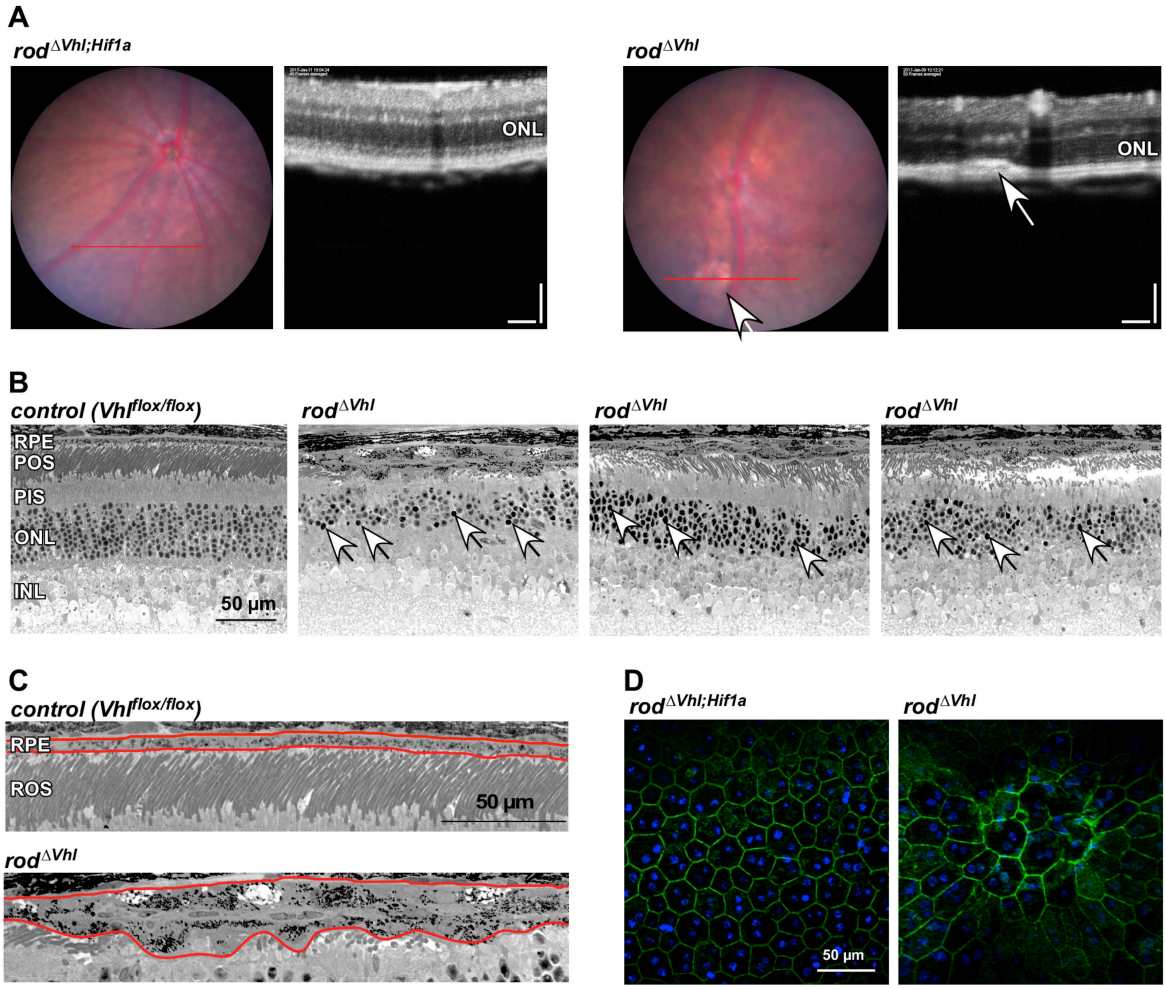

Fig 4. RPE phenotype in *rod*$^{\Delta Vhl}$ mice at 4 months of age.

A) Fundus imaging and OCT scans of *rod*$^{\Delta Vhl;Hif1a}$ mice (left, served as controls) and *rod*$^{\Delta Vhl}$ mice (right) at 4 months of age. Red lines indicate the positions of the OCT scans. White arrows point to RPE irregularities in *rod*$^{\Delta Vhl}$ mice. **B)** Morphology of a control and three different *rod*$^{\Delta Vhl}$ mice at 4 months of age. Shown are the focused regions where RPE irrgularities were detected. Arrows: examples of pyknotic nuclei. **C)** Higher magnifications of the RPE of a control and a *rod*$^{\Delta Vhl}$ mouse. Red lines indicate borders of the RPE. **D)** RPE flatmounts of *rod*$^{\Delta Vhl;Hif1a}$ and *rod*$^{\Delta Vhl}$ mice as indicated. Green: F-actin stained with phalloidin. Blue: nuclei stained with DAPI. RPE: retinal pigment epithelium; POS: photoreceptor outer segments; PIS: photoreceptor inner segments; ONL: outer nuclear layer; INL: inner nuclear layer. Scale bars: 100 µm (A) and 50 µm (B-D).

Figure 5

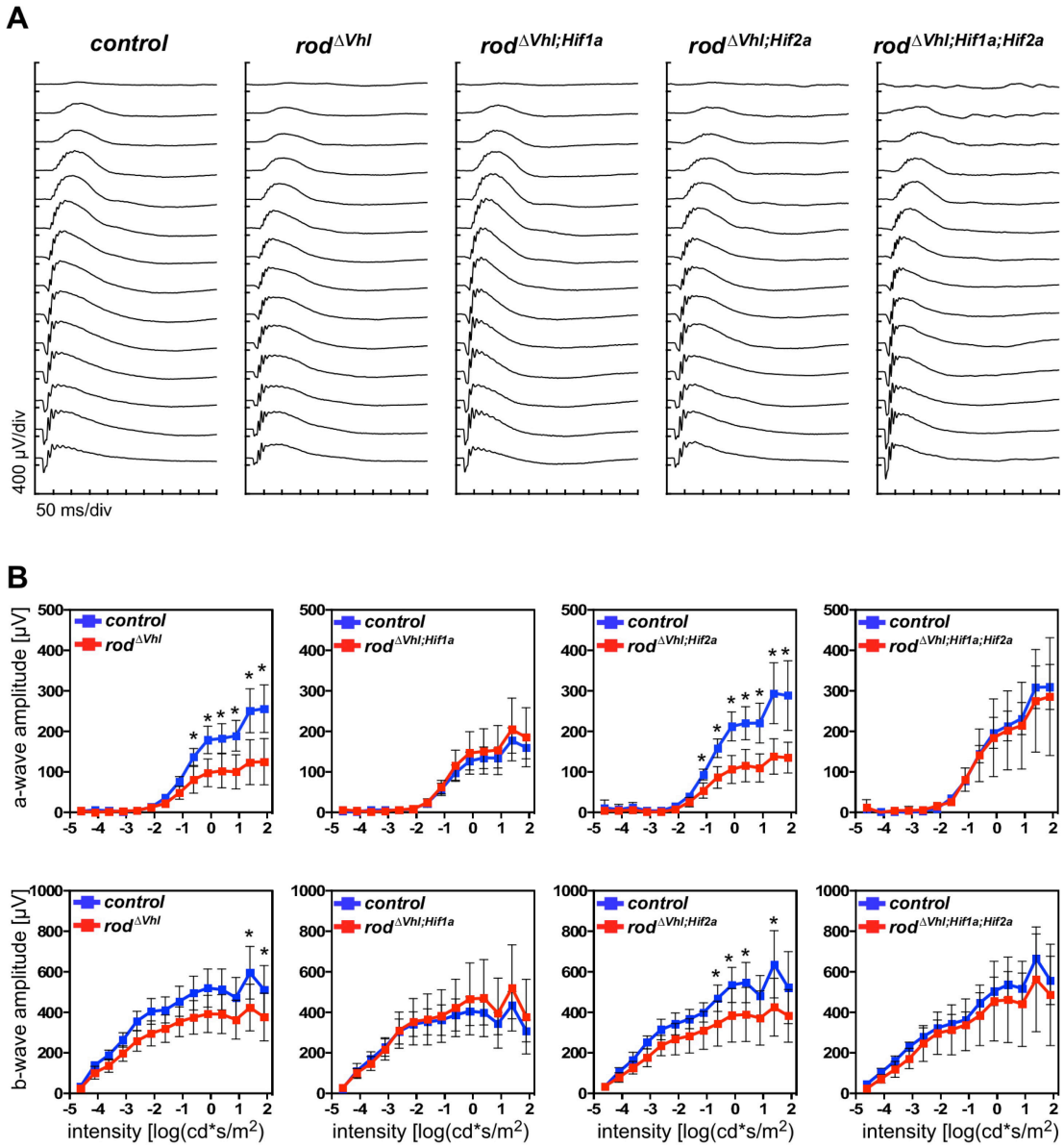

Fig 5. Scotopic retinal function of *rod*$^{\Delta Vhl}$, *rod*$^{\Delta Vhl;Hif1a}$, *rod*$^{\Delta Vhl;Hif2a}$, and *rod*$^{\Delta Vhl;Hif1a;Hif2a}$ mice at 6 months of age.

A) Scotopic ERG traces were recorded after light stimuli of increasing light intensities. Shown are representative traces. Cre-negative *Vhl*$^{flox/flox}$ mice served as controls. **B)** Scotopic a- and b-wave amplitudes plotted as a function of stimulus intensity. Control mice were Cre-negative littermates of the respective strains. Shown are averages ± SD. *N* = 6 eyes (3 mice), except for controls of *rod*$^{\Delta Vhl;Hif2a}$ (*N* = 5) and of *rod*$^{\Delta Vhl;Hif2a}$ (*N* = 7), and for *rod*$^{\Delta Vhl;Hif1a;Hif2a}$ (*N* = 4). *: P < 0.05. 2-way ANOVA with Sidak's multiple comparison test.

Figure 6

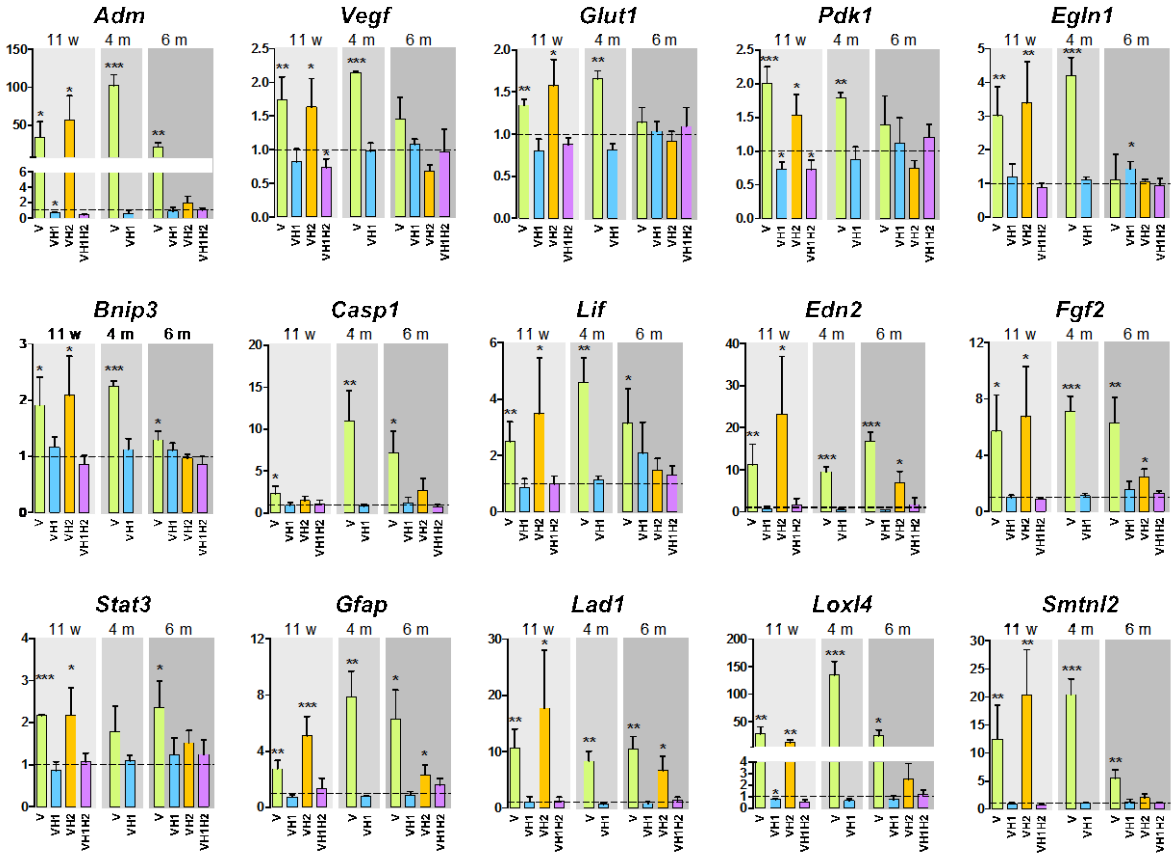

Fig 6. Retinal gene expression.

Retinal expression of indicated genes was tested in retinas of *rod*$^{\Delta Vhl}$ (V), *rod*$^{\Delta Vhl;Hif1a}$ (VH1), *rod*$^{\Delta Vhl;Hif2a}$ (VH2), and *rod*$^{\Delta Vhl;Hif1a;Hif2a}$ (VH1H2) mice at 11 weeks, 4 months and 6 months of age. Expression levels were calculated relative to their respective Cre-negative controls (set to 1; dotted line). Shown are means ± SD of N = 3-4. *: P < 0.05; **: P < 0.01; ***: P < 0.001. Individual comparisons between Cre-positive and Cre-negative mice of each genotype were done using Student's t-test.

Figure 7

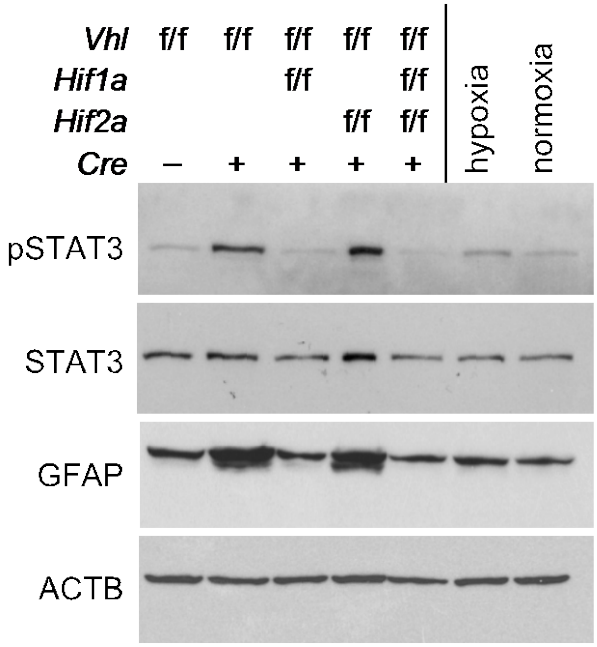

Fig 7. Protein levels in retinal homogenates.

Western blot for indicated proteins in mice at 10-11 weeks of age. Retinal homogenates of wild type mice exposed to 6 h of hypoxia (7% O_2) were used as positive controls. Homogenates of normoxic wild type mice served as negative controls. Note that homogenates were the same as those used for Fig. 2B and the same ACTB control is shown. *N* = 3.

Figure 8

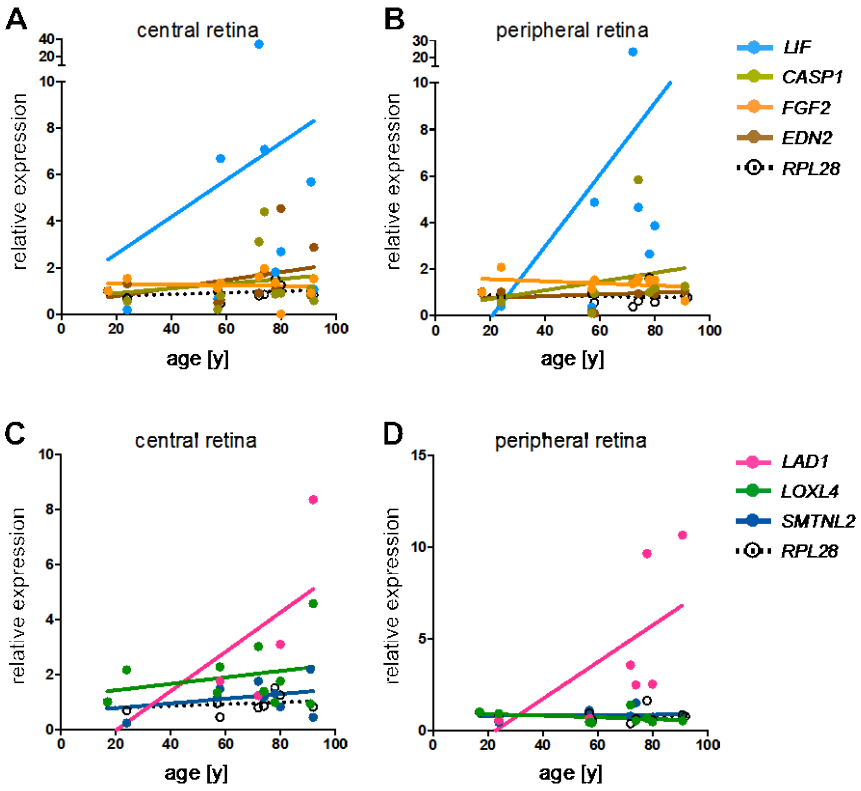

Fig 8. Age-dependent gene expression in the human retina.

A,B) Expression of *LIF*, *CASP1*, *FGF2* and *EDN2* in the central and peripheral human retina. **C,D)** Expression of *LOXL4*, *LAD1* and *SMTNL2* in the central and peripheral human retina. Expression levels were normalized to *ACTB* and are shown relative to the levels in the retina of a 17 year old donor. The housekeeping gene RLP28 served as control. Dots: individual values. Lines: linear regression through all values.

Figure 9

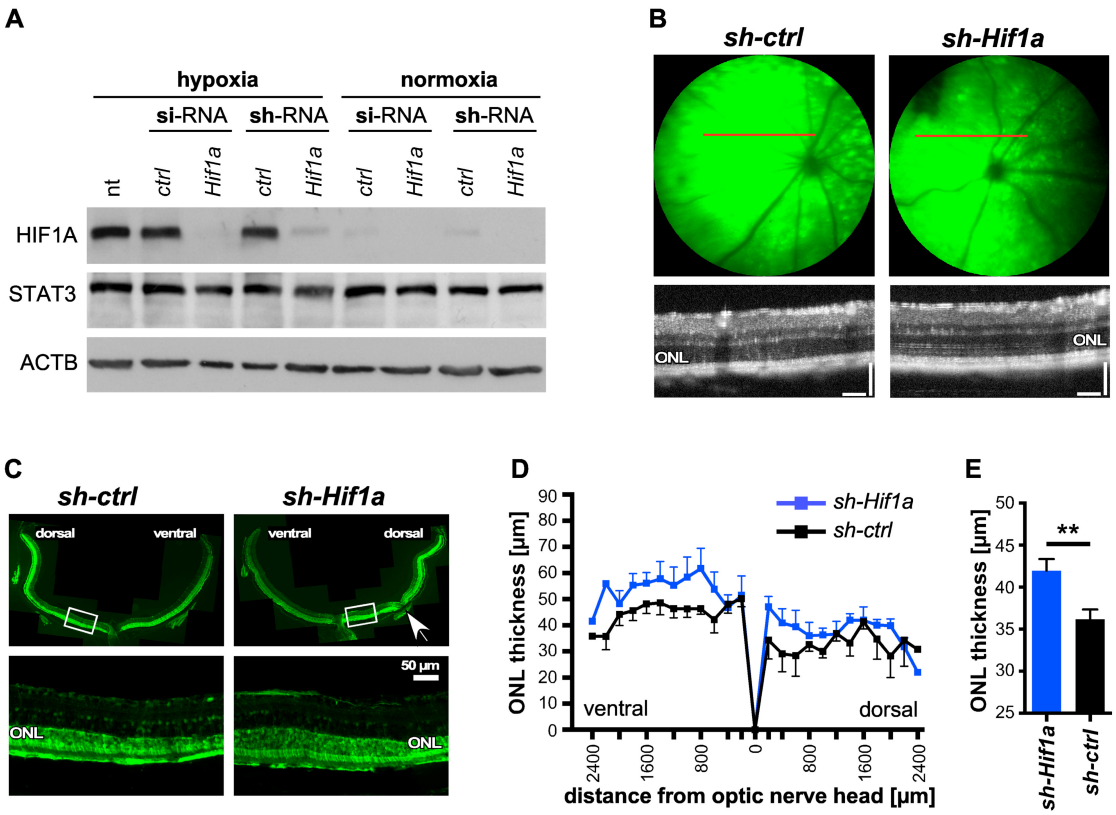

Fig 9. Efficacy of RNA interference and anti-*Hif1a* gene therapy.

A) NIH3T3 cells were transiently transfected with *si-Hif1a* RNA or stably transfected with *shHif1a,* or treated with the respective scrambled controls as indicated, followed by exposure to 0.2% oxygen (hypoxia) or normoxia. Not transfected cells (nt) exposed to hypoxia served as controls. Levels of HIF1A, STAT3 and ACTB were detected by Western blotting. **B)** Fluorescent fundus imaging (upper panels) and OCT scans (lower panels) of eyes that received a subretinal injection of AAV2/8(Y733F) particles expressing either the control sh-RNA sequence (left, *sh-ctrl*) or the *sh-Hif1a* sequence (*sh-Hif1a*, right) together with EGFP. The red line in the fundus image indicates the position of the OCT scan. **C)** Retinal cross sections of mice injected with the control (left, *sh-ctrl*) or the *sh-Hif1a* virus (right, *sh-Hif1a*). Lower panels are higher magnifications of retinal areas marked with a white square in the upper panels. White arrow: damage due to injection. Scale bar: 50 µm. **D)** Spidergram of the ONL thickness 5 months after injection of the control (black line, *sh-ctrl*) or the *sh-Hif1a* virus (blue line, *sh-Hif1a*). All mice were injected at 5 weeks and analysed at 6 months of age. Areas of obvious injection-inflicted damage (see white arrow in (C) as an example) were excluded from quantification. Shown are means ± SEM. $N = 6$. **E)** Quantification of the ONL thickness of *sh-Hif1a* (blue bar) and *sh-ctrl* (black bar) virus injected mice at 6 months of age. All data points (115 for *sh-Hif1a*; 99 for *sh-ctrl*) shown in (D) were included. Shown are means ± SEM. **: $P < 0.01$. ONL: outer nuclear layer.

Table 1. Human retina samples used in the study

Nr	Age	Gender	Post mortem-time	Cause of death
HE19	17	male	30 h	Accident
HE4	24	male	21 h	Heart failure
HE6	57	male	13 h	Multiorgan failure
HE11	58	male	31 h	Accident / brain trauma
HE1	72	male	13 h	Cardiogenic shock
HE16	74	male	35 h	Prostata adenocarcinoma
HE17	78	male	27 h	Heart failure
HE13	80	female	15 h	Cerebral ischemia
HE15	91	female	23 h	Aortic stenosis
HE3	92	male	36 h	Gastrointestinal bleeding

Table 2. Primers used for genotyping

Gene		Primer sequence (5' – 3')	Products [bp]	
Vhl	forward: reverse:	TGAGTATGGGATAACGGGTTGAAC AGAACTGACTGACTTCCACTGATGC	wt: 125	floxed: 317
Hif1a	forward: reverse:	GGAGCTATCTCTCTAGACC GCAGTTAAGAGCACTAGTTG	wt: 215	floxed: 260
Hif2a	forward: reverse:	TGTAGGCAAGGAAACCAAGG GAGAGCAGCTTCTCCTGGAA	wt: 182	floxed: 220
OpsinCre	forward: reverse:	AGGTGTAGAGAAGGCACTTAGC CTAATCGCCATCTTCCAGCAGG	wt: –	cre: 441

Table 3. Primers used to test for genomic excision

Gene	Primer sequence (5' – 3')		Product [bp]		
			wt	1-loxP	2-loxP
Vhl	forward-1 forward-2 reverse-1+2:	CTGGTACCCACGAAACTGTC CTAGGCACCGAGCTTAGAGGTTTGCG CTGACTTCCACTGATGCTTGTCACAG	286	~260	~460
Hif1a	forward-1: forward-2 reverse-1+2:	TTGGGGATGAAAACATCTGC GGAGCTATCTCTCTAGACC GCAGTTAAGAGCACTAGTTG	215	~270	~260
Hif2a	forward-1: forward-2 reverse-1+2:	GCTAACACTGTACTGTCTGAAAGAGTAGC CTTCTTCCATCATCTGGGATCTGGGACT CAGGCAGTATGCCTGGCTAATTCCAGTT	457	~300	~550

Table 4. Primers used for real-time PCR

Gene	Forward 5' – 3'	Reverse 5' – 3'	Product [bp]
Human-specific primers			
ACTB	CCTGGCACCCAGCACAAT	GGGCCGGACTCGTCATAC	144
GAPDH	CTTCGCTCTCTGCTCCTCCT	ATCCGTTGACTCCGACCTTC	111
RPL28	GCAATTCCTTCCGCTACAAC	TGTTCTTGCGGATCATGTGT	198
ADM	ATCACTCTCTTAGCAGGGTCT	CCACTTATTCCACTTCTTTCG	148
VEGFA	GTGGACATCTTCCAGGAGTACC	TGTTGTGCTGTAGGAAGCTCAT	205
GLUT1	ACTGTCGTGTCGCTGTTTG	CCAGGACCCACTTCAAAGAA	191
PDK1	CACGCTGGGTAATGAGGATT	GGAGGTCTCAACACGAGGT	127
RHO	ATCATGGTCATCGCTTTCCT	CTTGGACACGGTAGCAGAG	252
GNAT2	CTGCTACTGCTGGGTGCT	TGGTGAATAGCCATCCTGGT	84
PDE6A	CTACCAGATGAAATCCCAGAAC	CTTGAAATACAGGGCGAGGT	202
PDE6C	AACTGTTTCAAACTGCCGCT	TATTTTGGAGAGGCACCACC	100
LOXL4	AACTGCCTCTCCAAGTCTGC	AGGAGGTCGTAGTGGGTGAA	191
LAD1	CCTTTCGGATGAAACCCAAGA	CCCACAGGAGCCACGAATA	187
SMTNL2	AACTTCGAGCTGGCTTTCA	CATCACCATCATGTCCTCCA	81
LIF	TGCCAATGCCCTCTTTATTC	AGGTGCCAAGGTACACGACT	170
EDN2	TGTGCCACCTTCTGCCTTC	TGGAAATGTCCCTCAGCCTT	139
FGF2	AGAAGAGCGACCCTCACATCAAG	TCATCCGTAACACATTTAGAAGCCAG	139
CASP1	CCACAATGGGCTCTGTTTTT	GCTCTACCATCTGGCTGCTC	124
Mouse-specific primers			
Actb	CAACGGCTCCGGCATGTGC	CTCTTGCTCTGGGCCTCG	153
Adm	TCCTGGTTTCTCGGCTTCTC	ATTCTGTGGCGATGCTCTGA	133
Vegf	ACTTGTGTTGGGAGGAGGATGTC	AATGGGTTTGTCGTGTTTCTGG	171
Bnip3	CCTGTCGCAGTTGGGTTC	GAAGTGCAGTTCTACCCAGGAG	93
Egln1	CATTGTTGGCAGAAGGTGTG	CAAAGGACTACAGGGTCTCCA	70
Lif	AATGCCACCTGTGCCATACG	CAACTTGGTCTTCTCTGTCCCG	216
Edn2	AGACCTCCTCCGAAAGCTG	CTGGCTGTAGCTGGCAAAG	64
Fgf2	TGTGTCTATCAAGGGAGTGTGTGC	ACCAACTGGAGTATTTCCGTGACCG	158
Casp1	GGCAGGAATTCTGGAGCTTCAA	GTCAGTCCTGGAAATGTGCC	138
Pdk1	GTTGAAACGTCCCGTGCT	AGTCTCTCGACGGATTCTGT	170
Glut1	CAGTGTATCCTGTTGCCCTTCTG	GCCGACCCTCTTCTTTCATCTC	151
Stat3	CAAAACCCTCAAGAGCCAAGG	TCACTCACAATGCTTCTCCGC	132
Gfap	CCACCAAACTGGCTGATGTCTAC	TTCTCTCCAAATCCACACGAGC	240
Smtnl2	GCATCTTGGAGAACGGACA	CAGAGAATTTCTCGGAGACTCG	168
Lad1	CACCCAGAATGGAGCTCAG	CACCTGCCGCCTCTGTCTCCG	154
Loxl4	GTTGCACAACTGCCACACA	GGAGTGCAGTAATGGCTTC	108

Supplemental Information

Deletion of Vhl in rods may affect function in cones

Photopic ERG recordings of *rod$^{\Delta Vhl}$* mice at 6 months of age showed reduced b-wave amplitudes suggesting that cones were affected by the hypoxic response in rods. After the additional rod-specific deletion of *Hif1a*, of *Hif2a* or of both *Hif1a* and *Hif2a* photopic b-wave amplitudes of deletion strains were not distinguishable from their respective controls (Fig. S1). Importantly, photopic ERGs were recorded in the same mice and during the same experimental session used to determine the scotopic ERGs shown in Fig. 5. The reduced photopic response in *rod$^{\Delta Vhl}$* mice may not have been caused by a significant loss of cones since expression of cone specific transducin (*Gnat2*) was not affected at 6 months of age (Fig. 6), the timepoint of the functional tests. Thus, the hypoxic response of rods between 10 weeks and 6 months of age may have induced a lasting effect on cone function by unknown mechanisms. These putative mechanisms may depend on both HIF1 and HIF2 transcription factors as additional deletion of either factor in *rod$^{\Delta Vhl}$* mice prevented the effect.

Transcriptomic analysis

To detect genes that may be under transcriptional control of HIF1 and/or HIF2 in rods and that may contribute to the degenerative phenotype in *rod$^{\Delta Vhl}$* mice, we determined the retinal transcriptome of *rod$^{\Delta Vhl}$*, *rod$^{\Delta Vhl;Hif1a}$* and *Vhl$^{flox/flox}$;Hif1a$^{flox/flox}$* control mice and compared them to each other. Tables S1 – S3 show the top 20 up- and down regulated genes of each individual comparison. The full lists of genes analysed can be found in Files S1 – S3. Inactivation of *Vhl* in rods had a strong impact on the retinal transcriptome with 657 and 245 genes that were more than 2-fold ($P < 0.05$) up- or down-regulated, respectively. In contrast, only 30 genes were more than 2-fold ($P < 0.05$) up- and 29 genes down-regulated in *rod$^{\Delta Vhl;Hif1a}$* mice when compared to controls. Whereas the differentially regulated genes in *rod$^{\Delta Vhl}$* mice may be mostly controlled by HIF1, HIF2 and/or STAT3, the genes found in *rod$^{\Delta Vhl;Hif1a}$* mice may be primarily regulated by HIF2. When we compared differentially regulated genes in *rod$^{\Delta Vhl}$* to those in *rod$^{\Delta Vhl;Hif1a}$* mice we identified 493 genes that were expressed at least 2-fold higher than in *rod$^{\Delta Vhl}$* mice and 246 genes that were down regulated. These genes may be primarily regulated by HIF1 and/or STAT3, but not by HIF2. Venn diagrams of up- and down-regulated genes showed that genes differentially regulated in *rod$^{\Delta Vhl}$* mice were largely overlapping with those regulated in *rod$^{\Delta Vhl}$* when compared to *rod$^{\Delta Vhl;Hif1a}$* mice. But both had only little overlap to the differentially regulated genes *rod$^{\Delta Vhl;Hif1a}$* mice (Fig. S2A). *Rod$^{\Delta Vhl;Hif1a}$* mice had overlaps only with *rod$^{\Delta Vhl}$* mice since both mice had HIF2 activated. This was not the case in the list of genes that resulted from the comparison of *rod$^{\Delta Vhl}$* mice with *rod$^{\Delta Vhl;Hif1a}$* mice as already stated above. The gene that was commonly downregulated in all three gene lists was *Igh-VJ558*, a gene that has been implicated in the immune response, leukocyte migration and apoptosis (1, 2). The strongly different retinal transcriptome of *rod$^{\Delta Vhl}$* mice and the similarity of *rod$^{\Delta Vhl;Hif1a}$* to controls is also obvious from

the cluster heat map (Fig. S2B). Thus, inactivating *Hif1a* in mice lacking *Vhl* results in only few transcriptomic changes that may be attributable to HIF2.

To evaluate the regulation of the genes in more detail, we cross-compared the top regulated genes of all three lists. Table S4 uses the top 20 up- and down regulated genes in $rod^{\Delta Vhl}$ mice (see Table S1) as reference list. Fold-changes of these genes as detected in the other lists are shown for direct comparison. The same was done using the 20 top regulated genes in $rod^{\Delta Vhl}$ when compared to $rod^{\Delta Vhl;Hif1a}$ (see Table S2) as reference list (Table S5); and using the 20 top regulated in genes in $rod^{\Delta Vhl;Hif1a}$ (see Table S3) as reference list (Table S6). It is apparent that the transcriptome of $rod^{\Delta Vhl;Hif1a}$ mice differs strongly from $rod^{\Delta Vhl}$ mice. Genes that were differentially regulated in $rod^{\Delta Vhl;Hif1a}$ *and* $rod^{\Delta Vhl}$ mice compared to their respective controls, but not in $rod^{\Delta Vhl}$ mice when compared to $rod^{\Delta Vhl;Hif1a}$ are good candidates to be regulated by HIF2 in rod photoreceptors. These genes included five (*Prim2*, *Gadl1*, *Xlrb4*, *Slurp1*, *Mybph)* up- and eight (*Mns1*, *Lmod1*, *Lce1i*, *Lce1d*, *Lce1f*, *Cd27*, *Ak7*, *Calm4*) down-regulated genes that were not defined as HIF2 targets so far. Clearly, however, HIF2-regulated expression of these genes needs to be verified by additional tests in future experiments.

References

1. Bong, JJ, Kang, YM, Shin, SC, Choi, SJ, Lee, KM, Kim, HS. Identification of radiation-sensitive expressed genes in the ICR and AKR/J mouse thymus. *Cell Biol Int*. 2013;37(5):485–494.

2. Lin, M, Hu, Y, Chen, Y, Zhou, KK, Jin, J, Zhu, M, Le, YZ, Ge, J, Ma, JX. Impacts of hypoxia-inducible factor-1 knockout in the retinal pigment epithelium on choroidal neovascularization. *Invest Ophthalmol Vis Sci*. 2012;53(10):6197–6206.

Figure S1

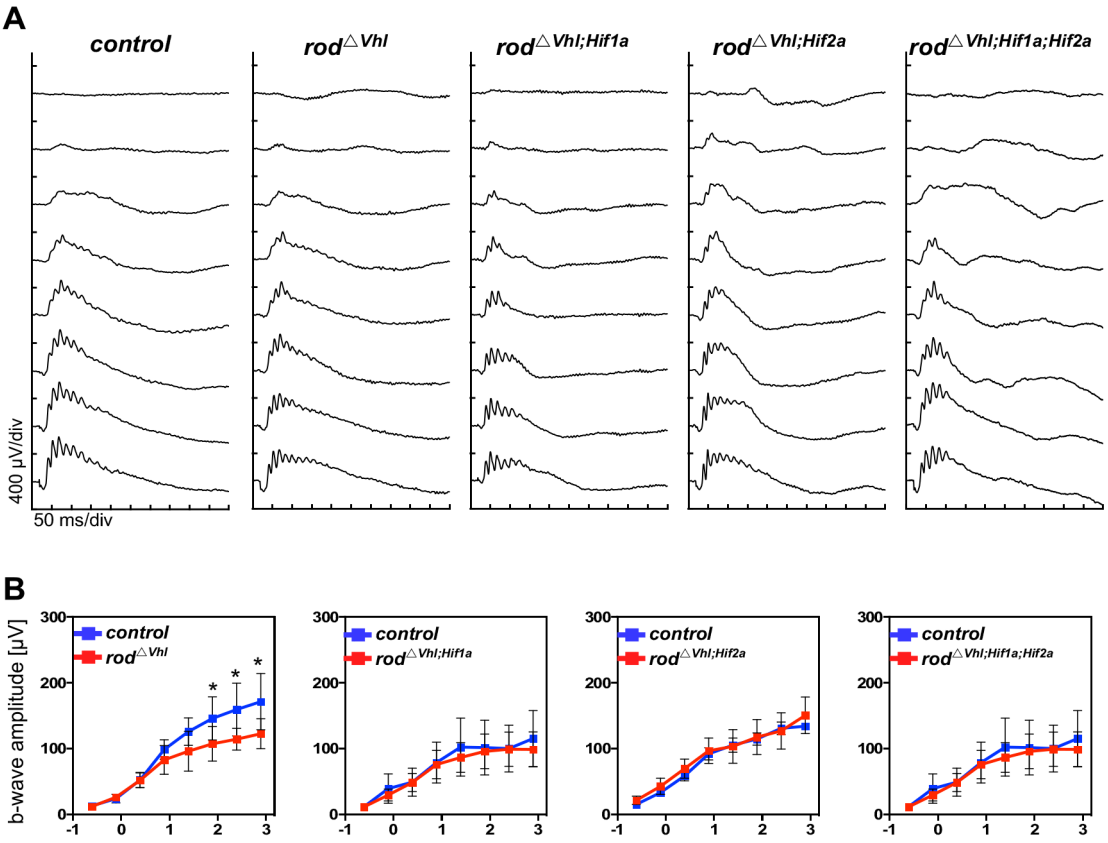

Fig. S1. Retinal function. Photopic retinal function was tested in 6 months old *rod*$^{\Delta Vhl}$, *rod*$^{\Delta Vhl;Hif1a}$, *rod*$^{\Delta Vhl;Hif2a}$, and *rod*$^{\Delta Vhl;Hif1a;Hif2a}$ mice. Cre-negative *Vhl*$^{flos/flox}$ mice served as controls. **A)** Representative photopic ERG traces recorded after light stimuli of increasing light intensities. **B)** Photopic b-wave amplitudes plotted as a function of stimulus intensity. Control mice were Cre-negative littermates of the respective strains. Shown are averages ± SD. *N* = 6 eyes (3 mice), except for controls of *rod*$^{\Delta Vhl;Hif2a}$ (N = 5), *rod*$^{\Delta Vhl;Hif2a}$ (N = 7) and *rod*$^{\Delta Vhl;Hif1a;Hif2a}$ (N = 4). *: P < 0.05. 2-way ANOVA with Sidak's multiple comparison test.

Figure S2

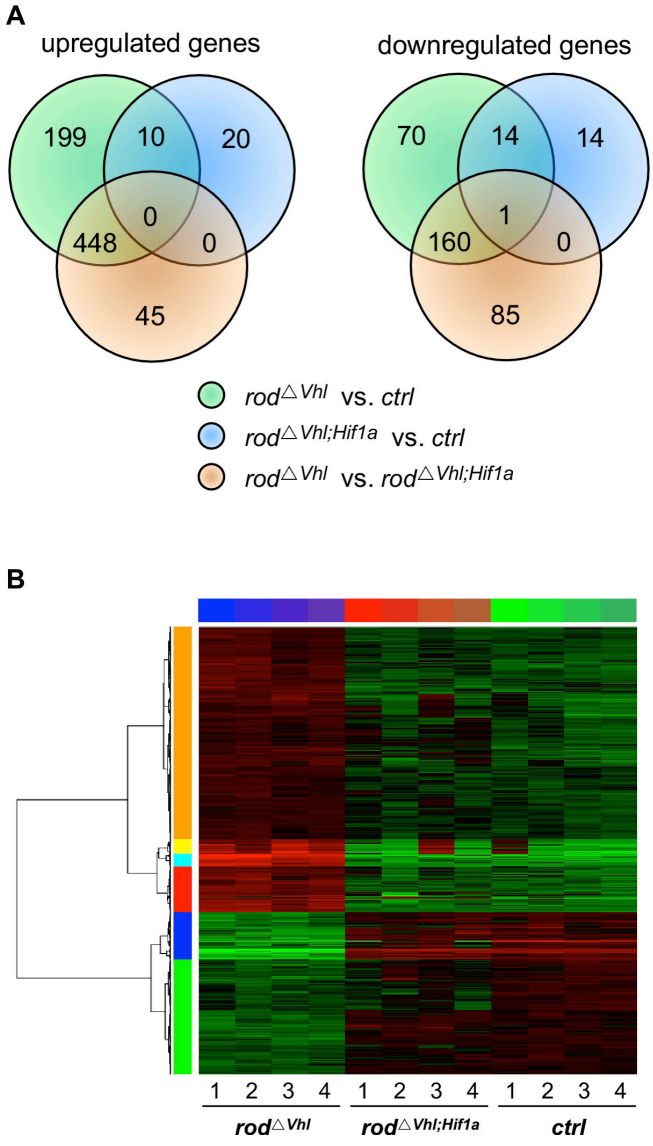

Fig. S2. Differentially regulated genes. **A)** Venn diagrams of genes differentially regulated in *rod*$^{\Delta Vhl}$ (compared to controls; green), *rod*$^{\Delta Vhl;Hif1a}$ (compared to controls; blue) and *rod*$^{\Delta Vhl}$ (compared to *rod*$^{\Delta Vhl;Hif1a}$; orange). Controls were *Vhl*$^{flox/flox}$;*Hif1a*$^{flox/flox}$ mice. Genes with a fold change of ≥ 2 and a P-value < 0.05 were included in the analysis. **B)** Cluster heat map of the transcriptomic data. Note the close relationship between *rod*$^{\Delta Vhl;Hif1a}$ and control mice.

Figure S3

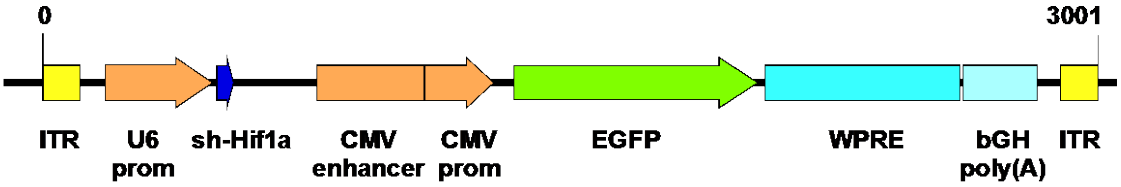

Fig. S3. Schematic representation of viral construct. Expression of *sh-Hif1a* is controlled by the U6 promoter. Expression of EGFP is driven by the CMV enhancer and CMV promoter. A woodchuck hepatitis post-transcriptional regulatory element (WPRE) is added before the bovine growth hormone (bGH) poly(A) signal. ITR: inverted terminal repeat. The entire cassette is 3001 bp in length.

Table S1. Top regulated genes in retinas of *rod$^{\Delta Vhl}$* mice, relative to *Vhl$^{flox/flox}$;Hif1a$^{flox/flox}$* ctrl mice

Top 20 genes upregulated in retinas of *rod$^{\Delta Vhl}$* mice				
Entrez Gene ID	**Gene Symbol**	**ratio**	**pValue**	**Description**
71957	***Ints11***	162.9	4.09E-07	integrator complex subunit 11
76487	***Ppp1r3g***	79.7	8.93E-10	protein phosphatase 1, regulatory (inhibitor) subunit 3G
223780	***Adm2***	71.9	9.09E-08	adrenomedullin 2
13615	***Edn2***	62.7	4.30E-08	endothelin 2
67573	***Loxl4***	33.9	1.83E-05	lysyl oxidase-like 4
240913	***Adamts4***	31.9	1.61E-04	a disintegrin-like and metallopeptidase (reprolysin type) with thrombospondin type 1 motif, 4
16763	***Lad1***	30.3	6.58E-07	ladinin
14663	***Glycam1***	25.2	3.39E-05	glycosylation dependent cell adhesion molecule 1
11535	***Adm***	23.7	1.12E-07	adrenomedullin
17339	***Mip***	22.9	8.08E-03	major intrinsic protein of eye lens fiber
214301	***Crygn***	22.3	6.26E-03	crystallin, gamma N
192199	***Rspo1***	21.7	7.82E-03	R-spondin homolog (Xenopus laevis)
233187	***Lim2***	21.6	4.19E-03	lens intrinsic membrane protein 2
12954	***Cryaa***	20.9	7.34E-03	crystallin, alpha A
20856	***Stc2***	20.7	1.13E-06	stanniocalcin 2
77998	***Grifin***	19.8	3.58E-03	galectin-related inter-fiber protein
12051	***Bcl3***	19.5	1.62E-06	B-cell leukemia/lymphoma 3
276829	***Smtnl2***	17.0	9.83E-08	smoothelin-like 2
381359	***Prdm12***	16.2	1.72E-05	PR domain containing 12
100039660	***Ect2l***	15.5	1.72E-05	epithelial cell transforming sequence 2 oncogene-like

Top 20 genes downregulated in retinas of *rod$^{\Delta Vhl}$* mice				
Entrez Gene ID	**Gene Symbol**	**ratio**	**pValue**	**Description**
258198	***Olfr224***	0.015	2.21E-06	olfactory receptor 224
80509	***Med8***	0.015	3.21E-07	mediator of RNA polymerase II transcription, subunit 8 homolog (yeast)
76681	***Trim12a***	0.024	2.23E-08	tripartite motif-containing 12A
30939	***Pttg1***	0.026	1.03E-09	pituitary tumor-transforming gene 1
54631	***Nphs1***	0.032	1.02E-07	nephrosis 1 homolog, nephrin (human)
14537	***Gcnt1***	0.039	1.14E-09	glucosaminyl (N-acetyl) transferase 1, core 2
75764	***Slx1b***	0.051	2.71E-09	SLX1 structure-specific endonuclease subunit homolog B (S. cerevisiae)
72154	***Zfp157***	0.058	4.90E-07	zinc finger protein 157
269209	***Stk36***	0.091	4.27E-06	serine/threonine kinase 36 (fused homolog, Drosophila)
214523	***Tmprss4***	0.095	2.39E-08	transmembrane protease, serine 4
17427	***Mns1***	0.100	1.01E-06	meiosis-specific nuclear structural protein 1
72461	***Prcp***	0.115	1.35E-08	prolylcarboxypeptidase (angiotensinase C)
16061	***Igh-VJ558***	0.117	4.18E-04	immunoglobulin heavy chain (J558 family)
140709	***Emid2***	0.120	1.01E-06	EMI domain containing 2
17921	***Myo7a***	0.124	1.77E-07	myosin VIIA
94216	***Col4a6***	0.129	3.29E-04	collagen, type IV, alpha 6
69611	***Lce1d***	0.148	1.60E-02	late cornified envelope 1D
71687	***Tmem25***	0.154	6.43E-08	transmembrane protein 25
12769	***Ccr9***	0.163	5.52E-03	chemokine (C-C motif) receptor 9
66442	***Spc25***	0.168	7.49E-05	SPC25, NDC80 kinetochore complex component, homolog (S. cerevisiae)

Genes with P > 0.05 were excluded from the analysis, as were 'Rik' sequences, 'expressed sequences', 'predicted genes' and 'hypothetical proteins'. Also excluded was '*Xist*' as this gene is X-linked and the number of females and males in the gene chip analyses were not balanced.

Table S2. Top regulated genes in retinas of *rod*$^{\Delta Vhl}$ mice, relative to *rod*$^{\Delta Vhl;Hif1a}$ mice

Top 20 genes upregulated in retinas of *rod*$^{\Delta Vhl}$ mice				
Entrez Gene ID	**Gene Symbol**	**ratio**	**pValue**	**Description**
71957	***Ints11***	282.8	5.20E-09	integrator complex subunit 11
223780	***Adm2***	70.9	1.19E-06	adrenomedullin 2
13615	***Edn2***	65.8	3.12E-08	endothelin 2
76487	***Ppp1r3g***	59.2	5.15E-06	protein phosphatase 1, regulatory (inhibitor) subunit 3G
240913	***Adamts4***	24.7	2.89E-04	a disintegrin-like and metallopeptidase (reprolysin type) with thrombospondin type 1 motif, 4
11535	***Adm***	23.5	6.34E-08	adrenomedullin
16763	***Lad1***	23.3	3.38E-05	ladinin
67573	***Loxl4***	22.4	2.51E-04	lysyl oxidase-like 4
381359	***Prdm12***	19.5	1.37E-05	PR domain containing 12
12051	***Bcl3***	18.7	4.52E-06	B-cell leukemia/lymphoma 3
233187	***Lim2***	17.0	2.37E-02	lens intrinsic membrane protein 2
17339	***Mip***	16.3	2.49E-02	major intrinsic protein of eye lens fiber
21818	***Tgm3***	15.6	4.76E-04	transglutaminase 3, E polypeptide
20856	***Stc2***	13.8	5.69E-07	stanniocalcin 2
276829	***Smtnl2***	13.2	2.79E-07	smoothelin-like 2
14663	***Glycam1***	13.0	1.27E-03	glycosylation dependent cell adhesion molecule 1
15006	***H2-Q1***	12.2	9.49E-06	histocompatibility 2, Q region locus 1
14173	***Fgf2***	11.6	7.27E-06	fibroblast growth factor 2
192199	***Rspo1***	11.3	2.04E-02	R-spondin homolog (Xenopus laevis)
12954	***Cryaa***	10.9	1.64E-02	crystallin, alpha A

Top 20 genes downregulated in retinas of *rod*$^{\Delta Vhl}$ mice				
Entrez Gene ID	**Gene Symbol**	**ratio**	**pValue**	**Description**
76681	***Trim12a***	0.014	8.54E-09	tripartite motif-containing 12A
80509	***Med8***	0.025	1.54E-06	mediator of RNA polymerase II transcription, subunit 8 homolog (yeast)
30939	***Pttg1***	0.026	1.81E-10	pituitary tumor-transforming gene 1
258198	***Olfr224***	0.027	2.80E-05	olfactory receptor 224
54631	***Nphs1***	0.028	4.80E-07	nephrosis 1 homolog, nephrin (human)
75764	***Slx1b***	0.034	4.22E-09	SLX1 structure-specific endonuclease subunit homolog B (S. cerevisiae)
14537	***Gcnt1***	0.035	3.59E-11	glucosaminyl (N-acetyl) transferase 1, core 2
109685	***Hyal3***	0.052	3.57E-06	hyaluronoglucosaminidase 3
72154	***Zfp157***	0.053	2.11E-07	zinc finger protein 157
17921	***Myo7a***	0.074	3.64E-08	myosin VIIA
214523	***Tmprss4***	0.084	2.07E-08	transmembrane protease, serine 4
72461	***Prcp***	0.101	9.91E-09	prolylcarboxypeptidase (angiotensinase C)
269209	***Stk36***	0.103	4.68E-06	serine/threonine kinase 36 (fused homolog, Drosophila)
94216	***Col4a6***	0.112	3.70E-04	collagen, type IV, alpha 6
140709	***Emid2***	0.112	9.73E-07	EMI domain containing 2
209760	***Tmc7***	0.129	1.24E-05	transmembrane channel-like gene family 7
68668	***Klk5***	0.134	1.22E-02	kallikrein related-peptidase 5
71687	***Tmem25***	0.156	7.66E-08	transmembrane protein 25
19223	***Ptgis***	0.167	2.71E-06	prostaglandin I2 (prostacyclin) synthase
18261	***Ocm***	0.175	1.41E-05	oncomodulin

Genes with P > 0.05 were excluded from the analysis, as were 'Rik' sequences, 'expressed sequences', 'predicted genes' and 'hypothetical proteins'. Also excluded was '*Xist*' as this gene is X-linked and the number of females and males in the gene chip analyses were not balanced.

Table S3. Top regulated genes in retinas of *rod*$^{\Delta Vhl;Hif1a}$ mice, relative to *Vhl*$^{flox/flox}$;*Hif1a*$^{flox/flox}$ control mice

Top 20 genes upregulated in retinas of *rod*$^{\Delta Vhl;Hif1a}$ mice				
Entrez Gene ID	**Gene Symbol**	**ratio**	**pValue**	**Description**
109685	***Hyal3***	7.0	1.26E-02	hyaluronoglucosaminidase 3
19076	***Prim2***	5.3	7.60E-09	DNA primase, p58 subunit
77044	***Arid2***	4.8	3.88E-02	AT rich interactive domain 2 (ARID, RFX-like)
434794	***Xlr4a***	4.5	8.59E-03	X-linked lymphocyte-regulated 4A
628171	***Olfr936***	3.4	5.31E-03	olfactory receptor 936
73748	***Gadl1***	3.3	1.48E-02	glutamate decarboxylase-like 1
545548	***Lce3a***	2.9	3.65E-03	late cornified envelope 3A
12534	***Cdk1***	2.9	8.44E-03	cyclin-dependent kinase 1
27083	***Xlr4b***	2.9	3.77E-02	X-linked lymphocyte-regulated 4B
57277	***Slurp1***	2.8	2.82E-02	secreted Ly6/Plaur domain containing 1
17748	***Mt1***	2.7	6.82E-08	metallothionein 1
53311	***Mybph***	2.7	3.58E-02	myosin binding protein H
67652	***Spaca1***	2.7	8.29E-05	sperm acrosome associated 1
194597	***Tmprss11a***	2.5	4.75E-03	transmembrane protease, serine 11a
230678	***Tmem125***	2.4	1.02E-03	transmembrane protein 125
244332	***Defb14***	2.3	5.00E-03	defensin beta 14
14428	***Galr2***	2.3	1.65E-02	galanin receptor 2
238393	***Serpina3f***	2.3	2.42E-05	serine (or cysteine) peptidase inhibitor, clade A, member 3F
22326	***Vax1***	2.2	3.28E-02	ventral anterior homeobox containing gene 1
69930	***Zfp715***	2.2	2.04E-02	zinc finger protein 715

Top 20 genes downregulated in retinas of *rod*$^{\Delta Vhl;Hif1a}$ mice				
Entrez Gene ID	**Gene Symbol**	**ratio**	**pValue**	**Description**
353371	***Oxct2b***	0.183	1.24E-02	3-oxoacid CoA transferase 2B
17427	***Mns1***	0.254	1.58E-02	meiosis-specific nuclear structural protein 1
51925	***D2Ertd640e***	0.260	2.78E-04	DNA segment, Chr 2, ERATO Doi 640, expressed
93689	***Lmod1***	0.324	3.44E-02	leiomodin 1 (smooth muscle)
76585	***Lce1i***	0.335	5.87E-03	late cornified envelope 1I
69611	***Lce1d***	0.338	2.88E-02	late cornified envelope 1D
56057	***Btg4***	0.356	4.73E-02	B-cell translocation gene 4
16061	***Igh-VJ558***	0.357	7.34E-03	immunoglobulin heavy chain (J558 family)
236904	***Klhl15***	0.375	1.83E-02	kelch-like 15 (Drosophila)
67828	***Lce1f***	0.376	1.43E-02	late cornified envelope 1F
20521	***Slc22a12***	0.377	3.41E-04	solute carrier family 22 (organic anion/cation transporter), member 12
21940	***Cd27***	0.380	1.84E-02	CD27 antigen
78801	***Ak7***	0.385	4.67E-04	adenylate kinase 7
68694	***Lce1e***	0.394	2.09E-02	late cornified envelope 1E
258692	***Olfr1442***	0.395	1.93E-02	olfactory receptor 1442
76117	***Arhgap15***	0.397	2.29E-03	Rho GTPase activating protein 15
246746	***Cd300lf***	0.398	4.89E-02	CD300 antigen like family member F
96875	***Prg4***	0.400	1.36E-04	proteoglycan 4 (megakaryocyte stimulating factor, articular superficial zone protein)
15130	***Hbb-b2***	0.402	2.54E-02	hemoglobin, beta adult minor chain
80796	***Calm4***	0.402	2.60E-02	calmodulin 4

Genes with P > 0.05 were excluded from the analysis, as were 'Rik' sequences, 'expressed sequences', 'predicted genes' and 'hypothetical proteins'. Also excluded was '*Xist*' as this gene is X-linked and the number of females and males in the gene chip analyses were not balanced.

Table S4. Comparison to top 20 genes that were differentially regulated in *rod*$^{\Delta Vhl}$ mice relative to *Vhl*$^{flox/flox}$;*Hif1a*$^{flox/flox}$ control mice

Reference list: Table S1: *rod*$^{\Delta Vhl}$ *vs ctrl* Upregulated genes Potential targets of: HIF1; HIF2; pSTAT3				*rod*$^{\Delta Vhl}$ *vs rod*$^{\Delta Vhl;Hif1a}$ potential targets of: HIF1; pSTAT3		*rod*$^{\Delta Vhl;Hif1a}$ *vs ctrl* potential targets of: HIF2	
Entrez Gene ID	Gene Symbol	ratio	pValue	ratio	pValue	ratio	pValue
71957	*Ints11*	162.9	4.09E-07	282.8	5.20E-09	–	–
76487	*Ppp1r3g*	79.7	8.93E-10	59.2	5.15E-06	–	–
223780	*Adm2*	71.9	9.09E-08	70.9	1.19E-06	–	–
13615	*Edn2*	62.7	4.30E-08	65.8	3.12E-08	–	–
67573	*Loxl4*	33.9	1.83E-05	22.4	2.51E-04	–	–
240913	*Adamts4*	31.9	1.61E-04	24.7	2.89E-04	–	–
16763	*Lad1*	30.3	6.58E-07	23.3	3.38E-05	–	–
14663	*Glycam1*	25.2	3.39E-05	13.0	1.27E-03	–	–
11535	*Adm*	23.7	1.12E-07	23.5	6.34E-08	–	–
17339	*Mip*	22.9	8.08E-03	16.3	2.49E-02	–	–
214301	*Crygn*	22.3	6.26E-03	† 10.3	† 1.19E-02	–	–
192199	*Rspo1*	21.7	7.82E-03	11.3	2.04E-02	–	–
233187	*Lim2*	21.6	4.19E-03	17.0	2.37E-02	–	–
12954	*Cryaa*	20.9	7.34E-03	10.9	1.64E-02	–	–
20856	*Stc2*	20.7	1.13E-06	13.8	5.69E-07	–	–
77998	*Grifin*	19.8	3.58E-03	† 10.7	† 1.75E-02	–	–
12051	*Bcl3*	19.5	1.62E-06	18.7	4.52E-06	–	–
276829	*Smtnl2*	17.0	9.83E-08	13.2	2.79E-07	† 1.3	† 1.34E-02
381359	*Prdm12*	16.2	1.72E-05	19.5	1.37E-05	–	–
100039660	*Ect2l*	15.5	1.72E-05	† 10.8	† 3.46E-05	–	–

Reference list: Table S1: *rod*$^{\Delta Vhl}$ *vs ctrl* Downregulated genes Potential targets of: HIF1; HIF2; pSTAT3				*rod*$^{\Delta Vhl}$ *vs rod*$^{\Delta Vhl;Hif1a}$ potential targets of: HIF1; pSTAT3		*rod*$^{\Delta Vhl;Hif1a}$ *vs ctrl* potential targets of: HIF2	
Entrez Gene ID	Gene Symbol	ratio	pValue	ratio	pValue	ratio	pValue
258198	*Olfr224*	0.015	2.21E-06	0.027	2.80E-05	–	–
80509	*Med8*	0.015	3.21E-07	0.025	1.54E-06	–	–
76681	*Trim12a*	0.024	2.23E-08	0.014	8.54E-09	† 1.68	† 3.77E-03
30939	*Pttg1*	0.026	1.03E-09	0.026	1.81E-10	–	–
54631	*Nphs1*	0.032	1.02E-07	0.028	4.80E-07	–	–
14537	*Gcnt1*	0.039	1.14E-09	0.035	3.59E-11	–	–
75764	*Slx1b*	0.051	2.71E-09	0.034	4.22E-09	† 1.49	† 9.70E-03
72154	*Zfp157*	0.058	4.90E-07	0.053	2.11E-07	–	–
269209	*Stk36*	0.091	4.27E-06	0.103	4.68E-06	–	–
214523	*Tmprss4*	0.095	2.39E-08	0.084	2.07E-08	–	–
17427	*Mns1*	0.100	1.01E-06	–	–	† 0.25	† 1.58E-02
72461	*Prcp*	0.115	1.35E-08	0.101	9.91E-09	† 1.14	† 2.83E-02
16061	*Igh-VJ558*	0.117	4.18E-04	† 0.313	† 2.28E-02	† 0.37	† 1.28E-02
140709	*Emid2*	0.120	1.01E-06	0.112	9.73E-07	–	–
17921	*Myo7a*	0.124	1.77E-07	0.074	3.64E-08	† 1.75	† 1.24E-04
94216	*Col4a6*	0.129	3.29E-04	0.112	3.70E-04	–	–
69611	*Lce1d*	0.148	1.60E-02	–	–	† 0.34	† 2.88E-02
71687	*Tmem25*	0.154	6.43E-08	0.156	7.66E-08	–	–
12769	*Ccr9*	0.163	5.52E-03	–	–	–	–
66442	*Spc25*	0.168	7.49E-05	† 0.183	† 1.35E-04	–	–

Genes with P > 0.05 were excluded from the analysis, as were 'Rik' sequences, 'expressed sequences', 'predicted genes' and 'hypothetical proteins'. Also excluded was '*Xist*' as this gene is X-linked and the number of females and males in the gene chip analyses were not balanced.

† : not present in the top 20 regulated genes of the respective list

– : not present in the respective list of genes, or P > 0.05

Table S5. Comparison to top 20 genes that were differentially regulated in *rod*$^{\Delta Vhl}$ relative to *rod*$^{\Delta rod;Hif1a}$ mice

Reference list: Table S2: *rod*$^{\Delta Vhl}$ *vs rod*$^{\Delta Vhl;Hif1a}$ Upregulated genes Potential targets of: HIF1; pSTAT3				*rod*$^{\Delta Vhl;Hif1a}$ *vs ctrl* potential targets of: HIF2		*rod*$^{\Delta Vhl}$ *vs ctrl* potential targets of: HIF1; HIF2; pSTAT3	
Entrez Gene ID	Gene Symbol	ratio	pValue	ratio	pValue	ratio	pValue
71957	***Ints11***	282.8	5.20E-09	–	–	162.9	4.09E-07
223780	***Adm2***	70.9	1.19E-06	–	–	71.9	9.09E-08
13615	***Edn2***	65.8	3.12E-08	–	–	62.7	4.30E-08
76487	***Ppp1r3g***	59.2	5.15E-06	–	–	79.7	8.93E-10
240913	***Adamts4***	24.7	2.89E-04	–	–	31.9	1.61E-04
11535	***Adm***	23.5	6.34E-08	–	–	23.7	1.12E-07
16763	***Lad1***	23.3	3.38E-05	–	–	30.3	6.58E-07
67573	***Loxl4***	22.4	2.51E-04	–	–	33.9	1.83E-05
381359	***Prdm12***	19.5	1.37E-05	–	–	16.2	1.72E-05
12051	***Bcl3***	18.7	4.52E-06	–	–	19.5	1.62E-06
233187	***Lim2***	17.0	2.37E-02	–	–	21.6	4.19E-03
17339	***Mip***	16.3	2.49E-02	–	–	22.9	8.08E-03
21818	***Tgm3***	15.6	4.76E-04	–	–	† 14.5	† 2.99E-05
20856	***Stc2***	13.8	5.69E-07	–	–	20.7	1.13E-06
276829	***Smtnl2***	13.2	2.79E-07	† 1.3	† 1.34E-02	17.0	9.83E-08
14663	***Glycam1***	13.0	1.27E-03	–	–	25.2	3.39E-05
15006	***H2-Q1***	12.2	9.49E-06	–	–	† 10.3	† 2.26E-06
14173	***Fgf2***	11.6	7.27E-06	–	–	† 9.86	† 1.01E-05
192199	***Rspo1***	11.3	2.04E-02	–	–	21.7	7.82E-03
12954	***Cryaa***	10.9	1.64E-02	–	–	20.9	7.34E-03

Reference list: Table S2: *rod*$^{\Delta Vhl}$ *vs rod*$^{\Delta Vhl;Hif1a}$ Downregulated genes Potential targets of: HIF1; pSTAT3				*rod*$^{\Delta Vhl;Hif1a}$ *vs ctrl* potential targets of: HIF2		*rod*$^{\Delta Vhl}$ *vs ctrl* potential targets of: HIF1; HIF2; pSTAT3	
Entrez Gene ID	Gene Symbol	ratio	pValue	ratio	pValue	ratio	pValue
76681	***Trim12a***	0.014	8.54E-09	† 1.68	† 3.77E-03	0.024	2.23E-08
80509	***Med8***	0.025	1.54E-06	–	–	0.015	3.21E-07
30939	***Pttg1***	0.026	1.81E-10	–	–	0.026	1.03E-09
258198	***Olfr224***	0.027	2.80E-05	–	–	0.015	2.21E-06
54631	***Nphs1***	0.028	4.80E-07	–	–	0.032	1.02E-07
75764	***Slx1b***	0.034	4.22E-09	† 1.49	† 9.70E-03	0.051	2.71E-09
14537	***Gcnt1***	0.035	3.59E-11	–	–	0.039	1.14E-09
109685	***Hyal3***	0.052	3.57E-06	6.96	1.26E-02	–	–
72154	***Zfp157***	0.053	2.11E-07	–	–	0.058	4.90E-07
17921	***Myo7a***	0.074	3.64E-08	† 1.75	† 1.24E-04	0.124	1.77E-07
214523	***Tmprss4***	0.084	2.07E-08	–	–	0.095	2.39E-08
72461	***Prcp***	0.101	9.91E-09	† 1.14	† 2.83E-02	0.115	1.35E-08
269209	***Stk36***	0.103	4.68E-06	–	–	0.091	4.27E-06
94216	***Col4a6***	0.112	3.70E-04	–	–	0.129	3.29E-04
140709	***Emid2***	0.112	9.73E-07	–	–	0.120	1.01E-06
209760	***Tmc7***	0.129	1.24E-05	† 1.45	† 2.99E-03	† 0.187	† 4.51E-05
68668	***Klk5***	0.134	1.22E-02	–	–	–	–
71687	***Tmem25***	0.156	7.66E-08	–	–	0.154	6.43E-08
19223	***Ptgis***	0.167	2.71E-06	† 1.49	† 9.72E-03	† 0.249	† 1.39E-06
18261	***Ocm***	0.175	1.41E-05	† 1.42	† 3.63E-02	† 0.403	† 4.41E-06

Genes with P > 0.05 were excluded from the analysis, as were 'Rik' sequences, 'expressed sequences', 'predicted genes' and 'hypothetical proteins'. Also excluded was '*Xist*' as this gene is X-linked and the number of females and males in the gene chip analyses were not balanced.

† : not present in the top 20 regulated genes of the respective list

– : not present in the respective list of genes, or P > 0.05

Table S6. Comparison to top 20 genes that were differentially regulated in *rod*$^{\Delta Vhl;Hif1a}$ relative to *Vhl*$^{flox/flox}$;*Hif1a*$^{flox/flox}$ control mice

Reference list: Table S3: *rod*$^{\Delta Vhl;Hif1a}$ *vs ctrl* Upregulated genes Potential targets of: HIF2				*rod*$^{\Delta Vhl}$ *vs rod*$^{\Delta Vhl;Hif1a}$ potential targets of: HIF1; pSTAT3		*rod*$^{\Delta Vhl}$ *vs ctrl* potential targets of: HIF1; HIF2; pSTAT3	
Entrez Gene ID	Gene Symbol	ratio	pValue	ratio	pValue	ratio	pValue
109685	*Hyal3*	7.0	1.26E-02	0.05	3.57E-06	–	–
19076	*Prim2*	5.3	7.60E-09	–	–	† 4.7	† 3.02E-05
77044	*Arid2*	4.8	3.88E-02	–	–	–	–
434794	*Xlr4a*	4.5	8.59E-03	–	–	–	–
628171	*Olfr936*	3.4	5.31E-03	–	–	–	–
73748	*Gadl1*	3.3	1.48E-02	–	–	† 5.0	† 9.08E-04
545548	*Lce3a*	2.9	3.65E-03	† 0.2	† 2.17E-03	–	–
12534	*Cdk1*	2.9	8.44E-03	–	–	–	–
27083	*Xlr4b*	2.9	3.77E-02	–	–	† 2.6	† 5.27E-03
57277	*Slurp1*	2.8	2.82E-02	–	–	† 2.5	† 8.05E-03
17748	*Mt1*	2.7	6.82E-08	† 0.8	† 9.22E-03	† 2.0	† 4.22E-05
53311	*Mybph*	2.7	3.58E-02	–	–	† 1.9	† 3.72E-02
67652	*Spaca1*	2.7	8.29E-05	–	–	–	–
194597	*Tmprss11a*	2.5	4.75E-03	–	–	–	–
230678	*Tmem125*	2.4	1.02E-03	–	–	–	–
244332	*Defb14*	2.3	5.00E-03	–	–	–	–
14428	*Galr2*	2.3	1.65E-02	† 0.3	† 1.33E-02	–	–
238393	*Serpina3f*	2.3	2.42E-05	† 1.44	† 2.38E-03	† 3.3	† 2.46E-07
22326	*Vax1*	2.2	3.28E-02	–	–	–	–
69930	*Zfp715*	2.2	2.04E-02	† 0.4	† 1.87E-02	† 0.8	† 9.99E-03

Reference list: Table S3: *rod*$^{\Delta Vhl;Hif1a}$ *vs ctrl* Downregulated genes Potential targets of: HIF2				*rod*$^{\Delta Vhl}$ *vs rod*$^{\Delta Vhl;Hif1a}$ potential targets of: HIF1; pSTAT3		*rod*$^{\Delta Vhl}$ *vs ctrl* potential targets of: HIF1; HIF2; pSTAT3	
Entrez Gene ID	Gene Symbol	ratio	pValue	ratio	pValue	ratio	pValue
353371	*Oxct2b*	0.183	1.24E-02	–	–	–	–
17427	*Mns1*	0.254	1.58E-02	–	–	0.100	1.01E-06
51925	*D2Ertd640e*	0.260	2.78E-04	–	–	–	–
93689	*Lmod1*	0.324	3.44E-02	–	–	† 0.322	† 3.25E-02
76585	*Lce1i*	0.335	5.87E-03	–	–	† 0.207	† 1.09E-02
69611	*Lce1d*	0.338	2.88E-02	–	–	0.148	1.60E-02
56057	*Btg4*	0.356	4.73E-02	–	–	–	–
16061	*Igh-VJ558*	0.357	7.34E-03	† 0.31	† 2.28E-02	0.117	4.18E-04
236904	*Klhl15*	0.375	1.83E-02	–	–	–	–
67828	*Lce1f*	0.376	1.43E-02	–	–	† 0.175	† 4.43E-03
20521	*Slc22a12*	0.377	3.41E-04	–	–	–	–
21940	*Cd27*	0.380	1.84E-02	–	–	† 0.329	† 3.02E-02
78801	*Ak7*	0.385	4.67E-04	–	–	–	–
68694	*Lce1e*	0.394	2.09E-02	–	–	† 0.180	† 3.60E-03
258692	*Olfr1442*	0.395	1.93E-02	† 4.50	† 4.86E-02	–	–
76117	*Arhgap15*	0.397	2.29E-03	† 0.68	† 8.86E-04	–	–
246746	*Cd300lf*	0.398	4.89E-02	† 0.74	† 4.34E-03	–	–
96875	*Prg4*	0.400	1.36E-04	–	–	–	–
15130	*Hbb-b2*	0.402	2.54E-02	† 2.29	† 1.86E-02	–	–
80796	*Calm4*	0.402	2.60E-02	–	–	† 0.239	† 1.79E-02

Genes with P > 0.05, were excluded from the analysis, as were 'Rik' sequences, 'expressed sequences', 'predicted genes' and 'hypothetical proteins'. Also excluded was '*Xist*' as this gene is X-linked and the number of females and males in the gene chip analyses were not balanced.

† : not present in the top 20 regulated genes of the respective list

– : not present in the respective list of genes, or P > 0.05

3.3 Article 3: Blue light-induced retinal lesions, intraretinal vascular leakage and edema formation in the all-cone mouse retina

Philipp Geiger[1,2], **Maya Barben[1,2,3]**, Christian Grimm[2,3,4], Marijana Samardzija[2]

[1]Equal contributions, **shared authorship.**

[2]Lab for Retinal Cell Biology, Dept. Ophthalmology, University Hospital Zurich, University of Zurich, Switzerland

[3]Neuroscience Center Zurich (ZNZ), University of Zurich, Switzerland

[4]Zurich Center for Integrative Human Physiology (ZIHP), University of Zurich, Switzerland

Status of the manuscript:

Published in *Cell Death Dis., 2015 Nov 19;6:e1985. doi: 10.1038/cddis.2015.333.*

Personal Contribution

In situ cell death detection (TUNEL), semi-quantitative real-time PCR, OCT analysis, data interpretation, manuscript editing.

OPEN

Citation: Cell Death and Disease (2015) 6, e1985; doi:10.1038/cddis.2015.333

www.nature.com/cddis

Blue light-induced retinal lesions, intraretinal vascular leakage and edema formation in the all-cone mouse retina

P Geiger[1,2], M Barben[1,2], C Grimm[1] and M Samardzija*[,1]

Little is known about the mechanisms underlying macular degenerations, mainly for the scarcity of adequate experimental models to investigate cone cell death. Recently, we generated *R91W;Nrl*$^{-/-}$ double-mutant mice, which display a well-ordered all-cone retina with normal retinal vasculature and a strong photopic function that generates useful vision. Here we exposed *R91W;Nrl*$^{-/-}$ and wild-type (*wt*) mice to toxic levels of blue light and analyzed their retinas at different time points post illumination (up to 10 days). While exposure of *wt* mice resulted in massive pyknosis in a focal region of the outer nuclear layer (ONL), the exposure of *R91W;Nrl*$^{-/-}$ mice led to additional cell death detected within the inner nuclear layer. Microglia/macrophage infiltration at the site of injury was more pronounced in the all-cone retina of *R91W;Nrl*$^{-/-}$ than in *wt* mice. Similarly, vascular leakage was abundant in the inner and outer retina in *R91W;Nrl*$^{-/-}$ mice, whereas it was mild and restricted to the subretinal space in *wt* mice. This was accompanied by retinal swelling and the appearance of cystoid spaces in both inner and ONLs of *R91W;Nrl*$^{-/-}$ mice indicating edema in affected areas. In addition, basal expression levels of tight junction protein-1 encoding ZO1 were lower in *R91W;Nrl*$^{-/-}$ than in *wt* retinas. Collectively, our data suggest that exposure of *R91W;Nrl*$^{-/-}$ mice to blue light not only induces cone cell death but also disrupts the inner blood–retinal barrier. Macular edema in humans is a result of diffuse capillary leakage and microaneurysms in the macular region. Blue light exposure of the *R91W;Nrl*$^{-/-}$ mouse could therefore be used to study molecular events preceding edema formation in a cone-rich environment, and thus potentially help to develop treatment strategies for edema-based complications in macular degenerations.
Cell Death and Disease (2015) **6,** e1985; doi:10.1038/cddis.2015.333; published online 19 November 2015

Human vision largely depends on cone photoreceptors. As the incidence of cone degenerative diseases such as age-related macular degeneration is expected to rise in the future, the understanding of cone physiology and pathophysiology is urgently needed to develop therapeutic approaches for the preservation of cone-mediated vision in patients. Recently, we engineered an *R91W;Nrl*$^{-/-}$ mouse model[1] to analyze the impact of a human-blinding mutation found in RPE65 (the R91W) specifically on cone photoreceptors.[2,3] The lack of the neural retina leucine zipper (NRL) transcription factor drives all photoreceptor progenitor cells to a cone fate.[4] Therefore, the impact of the R91W mutation on cones can be analyzed without the 'contaminating' presence of rods in *R91W;Nrl*$^{-/-}$ mice. In addition, as the *R91W* mutation leads to a hypomorphic RPE65 protein substantially reducing levels of 11-*cis*-retinal in the retina,[2,5] the disturbed cone layering with rosette formation typically found in the *Nrl*$^{-/-}$ mouse retinas is corrected in double-mutant *R91W;Nrl*$^{-/-}$ mice. Thus, the *R91W;Nrl*$^{-/-}$ mouse constitutes a model with a well-ordered and functional all-cone retina.[1]

The acute model of light-induced retinal degeneration uses short exposure to bright white light to study photoreceptor cell death leading to loss of vision.[6,7] High photon flux, oxygen tension and the high levels of polyunsaturated fatty acids present in rod outer segment membranes make rod photoreceptor cells especially vulnerable to photochemical damage. Although light affects rod photoreceptors primarily, cones seem to be more resilient surviving for a prolonged period of time after light exposure.[8] Cones eventually do die, but secondarily to the loss of rod cells. Endotoxins released by degenerating rods,[9] the lack of trophic and mechanical support[10,11] after loss of rod cells or sudden exposure to increased oxygen levels in the absence of rods[12] have been implicated in the secondary cone cell death.

Mammalian animal models with higher cone percentage such as gray squirrels (60% cones) or Nile rats (33% cones) showed high resistance of cones to light-induced damage.[13] Similarly, short-term (hours) or constant (up to several months) exposure of *Nrl*$^{-/-}$ mice to bright white light did not induce cone degeneration.[14,15] However, in the monkey retina S-cones were irreversibly damaged with high levels of monochromatic

[1]Laboratory for Retinal Cell Biology, Department Ophthalmology, USZ, University of Zurich, Switzerland
*Corresponding author: M Samardzija, Laboratory for Retinal Cell Biology, Department Ophthalmology, USZ, University of Zurich, Wagistr. 14, Schlieren, CH-8952, Switzerland. Tel: +41 44 5563 007; Fax: +41 44 5563 999; E-mail: marijana.samardzija@usz.uzh.ch
[2]These authors contributed equally to this work.
Abbreviations: ALB, albumin; Aqp, aquaporin; BLD, blue light damage; BRB, blood–retinal barrier; CALB1, calbindin; Cldn, claudin; CR, calretinin; GCL, ganglion cell layer; IBA1, ionized calcium-binding adaptor molecule 1; Il1b, interleukin 1 beta; INL, inner nuclear layer; IPL, inner plexiform layer; IS, inner segments; NRL, neural retina leucine zipper; OCT, optical coherence tomography; ONL, outer nuclear layer; OPL, outer plexiform layer; OS, outer segments; PS, photoreceptor segments; RPE, retinal pigment epithelium; Tjp, tight junction protein; Tnf, tumor necrosis factor; *wt*, wild-type
Received 22.7.15; revised 30.9.15; accepted 06.10.15; Edited by A Verkhratsky

blue light.[16] In rats and mice, high irradiances to shorter wavelengths are also more damaging to photoreceptors than broad-bandwidth light.[17] This suggests that if conditions including exposure duration, light intensity and wavelength are appropriately chosen, the light damage model can be applied to study cone degenerations.

Here we exposed the *R91W;Nrl*$^{-/-}$ mice to toxic blue light levels to induce cone cell death. We show that the all-cone retina of *R91W;Nrl*$^{-/-}$ mice can be damaged, although to a lesser extent than the rod-dominant mouse retina. While blue light damage (BLD) in wild-type (*wt*) mice causes breakdown of the retinal pigment epithelium (RPE), it affects the inner blood–retinal barrier (BRB) in *R91W;Nrl*$^{-/-}$ mice. Vascular leakage is accompanied by retinal swelling and edema, which seems to be more prominent in the all-cone retina.

Results

To establish the blue light sensitivity of the all-cone retina we exposed *R91W;Nrl*$^{-/-}$ mice to 410 nm light for up to 30 min and measured retinal cell death by ELISA 48 h after BLD (Figure 1a). As little as 2 min of exposure induced loss of photoreceptors in *wt* mice (not shown[18]). In contrast, *R91W;Nrl*$^{-/-}$ mice were much more resistant to BLD and only prolonged exposure (20 and 30 min) led to cell death (Figure 1a). As the 20 min exposure led to a higher variability in damage severity, we used a 30 min exposure for all further experiments.

To localize dying cells, *R91W;Nrl*$^{-/-}$ and *wt* mice were analyzed by TUNEL assay 24 h, 3 and 10 days after BLD and compared with non-exposed controls (ctrl). TUNEL-positive cells in *wt* mice were detected only in a focal area (termed hotspot[17]) in the central retina (Figure 1b). At 24 h and 3 days post exposure, almost all TUNEL-positive cells were found in the outer nuclear layer (ONL) and only occasionally in the inner nuclear layer (INL) of *wt* mice. Ten days after BLD almost all nuclei in the hotspot area were lost (Figure 1b). In *R91W;Nrl*$^{-/-}$ mice, however, TUNEL-positive cells were not only found centrally but also in the periphery (Figure 1b). Dying cells were detected both in the ONL and INL at 24 h and 3 days post exposure. Overall, *R91W;Nrl*$^{-/-}$ mice had fewer TUNEL-positive cells than *wt* mice, suggesting that BLD was less severe than in *wt* mice.

BLD induces focal photoreceptor death and accumulation of microglia/macrophages in the hotspot region of *wt* mice.[18] Therefore, we stained retinal flat mounts for IBA1, a marker for microglia and macrophages (Figures 2 and 3). In *wt* mice, density of IBA1-positive cells was clearly increased in a focal area at 3 days and remained detectable even 10 days after the light insult (Figure 2, left dotted circle). A similar IBA1-positive region was identified in *R91W;Nrl*$^{-/-}$ mice. However, it was smaller in diameter and stronger in signal intensity at 3 days (Figure 2, right). Ten days after BLD, an intensely stained region was still visible in *R91W;Nrl*$^{-/-}$ mice, but reduced in size suggesting disappearance of IBA1-positive cells (Figure 2, right). A closer inspection of the hotspot regions revealed accumulation of ameboid microglia in both *wt* and *R91W;Nrl*$^{-/-}$ retinas at 3 days after BLD (Figures 3a and e, respectively). The number of ameboid microglia appeared higher in *R91W;Nrl*$^{-/-}$, and occupied all retinal layers especially the plexiform layers as opposed to the *wt* (Figures 3c and g). Compared with the adjacent unexposed region, the hotspot area in *R91W;Nrl*$^{-/-}$ seemed to be swollen with less-densely packed nuclei, especially in the INL (Figure 3, compare g with h). As expected, microglia were ramified in regions outside this central region in both mouse lines (Figures 3b, d, f and h).

Blue light was shown previously to damage RPE cells thereby disrupting the outer BRB.[19] A strong albumin staining

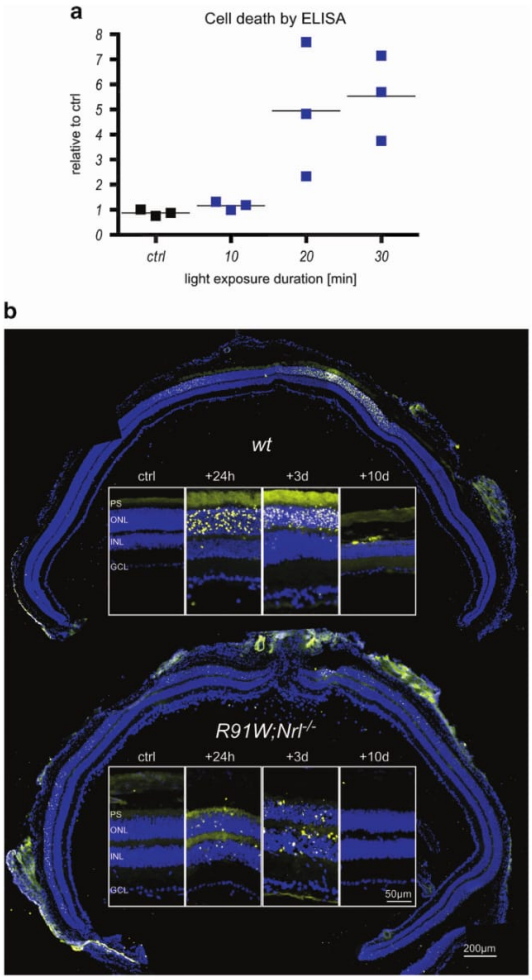

Figure 1 Retinal cell death after blue light exposure. (**a**) Dose–response for blue light-induced damage in the *R91W;Nrl*$^{-/-}$ all-cone retina. *R91W;Nrl*$^{-/-}$ mice were exposed for 10–30 min to blue light (410 ± 10 nm; 60 mW/cm^2) and cytoplasmic nucleosomes in the retina were quantified using an ELISA-based cell death detection kit 48 h after exposure. Horizontal lines represent mean values of $N = 3$ animals. Levels of unexposed control (ctrl) retinas were set to 1. (**b**) Apoptotic cells detected by TUNEL on retinal cross-sections of unexposed control (ctrl) and exposed eyes at the time points indicated. DAPI (blue) was used to visualize cell nuclei. Retinal panoramas show representative examples at 24 h following BLD. Panels show most affected retinal areas at a higher magnification. PS: photoreceptor segments; ONL: outer nuclear layer; INL: inner nuclear layer; GCL: ganglion cell layer. $N = 3$. Scale bars as indicated

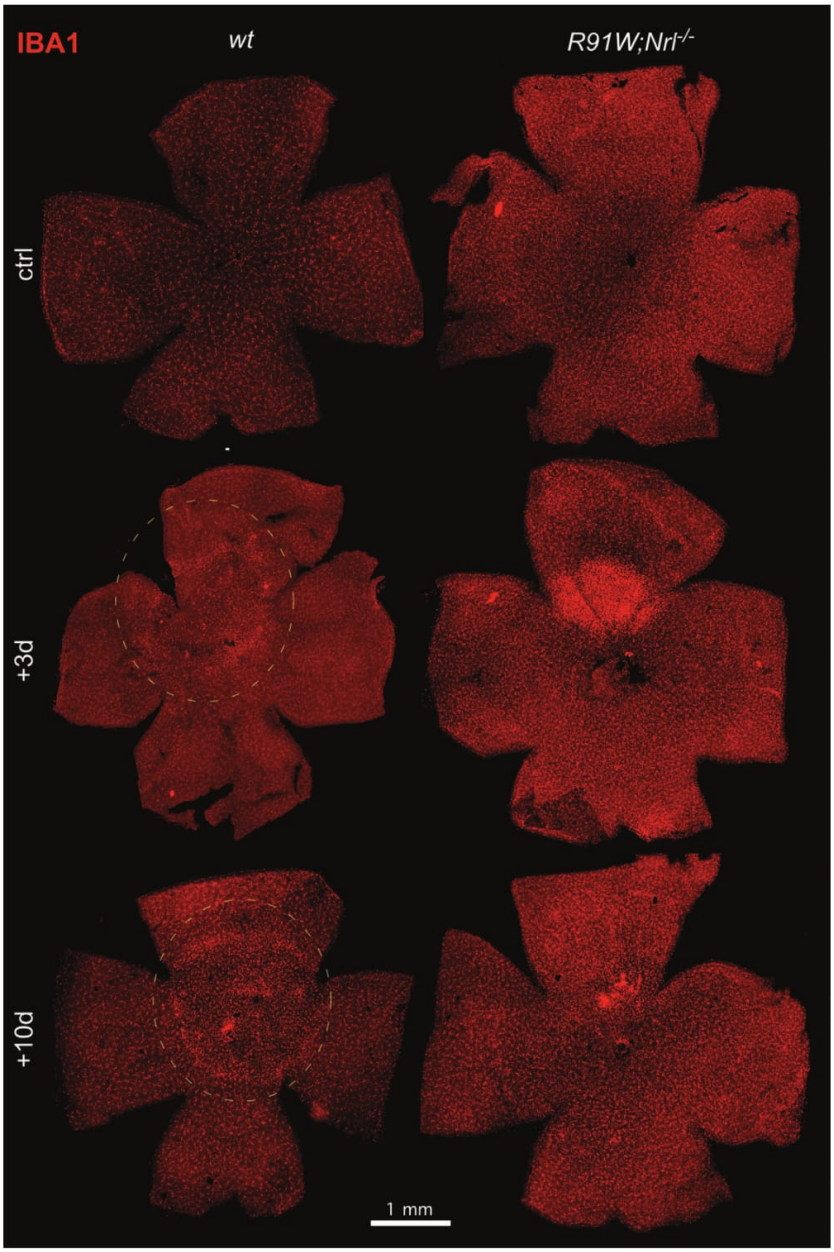

Figure 2 Retinal flat mounts of *wt* and *R91W;Nrl*$^{-/-}$ mice before (ctrl) or at 3 and 10 days after BLD stained for IBA1, a microglia/macrophage marker. Dotted circular line marks the hotspot region in *wt*. Note that the hotspot region is visible in all light-damaged retinas, but larger regions were affected in *wt* mice. $N = 3$. Scale bar as indicated

was detected in the region between the RPE and ONL corresponding to the inner and outer photoreceptor segments (IS and OS) at 3 days post exposure in *wt* mice (Figure 4a). Albumin staining was also visible in the OS of a control region outside of the hotspot (Figure 4b). This can probably be attributed to lateral diffusion to the neighboring non-damaged area, as non-exposed *wt* retinas showed no signal in the IS and OS (Figure 4c). In contrast to *wt* mice, albumin-positive signals were found in all retinal layers in the hotspot area of *R91W;Nrl*$^{-/-}$ mice (Figure 4d). This signal was specific, as the staining was restricted to the vessels of the three vascular plexi outside of the hotspot region (Figures 4e and j–m).

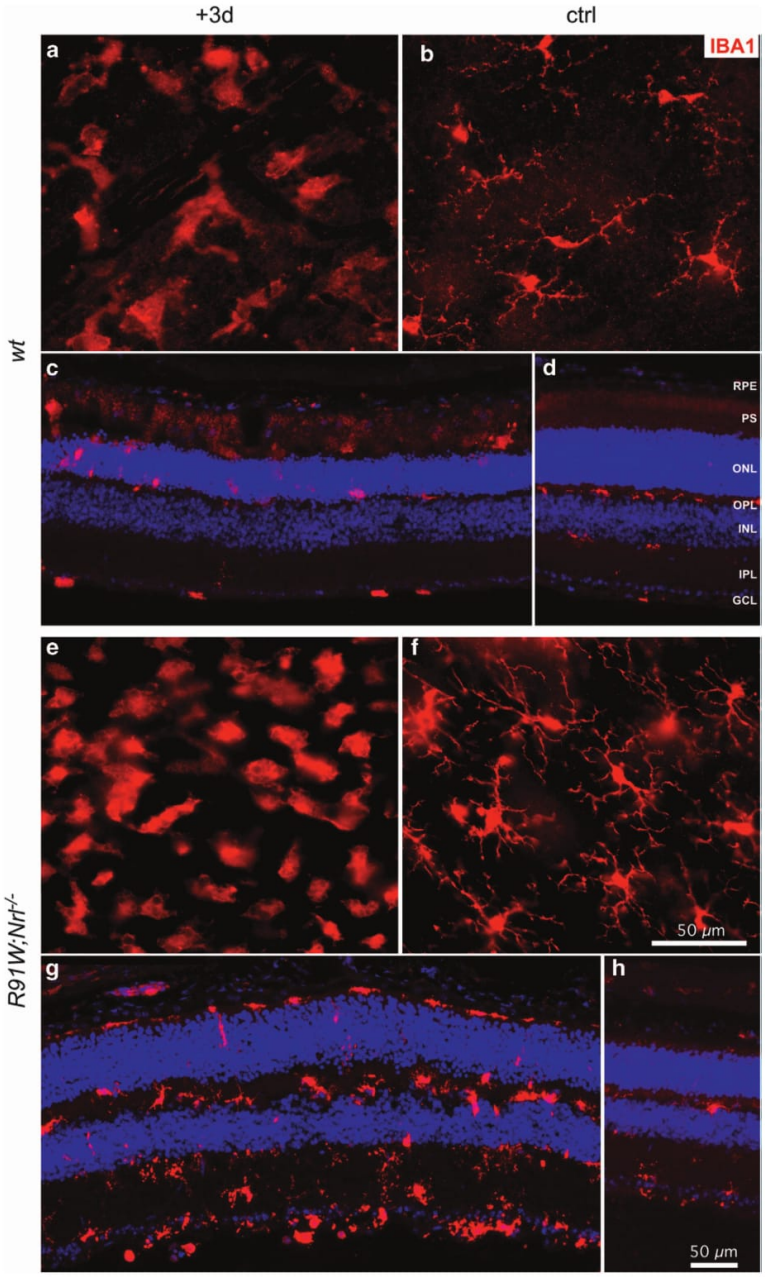

Figure 3 Microglia/macrophage accumulation within the hotspot area at 3 days (+3d; **a**, **c**, **e**, **g**) following BLD in *wt* and *R91W;Nrl*$^{-/-}$ retinas. Undamaged regions outside the hotspot served as internal controls (ctrl; **b**, **d**, **f**, **h**). Shown are retinal flat mounts (**a**, **b**, **e**, **f**; the focal plane in the outer plexiform layer) or retinal cryosections (**c**, **d**, **g**, **h**) immunostained for IBA1. RPE: retinal pigment epithelium; OPL: outer plexiform layer; IPL: inner plexiform layer; other abbreviations as in Figure 1. $N = 3$. Scale bars as indicated

To test if cells within the inner retina were affected by BLD we labeled horizontal cells with anti-calbindin, and amacrine and ganglion cells with anti-calretinin antibodies, respectively. Normal distribution for both markers was found in *wt* mice (Figures 4f and g). In *R91W;Nrl*$^{-/-}$ mice calbindin-positive horizontal cells were especially enlarged and displaced in the damaged region, whereas signal distribution and intensity in undamaged neighboring areas were similar to *wt* (Figures 4h and i).

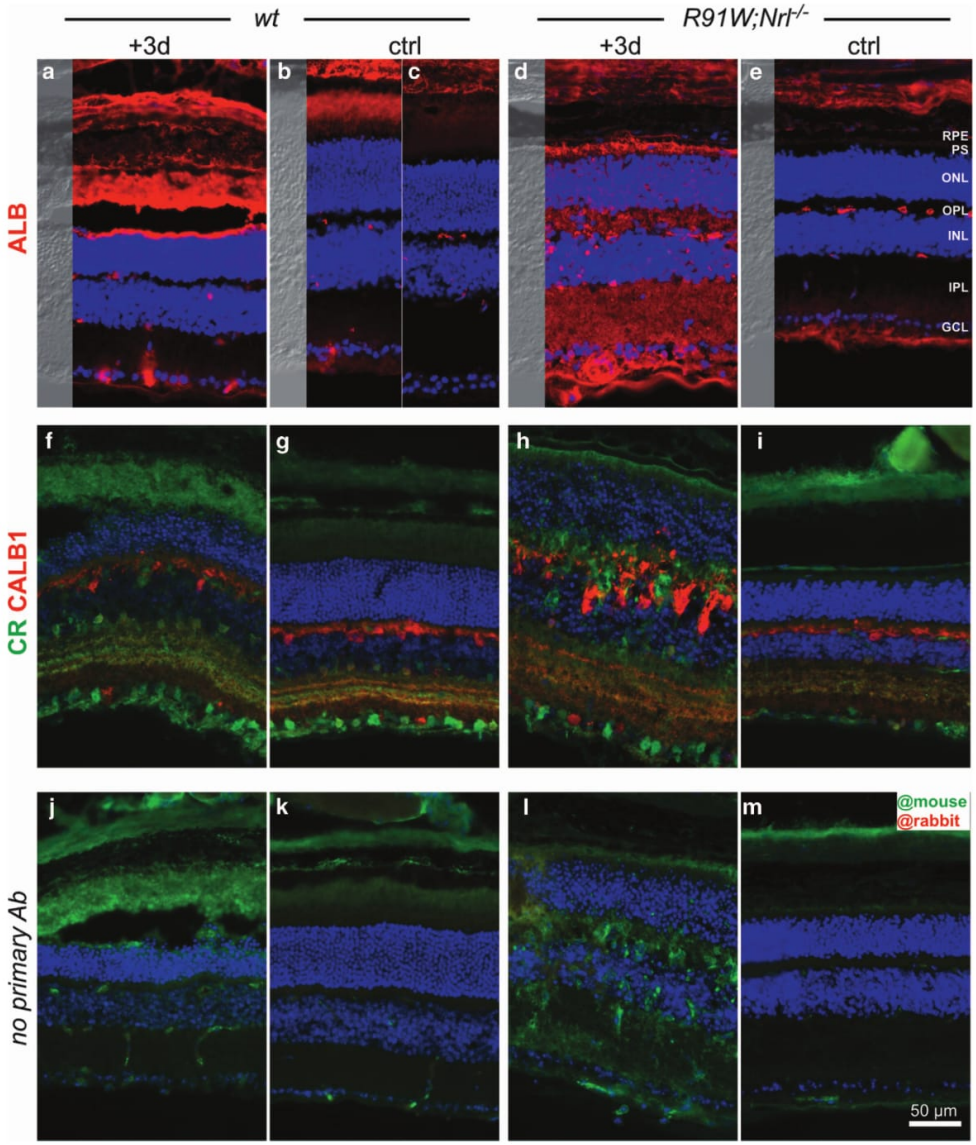

Figure 4 Blue light damage causes vascular leakage in the inner retina of *R91W;Nrl*$^{-/-}$ mice. Mice were exposed for 30 min and analyzed 3 days following BLD. Non-damaged retinal regions outside the hotspot (ctrl; **b**, **e**, **g**, **i**, **k** and **m**) and unexposed *wt* retina (**c**) were used as controls. Staining for albumin (ALB) in *wt* (**a**–**c**) and *R91W;Nrl*$^{-/-}$ (**d**, **e**) mice indicated presence of blood components. Note that ALB immunoreactivity outside the blood vessels was mostly detected in the outer retina of *wt* mice (**a**), whereas both the inner and outer retina of *R91W;Nrl*$^{-/-}$ were ALB-positive (**d**). Calbindin (CALB1) and calretinin (CR) were used as markers for horizontal, amacrine and ganglion cells (**f**–**i**). CALB1 staining revealed severe disturbance of horizontal cell morphology in *R91W;Nrl*$^{-/-}$ mice (**h**). Control stainings with anti-mouse secondary antibodies only showed immunoreactivity (green) in damaged (**j** and **l**) but not in neighboring undamaged retinal regions (**k** and **m**) likely due to cross-reactivity with immunoglobulins from blood that leaked to injured areas. Application of anti-rabbit secondary antibodies (**j**–**m**) did not result in a detectable signal (red). Abbreviations as in Figures 1 and 3. $N = 3$. Scale bar as indicated

Thus BLD increased vascular permeability, but affected *wt* and *R91W;Nrl*$^{-/-}$ mice differently. In *wt* mice, the leakage was found predominantly in the subretinal region and probably originated from disruption of the RPE. In all-cone retinas, BLD affected the inner BRB, which was accompanied by horizontal cell disorganization.

We next analyzed retinal morphology of both strains up to 10 days after BLD. In *wt* mice, almost all photoreceptor nuclei within the hotspot region were pyknotic 24 h after BLD (Figure 5, compare a and b). Pyknosis was accompanied by vesiculation of IS and OS and swelling of the RPE (Figure 5b). RPE ruptured 3 days post exposure and large macrophages

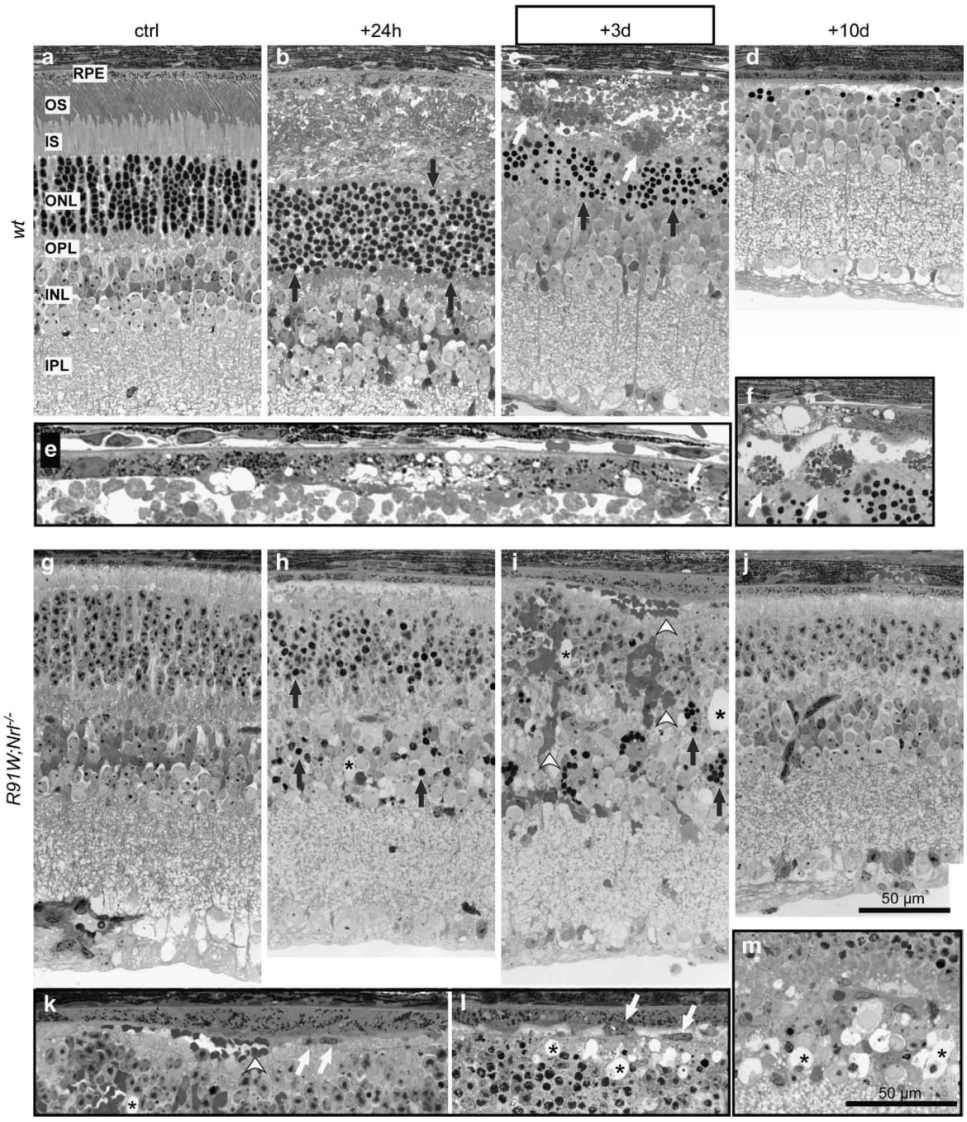

Figure 5 Retinal morphology of *wt* (**a**–**f**) and *R91W;Nrl*$^{-/-}$ (**g**–**m**) mice at indicated time points after blue light exposure. Boxed images (**e**, **f**, **k**–**m**) are high-magnification images of retinas at the +3d time point. All photoreceptors within the hotspot were pyknotic (black arrows) in *wt* mice at 24 h (**b**). ONL thinning, subretinal accumulation of large cells, presumably microglia/macrophages (white arrows), disruption and vesiculation of the RPE was detected 3 days after the insult (**c**, **e**, **f**). No photoreceptors remained in the hotspot region of *wt* at 10 days after exposure (**d**). In *R91W;Nrl*$^{-/-}$ mice pyknotic nuclei were detected in the ONL but also in the INL at 24 h after BLD (**h**). Three days following light damage (**i**, **k**–**m**) blood cells (white arrowheads) appeared in the OPL, ONL and in the subretinal space (**i**, **k**). Cystoid spaces (*) emerged throughout the outer retina (**i**, **k**, **l**) including the INL (**m**). The RPE occasionally thickened (**i**, **k**) and macrophage/microglia (white arrows) cells were detected in the subretinal space (**l**). Ten days after BLD, only a reduced number of nuclei in the ONL revealed the position of the hotspot. All other signs of blue light-induced damage have been resolved (**j**). Black arrows: pyknotic nuclei. White arrows: macrophage/microglia. Arrowheads: blood cells. *: cystoid spaces. OS: outer segments, IS: inner segments, other abbreviations as in Figures 1 and 3. Scale bars are as indicated for boxed and unboxed images. $N = 3$ per time point and strain

were mobilized to the region between the RPE and ONL (Figures 5c, e and f). Ten days after BLD, the RPE recovered but almost all photoreceptor nuclei were lost and no OS and IS remained in the hotspot area (Figure 5d).

In *R91W;Nrl*$^{-/-}$ mice, fewer pyknotic cells were detected in the ONL 24 h after BLD (Figure 5h). Consistent with the TUNEL stainings (Figure 1b), some pyknotic nuclei were also visible in the INL (Figure 5h). Three days after BLD some retinal areas showed massive vascular leakage extending from the inner retina to the subretinal space (Figure 5i). Cystoid spaces were detected in INL, outer plexiform layer, ONL and subretinally (∗ in Figures 5h, i and k–m). In some

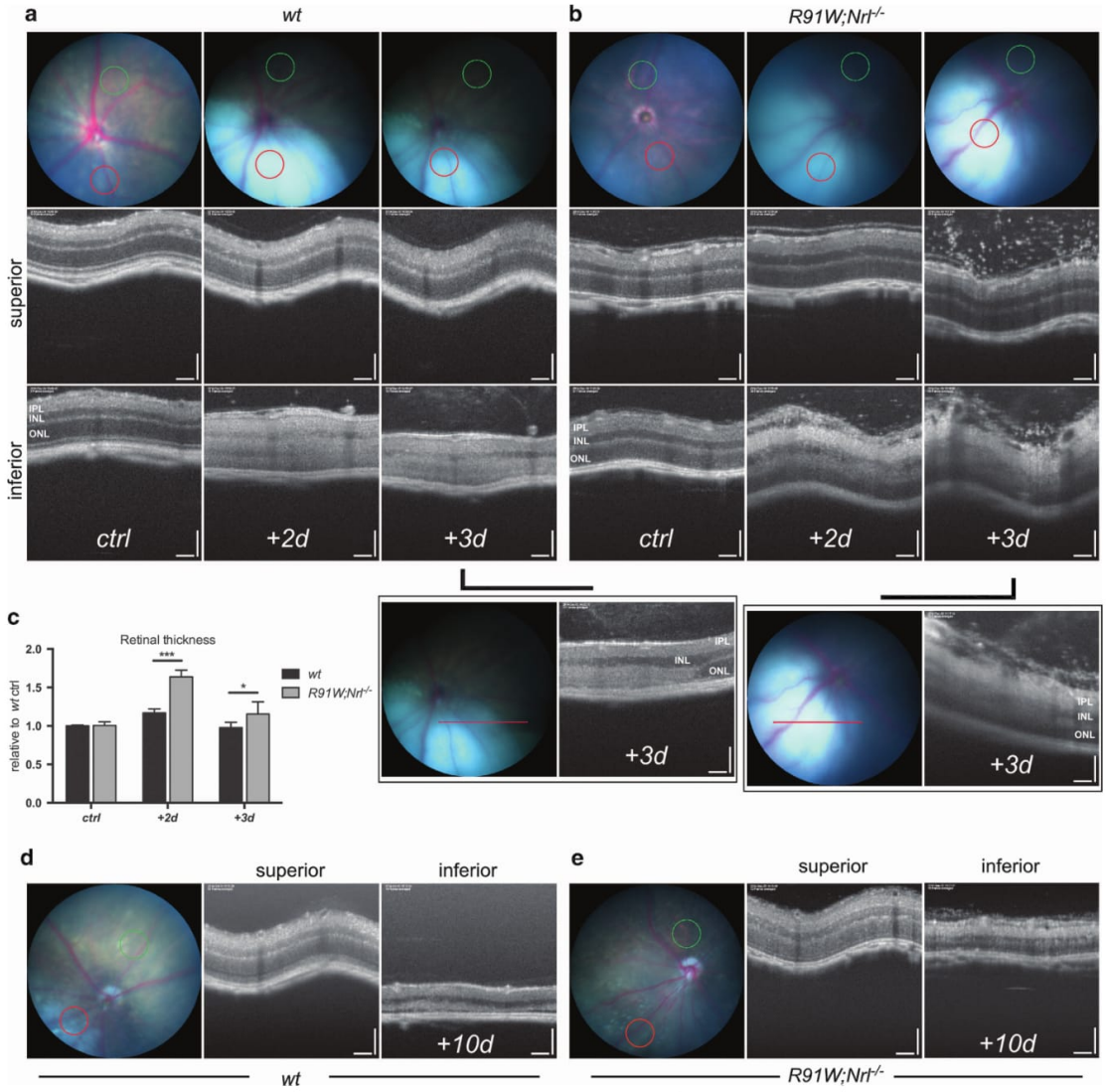

Figure 6 Fundus (color) and corresponding OCT (black and white) images of *wt* (**a**, **d**) and *R91W;Nrl*$^{-/-}$ (**b**, **e**) mice taken up to 10 days following BLD. The positions of OCT scans are shown in fundi as colored circles/lines (green, superior; red, inferior). At 2 and 3 days after BLD the hotspot regions appeared as a pale bluish spot, much lighter than the rest of the fundus (**a**, **b**). OCT revealed that INL and ONL in the damaged (inferior) but not the control area (superior) became hyperreflective in *wt*, whereas hyperreflectivity was very pronounced in the IPL but absent in the ONL in *R91W;Nrl*$^{-/-}$ mice. Boxed panels in (**a**) and (**b**) show linear scans of the transition zones analyzed 3 days following BLD. Increased retinal thickness was especially prominent in *R91W;Nrl*$^{-/-}$ mice. Quantification of retinal thickness in *R91W;Nrl*$^{-/-}$ and *wt* eyes that were unexposed (ctrl) or exposed to blue light, as indicated (**c**). Values are expressed relative to mean value of unexposed *wt* mice that was set to 1 ($N=4$ *wt*, 5 *R91W;Nrl*$^{-/-}$; $^{*}P<0.05$; $^{***}P<0.001$). At 10 days after BLD the hotspot regions can be recognized by whitish material appearing in the fundus and by a thinned retina in OCT (**d**, **e**). Note: the second and third time points in panels (**a**) and (**b**) show data from the same mouse followed for two consecutive days. Scale bars 100 μm

instances blood cells were observed subretinally close to the RPE (Figures 5i and k). In the most affected regions variations in RPE thickness were visible but no obvious rupture was detected (Figures 5k and l). Larger cells, presumably activated microglia or macrophages were detected in the subretinal space (Figure 5l, white arrows). Ten days after the insult the remaining cones and RPE seemed to have recovered completely in the most affected areas of *R91W;Nrl*$^{-/-}$ mice (Figure 5j).

Our data suggested an outer BRB breakdown after BLD in *wt* retinas supporting an earlier work reporting RPE disruption and retinal fluid influx after blue light exposure.[19] This prompted us to analyze the consequences of possible fluid leakage in each model *in vivo*. Mice were examined at 2, 3 and

10 days after BLD by funduscopy and optical coherence tomography (OCT) imaging (Figure 6). Retinal funduscopy revealed a well-defined hotspot paler than the remaining retina 2 and 3 days after BLD (Figures 6a and b). This color change was previously postulated to be the result of subretinal fluid accumulation.[18] The fundus appearance was very similar in *wt* and *R91W;Nrl*$^{-/-}$ mice up to 3 days post illumination (Figures 6a and b). However, at 10 days post illumination more autofluorescent material was visible in the hotspot region in the inferior *wt* mouse retina (Figure 6d). OCT images were taken to compare the retinal structure in the superior (control) and inferior (hotspot) region of the same eye. OCT scans of the injured areas revealed an overall change in retinal reflectivity at 2 and 3 days after light exposure (Figures 6a and b). This change in reflectivity was particularly visible on linear scans of transition zones covering both the hotspot and neighboring, non-exposed area (Figures 6a and b, boxed panels). In the injured area of *wt* mice a clear distinction between the layers was lost and both nuclear layers became hyperreflective (Figure 6a). Retinas appeared swollen especially at 2 days after light damage, which was confirmed by measurement of the retinal thickness (Figure 6c). In *R91W;Nrl*$^{-/-}$ mice the ONL retained its darker appearance while the INL and especially the IPL showed hyperreflectivity (Figure 6b). A strong increase in retinal thickness and loss of a clear separation between the layers within the inner retina was visible 2 and 3 days after BLD in *R91W;Nrl*$^{-/-}$ mice (Figures 6b and c). In addition, a number of punctate spots were observed epiretinally (vitreal side) in both superior and inferior OCT scans especially 3 days after BLD (Figure 6b). Ten days following the light insult, OCT scans showed a clear reduction in retinal thickness in the hotspot of both mouse lines (Figures 6d and e).

OCT and morphological analysis revealed edema formation in both mouse models. This prompted us to analyze the gene expression levels of aquaporins (*Aqp*) and tight junction proteins as they are important for maintaining the retinal fluid balance and the integrity of the BRB. Alterations in AQP1 and AQP4 expression have previously been detected in a rat model of BLD.[20] Decreased retinal expression of *Aqp1* was found in *wt* mice during the first 3 days following BLD. After that, expression recovered and reached or even surpassed control levels at 10 days after exposure (Figure 7). Surprisingly, retinas of *R91W;Nrl*$^{-/-}$ mice showed very low expression levels of *Aqp1* at all time points tested (Figure 7). As strong *Aqp1* expression was previously found in photoreceptors[21] our data suggest that *Aqp1* is mainly expressed by rods but not by cones. A similar pattern of expression characterized by an initial sharp decrease following the light insult was observed for *Aqp4* in both mouse strains. *Wt* mice had a slightly delayed recovery of expression as judged by the 12 h time point (Figure 7). Claudins, including CLDN5, compose the major structural and functional elements of tight junctions between endothelial cells forming the inner BRB. In both mouse lines BLD caused an initial drop in transcription (6 h time point). *Cldn5* expression levels recovered fast and were stabilized at 24 h in *wt,* whereas in *R91W;Nrl*$^{-/-}$ mice they peaked at 3 days after BLD. The expression of tight junction protein-1 (*Tjp1)* dropped in the *wt* and *R91W;Nrl*$^{-/-}$ mice 6 h after BLD. Surprisingly, *Tjp1* levels were low in *R91W;Nrl*$^{-/-}$ mice in general. In addition, the expression of the proinflammatory cytokines *Il1b* and *Tnf* was highly increased in *R91W;Nrl*$^{-/-}$, especially 24 h after BLD (Figure 7). Both cytokines were also upregulated in *wt* mice after BLD insult, but to a lesser extent (Figure 7).

Collectively, our data suggest low basal expression of *Aqp1* and *Tjp1* in *R91W;Nrl*$^{-/-}$ mice. Differential expression of these genes and thus alterations in water homeostasis and tight junction formation in retinas of the all-cone *R91W;Nrl*$^{-/-}$ mice may account for the strong edema formation observed in *R91W;Nrl*$^{-/-}$ mice after BLD.

Discussion

The aim of this study was to analyze light-induced retinal degeneration in the all-cone *R91W;Nrl*$^{-/-}$ mouse and compare it to the rod-dominant *wt* mouse. By using the *R91W;Nrl*$^{-/-}$ mouse model, we directly showed that blue light could induce cone cell death. However, cone photoreceptors were more resistant to BLD than rods. Degeneration was accompanied by the appearance of microglial cells in the injured area. Although activated microglia were mostly restricted to the damaged outer retina in *wt* mice, microglial cells were detected in all layers of the damaged *R91W;Nrl*$^{-/-}$ retina. Degeneration was accompanied by a more pronounced edema formation in *R91W;Nrl*$^{-/-}$ mice, and a strongly reduced basal expression of *Aqp1* and *Tjp1* that are involved in water extrusion and the formation of tight junctions, respectively. Also, an increased expression of *Tnf* and *Il1b* further corroborates a stronger local inflammatory response and edema in *R91W;Nrl*$^{-/-}$ mice after BLD.

Photoreceptor damage after blue light exposure was more pronounced in rod-dominant *wt* retinas with almost all photoreceptors lost within the hotspot in *wt* mice (Figure 5). This was accompanied by impairment of RPE integrity 3 days after light exposure. Although RPE changes were observed also in *R91W;Nrl*$^{-/-}$ mice, vesiculations and RPE rupture were only detected in exposed *wt* retinas. In theory, RPE cells of *R91W;Nrl*$^{-/-}$ mice should receive much more light due to the reduced levels of visual pigments, which are the main light absorbers in the retina. This argues that the RPE rupture observed in *wt* mice was not a result of direct photon-damage (photostress) to the RPE cells, but that it may be a secondary event. Organisciak and colleagues[7] hypothesized that the removal of light-damaged outer segments by the phagocytic activity of RPE cells may be responsible for oxidative stress and consequent RPE injury. In other words, RPE cells of *wt* mice may be poisoned by a surplus of toxic phagocytic material. In addition, an excess of all-trans-retinal diffusing from damaged photoreceptors could also be toxic for RPE cells.[22] As the photoreceptor damage in *R91W;Nrl*$^{-/-}$ is not as strong and photoreceptor segments are shorter with less-chromophore present, phagocytosis of the debris after BLD may be less challenging for the RPE, and the potential toxicity of all-*trans*-retinal may be reduced in the all-cone retina. Alternatively, basic antioxidative defense mechanisms might be enhanced in the RPE of *R91W;Nrl*$^{-/-}$ mice as an adaptation to the potentially increased light levels reaching the RPE. This may render RPE cells in *R91W;Nrl*$^{-/-}$ mice more resistant, a hypothesis that will be tested in future experiments.

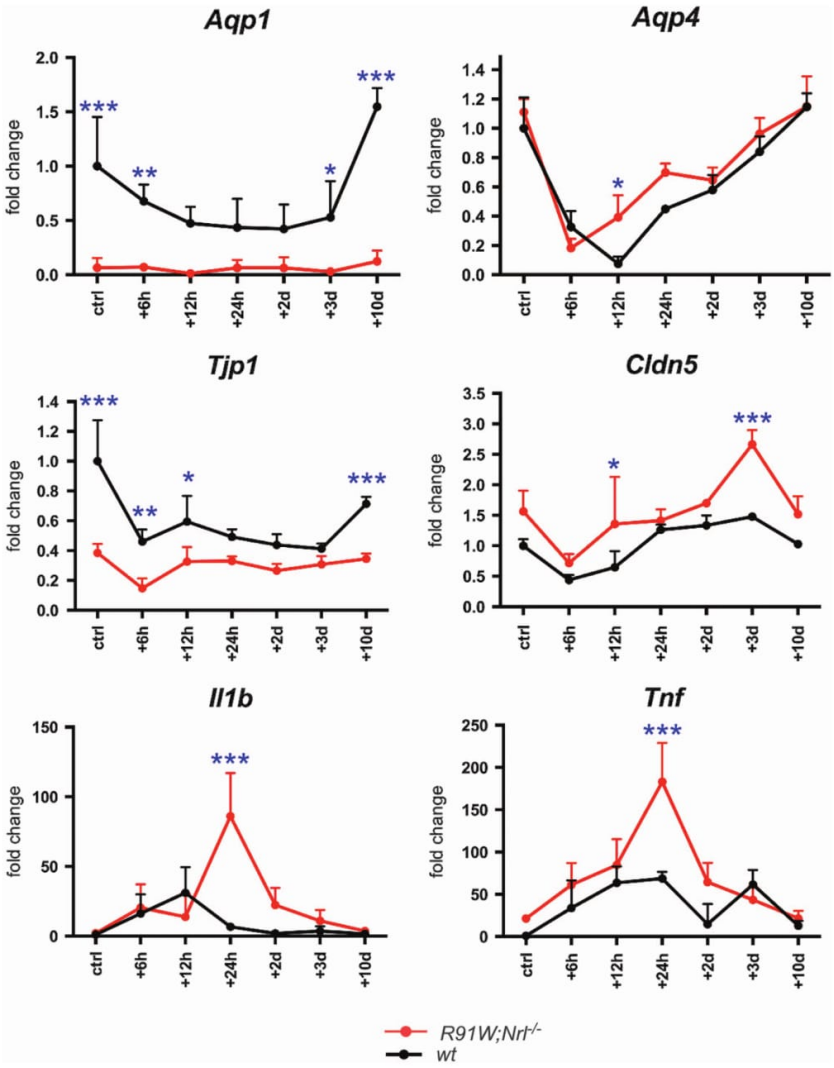

Figure 7 Reduced basal expression of *Aqp1* and *Tjp1* in the retina of *R91W;Nrl*$^{-/-}$ all-cone mice. Expression levels of indicated genes were analyzed before (ctrl) and at six time points (as indicated) after BLD by semiquantitative real-time PCR. Expression is shown relatively to unexposed *wt* (ctrl), which was set to 1. Shown are means ± S.D. $N = 3$. Two-way ANOVA was used to compare expression levels between *R91W;Nrl*$^{-/-}$ (red line) and *wt* (black line) mice at individual time points. *$P < 0.05$; **$P < 0.01$; ***$P < 0.001$. *Aqp*, aquaporin; *Tjp*, tight junction protein; *Cldn*, claudin; *Il1b*, interleukin 1 beta; *Tnf*, tumor necrosis factor

Shorter outer segments and lower chromophore levels reduce the maximal photon catch capacity of cones leading to a reduced light absorption in retinas of *R91W;Nrl*$^{-/-}$ mice in general. As a consequence, incoming light is not efficiently absorbed by photoreceptors and photons are thus more likely to scatter in the retina. Such an increased intraretinal light scattering in *R91W;Nrl*$^{-/-}$ mice may explain the increased number of TUNEL-positive cells in the retinal periphery of these mice (Figure 1) as well as the damage in the inner retina where we detected vascular leakage, appearance of cystoid spaces, retinal swelling and horizontal cell hypertrophy. Although it is unclear, which cells were damaged in the INL, we speculate that some Müller glia cells might have been affected. Indeed, it was recently shown that ablation of Müller cells caused partial breakdown of the inner BRB leading to vascular leakage,[23] a phenomenon resembling our observations presented here (see below). We cannot exclude, however, that also some interneurons were affected but as no gross changes in INL thickness and morphology were detected at late time points (10 days, Figure 5j), BLD only mildly affected cells of the INL.

Albumin staining revealed that BLD caused an outer BRB breakdown in *wt* mice (Figure 4). The resulting edema was especially prominent 2 days post exposure as evidenced by

OCT analysis (Figure 6). Development of local edema within the outer retina after excessive light exposure has been described in the literature as a consequence of RPE damage as well as of the normotonic shrinkage of cells undergoing apoptosis.[24] Although the outer BRB was compromised in *wt* mice, the inner BRB was affected in addition in *R91W;Nrl*$^{-/-}$ mice: intraretinal vascular leakage and albumin immunoreactivity was detected in all retinal layers (Figures 4 and 5). Furthermore, erythrocytes were found in the subretinal space next to a thickened but not ruptured RPE (Figure 5i). Although data suggest a disruption of the inner BRB, it is still possible that tight junctions in the RPE were affected loosening cell–cell contacts and contributing to edema formation in the all-cone retinas of *R91W;Nrl*$^{-/-}$ mice after BLD. Retinal hemorrhages can cause serious problems and vision loss in human patients. Yet, little is known which direct cytotoxic consequences the extravasated blood components have on cells and tissues. Protoporphyrin IX, a blood-borne photosensitizer, was shown to produce free radicals that can damage cells.[25] An early work in a rabbit model of experimental subretinal hemorrhages suggested hemoglobin toxicity[26] that was further substantiated in various models showing that cell-free hemoglobin and iron are strong neurotoxins.[27] Thus, it seems likely that apoptosis detected in the INL of *R91W;Nrl*$^{-/-}$ mice was not a direct consequence of light exposure but was indirectly caused by toxic effects of extravasated blood components. A recent report attributed photoreceptor degeneration in a mouse model of subretinal hemorrhage to the presence of blood constituents in the tissue and demonstrated the involvement of an inflammatory reaction in governing the severity of degeneration.[28] In our model, large macrophages and activated microglia were mobilized to the outer retina in *wt* mice. In *R91W;Nrl*$^{-/-}$ mice, however, these immune cells were increased in numbers and not only restricted to the outer retina but found in all layers. This was accompanied by a significantly stronger induction of *Tnf* and *Il1b* expression in *R91W;Nrl*$^{-/-}$ than in *wt* mice (Figure 7). It is important to note that microglial activation impairs BBB function by the release of various proinflammatory factors including TNF and IL1β, leading to a hyperpermeability shown to be associated with neurodegenerative disorders such as Alzheimers disease and multiple sclerosis (reviewed in ref. 29).

We detected BLD-induced edema formation in both mouse models by fundus imaging and OCT (Figure 6). However, swelling was not only more pronounced in *R91W;Nrl*$^{-/-}$ but it also persisted for a longer period than in *wt* mice (Figures 6a–c). The integrity of blood vessels and the regulation of water flux are important for the BRB and the maintenance of a physiologic tissue environment, respectively. Barrier function depends on tight junction proteins such as TJP1 (ZO1) in endothelial cells and water flux in the outer retina is at least partly regulated through AQP1 channels residing in the RPE and photoreceptor cells.[30] Reduced expression of *Tjp1* increases barrier permeability[31] and downregulation of *Aqp1*, among other factors, has been proposed to contribute to edema development in a rat model of branch retinal vein occlusion.[32] As *R91W;Nrl*$^{-/-}$ mice had significantly reduced basal expression levels of both, *Tjp1* and *Aqp1* in the retina (Figure 7), they may not only be prone to increased vascular leakage upon stress, but may also clear accumulated liquid less efficiently from the retinal tissue leading to prolonged edema.

In summary, we have analyzed the consequence of BLD for the all-cone retina. We show substantial cone degeneration after BLD that is accompanied with vascular leakage and strong edema formation. BLD *R91W;Nrl*$^{-/-}$ mice can be used as a platform to test potential therapeutic agents to prevent osmotic swelling and impaired fluid absorption, which, if left untreated in patients, may result in a severe visual impairment and blindness. Pharmacologic stimulation of purinergic receptor signaling may be a promising direction of research[33] and has already shown efficacy in a brain injury model.[34]

Materials and Methods

Mice. All animal experimentation adhered to the ARVO Statement for the Use of Animals in Ophthalmic and Vision Research and the regulations of the Veterinary Authorities of Kanton Zurich, Switzerland. The *R91W;Nrl*$^{-/-}$ strain was described recently.[1] 129S6 wild-type mice (Taconic, Ejby, Denmark) served as controls. Both mouse lines were housed in the animal facility of the University of Zurich in a 12 h:12 h light–dark cycle with access to food and water *ad libitum*. At the time of experimentation, the mice were between 6 and 8 weeks of age.

Blue light exposure and quantification of retinal damage. Blue light exposure was described recently in detail.[35] In brief, mice were dark-adapted overnight, pupils were dilated with cyclogyl 1% (Alcon Pharmaceuticals, Fribourg, Switzerland) and phenylephrine 5% (Ursapharm, Saarbrücken, Germany) in dim red light. Approximately 5 min before exposure, the mice were anesthetized subcutaneously with ketamine (85 mg/kg; Inresa Arzneimittel, Freiburg, Germany) and xylazine (4 mg/kg Bayer AG, Leverkusen, Germany) and placed on a pre-warmed surface. To keep both eyes moist during exposure, 2% methocel (OmniVision AG, Neuhausen, Switzerland) was applied. The left eyes were exposed for 10–30 min to blue light (410 $\pm$ 10 nm; 60 mW/cm^2 at the level of the cornea). Unexposed eyes served as controls. Following light exposure mice were kept in darkness overnight; and then returned to the normal light/dark cycle until analysis.

The extent of light-induced damage was assessed in retinas of *R91W;Nrl*$^{-/-}$ mice exposed for 10, 20 and 30 min to blue light. Forty-eight hours after light exposure, apoptotic cell death was quantified in isolated retinas using the ELISA-based determination of free nucleosomes in the cytoplasm (Cell Death Detection ElisaPlus, 1920685; Roche Diagnostics, Basel, Switzerland) according to the manufacturer's recommendation.

Immunofluorescence and retinal flat mounts. Mice were euthanized and eyes were marked dorsally by cauterization, enucleated, fixed in 4% PFA and processed for cryosectioning, as described earlier.[36] Naso-temporal cryosections (12 μm) were blocked for 1 h with 3% normal goat serum (containing 0.3% Triton X-100 in PBS), and incubated overnight at 4 °C with the following primary antibodies: rabbit anti-albumin (ALB) (1 : 500, RARaAlb; Nordic Immunology, Tilburg, Netherlands), rabbit anti-calbindin (CALB) (1 : 500, AB1778; Chemicon, Temecula, CA, USA), mouse anti-calretinin (CR) (1 : 1000, AB5054; Chemicon), and rabbit anti-allograft inflammatory factor 1 (alias IBA1) (1 : 1000, 019-19741; Wako, Neuss, Germany). After washing, slides were incubated with appropriate secondary antibodies labeled with Cy2 or Cy3 (Jackson ImmunoResearch Laboratories, Soham, UK), counterstained with 4′,6-diamidino-2-phenylindole (DAPI; Life Technologies, Zug, Switzerland), and analyzed with a digitalized microscope (Zeiss Axioplan, Jena, Germany).

For preparation of retinal flat mounts enucleated eyes were incubated for 20–30 min in 2% PFA prepared in PBS. Cornea and lens were removed and the retina was dissected from the sclera and flat-mounted in PBS. Retinal flat mounts were postfixed in 4% PFA for 10 min, washed in PBS, and blocked with 3% normal goat serum for 1 h. Flat mounts were incubated with anti-IBA1 (1 : 500, Wako) overnight. After washing in PBS, flat mounts were incubated with Cy3-labeled secondary antibody (Jackson ImmunoResearch Laboratories), washed, mounted and immunofluorescence staining was analyzed with microscope (Zeiss Axioplan).

Table 1 Primers used for semiquantitative real-time PCR

Gene	Forward	Reverse	Size (bp)
Actb	*CAACGGCTCCGGCATGTGC*	*CTCTTGCTCTGGGCCTCG*	*153*
Aqp1	*CACTTGGCCGCAATGACCT*	*CCAGAACGCACAGTACCAGC*	*96*
Aqp4	*TACTGGAGCCAGCATGAATC*	*CCACATCAGGACAGAAGACA*	*149*
Tjp1	*CAGCAGCTAAGGAAGAGTGG*	*ATTATCAGACACCGGCTCAG*	*105*
Cldn5	*TGCCTTCCTGGACCACAA*	*GCGCCAGCACAGATTCATA*	*119*
Il1b	*GCTATGGCAACTGTTCCTGA*	*GATGTGCTGCTGCGAGATT*	*171*
Tnf	*CCACGCTCTTCTGTCTACTGA*	*GGCCATAGAACTGATGAGAGG*	*95*

***In situ* cell death detection (TUNEL).** For TUNEL assay air-dried cryosections were postfixed for 10 min with 4% PFA, washed for 10 min in PBS before the tissue was permeabilized with freshly prepared 0.1% Triton X-100 in 0.1% sodium citrate for 3 min. The slides were washed in PBS twice for 1 min and labeled with the *In Situ* Cell Death Detection Kit (Roche Diagnostics, Rotkreuz, Switzerland, Cat. No. 11 684 795 910). Five μl terminal deoxynucleotidyl transferase enzyme solution and 45 μl label solution, containing fluorescein labeled deoxyuridine-triphosphate, were mixed and applied to the slides and incubated for 1 h at 37 °C in a humid chamber. Slides were washed, counterstained with DAPI (Life Technologies), mounted and analyzed as described above.

Morphology. The detailed procedure was described recently.[36] In brief, eyes were marked dorsally, enucleated and fixed in 2.5% glutaraldehyde. Dorsal and ventral eye halves were separated by a cut through the optic nerve head and separately embedded in epon plastic. For light microscopy, semithin cross-sections (0.5 μm) were counterstained with toluidine blue and analyzed with a digitalized microscope (Zeiss Axioplan).

Fundus imaging and OCT. Five minutes prior to fundus imaging, the pupils were dilated and mice were anesthetized as described above. During imaging, the eyes were lubricated with methocel 2% (OmniVision AG). Retinal fundus images were taken during the same session as corresponding OCT scans using the MicronIV fundus camera and OCT Scan Head equipped with the mouse objective nosepiece with integrated polarizing beam splitter (Phoenix Research Labs, Pleasanton, CA, USA). The MicronIV was equipped with a Xenon lamp as a light source and Semrock FF01-554/211 filter limiting the wavelength range for bright filed imaging from 450 to 680 nm. The OCT device featured a broadband superluminescent diode at 830 nm customized for retinal imaging of mice. The scan region on the mouse retina was 1.8 mm in the X and the Y direction. Linear or circle OCT scans consisted of a series of 1024 single point A-Scans. OCT circle scans started at the 9 : 00 position and traveled counterclockwise. Scans from superior and inferior (damaged) retinal areas were taken and compared among the strains and conditions. Images were captured using StreamPix 5 and Micron OCT commercial softwares (Phoenix Research Labs). The two fundus images showing the upper (green circle) and lower (red circle) scan position were superimposed using Adobe Photoshop CS3 (Adobe Systems, Inc., San Jose, CA, USA). At least three mice per condition and strain were analyzed. Scale bars 100 μm. Average retinal thickness, representing the distance between nerve fiber layer and the RPE (apical side), was determined using the InSight—Animal OCT Segmentation Software (Phoenix Research Labs). Retinal thickness was measured in the most affected area of the hotspot and in the unexposed contralateral eye that served as control (ctrl). Numerical data were exported for statistical analysis described below.

RNA isolation and semiquantitative real-time PCR. Retinas were removed trough a slit in the cornea and snap-frozen in liquid nitrogen. Total retinal RNA was isolated using an RNA isolation kit (RNeasy, Qiagen, Hilden, Germany), which included a DNase treatment. One microgram of total RNA was used for reverse transcription using oligo(dT) and M-MLV reverse transcriptase (Promega, Dübendorf, Switzerland). Gene expression was analyzed by real-time PCR on 10 ng template cDNA using PCR polymerase ready mix (LightCycler480 SYBR Green I Master; Roche Diagnostics), and a LightCycler480 thermocycler (Roche Diagnostics). Specific primer pairs (Table 1) were designed to span a large intronic region or an exon/exon boundary of the target genes. Signals were normalized to *Actb* and relative expression was calculated using LightCycler480 software (Roche Diagnostics) using a calibrator sample.

Statistical analysis. Statistical analysis was performed using Prism4 software (GraphPad, San Diego, CA, USA). All data are presented as mean values $\pm$ S.D.; $N \geq 3$. Two-way ANOVA followed by a Bonferroni's *post hoc* test was used to determine significance. *P*-values below 0.05 were considered significant.

Conflict of Interest

The authors declare no conflict of interest.

Acknowledgements. The authors thank Andrea Gubler, Cornelia Imsand and Christel Beck for their excellent technical support. Supported by the Swiss National Science Foundation (SNF #31003A_133043), University of Zurich Forschungskredit, Vontobel Foundation, Hermann Kurz Foundation and SwissLife.

1. Samardzija M, Caprara C, Heynen SR, Willcox DeParis S, Meneau I, Traber G *et al.* A mouse model for studying cone photoreceptor pathologies. *Invest Ophthalmol Vis Sci* 2014; **55**: 5304–5313.
2. Samardzija M, von Lintig J, Tanimoto N, Oberhauser V, Thiersch M, Reme CE *et al.* R91W mutation in Rpe65 leads to milder early-onset retinal dystrophy due to the generation of low levels of 11-cis-retinal. *Hum Mol Genet* 2008; **17**: 281–292.
3. Samardzija M, Tanimoto N, Kostic C, Beck S, Oberhauser V, Joly S *et al.* In conditions of limited chromophore supply rods entrap 11-cis-retinal leading to loss of cone function and cell death. *Hum Mol Genet* 2009; **18**: 1266–1275.
4. Mears AJ, Kondo M, Swain PK, Takada Y, Bush RA, Saunders TL *et al.* Nrl is required for rod photoreceptor development. *Nat Genet* 2001; **29**: 447–452.
5. Takahashi Y, Chen Y, Moiseyev G, Ma JX. Two point mutations of RPE65 from patients with retinal dystrophies decrease the stability of RPE65 protein and abolish its isomerohydrolase activity. *J Biol Chem* 2006; **281**: 21820–21826.
6. Wenzel A, Grimm C, Samardzija M, Reme CE. Molecular mechanisms of light-induced photoreceptor apoptosis and neuroprotection for retinal degeneration. *Prog Retin Eye Res* 2005; **24**: 275–306.
7. Organisciak DT, Vaughan DK. Retinal light damage: mechanisms and protection. *Prog Retin Eye Res* 2010; **29**: 113–134.
8. Cicerone CM. Cones survive rods in the light-damaged eye of the albino rat. *Science* 1976; **194**: 1183–1185.
9. Mohand-Said S, Deudon-Combe A, Hicks D, Simonutti M, Forster V, Fintz AC *et al.* Normal retina releases a diffusible factor stimulating cone survival in the retinal degeneration mouse. *Proc Natl Acad Sci USA* 1998; **95**: 8357–8362.
10. Leveillard T, Mohand-Said S, Lorentz O, Hicks D, Fintz AC, Clerin E *et al.* Identification and characterization of rod-derived cone viability factor. *Nat Genet* 2004; **36**: 755–759.
11. Punzo C, Kornacker K, Cepko CL. Stimulation of the insulin/mTOR pathway delays cone death in a mouse model of retinitis pigmentosa. *Nat Neurosci* 2009; **12**: 44–52.
12. Stone J, Maslim J, Valter-Kocsi K, Mervin K, Bowers F, Chu Y *et al.* Mechanisms of photoreceptor death and survival in mammalian retina. *Prog Retin Eye Res* 1999; **18**: 689–735.
13. Collier RJ, Waldron WR, Zigman S. Temporal sequence of changes to the gray squirrel retina after near-UV exposure. *Invest Ophthalmol Vis Sci* 1989; **30**: 631–637.
14. Yetemian RM, Brown BM, Craft CM. Neovascularization, enhanced inflammatory response, and age-related cone dystrophy in the Nrl$^{-/-}$Grk1$^{-/-}$ mouse retina. *Invest Ophthalmol Vis Sci* 2010; **51**: 6196–6206.
15. Okano K, Maeda A, Chen Y, Chauhan V, Tang J, Palczewska G *et al.* Retinal cone and rod photoreceptor cells exhibit differential susceptibility to light-induced damage. *J Neurochem* 2012; **121**: 146–156.
16. Sperling HG. Spectral sensitivity, intense spectral light studies and the color receptor mosaic of primates. *Vision Res* 1986; **26**: 1557–1571.
17. Grimm C, Wenzel A, Williams T, Rol P, Hafezi F, Reme C. Rhodopsin-mediated blue-light damage to the rat retina: effect of photoreversal of bleaching. *Invest Ophthalmol Vis Sci* 2001; **42**: 497–505.
18. Joly S, Francke M, Ulbricht E, Beck S, Seeliger M, Hirrlinger P *et al.* Cooperative Phagocytes: Resident Microglia and Bone Marrow Immigrants Remove Dead Photoreceptors in Retinal Lesions. *Am J Pathol* 2009; **174**: 2310–2323.

19. Putting BJ, Zweypfenning RC, Vrensen GF, Oosterhuis JA, van Best JA. Blood-retinal barrier dysfunction at the pigment epithelium induced by blue light. *Invest Ophthalmol Vis Sci* 1992; **33**: 3385–3393.
20. Iandiev I, Wurm A, Hollborn M, Wiedemann P, Grimm C, Reme CE *et al.* Muller cell response to blue light injury of the rat retina. *Invest Ophthalmol Vis Sci* 2008; **49**: 3559–3567.
21. Iandiev I, Pannicke T, Reichel MB, Wiedemann P, Reichenbach A, Bringmann A. Expression of aquaporin-1 immunoreactivity by photoreceptor cells in the mouse retina. *Neurosci Lett* 2005; **388**: 96–99.
22. Maeda A, Maeda T, Golczak M, Chou S, Desai A, Hoppel CL *et al.* Involvement of all-trans-retinal in acute light-induced retinopathy of mice. *J Biol Chem* 2009; **284**: 15173–15183.
23. Shen W, Fruttiger M, Zhu L, Chung SH, Barnett NL, Kirk JK *et al.* Conditional Mullercell ablation causes independent neuronal and vascular pathologies in a novel transgenic model. *J Neurosci* 2012; **32**: 15715–15727.
24. Cachafeiro M, Bemelmans AP, Samardzija M, Afanasieva T, Pournaras JA, Grimm C *et al.* Hyperactivation of retina by light in mice leads to photoreceptor cell death mediated by VEGF and retinal pigment epithelium permeability. *Cell Death Dis* 2013; **4**: e781.
25. Bynoe LA, Del Priore LV, Hornbeck R. Photosensitization of retinal pigment epithelium by protoporphyrin IX. *Graefes Arch Clin Exp Ophthalmol* 1998; **236**: 230–233.
26. Glatt H, Machemer R. Experimental subretinal hemorrhage in rabbits. *Am J Ophthalmol* 1982; **94**: 762–773.
27. Regan RF, Panter SS. Neurotoxicity of hemoglobin in cortical cell culture. *Neurosci Lett* 1993; **153**: 219–222.
28. Zhao L, Ma W, Fariss RN, Wong WT. Minocycline attenuates photoreceptor degeneration in a mouse model of subretinal hemorrhage microglial: inhibition as a potential therapeutic strategy. *Am J Pathol* 2011; **179**: 1265–1277.
29. da Fonseca AC, Matias D, Garcia C, Amaral R, Geraldo LH, Freitas C *et al.* The impact of microglial activation on blood-brain barrier in brain diseases. *Front Cell Neurosci* 2014; **8**: 362.
30. Stamer WD, Bok D, Hu J, Jaffe GJ, McKay BS. Aquaporin-1 channels in human retinal pigment epithelium: role in transepithelial water movement. *Invest Ophthalmol Vis Sci* 2003; **44**: 2803–2808.
31. Liu W, Wang P, Shang C, Chen L, Cai H, Ma J *et al.* Endophilin-1 regulates blood-brain barrier permeability by controlling ZO-1 and occludin expression via the EGFR-ERK1/2 pathway. *Brain Res* 2014; **1573**: 17–26.
32. Rehak M, Hollborn M, Iandiev I, Pannicke T, Karl A, Wurm A *et al.* Retinal gene expression and Muller cell responses after branch retinal vein occlusion in the rat. *Invest Ophthalmol Vis Sci* 2009; **50**: 2359–2367.
33. Reichenbach A, Bringmann A. Purinergic signaling in retinal degeneration and regeneration. *Neuropharmacology* 2015, in press.
34. Talley Watts L, Sprague S, Zheng W, Garling RJ, Jimenez D, Digicaylioglu M *et al.* Purinergic 2Y1 receptor stimulation decreases cerebral edema and reactive gliosis in a traumatic brain injury model. *J Neurotrauma* 2013; **30**: 55–66.
35. Grimm C, Reme CE. Light damage as a model of retinal degeneration. *Methods Mol Biol* 2013; **935**: 87–97.
36. Heynen SR, Tanimoto N, Joly S, Seeliger MW, Samardzija M, Grimm C. Retinal degeneration modulates intracellular localization of CDC42 in photoreceptors. *Mol Vis* 2011; **17**: 2934–2946.

4 DISCUSSION

Our knowledge about cone cell death is still limited. Using different experimental mouse models, we analyzed and compared the effects of a chronically activated hypoxic response in cones and rods. Additionally, we analyzed retinal degenerative processes in *R91W;Nrl*$^{-/-}$ mice which were exposed to blue light.

4.1 The effects of a chronic hypoxia-like response on photoreceptors

Accumulating evidence suggests a role for reduced tissue oxygenation in the pathogenesis of several retinal diseases. Hypoxia is not only relevant for neovascular diseases such as diabetic retinopathy and retinopathy of prematurity, but it might also play an important role in the aging retina and contribute to the development of age-related diseases such as AMD. In the first part of this thesis, we analyzed the effects of a chronic hypoxia-like situation on photoreceptors. To assess the significance of hypoxia in the aged human retina (see 3.2), we analyzed gene expression levels in retinas of human donors. We observed an age-dependent tendency of increased expression of hypoxia-regulated genes, supporting our hypothesis that oxygen delivery in older eyes is reduced and may lead to mild but chronic hypoxia during the aging process.

To model such a chronic hypoxic response related to the human situation, we generated *BPCre;R91W;Nrl*$^{-/-}$*;Vhl*$^{f/f}$ (*cone*$^{\Delta Vhl}$, all-cone retina) and *OpsinCre;Vhl*$^{f/f}$ (*rod*$^{\Delta Vhl}$, rod-dominant retina) mice. We showed that cone-specific deletion of *Vhl* in *cone*$^{\Delta Vhl}$ mice caused pathological vessel growth into the photoreceptor layer and severe, progressive cone degeneration (see 3.1). Additionally, we found increased expression of *Timp3*, an important regulator of extracellular matrix remodeling associated with Sorsby's fundus dystrophy and neovascular AMD (Weber et al. 1994, Lin et al. 2006, Ardeljan et al. 2013). We clearly demonstrated that the observed neovascularization in *cone*$^{\Delta Vhl}$ mice is *Hif1*-dependent, as additional deletion of *Hif1a* (*BPCre;R91W;Nrl*$^{-/-}$*;Vhl*$^{f/f}$*;Hif1a*$^{f/f}$ (*cone*$^{\Delta VhlHif1a}$) mice) fully rescued the phenotype. *Cone*$^{\Delta Vhl}$ mice recapitulate some of the features of AMD pathology, particularly of a distinct form of neovascular AMD known as RAP. In RAP, vessels grow from the deep retinal plexus into the photoreceptor layer and subretinal space (see 1.3.2; (Hartnett et al. 1996, Yannuzzi et al. 2008)). By using *rod*$^{\Delta Vhl}$ mice, we showed that a chronic hypoxia-like response induced photoreceptor degeneration, which was dependent on chronic activation of HIF1 but not of HIF2 (see 3.2). *Rod*$^{\Delta Vhl}$ mice represent some features of dry AMD such as age-related photoreceptor degeneration and RPE defects. Although both *cone*$^{\Delta Vhl}$ and *rod*$^{\Delta Vhl}$ mice may not recapitulate all the features of the disease, as for example drusen accumulation, they provide suitable models to study hypoxia-related degeneration and test potential treatments.

4.1.1 Similarities and differences between *cone$^{\Delta Vhl}$* and *rod$^{\Delta Vhl}$* mouse models

Cone$^{\Delta Vhl}$ and *rod$^{\Delta Vhl}$* mice are used as models to simulate a chronic hypoxia-like situation in cones and rods, respectively. Even though the hypoxic response is triggered in different types of photoreceptors, the two models share similar aspects. As expected, in both models chronic activation of the hypoxic response led to increased expression of hypoxia-regulated genes. Increased expression of hypoxic target genes associated with glycolysis (e.g. *Glut1*, *Pdk1*) indicated a metabolic shift that may result in reduced oxidative phosphorylation and thus reduced ATP production. Affected energy metabolism might have detrimental consequences for photoreceptor survival. Indeed, we observed progressive photoreceptor degeneration in both *cone$^{\Delta Vhl}$* and *rod$^{\Delta Vhl}$* mice. Although the individual mechanisms leading to cell death and the contribution of a metabolic shift are still elusive, we provide evidence for a HIF1A-regulated process: the degenerative phenotype was rescued by genetic inactivation of HIF1A in both models. Consequently, we identify HIF1A as a therapeutic target to rescue hypoxia-mediated photoreceptor loss in patients. Interestingly, recently published work by Kurihara and colleagues suggests that another HIF isoform, HIF2A, affects survival of RPE cells and photoreceptors in a different mouse model of chronic hypoxia (Kurihara et al. 2016). In their study, they used VMD2-*Cre* to delete *Vhl* in the RPE and showed that chronic HIF2A-mediated metabolic stress (i.e. altered glucose and lipid metabolism) in RPE cells induced photoreceptor dysfunction and degeneration. Given the different impact of chronically active HIF1A and HIF2A in photoreceptor cells and the RPE, cell type-specific targeting of both HIF1A and HIF2A might be required to develop a successful therapy for AMD.

Additionally, in both *cone$^{\Delta Vhl}$* and *rod$^{\Delta Vhl}$* mice we observed RPE changes, albeit with variable severity. RPE damage was more pronounced in *cone$^{\Delta Vhl}$* mice as compared to *rod$^{\Delta Vhl}$* mice. Thicker RPE and/or partial loss of the RPE indicated RPE stress, which could be explained by several possible causes. At first, unspecific *Cre* expression could activate a hypoxic response in the RPE. However, since in both models *Cre* expression was found predominantly in the ONL and no sign of *Cre* activity was detected in the RPE (analyzed by using reporter mouse lines) this option can be ruled out. Secondly, RPE stress could be secondary to photoreceptor cell death due to increased amounts of phagocytic material. However, debris of degenerated rods in *rod$^{\Delta Vhl}$* mice should not represent a major problem for the RPE, as progression of degeneration in *rod$^{\Delta Vhl}$* mice is rather slow. Nevertheless, ingestion and accumulation of toxic byproducts resulting from activated HIF1A in photoreceptors may cause RPE stress. Additionally, secreted factors or reduced metabolic support may result in RPE damage. Clearly, more research is required to define these mechanisms.

In both *cone$^{\Delta Vhl}$* and *rod$^{\Delta Vhl}$* mice, we observed activation of the *Lif*/*Edn2*/*Fgf2* pathway (*cone$^{\Delta Vhl}$* mice not shown, *rod$^{\Delta Vhl}$* mice see 3.2 and (Lange et al. 2011b)). Expression of leukemia inhibitory factor (*Lif*) by a subset of Müller cells is strongly induced upon photoreceptor cell death (Joly et al. 2008). Different models for inherited and light-induced degeneration may activate LIF and an endogenous rescue defense system that involves the Janus kinase/signal transducer and activator of

transcription (Jak/STAT) signaling pathway (Samardzija et al. 2006, Burgi et al. 2009). Additionally, *Lif* has been shown to be involved in retinal neuroprotective signaling (Samardzija et al. 2006, Joly et al. 2008, Burgi et al. 2009, Leibinger et al. 2009). Despite the documented neuroprotective role of LIF in the retina, the regulation of *Lif* signaling and LIF target molecules are still under debate (Agca et al. 2013). In addition, it remains to be elucidated if modulating *Lif* could activate neuroprotective signaling and reduce degeneration in *cone*$^{\Delta Vhl}$ and *rod*$^{\Delta Vhl}$ mice.

Despite the similar aspects observed in *cone*$^{\Delta Vhl}$ and *rod*$^{\Delta Vhl}$ mice, the two models differ in some features. While *cone*$^{\Delta Vhl}$ and *rod*$^{\Delta Vhl}$ mice both represent some aspects of dry AMD such as age-related photoreceptor degeneration and RPE defects, the phenotype of *cone*$^{\Delta Vhl}$ mice additionally recapitulates features of a distinct form of neovascular AMD known as RAP, including vascular defects with vessels extending from the deep plexus into the ONL/subretinal space. Although photoreceptor degeneration was evident in both models, the progression of the degenerative process varied. While we observed severe cone degeneration in *cone*$^{\Delta Vhl}$ mice already at early time points, rod cell death in *rod*$^{\Delta Vhl}$ was milder and progressed more slowly. A possible explanation for the different pathological phenotypes in the two mouse lines could arise from the different characteristics of rods and cones. Several studies suggest that cones are particularly sensitive to reduced oxygen and nutrient levels compared to rods. RPE-specific *Vegfa* ablation (*VMD2-Cre;Vegfa*$^{f/f}$ mice) leads to severe choriocapillaris deficits that in turn induce hypoxia in the RPE and promote photoreceptor degeneration. While dysfunction of cone photoreceptors was deteced already within one week after *Vegfa* deletion, defects in rod function were not detected until 11 months post deletion. Thus, cones seem to be more sensitive to oxygen deprivation than rods (Kurihara et al. 2012, Kurihara et al. 2016). Additionally, metabolic dysregulation has been associated with cone cell death in retinitis pigmentosa, a genetic disorder that causes severe vision impairment due to loss of rods and secondary loss of cones (Punzo et al. 2009, Punzo et al. 2012). Although the reasons for secondary cone cell death are still elusive, one hypothesis by Punzo and colleagues suggested that upon rod cell loss cones die, at least in part, as a result of starvation and nutritional imbalance (Punzo et al. 2009). Although the higher sensitivity of cones may contribute to the stronger phenotype observed in *cone*$^{\Delta Vhl}$ compared to *rod*$^{\Delta Vhl}$ mice, for a precise interpretation of the observed phenotypes we need to emphasize the different timing to trigger the hypoxic response in the two models. In *cone*$^{\Delta Vhl}$ mice, BP*Cre* drives strong *Cre* expression in almost all cells of the ONL and is already active at PND1 (not shown). In *rod*$^{\Delta Vhl}$ mice, rod-specific *Cre* expression is patchy and evident in 50-70% of rod photoreceptors (Le et al. 2006, Lange et al. 2011b). Opsin*Cre* expression starts around PND7 and increases up to 6 weeks of age (Le et al. 2006). Thus, based on *Cre* expression, the hypoxic response in *cone*$^{\Delta Vhl}$ mice should be triggered at an earlier time point and in an increased number of photoreceptors as compared to *rod*$^{\Delta Vhl}$ mice. The early hypoxic response in *cone*$^{\Delta Vhl}$ mice interferes with the development of the retinal vasculature and causes vessel growth from the deep plexus into the photoreceptor layer and subretinal space. It remains unclear which angiogenic factor(s) are misguiding the vessels to extend into the ONL and subretinal

space. However, a prominent candidate factor responsible for neovascularization is VEGF, as *Vegf* overexpression has been shown to cause abnormal vessel growth (Okamoto et al. 1997, Ohno-Matsui et al. 2002, Ida et al. 2003). We also observed increased *Vegf* gene expression levels in *rod*$^{\Delta Vhl}$ mice (tested at 11 weeks of age, see 3.2). However, given the crucial role of a VEGF gradient during vascular development (see 1.2.3), timing of increased *Vegf* expression might be the key factor for misguiding the vessels to the ONL in *cone*$^{\Delta Vhl}$ mice. The observed pathological vascular defects and retinal hemorrhages (as shown by albumin immunostaining) in *cone*$^{\Delta Vhl}$ mice may exacerbate cone photoreceptor degeneration, as suggested for other models ((Zhao et al. 2011) and see 3.3, 4.3).

Collectively, our results suggest that timing and dosage (i.e. the amount of cells with active *Cre* recombinase) are decisive factors for neovascularization, which, subsequently, may accelerate neurodegeneration in response to an activated hypoxic response. This, together with stronger *Cre* activity in *cone*$^{\Delta Vhl}$ mice, might explain the different progression of the degenerative process in *cone*$^{\Delta Vhl}$ and *rod*$^{\Delta Vhl}$ mice.

4.1.2 Future directions: cone degeneration and a hypoxia-like response in *cone*$^{\Delta Vhl}$ mice

To date, it remains unclear whether cones in *cone*$^{\Delta Vhl}$ mice degenerate due to chronic activation of the hypoxic response, due to vascular defects or due to a combination of the two. In *cone*$^{\Delta Vhl}$ mice, early *Cre* activity triggered a hypoxic response that caused vessel growth from the deep plexus into the photoreceptor layer and subretinal space. To further clarify the impact of a chronic hypoxia-like response on mature photoreceptors, a delayed trigger of *Cre* expression, at the time when developmental vascularization is completed, should be pursued. For this purpose, an AAV expressing *Cre* under the transcriptional control of a photoreceptor-specific promoter (e.g. G protein-coupled receptor kinase 1 (GRK1), a component of phototransduction expressed in rods and cones) can be delivered to adult *R91W;Nrl*$^{-/-}$*;Vhl*$^{f/f}$ mice by subretinal injections. Testing of this approach is currently ongoing and may assist in elucidating the influence of chronic hypoxia on cone photoreceptors in the adult all-cone retina. However, separating a potential degenerative phenotype triggered by *Vhl* excision and injection-inflicted damage will be challenging. Furthermore, we generated *BPCre;Vhl*$^{f/f}$ mice (rod-dominant retina) to assess the effects of *Vhl* ablation on cones in retinas with normal photoreceptor ratio (3% cones, 97% rods). Based on preliminary results, retinal vasculature is normal in these mice. Further analysis will focus on cell death mediated by the lack of *Vhl* in cones in the rod-dominant retina. With this model, we will be able to study hypoxia-mediated cone cell death in a normally vascularized retina with a mixed rod/cone composition. However, due to the low number of cones in the rod-dominant retina, cone cell death analysis will be challenging as potential differences between *Vhl* knockout and control mice are expected to be small.

To further elucidate the contribution of VEGF on vascular defects in *cone$^{\Delta Vhl}$* mice, VEGF could be targeted. FLT1-Fc is a VEGF receptor-1/Fc chimeric protein that binds VEGF and decreases its activity. Intraocular injections of FLT1-Fc have been proven to prevent vascular defects in distal-retina-specific *α-Cre;Vhl$^{f/f}$* mice that express *Cre* under the α-element of the Pax6-promotor (Kurihara et al. 2010). Apart from the vessel phenotype such as abnormal vessel growth into the ONL in the retinal periphery, reduced vascular density as well as persistent hyaloid vasculature, the *α-Cre;Vhl$^{f/f}$* mice show also photoreceptor degeneration (Kurihara et al. 2010, Lange et al. 2011a). FLT1-Fc or AAV-sFLT1 injections were used in mouse models and subsequently in clinical trials to treat neovascular AMD (see 1.3.5). Such an approach, applied early (PND4/PND7), could be considered to address the neovascular phenotype in *cone$^{\Delta Vhl}$* mice and evaluate the impact of *Vegf* on the cone pathology. Another strategy to study the role of *Vegf* would be a genetic approach: crossing *BPCre;R91W;Nrl$^{-/-}$;Vhl$^{f/f}$* and *Vegfa$^{f/f}$* (Gerber et al. 1999) mice would allow analyzing the phenotype in absence of cone-specific *Vegf* expression.

With the above discussed strategies, the effects of chronic hypoxia on cones and the role of *Vegf* on vascular defects in *cone$^{\Delta Vhl}$* mice should be further clarified.

4.1.3 Future directions: optimization of gene therapy approach in *rod$^{\Delta Vhl}$* mice

Currently, no treatment is available for patients suffering from AMD, apart from repeated intravitreal anti-VEGF injections for the less common neovascular form of AMD. First clinical trials using different AAVs to treat AMD were initiated (see 1.3.5), however these studies reported limited success of the treatment in patients. Therefore, new therapeutic approaches are urgently needed. In an attempt to establish an interventional therapy, we aimed at targeting HIF1A in the adult retina of *rod$^{\Delta Vhl}$* mice. To reduce toxic HIF1A levels, we used RNA interference through expression of an shRNA against HIF1A. First, we tested our s*hHif1a* in NIH3t3 cells and showed an efficient downregulation of HIF1A in *shHif1a*-transfected cells following exposure to 0.2% oxygen (hypoxia). In a next step, viral particles carrying the *shHif1a* sequence (AAV2/8Y733F-*shHif1a*) were injected into the subretinal space of *rod$^{\Delta Vhl}$* mice. We provided evidence that anti-*Hif1a* gene therapy reduced the degenerative phenotype in mice (see 3.2), which supports the hypothesis of targeting *Hif1a* to protect photoreceptors in hypoxia-related diseases such as AMD. To achieve robust *shRNA* expression, we used the ubiquitous polymerase III promoter U6 to drive *shHif1a*. We observed widespread expression, predominantly localized in the ONL and RPE but we also detected weak expression in some other retinal cells. HIF1A can be safely inactivated in adult cones (see 3.1), rods (Thiersch et al. 2009), and 3.2) and RPE (Kurihara et al. 2012, Kurihara et al. 2016). However, the consequences of HIF1A inactivation in other adult retinal cell types is unknown. As we did not observe AAV-*shHif1a*-mediated toxicity in other cells, our data suggest that *Hif1a* inactivation does not have adverse effects. Nevertheless, further thorough analysis is required to make that conclusion.

Clearly, far more research is needed to further test and improve our gene therapy approach. Besides the above-mentioned specificity of our AAV vector, an open question that needs to be addressed is the route of delivery. We delivered AAV-*shHif1a* by subretinal injections, which is currently the preferred route to target photoreceptor cells. However, injection-inflicted damage was unavoidable due to the small size of the mouse eye. Recently, successful transduction of the outer retina following intravitreal injection has been reported. Vitreous aspiration prior to intravitreal injections results in retina-wide AAV transduction, but occasionally leads to side effects such as cataracts or retinal remodeling due to retinal detachment (see 5.2.3, (Da Costa et al. 2016)). Intravitreal administration of a newly engineered AAV capsid (AAV2-7m8) may provide a less invasive alternative to target photoreceptors (Dalkara et al. 2013). The AAV2-7m8 vector has a capsid-displayed peptide-insertion of 10 amino acids (referred to as 7m8) which leads to increased efficacy of cellular entry and allows transduction of the outer retina after non-invasive injection into the vitreous (Khabou et al. 2016). However, in contrast to subretinal injections, intravitreal injections were shown to trigger an immune response. Although both the intravitreal and subretinal space possess immune privilege, apparently they respond to AAV-injection differently (Li et al. 2008). Even though the precise mechanisms still need to be determined, anatomical characteristics might partially explain the difference in humoral immune response. The vitreous is located in close proximity to the vasculature system, which offers the potential to present capsid antigens to the immune system. The subsequent humoral immune response may reduce the therapeutical dose by decreasing transgene expression upon re-administration and limit the therapeutical benefit if sequential treatment is needed (Li et al. 2008). In contrast, the subretinal space is separated from blood vessels of the choriocapillaris by RPE cells, which form the outer BRB. In addition, RPE cells secrete anti-inflammatory and immune-suppressive molecules which contribute to ocular immune privilege (Li et al. 2008). Therefore, injections into the subretinal space might not induce a humoral immune response.

Taken together, packaging of our *shHif1a* in an optimized AAV capsid (e.g. AAV2-7m8) would possibly allow targeting of photoreceptors by intravitreal injection, a technique that is methodologically less complicated and less invasive. However, for a potential future application in clinical trials, subretinal injections may be the safer route regarding the activation of the immune response. Additionally, as discussed earlier, development and testing of a an AAV-mediated cell type-specific targeting of HIF1A and HIF2A should be considered in future experiments (see above, and results from 3.2 and (Kurihara et al. 2016)).

4.2 Light-induced retinal degeneration in the all-cone *R91W;Nrl*$^{-/-}$ mouse

To further understand the underlying mechanisms of cone cell death, we analyzed retinal degenerative processes in *R91W;Nrl*$^{-/-}$ mice which were exposed to blue light. Interestingly, exposure to light may act as co-factor in retinal diseases (Taylor et al. 1990, Margrain et al. 2004).

In our study, we exposed wild-type (*wt*, *129S6*) and all-cone *R91W;Nrl*$^{-/-}$ mice to toxic levels of blue light. Our data suggest significant differences between rod- and cone-dominant retinas, regarding not only photoreceptor degeneration but also BRB integrity. Interestingly, although cones seem to be more sensitive to reduced oxygen and nutrient levels compared to rods (Punzo et al. 2012, Kurihara et al. 2016), they are more resistant to light-induced damage (Cicerone 1976, Okano et al. 2012). In line with these results, cone photoreceptors of *R91W;Nrl*$^{-/-}$ mice were more resistant to blue-light damage compared to rods of *wt* mice (see 3.3). Although cones in *R91W;Nrl*$^{-/-}$ mice survived the toxic insult to a higher extent, we identified dying cells in the INL in *R91W;Nrl*$^{-/-}$ mice but not in *wt* mice. In *wt* mice, blue light exposure led to the disruption of the outer BRB, which is maintained by the RPE. In contrast, cell death in the INL of *R91W;Nrl*$^{-/-}$ mice was accompanied by retinal hemorrhages, suggesting vessel leakage and breakdown of the inner BRB which is formed by tight junctions between retinal capillary endothelial cells. As a result, retinal swelling and edema formation was more pronounced in *R91W;Nrl*$^{-/-}$ than in *wt* mice. This resulted in neuroinflammation and increased expression levels of the proinflammatory cytokines *Tnf* and *Il1b* in *R91W;Nrl*$^{-/-}$ mice. Similarly, increased levels of TNFa and IL1B were found in aqueous humor of patients suffering from proliferative diabetic retinopathy (Demircan et al. 2006), a disease affecting retinal blood vessels that ultimately leads to dysfunction of the BRB, vascular leakage and vision loss (see 1.3.1). In patients, macular edema is often associated with DR, but a wide variety of pathologic conditions may cause its formation. Compromised retinal blood barrier function has also been suggested to play an important role in several other retinal diseases including AMD and other chronic retinal diseases (Klaassen et al. 2013).

Blue light damage in *R91W;Nrl*$^{-/-}$ mice can be used to study mechanisms leading to edema formation in a cone-exclusive environment, resembling partially the human rod-free central macula. Additionally, our model allows testing of potential therapeutic agents that may prevent edema formation and restore proper vessel function. Besides anti-inflammatory therapy (Das et al. 2015), purinergic receptor activation improving the retinal water transport may be a promising research area to test therapeutic agents for prevention of cell death in degenerative and proliferative retinopathies (Reichenbach et al. 2016).

4.3 Vascular leakage: a common feature of *cone*$^{\Delta Vhl}$ and blue-light damaged all-cone *R91W;Nrl*$^{-/-}$ mice

We investigated photoreceptor degeneration based on a chronic hypoxic response or on toxic levels of blue light exposure. Certainly, the experimental setup including stimuli (hypoxia versus light) and timing (acute versus chronic) varies greatly. Nevertheless, in both blue-light damaged all-cone *R91W;Nrl*$^{-/-}$ and *cone*$^{\Delta Vhl}$ mice, we observed breakdown of the inner BRB and vascular leakage (see 3.1, 3.3 and discussion above). The molecular mechanisms underlying vascular leakage possibly differ in the two models. While *Vegf* is a prominent candidate factor responsible for vascular

pathology in *cone$^{\Delta Vhl}$* mice, we did not find upregulation of *Vegf* expression in *R91W;Nrl$^{-/-}$* mice following blue light damage (not shown). However, leakage may have detrimental consequences in both *cone$^{\Delta Vhl}$* and blue-light damaged all-cone *R91W;Nrl$^{-/-}$* mice. Extravasated blood components such as hemoglobin and iron can have toxic effects on surrounding cells (Regan et al. 1993, Gelfand et al. 2015). Although iron is essential for retinal function, excess iron has been associated with retinal degeneration (Hahn et al. 2004, Dunaief 2006, Song et al. 2013). Besides inducing oxidative damage, iron accumulation has been shown to activate the NLRP3 inflammasome and promote RPE degeneration (Gelfand et al. 2015). Another report by Zhao and colleagues supports the involvement of an inflammatory reaction to extravasated blood components, as blood constituents have been shown to cause an inflammatory response that causes photoreceptor degeneration (Zhao et al. 2011). Blood leakage and BRB disruption may have additional adverse effects by impairing the influx of nutrients and oxygen supply to the retina. The inner retina is nourished by the retinal vasculature and diffusion of molecules is controlled by the inner BRB. The outer retina including photoreceptors is supplied mainly by the choroidal vasculature and diffusion of solutes is regulated by the outer BRB (see 1.2.1). Thus, it is conceivable that while dysfunctional blood vessels and inner BRB disruption might impair oxygen supply for the inner retina, outer BRB disruption may affect oxygen supply for photoreceptors. However, experiments substantiating this hypothesis would be required.

Clearly, more experiments are needed to clarify the exact mechanisms and consequences of vascular leakage in blue-light damaged all-cone *R91W;Nrl$^{-/-}$* and *cone$^{\Delta Vhl}$* mice. Further testing should investigate the impact of extravasated blood components and the effects of BRB disruption on nutrient and oxygen supply.

4.4 Concluding Remarks

In our work, we analyzed the retinal response to toxic levels of light and chronic hypoxia-like conditions, two important features of retinal degenerative diseases. Our research revealed different responses of rod- and cone-dominant retinas: cone photoreceptors are not only resistant to light damage induced by white light, even strong blue light affected cones less severely than rods. Our data confirmed the previous notion that rod photoreceptors are more susceptible than cones in a light-damage paradigm used to study retinal degenerations. However, cone degeneration induced by blue light in the all-cone *R91W;Nrl$^{-/-}$* mice was accompanied by vascular leakage and edema. Thus, our blue light damaged *R91W;Nrl$^{-/-}$* mouse model can be used to study edema-based complications in different macular degenerations and may serve as a platform to test therapeutic agents.

Vascular leakage was also a prominent feature of all-cone *R91W;Nrl$^{-/-}$* mice with a cone-specific activation of the molecular hypoxic response. Chronic activation of HIF transcription factors caused severe early-onset cone degeneration and neovascularization – features that are central to a distinct

form of neovascular AMD known as retinal angiomatous proliferation (RAP). The phenotype of mice with a rod-specific activation of the molecular hypoxic response in a rod-dominant retina recapitulates features of dry AMD such as slow, age-dependent photoreceptor death and loss of vision. We identified HIF1A as causative factor and showed that targeting HIF1A might be an applicable strategy to rescue vision in hypoxia-mediated retinal degenerative diseases. However, many open questions remain to be answered. An important point that needs to be addressed is whether it is safe to inactivate a protein with pleiotropic effects such as HIF1A. Our data and data from others suggest that HIF1A can be safely inactivated in adult photoreceptors and RPE. Future experiments will assist in elucidating safety and effectiveness of our gene therapy approach. Additionally, a cell type-specific targeting of HIF1A and HIF2A may further increase treatment success. With our research, we hope to contribute to the development of therapeutic strategies to protect invaluable high-acuity vision.

References

Agca C., Gubler A., Traber G., Beck C., Imsand C., Ail D., Caprara C. and Grimm C. (2013). p38 MAPK signaling acts upstream of LIF-dependent neuroprotection during photoreceptor degeneration. *Cell Death Dis* **4**: e785.

Ardeljan D., Meyerle C. B., Agron E., Wang J. J., Mitchell P., Chew E. Y., Zhao J., Maminishkis A., Chan C. C. and Tuo J. (2013). Influence of TIMP3/SYN3 polymorphisms on the phenotypic presentation of age-related macular degeneration. *Eur J Hum Genet* **21**(10): 1152-1157.

Burgi S., Samardzija M. and Grimm C. (2009). Endogenous leukemia inhibitory factor protects photoreceptor cells against light-induced degeneration. *Mol Vis* **15**: 1631-1637.

Cicerone C. M. (1976). Cones survive rods in the light-damaged eye of the albino rat. *Science* **194**(4270): 1183-1185.

Da Costa R., Roger C., Segelken J., Barben M., Grimm C. and Neidhardt J. (2016). A Novel Method Combining Vitreous Aspiration and Intravitreal AAV2/8 Injection Results in Retina-Wide Transduction in Adult Mice. *Invest Ophthalmol Vis Sci* **57**(13): 5326-5334.

Dalkara D., Byrne L. C., Klimczak R. R., Visel M., Yin L., Merigan W. H., Flannery J. G. and Schaffer D. V. (2013). In vivo-directed evolution of a new adeno-associated virus for therapeutic outer retinal gene delivery from the vitreous. *Sci Transl Med* **5**(189): 189ra176.

Das A., McGuire P. G. and Rangasamy S. (2015). Diabetic Macular Edema: Pathophysiology and Novel Therapeutic Targets. *Ophthalmology* **122**(7): 1375-1394.

Demircan N., Safran B. G., Soylu M., Ozcan A. A. and Sizmaz S. (2006). Determination of vitreous interleukin-1 (IL-1) and tumour necrosis factor (TNF) levels in proliferative diabetic retinopathy. *Eye* **20**(12): 1366-1369.

Dunaief J. L. (2006). Iron induced oxidative damage as a potential factor in age-related macular degeneration: the Cogan Lecture. *Invest Ophthalmol Vis Sci* **47**(11): 4660-4664.

Gelfand B. D., Wright C. B., Kim Y., Yasuma T., Yasuma R., Li S., Fowler B. J., Bastos-Carvalho A., Kerur N., Uittenbogaard A., Han Y. S., Lou D., Kleinman M. E., McDonald W. H., Nunez G., Georgel P., Dunaief J. L. and Ambati J. (2015). Iron Toxicity in the Retina Requires Alu RNA and the NLRP3 Inflammasome. *Cell Rep* **11**(11): 1686-1693.

Gerber H. P., Hillan K. J., Ryan A. M., Kowalski J., Keller G. A., Rangell L., Wright B. D., Radtke F., Aguet M. and Ferrara N. (1999). VEGF is required for growth and survival in neonatal mice. *Development* **126**(6): 1149-1159.

Hahn P., Qian Y., Dentchev T., Chen L., Beard J., Harris Z. L. and Dunaief J. L. (2004). Disruption of ceruloplasmin and hephaestin in mice causes retinal iron overload and retinal degeneration with features of age-related macular degeneration. *Proc Natl Acad Sci U S A* **101**(38): 13850-13855.

Hartnett M. E., Weiter J. J., Staurenghi G. and Elsner A. E. (1996). Deep retinal vascular anomalous complexes in advanced age-related macular degeneration. *Ophthalmology* **103**(12): 2042-2053.

Ida H., Tobe T., Nambu H., Matsumura M., Uyama M. and Campochiaro P. A. (2003). RPE cells modulate subretinal neovascularization, but do not cause regression in mice with sustained expression of VEGF. *Invest Ophthalmol Vis Sci* **44**(12): 5430-5437.

Joly S., Lange C., Thiersch M., Samardzija M. and Grimm C. (2008). Leukemia inhibitory factor extends the lifespan of injured photoreceptors in vivo. *J Neurosci* **28**(51): 13765-13774.

Khabou H., Desrosiers M., Winckler C., Fouquet S., Auregan G., Bemelmans A. P., Sahel J. A. and Dalkara D. (2016). Insight into the mechanisms of enhanced retinal transduction by the engineered AAV2 capsid variant -7m8. *Biotechnol Bioeng* **113**(12): 2712-2724.

Klaassen I., Van Noorden C. J. and Schlingemann R. O. (2013). Molecular basis of the inner blood-retinal barrier and its breakdown in diabetic macular edema and other pathological conditions. *Prog Retin Eye Res* **34**: 19-48.

Kurihara T., Kubota Y., Ozawa Y., Takubo K., Noda K., Simon M. C., Johnson R. S., Suematsu M., Tsubota K., Ishida S., Goda N., Suda T. and Okano H. (2010). von Hippel-Lindau protein regulates transition from the fetal to the adult circulatory system in retina. *Development* **137**(9): 1563-1571.

Kurihara T., Westenskow P. D., Bravo S., Aguilar E. and Friedlander M. (2012). Targeted deletion of Vegfa in adult mice induces vision loss. *J Clin Invest* **122**(11): 4213-4217.

Kurihara T., Westenskow P. D., Gantner M. L., Usui Y., Schultz A., Bravo S., Aguilar E., Wittgrove C., Friedlander M. S., Paris L. P., Chew E., Siuzdak G. and Friedlander M. (2016). Hypoxia-induced metabolic stress in retinal pigment epithelial cells is sufficient to induce photoreceptor degeneration. *Elife* **5**.

Lange C., Caprara C., Tanimoto N., Beck S., Huber G., Samardzija M., Seeliger M. and Grimm C. (2011a). Retina-specific activation of a sustained hypoxia-like response leads to severe retinal degeneration and loss of vision. *Neurobiol Dis* **41**(1): 119-130.

Lange C., Heynen S. R., Tanimoto N., Thiersch M., Le Y. Z., Meneau I., Seeliger M. W., Samardzija M., Caprara C. and Grimm C. (2011b). Normoxic activation of hypoxia-inducible factors in photoreceptors

provides transient protection against light-induced retinal degeneration. *Invest Ophthalmol Vis Sci* **52**(8): 5872-5880.

Le Y. Z., Zheng L., Zheng W., Ash J. D., Agbaga M. P., Zhu M. and Anderson R. E. (2006). Mouse opsin promoter-directed Cre recombinase expression in transgenic mice. *Mol Vis* **12**: 389-398.

Leibinger M., Muller A., Andreadaki A., Hauk T. G., Kirsch M. and Fischer D. (2009). Neuroprotective and axon growth-promoting effects following inflammatory stimulation on mature retinal ganglion cells in mice depend on ciliary neurotrophic factor and leukemia inhibitory factor. *J Neurosci* **29**(45): 14334-14341.

Li Q., Miller R., Han P. Y., Pang J., Dinculescu A., Chiodo V. and Hauswirth W. W. (2008). Intraocular route of AAV2 vector administration defines humoral immune response and therapeutic potential. *Mol Vis* **14**: 1760-1769.

Lin R. J., Blumenkranz M. S., Binkley J., Wu K. and Vollrath D. (2006). A novel His158Arg mutation in TIMP3 causes a late-onset form of Sorsby fundus dystrophy. *Am J Ophthalmol* **142**(5): 839-848.

Margrain T. H., Boulton M., Marshall J. and Sliney D. H. (2004). Do blue light filters confer protection against age-related macular degeneration? *Prog Retin Eye Res* **23**(5): 523-531.

Ohno-Matsui K., Hirose A., Yamamoto S., Saikia J., Okamoto N., Gehlbach P., Duh E. J., Hackett S., Chang M., Bok D., Zack D. J. and Campochiaro P. A. (2002). Inducible expression of vascular endothelial growth factor in adult mice causes severe proliferative retinopathy and retinal detachment. *Am J Pathol* **160**(2): 711-719.

Okamoto N., Tobe T., Hackett S. F., Ozaki H., Vinores M. A., LaRochelle W., Zack D. J. and Campochiaro P. A. (1997). Transgenic mice with increased expression of vascular endothelial growth factor in the retina: a new model of intraretinal and subretinal neovascularization. *Am J Pathol* **151**(1): 281-291.

Okano K., Maeda A., Chen Y., Chauhan V., Tang J., Palczewska G., Sakai T., Tsuneoka H., Palczewski K. and Maeda T. (2012). Retinal cone and rod photoreceptor cells exhibit differential susceptibility to light-induced damage. *J Neurochem* **121**(1): 146-156.

Punzo C., Kornacker K. and Cepko C. L. (2009). Stimulation of the insulin/mTOR pathway delays cone death in a mouse model of retinitis pigmentosa. *Nat Neurosci* **12**(1): 44-52.

Punzo C., Xiong W. and Cepko C. L. (2012). Loss of daylight vision in retinal degeneration: are oxidative stress and metabolic dysregulation to blame? *J Biol Chem* **287**(3): 1642-1648.

Regan R. F. and Panter S. S. (1993). Neurotoxicity of hemoglobin in cortical cell culture. *Neurosci Lett* **153**(2): 219-222.

Reichenbach A. and Bringmann A. (2016). Purinergic signaling in retinal degeneration and regeneration. *Neuropharmacology* **104**: 194-211.

Samardzija M., Wenzel A., Aufenberg S., Thiersch M., Reme C. and Grimm C. (2006). Differential role of Jak-STAT signaling in retinal degenerations. *FASEB J* **20**(13): 2411-2413.

Song D. and Dunaief J. L. (2013). Retinal iron homeostasis in health and disease. *Front Aging Neurosci* **5**: 24.

Taylor H. R., Munoz B., West S., Bressler N. M., Bressler S. B. and Rosenthal F. S. (1990). Visible light and risk of age-related macular degeneration. *Trans Am Ophthalmol Soc* **88**: 163-173; discussion 173-168.

Thiersch M., Lange C., Joly S., Heynen S., Le Y. Z., Samardzija M. and Grimm C. (2009). Retinal neuroprotection by hypoxic preconditioning is independent of hypoxia-inducible factor-1 alpha expression in photoreceptors. *Eur J Neurosci* **29**(12): 2291-2302.

Weber B. H., Vogt G., Pruett R. C., Stohr H. and Felbor U. (1994). Mutations in the tissue inhibitor of metalloproteinases-3 (TIMP3) in patients with Sorsby's fundus dystrophy. *Nat Genet* **8**(4): 352-356.

Yannuzzi L. A., Freund K. B. and Takahashi B. S. (2008). Review of retinal angiomatous proliferation or type 3 neovascularization. *Retina* **28**(3): 375-384.

Zhao L., Ma W., Fariss R. N. and Wong W. T. (2011). Minocycline attenuates photoreceptor degeneration in a mouse model of subretinal hemorrhage microglial: inhibition as a potential therapeutic strategy. *Am J Pathol* **179**(3): 1265-1277.

5 APPENDIX

5.1 List of Abbreviations

AAV	adeno-associated virus
ABCA4	ATP binding cassette subfamily A member 4
Adm	adrenomedullin
AMD	age-related macular degeneration
AMPA	α-amino-3-hydroxy-5-methyl-4-isoxazolepropionic acid
ARMS2	age-related maculopathy susceptibility 2
ARNT	aryl hydrocarbon receptor nuclear translocator
ARNTL	ARNT-like
ATP	adenosine triphosphate
bHLH	basic-helix-loop-helix
BMAL1	brain and muscle Arnt-like protein 1
Bnip3	BCL2/adenovirus E1B interacting protein 3
BRB	blood-retinal barrier
C-TAD	C-terminal transactivation domain
C2	complement 2
C3	complement 3
cap	capsid
CBP	CREB-binding protein
CEP	carboxyethylpyrrole
CFB	complement factor B
CFH	complement factor H
cGMP	cyclic guanosine monophosphate
CNTF	ciliary neurotrophic factor
CNV	choroidal neovascularization
cpfl1	cone photoreceptor function loss 1
CRALBP	cellular retinaldehyde-binding protein
CRBP	cellular retinol binding protein
CREB	cAMP-response element-binding protein
DR	diabetic retinopathy
EIAV	Equine Infectious Anemia Virus
EPAS1	endothelial PAS domain protein 1
Epo	erythropoietin
FIH	factor inhibiting HIF1
FLT1	fms related tyrosine kinase 1
GCL	ganglion cell layer
GDP	guanosine diphosphate
Glut1	glucose transporter 1
GRK1	G protein-coupled receptor kinase 1
GTP	guanosine triphosphate
hESC	human embryonic stem cell
HIF	hypoxia-inducible factor
HLA	human leukocyte antigen
Hmox1	heme oxygenase (decycling) 1
HRE	hypoxia response element
Htra1	HtrA serine peptidase 1
INL	inner nuclear layer
IPL	inner plexiform layer
iPSCs	induced pluripotent stem cells
IRBP	interphotoreceptor retinol binding protein
ITR	inverted terminal repeats
Jak/STAT	Janus kinase / signal transducer and activator of transcription
Ldha	lactate dehydrogenase A

Lif	leukemia inhibitory factor
LRAT	lecithin retinol acyltransferase
mGluR6	G protein-coupled metabotropic glutamate receptor 6
MNU	*N*-methyl-*N*-nitrosourea
Nrl	neural retina leucine zipper
OCT	optical coherence tomography
ONL	outer nuclear layer
OPL	outer plexiform layer
PAS	Per/ARNT/Sim
PCR	polymerase chain reaction
PDE	phosphodiesterase
PDGF	platelet-derived growth factor
PEDF	pigment epithelium-derived factor
Phd	prolyl hydroxylase domain
PND	postnatal day
RAP	retinal angiomatous proliferation
Rd	retinal degeneration
rep	replication
RPE	retinal pigment epithelium
RPE65	RPE-specific 65kDa protein
sFLT1	soluble fms related tyrosine kinase 1
shRNA	short hairpin RNA
siRNA	small interfering RNA
Timp3	tissue inhibitor of metalloproteinase 3
Vegf	vascular endothelial growth factor
VHL	von Hippel Lindau
VLDLR	very low density lipoprotein receptor
wt	wild-type

5.2 Additional Publications

5.2.1 The role of hypoxia, hypoxia-inducible factor (HIF) and VEGF in retinal angiomatous proliferation (book chapter)

Maya Barben[1,2], Marijana Samardzija[1], Christian Grimm[1,2,3]

[1]Lab for Retinal Cell Biology, Dept. Ophthalmology, University Hospital Zurich, University of Zurich, Switzerland

[2]Neuroscience Center Zurich (ZNZ), University of Zurich, Switzerland

[3]Zurich Center for Integrative Human Physiology (ZIHP), University of Zurich, Switzerland

Status of the manuscript:

Adv Exp Med Biol, in press

Personal Contribution

Literature search, manuscript writing.

Abstract

In industrialized countries, age-related macular degeneration (AMD) is the leading cause of blindness in elderly people. Hallmarks of the non-neovascular (dry) form of AMD are the formation of drusen and geographic atrophy, whereas the exudative (wet) form of the disease is characterized by invading blood vessels. In retinal angiomatous proliferation (RAP), a special form of wet AMD, intraretinal vessels grow from the deep plexus into the subretinal space. Little is known about the mechanisms leading to intraretinal neovascularization but age-related changes such as reduction of choroidal blood flow, accumulation of drusen and thickening of the Bruch's membrane may lead to reduced oxygen availability in photoreceptors. Such a chronic hypoxic situation may induce several cellular response pathways including the stabilization of hypoxia-inducible factors (HIFs) and the production of angiogenic factors, such as vascular endothelial growth factor (VEGF). Here, we discuss the potential contribution of hypoxia and HIFs in RAP disease pathology and in some mouse models for subretinal neovascularization.

XX.1 Introduction

Retinal function can be affected by three variants of neovascularization (Grossniklaus et al. 2010). In retinal neovascular diseases such as diabetic retinopathy, central retinal vein occlusion and retinopathy of prematurity, retinal vessels grow along the inner retinal surface and/or extend into the vitreous (Grossniklaus et al. 2010) due to retinal ischemia and increased concentrations of vascular endothelial growth factor (VEGF) (Aiello et al. 1994, Lashkari et al. 2000). In choroidal neovascularization (CNV) new vessels originate in the choroid and grow towards the retina, characteristic for wet age-related macular degeneration (AMD) (Bressler et al. 1988, Spaide 2013). Additionally, retinal angiomatous proliferation (RAP), also known as deep retinal vascular anomalous complexes, has been described (Yannuzzi et al. 2001). RAP is a distinct form of neovascular AMD, characterized by the growth of vessels that invade the subretinal space not from the choroid but from the retina. In RAP, vessels originate from the deep retinal plexus and cause intraretinal neovascularization mainly in the photoreceptor layer resulting in an abnormal communication between retinal and choroidal vasculatures (Hartnett et al. 1996, Yannuzzi et al. 2008, Atmani et al.

2010). However, since vessels originating from the choroid in CNV of late stage neovascular AMD can form connections with the retinal vasculature known as retinal-choroidal anastomosis, the distinction between a retinal or choroidal origin of vessel growth is sometimes difficult (Slakter et al. 2000, Scott et al. 2010). Therefore, the more general term “type 3 neovascularization” has been suggested (Freund et al. 2008) but RAP is still the most frequently used designation. RAP has a poor clinical prognosis and treatment of RAP remains difficult (Bottoni et al. 2005, Gross et al. 2005). The prevalence of RAP is estimated at 15-20% of neovascular AMD (Cohen et al. 2007, Massacesi et al. 2008).

XX.2 Hypoxia and Hypoxia-Inducible Factors

The exact cause for neovascular AMD and particularly RAP is still unclear. Although VEGF plays a critical role in neovascularization the triggering factor is still largely unknown. Hypoxia activates regulatory systems in the body with hypoxia-inducible factor 1 (HIF1) playing a central role. HIF1 heterodimers are composed of an oxygen-labile α-subunit and a constitutively expressed β-subunit. Under normal oxygen levels, the HIF1A protein is rapidly degraded, which is mediated by hydroxylation of HIF1A by prolyl hydroxylases promoting its interaction with the von-Hippel-Lindau ubiquitin E3 ligase complex. As a result, the HIF1A protein is degraded via the proteosomal pathway. Under hypoxia, hydroxylation does not occur and hence, HIF1A gets stabilized, translocates into the nucleus and enables transcription of target genes such as *VEGF* (Jaakkola et al. 2001, Grimm et al. 2002, Caprara et al. 2012). This can trigger neovascularization in an attempt to resolve the long-term tissue hypoxia. Besides hypoxia, other factors such as oxidative stress, inflammation and disturbance in energy metabolism may also be involved in HIF1A stabilization (Cash et al. 2007, Dehne et al. 2009, Joyal et al. 2016). Since a chronic hypoxic situation has been suggested to play an important role in RAP and AMD pathology (Arjamaa et al. 2009, Kent 2014) we discuss the potential contribution of tissue hypoxia and HIF1A stabilization for disease development.

XX.3 Hypoxia and HIF in Neovascular AMD and RAP Pathology

In AMD patients, abnormalities in choroidal perfusion and vascular defects were described (reviewed in (Harris et al. 1999)), suggesting tissue hypoxia. In effect, strong VEGF protein immunoreactivity

has been shown in surgically excised CNV membranes and transdifferentiated retinal pigment epithelial (RPE) cells of AMD patients (Kvanta et al. 1996, Lopez et al. 1996). Additionally, stabilized HIF1A and HIF2A were detected in the endothelium and macrophages of human choroidal neovascular membranes associated with AMD (Inoue et al. 2007).

In human patients with RAP, vitreous VEGF levels determined by ELISA are higher compared to control subjects (Joyal et al. 2016). Intravitreally injected anti-VEGF agents have been shown to be effective in blocking vessel growth and improving vision in neovascular AMD (Solomon et al. 2014) and in RAP (Engelbert et al. 2009, Atmani et al. 2010). Evidence indicates that hypoxia and HIF transcription factors are important driving forces in RAP disease development. For example, Hartnett and colleagues hypothesized that large drusen and Bruch's membrane deposits observed in RAP could decrease retinal oxygenation and create a hypoxic microenvironment in the outer retina which may stimulate angiogenic growth factor release, vessel growth and retinal degeneration (Hartnett et al. 1996). A thinner choroid and greater density of drusen has been observed in RAP patients compared to typical neovascular AMD patients, two factors that may cause ischemia and/or restrict oxygen availability for photoreceptors (Kim et al. 2013). Additionally, RPE detachment could intensify the hypoxic challenge by increasing the distance between the photoreceptors and the choroid (Hartnett et al. 1996). Shimada et al. reported HIF1A and HIF2A expression in the surroundings of VEGF-positive retinal neovascular areas in RAP specimens (Shimada et al. 2007). This suggests a hypoxia-mediated mechanism leading to VEGF expression in RAP.

In summary, hypoxic factors such as VEGF and HIF1 may be involved in both typical neovascular AMD and RAP disease pathology. However, RAP does not require perturbation of Bruch's membrane and/or RPE, unlike CNV (Campochiaro 2013).

XX.4 *Rho/VEGF* and *Vldlr*$^{-/-}$ Mice: Two Animal Models for RAP

Transgenic mice expressing VEGF driven by the rhodopsin promoter (*rho/VEGF*) develop vessels that originate in the deep capillary bed of the retina and extend through the outer nuclear layer into the subretinal space (Okamoto et al. 1997). CNV has not been observed in these mice (Tobe et al. 1998). In addition, VEGF overexpression caused retinal neovascularization even in adult mice with

completely developed retinal vasculature (Ohno-Matsui et al. 2002). Less neovascularization has been observed in mice with ischemic retinopathy lacking the hypoxia response element in the *Vegf* promoter compared to control mice (Vinores et al. 2006), suggesting an important role for HIF1 in the regulation of VEGF-mediated neovascularization.

Mice with a partial deletion of exon 5 of the very low density lipoprotein receptor gene lack functional VLDLR (*Vldlr*$^{-/-}$) (Frykman et al. 1995) and show a retinal phenotype resembling RAP lesions (Heckenlively et al. 2003). Due to increased VEGF levels (see below) *Vldlr*$^{-/-}$ mice exhibit retinal neovascularization with vessels originating within the outer plexiform layer. Vessels start to grow at postnatal day (PND) 15, reach the subretinal space by PND20, and anastomoses with the choriocapillaries are observed at 3 months of age. This is accompanied by photoreceptor degeneration affecting predominantly cone cells (Hu et al. 2008, Dorrell et al. 2009). The increased VEGF levels observed in *Vldlr*$^{-/-}$ mice were initially suggested to be linked to the negative regulatory role of VLDLR on Wnt signaling, which targets VEGF (Dorrell et al. 2009). However, since VLDLR has important functions in cholesterol homeostasis, lipid metabolism and transport (Tiebel et al. 1999), Joyal and colleagues demonstrated that impaired fatty acid uptake in *Vldlr*$^{-/-}$ mice results in a reduction of α-ketoglutarate, which decreases prolyl hydroxylase dehydrogenase activity and promotes the stabilization of HIF1A. Subsequently, VEGF levels are increased, leading to a RAP-like neovascular phenotype (Joyal et al. 2016). Thus, dysregulated energy metabolism might drive pathological neovascularization by stabilizing HIF1A.

XX.5 Concluding Remarks and Future Therapeutic Perspectives

Pathological vessel growth in wet AMD and RAP are both associated with increased VEGF levels and are currently treated by frequent intraocular injections of anti-VEGF agents. However, such treatment should not downregulate VEGF below basal concentrations since physiological levels of VEGF are needed for proper visual function. It has been shown for example that an RPE-specific *Vegf* deletion leads to atrophy of the choriocapillaris and cone degeneration (Kurihara et al. 2012, Kurihara et al. 2016). Its hypoxia-specific regulator *Hif1a*, however, can be safely inactivated in RPE (Kurihara et al. 2012), adult rods (Thiersch et al. 2009) and cones (author's unpublished

data). Therefore, tissue-specific targeting HIF1A may provide a valid and safe therapeutical approach to treat RAP and potentially AMD. Animal models such as *rho/VEGF* and *Vldlr*$^{-/-}$ mice are clearly important to test and improve such treatment strategies. However, considering that these mice lack a cone-rich region resembling the human macular region, more research is needed to determine the influence of hypoxia, HIF1A and VEGF on cone survival and function.

References

Aiello L. P., Avery R. L., Arrigg P. G., Keyt B. A., Jampel H. D., Shah S. T., Pasquale L. R., Thieme H., Iwamoto M. A., Park J. E. and et al. (1994). Vascular endothelial growth factor in ocular fluid of patients with diabetic retinopathy and other retinal disorders. *N Engl J Med* **331**(22): 1480-1487.

Arjamaa O., Nikinmaa M., Salminen A. and Kaarniranta K. (2009). Regulatory role of HIF-1 a in the pathogenesis of age-related macular. *Ageing Research Reviews* **8**: 349-358.

Atmani K., Voigt M., Le Tien V., Querques G., Coscas G., Soubrane G. and Souied E. H. (2010). Ranibizumab for retinal angiomatous proliferation in age-related macular degeneration. *Eye (Lond)* **24**(7): 1193-1198.

Bottoni F., Massacesi A., Cigada M., Viola F., Musicco I. and Staurenghi G. (2005). Treatment of retinal angiomatous proliferation in age-related macular degeneration: a series of 104 cases of retinal angiomatous proliferation. *Arch Ophthalmol* **123**(12): 1644-1650.

Bressler N. M., Bressler S. B. and Fine S. L. (1988). Age-related macular degeneration. *Surv Ophthalmol* **32**(6): 375-413.

Campochiaro P. A. (2013). Ocular neovascularization. *J Mol Med (Berl)* **91**(3): 311-321.

Caprara C. and Grimm C. (2012). From oxygen to erythropoietin: Relevance of hypoxia for retinal development, health and disease. *Progress in Retinal and Eye Research* **31**: 89-119.

Cash T. P., Pan Y. and Simon M. C. (2007). Reactive oxygen species and cellular oxygen sensing. *Free Radic Biol Med* **43**(9): 1219-1225.

Cohen S. Y., Creuzot-Garcher C., Darmon J., Desmettre T., Korobelnik J. F., Levrat F., Quentel G., Palies S., Sanchez A., de Gendre A. S., Schluep H., Weber M. and Delcourt C. (2007). Types of choroidal neovascularisation in newly diagnosed exudative age-related macular degeneration. *Br J Ophthalmol* **91**(9): 1173-1176.

Dehne N. and Brune B. (2009). HIF-1 in the inflammatory microenvironment. *Experimental Cell Research* **315**(11): 1791-1797.

Dorrell M. I., Aguilar E., Jacobson R., Yanes O., Gariano R., Heckenlively J., Banin E., Ramirez G. A., Gasmi M., Bird A., Siuzdak G. and Friedlander M. (2009). Antioxidant or neurotrophic factor treatment preserves function in a mouse model of neovascularization-associated oxidative stress. *J Clin Invest* **119**(3): 611-623.

Engelbert M., Zweifel S. A. and Freund K. B. (2009). "Treat and extend" dosing of intravitreal antivascular endothelial growth factor therapy for type 3 neovascularization/retinal angiomatous proliferation. *Retina* **29**(10): 1424-1431.

Freund K. B., Ho I. V., Barbazetto I. A., Koizumi H., Laud K., Ferrara D., Matsumoto Y., Sorenson J. A. and Yannuzzi L. (2008). Type 3 neovascularization: the expanded spectrum of retinal angiomatous proliferation. *Retina* **28**(2): 201-211.

Frykman P. K., Brown M. S., Yamamoto T., Goldstein J. L. and Herz J. (1995). Normal plasma lipoproteins and fertility in gene-targeted mice homozygous for a disruption in the gene encoding very low density lipoprotein receptor. *Proc Natl Acad Sci U S A* **92**(18): 8453-8457.

Grimm C., Wenzel A., Groszer M., Mayser H., Seeliger M., Samardzija M., Bauer C., Gassmann M. and Reme C. E. (2002). HIF-1-induced erythropoietin in the hypoxic retina protects against light-induced retinal degeneration. *Nat Med* **8**(7): 718-724.

Gross N. E., Aizman A., Brucker A., Klancnik J. M., Jr. and Yannuzzi L. A. (2005). Nature and risk of neovascularization in the fellow eye of patients with unilateral retinal angiomatous proliferation. *Retina* **25**(6): 713-718.

Grossniklaus H. E., Kang S. J. and Berglin L. (2010). Animal models of choroidal and retinal neovascularization. *Prog Retin Eye Res* **29**(6): 500-519.

Harris A., Chung H. S., Ciulla T. A. and Kagemann L. (1999). Progress in measurement of ocular blood flow and relevance to our understanding of glaucoma and age-related macular degeneration. *Prog Retin Eye Res* **18**(5): 669-687.

Hartnett M. E., Weiter J. J., Staurenghi G. and Elsner A. E. (1996). Deep retinal vascular anomalous complexes in advanced age-related macular degeneration. *Ophthalmology* **103**(12): 2042-2053.

Heckenlively J. R., Hawes N. L., Friedlander M., Nusinowitz S., Hurd R., Davisson M. and Chang B. (2003). Mouse model of subretinal neovascularization with choroidal anastomosis. *Retina* **23**(4): 518-522.

Hu W., Jiang A., Liang J., Meng H., Chang B., Gao H. and Qiao X. (2008). Expression of VLDLR in the retina and evolution of subretinal neovascularization in the knockout mouse model's retinal angiomatous proliferation. *Invest Ophthalmol Vis Sci* **49**(1): 407-415.

Inoue Y., Yanagi Y., Matsuura K., Takahashi H., Tamaki Y. and Araie M. (2007). Expression of hypoxia-inducible factor 1alpha and 2alpha in choroidal neovascular membranes associated with age-related macular degeneration. *Br J Ophthalmol* **91**(12): 1720-1721.

Jaakkola P., Mole D. R., Tian Y. M., Wilson M. I., Gielbert J., Gaskell S. J., von Kriegsheim A., Hebestreit H. F., Mukherji M., Schofield C. J., Maxwell P. H., Pugh C. W. and Ratcliffe P. J. (2001). Targeting of

HIF-alpha to the von Hippel-Lindau ubiquitylation complex by O2-regulated prolyl hydroxylation. *Science* **292**(5516): 468-472.

Joyal J. S., Sun Y., Gantner M. L., Shao Z., Evans L. P., Saba N., Fredrick T., Burnim S., Kim J. S., Patel G., Juan A. M., Hurst C. G., Hatton C. J., Cui Z., Pierce K. A., Bherer P., Aguilar E., Powner M. B., Vevis K., Boisvert M., Fu Z., Levy E., Fruttiger M., Packard A., Rezende F. A., Maranda B., Sapieha P., Chen J., Friedlander M., Clish C. B. and Smith L. E. (2016). Retinal lipid and glucose metabolism dictates angiogenesis through the lipid sensor Ffar1. *Nat Med* **22**(4): 439-445.

Kent D. L. (2014). Age-related macular degeneration: beyond anti-angiogenesis. *Mol Vis* **20**: 46-55.

Kim J. H., Kim J. R., Kang S. W., Kim S. J. and Ha H. S. (2013). Thinner choroid and greater drusen extent in retinal angiomatous proliferation than in typical exudative age-related macular degeneration. *Am J Ophthalmol* **155**(4): 743-749, 749 e741-742.

Kurihara T., Westenskow P. D., Bravo S., Aguilar E. and Friedlander M. (2012). Targeted deletion of Vegfa in adult mice induces vision loss. *J Clin Invest* **122**(11): 4213-4217.

Kurihara T., Westenskow P. D., Gantner M. L., Usui Y., Schultz A., Bravo S., Aguilar E., Wittgrove C., Friedlander M. S., Paris L. P., Chew E., Siuzdak G. and Friedlander M. (2016). Hypoxia-induced metabolic stress in retinal pigment epithelial cells is sufficient to induce photoreceptor degeneration. *Elife* **5**.

Kvanta A., Algvere P. V., Berglin L. and Seregard S. (1996). Subfoveal fibrovascular membranes in age-related macular degeneration express vascular endothelial growth factor. *Invest Ophthalmol Vis Sci* **37**(9): 1929-1934.

Lashkari K., Hirose T., Yazdany J., McMeel J. W., Kazlauskas A. and Rahimi N. (2000). Vascular endothelial growth factor and hepatocyte growth factor levels are differentially elevated in patients with advanced retinopathy of prematurity. *Am J Pathol* **156**(4): 1337-1344.

Lopez P. F., Sippy B. D., Lambert H. M., Thach A. B. and Hinton D. R. (1996). Transdifferentiated retinal pigment epithelial cells are immunoreactive for vascular endothelial growth factor in surgically excised age-related macular degeneration-related choroidal neovascular membranes. *Invest Ophthalmol Vis Sci* **37**(5): 855-868.

Massacesi A. L., Sacchi L., Bergamini F. and Bottoni F. (2008). The prevalence of retinal angiomatous proliferation in age-related macular degeneration with occult choroidal neovascularization. *Graefe's Archive for Clinical and Experimental Ophthalmology* **246**(1): 89-92.

Ohno-Matsui K., Hirose A., Yamamoto S., Saikia J., Okamoto N., Gehlbach P., Duh E. J., Hackett S., Chang M., Bok D., Zack D. J. and Campochiaro P. A. (2002). Inducible expression of vascular endothelial growth factor in adult mice causes severe proliferative retinopathy and retinal detachment. *Am J Pathol* **160**(2): 711-719.

Okamoto N., Tobe T., Hackett S. F., Ozaki H., Vinores M. A., LaRochelle W., Zack D. J. and Campochiaro P. A. (1997). Transgenic mice with increased expression of vascular endothelial growth factor in the retina: a new model of intraretinal and subretinal neovascularization. *Am J Pathol* **151**(1): 281-291.

Scott A. W. and Bressler S. B. (2010). Retinal angiomatous proliferation or retinal anastomosis to the lesion. *Eye (Lond)* **24**(3): 491-496.

Shimada H., Kawamura A., Mori R. and Yuzawa M. (2007). Clinicopathological findings of retinal angiomatous proliferation. *Graefes Arch Clin Exp Ophthalmol* **245**(2): 295-300.

Slakter J. S., Yannuzzi L. A., Schneider U., Sorenson J. A., Ciardella A., Guyer D. R., Spaide R. F., Freund K. B. and Orlock D. A. (2000). Retinal choroidal anastomoses and occult choroidal neovascularization in age-related macular degeneration. *Ophthalmology* **107**(4): 742-753; discussion 753-744.

Solomon S. D., Lindsley K., Vedula S. S., Krzystolik M. G. and Hawkins B. S. (2014). Anti-vascular endothelial growth factor for neovascular age-related macular degeneration. *Cochrane Database Syst Rev*(8): CD005139.

Spaide R. F. (2013). Clinical Manifestations of Choroidal Neovascularization in AMD. Age-related Macular Degeneration. F. G. Holz, D. Pauleikhoff, R. F. Spaide and A. C. Bird. Berlin, Heidelberg, Springer Berlin Heidelberg**:** 111-119.

Thiersch M., Lange C., Joly S., Heynen S., Le Y. Z., Samardzija M. and Grimm C. (2009). Retinal neuroprotection by hypoxic preconditioning is independent of hypoxia-inducible factor-1 alpha expression in photoreceptors. *Eur J Neurosci* **29**(12): 2291-2302.

Tiebel O., Oka K., Robinson K., Sullivan M., Martinez J., Nakamuta M., Ishimura-Oka K. and Chan L. (1999). Mouse very low-density lipoprotein receptor (VLDLR): gene structure, tissue-specific expression and dietary and developmental regulation. *Atherosclerosis* **145**(2): 239-251.

Tobe T., Okamoto N., Vinores M. A., Derevjanik N. L., Vinores S. A., Zack D. J. and Campochiaro P. A. (1998). Evolution of neovascularization in mice with overexpression of vascular endothelial growth factor in photoreceptors. *Invest Ophthalmol Vis Sci* **39**(1): 180-188.

Vinores S. A., Xiao W. H., Aslam S., Shen J., Oshima Y., Nambu H., Liu H., Carmeliet P. and Campochiaro P. A. (2006). Implication of the hypoxia response element of the Vegf promoter in mouse models of retinal and choroidal neovascularization, but not retinal vascular development. *J Cell Physiol* **206**(3): 749-758.

Yannuzzi L. A., Freund K. B. and Takahashi B. S. (2008). Review of retinal angiomatous proliferation or type 3 neovascularization. *Retina* **28**(3): 375-384.

Yannuzzi L. A., Negrao S., Iida T., Carvalho C., Rodriguez-Coleman H., Slakter J., Freund K. B., Sorenson J., Orlock D. and Borodoker N. (2001). Retinal angiomatous proliferation in age-related macular degeneration. *Retina* **21**(5): 416-434.

5.2.2 Digoxin-induced retinal degeneration depends on rhodopsin

Britta Landfried[1], Marijana Samardzija[1], **Maya Barben[1,2]**, Christian Schori [1,3], Katrin Klee[1,3], Federica Storti[1], Christian Grimm[1,2,3]

[1]Lab for Retinal Cell Biology, Dept. Ophthalmology, University Hospital Zurich, University of Zurich, Switzerland

[2]Neuroscience Center Zurich (ZNZ), University of Zurich, Switzerland

[3]Zurich Center for Integrative Human Physiology (ZIHP), University of Zurich, Switzerland

Status of the manuscript:

Published in *Cell Death Dis., 2015,* **8**(3): e2670

Personal Contribution

Preparation of digoxin, interpretation of results, manuscript editing and proofreading.

OPEN

Citation: Cell Death and Disease (2017) 8, e2670; doi:10.1038/cddis.2017.94
Official journal of the Cell Death Differentiation Association
www.nature.com/cddis

Digoxin-induced retinal degeneration depends on rhodopsin

Britta Landfried[1], Marijana Samardzija[1], Maya Barben[1,2], Christian Schori[1,3], Katrin Klee[1,3], Federica Storti[1] and Christian Grimm*[,1,2,3]

Na,K-ATPases are energy consuming ion pumps that are required for maintaining ion homeostasis in most cells. In the retina, Na,K-ATPases are especially important to sustain the dark current in photoreceptor cells needed for rapid hyperpolarization of rods and cones in light. Cardiac glycosides like digoxin inhibit the activity of Na,K-ATPases by targeting their catalytic alpha subunits. This leads to a disturbed ion balance, which can affect cellular function and survival. Here we show that the treatment of wild-type mice with digoxin leads to severe retinal degeneration and loss of vision. Digoxin induced cell death specifically in photoreceptor cells with no or only minor effects in other retinal cell types. Photoreceptor-specific cytotoxicity depended on the presence of bleachable rhodopsin. Photoreceptors of *Rpe65* knockouts, which have no measurable rhodopsin and photoreceptors of *Rpe65*^{R91W} mice that have $<$10% of the rhodopsin found in retinas of wild-type mice were not sensitive to digoxin treatment. Similarly, cones in the all-cone retina of *Nrl* knockout mice were also not affected. Digoxin induced expression of several genes involved in stress signaling and inflammation. It also activated proteins such as ERK1/2, AKT, STAT1, STAT3 and CASP1 during a period of up to 10 days after treatment. Activation of signaling genes and proteins, as well as the dependency on bleachable rhodopsin resembles mechanisms of light-induced photoreceptor degeneration. Digoxin-mediated photoreceptor cell death may thus be used as an inducible model system to study molecular mechanisms of retinal degeneration.
Cell Death and Disease (2017) **8,** e2670; doi:10.1038/cddis.2017.94; published online 16 March 2017

Retinal degenerative diseases like retinitis pigmentosa or age-related macular degeneration (AMD) lead to strong visual impairment or blindness and have a high socio-economic impact. Although they affect a large number of patients and the incidence is expected to increase during the next decades especially for AMD,[1] an efficient treatment option is still an unmet medical need. A main reason for the lack of therapies is the insufficient understanding of the pathophysiological mechanisms responsible for disease initiation and progression even though many animal models have been developed and studied.[2] These models are either based on genetic manipulations or on the application of toxic stimuli such as light[3] or N-methyl-N-nitrosourea (MNU)[4] and may give insights into specific aspects of disease pathology. Nevertheless, additional models based on different molecules or pathways are desirable to further broaden approaches and experimental possibilities for investigations.

Cardiac glycosides like digoxin or ouabain inhibit Na,K-ATPases and are traditionally used to treat atrial fibrillation and atrial flutter.[5] Owing to their cytotoxic properties, they are also discussed as possible anticancer agents.[6] Although different cardiac glycosides have slightly different specificities for different isoforms of the Na,K-ATPases,[7] their inhibitory action on the ion pump causes increased intracellular Na^+ and Ca^{2+} and decreased K^+ concentrations.[8] This disturbance of the ion homeostasis may affect cellular function and viability. As cardiac glycosides inhibit Na,K-ATPases in all tissues including the retina, it is not surprising that several reports suggest an effect of digoxin on vision, with strongest disturbances of the cone pathway.[9,10]

Na,K-ATPases are heterodimers, composed of an alpha- and a beta-subunit.[11] In addition, they can be regulated by an auxiliary FXYD protein.[12,13] Cardiac glycosides target primarily the catalytic alpha subunit of the Na,K-ATPase.[14,15] Four alpha subunits have been identified that are encoded by different genes (*Atp1a1–Atp1a4*) and show tissue-specific expression. Whereas α1 is quite ubiquitously expressed in many tissues including the retina, α2 and α3 show a more specific pattern and have also been found in brain and retina.[16] Whereas α2 may be specific for Müller glia cells, α3 has been identified on all retinal neurons with particularly strong expression in photoreceptors, but not on Müller cells or the retinal pigment epithelium (RPE).[17] In contrast, α4 may be restricted to testis where it is important for sperm maturation.[18]

Since digoxin shows some preference for α2 and α3 isoforms[7] it may affect activity of Na,K-ATPases in the retina. Reports of patients describing visual disturbances, blurred vision, central scotomas or seeing yellowish[19] after digoxin treatment support this conclusion. Similarly, studies in monkeys demonstrated that digoxin can affect function especially of the cone system,[10] and a recent report showed that treating mice with high doses of digoxin causes retinal degeneration.[20] Thus, we investigated the effect of digoxin on the mouse retina and focused on its potential cytotoxicity for photoreceptor cells in different wild type and transgenic mouse lines. We established a treatment protocol that induces severe

[1]Lab for Retinal Cell Biology, Department of Ophthalmology, University of Zürich, Zürich, Switzerland; [2]Neuroscience Center Zürich (ZNZ), University of Zürich, Zürich, Switzerland and [3]Center for Integrative Human Physiology (ZIHP), University of Zürich, Zürich, Switzerland
*Corresponding author: C Grimm, Lab for Retinal Cell Biology, Department of Ophthalmology, University of Zürich, Wagistrasse 14, Schlieren, CH 8952, Switzerland. Tel: +41 44 556 3001; Fax: +41 44 556 3999; E-mail: cgrimm@opht.uzh.ch
Received 20.11.16; revised 09.2.17; accepted 10.2.17; Edited by A Verkhrtasky

loss of photoreceptors and propose that digoxin-mediated photoreceptor cell death may be used as a novel model to study mechanisms of retinal degeneration.

Results

Digoxin-induced retinal degeneration. To characterize the morphological, functional and molecular response to digoxin treatment, we titrated the amount of digoxin and the number of intraperitoneal (ip) injections needed for the induction of photoreceptor degeneration in C57BL/6 mice. In a first set of experiments, we used a dose of 2 mg/kg that was reported by Hinshaw *et al*.[20] to cause photoreceptor degeneration after 5 (least number of injections reported) or more intraperitoneal injections. This dose induced severe retinal degeneration already after three daily ip injections whereas one and two injections did not noticeably alter retinal morphology (Figure 1a). Although the extent of degeneration was slightly variable, cell death was largely restricted to the outer nuclear layer (ONL) as almost no TUNEL-positive cells were detected in other retinal layers (Figure 1a). Three injections of a lower dose (up to 1 mg/kg) did not cause degeneration (Figure 1b). Consequently, a treatment protocol of one digoxin injection on each of three consecutive days at a dose of 2 mg/kg was established and used for most of the following experiments. Although strong morphological damage was observed at 2 days, we detected pyknotic nuclei in the ONL as early as 1 day after the last injection (Figure 1c, white arrowheads). This was followed by a complete disruption of the outer and inner segments and loss of photoreceptors in the central retina between 2 and 10 days, the last time point analyzed (Figure 1c). Degeneration was accompanied by macrophage infiltration to the subretinal space (Figure 1c, black arrow). Loss of photoreceptor cells was most significant in the central retina whereas the retinal periphery was largely spared (Figures 2a and 6f). Consequences of digoxin treatment were also followed *in vivo* by fundus photography and optical coherence tomography (OCT) at 9 days after treatment (Figure 2b). Injections of digoxin caused the fundus to appear more intensely pigmented, probably due to the thinned retinal tissue. OCT images confirmed severe thinning of the ONL in digoxin-treated but not in control mice. Some regions of the retina in digoxin-treated mice were detached from the RPE suggesting potential subretinal fluid accumulation (Figure 2b).

TUNEL staining (Figure 1a) suggested that the toxic effect of digoxin was largely restricted to photoreceptor cells. This conclusion was further supported by immunofluorescence staining of retinal cell markers in retinas at 10 days after digoxin or PBS treatment. Distribution of peanut agglutinin (PNA) and G-protein subunit alpha transducin 1 (GNAT1) showed that both cones and rods were directly or indirectly affected by digoxin (Figure 3a). In contrast, normal distribution of visual system homeobox 2 (VSX2), pou domain, class4, transcription factor 1 (POU4F1), calbindin 1 (CALB1) and calretinin (CR) suggested that bipolar cells, ganglion cells, horizontal cells and amacrine cells, respectively, were largely unaffected (Figures 3b and c). Nevertheless, digoxin induced degeneration of photoreceptors activated Müller glia cells as indicated by increased GFAP staining and stimulated resident IBA1-positive microglia and/or macrophages to migrate to the subretinal space (Figure 3d).

As expected, digoxin-induced loss of photoreceptors affected scotopic and photopic retinal function at 10 days after treatment. Scotopic and photopic b-wave, as well as scotopic a-wave amplitudes were reduced indicating loss of function (Figures 4a and c). Even though morphological and immunofluorescence analyses suggested that digoxin toxicity was confined to photoreceptors in the outer retina, cells of the inner retina may have been affected functionally. ERG recordings one day after two digoxin injections (2 mg/kg), a treatment that did not induce photoreceptor degeneration (Figure 1a), showed prolonged responses at low light intensities, a reduction of the maximal b-wave amplitudes and strongly reduced oscillatory potentials for both the scotopic and the photopic ERG (Figures 4b and c). These observations resemble functional consequences reported for ocular ischemia[21] that is characterized by a reduced supply of oxygen to the inner retina.[22] Interestingly, digoxin can reduce heart rate[23] and cause vasoconstriction of peripheral arteries,[24] and may thus potentially lead to a reduced blood flow in peripheral organs including the retina. Clearly, further experimentation is required to evaluate the influence of digoxin on retinal function.

Molecular signaling. Digoxin inhibits Na,K-ATPases[25] through interaction with the regulatory alpha subunits, with a preference for α2 and α3 (ref. 26) (see 'Introduction' section). As α4 was reported to be specifically expressed in testis,[18] we focused on α1, α2 and α3 for our analysis. As reported before[17] all three alpha subunits were expressed in the normal mouse retina (Figure 5a). Treatment with digoxin increased expression of *Atp1a1* at 1 d and 10 d, did not affect *Atp1a2* and reduced the expression of *Atp1a3* (Figure 5a). As α3 shows a strong expression in photoreceptors whereas α1 and α2 may be expressed preferentially by other retinal cells,[17] downregulation of *Atp1a3* expression may reflect the degenerative process with photoreceptor injury and death. In addition, digoxin treatment induced retinal expression of several genes involved in stress signaling such as endothelin-2 (*Edn2*), fibroblast growth factor 2 (*Fgf2*) and glial fibrillary acidic protein (*Gfap*), in degeneration and inflammation including caspase 1 (*Casp1*) and tumor necrosis factor alpha (*Tnf*), and in oxidative stress like heme oxygenase 1 (*Hmox1*; Figure 5b). Peak of activation was at 2 days after the last digoxin injection. Expression levels returned to basal levels at 10 days after injections suggesting a general recovery from treatment. This interpretation was supported by the pattern of protein activation (Figure 5c). Phosphorylation of the signaling proteins extracellular signal regulated kinase (ERK), protein kinase B (alias AKT), signal transducer and activator of transcription 1 (STAT1) and of STAT3 peaked at 1 and 2 days after treatment, reaching basal levels thereafter. Interestingly, we consistently observed that levels of pERK1/2 were strongly reduced at 5 and 10 days post treatment. The reason and the functional consequences for such a reduced pERK signaling are unknown and remain to be evaluated. It has been reported that digoxin increases phosphorylation of protein kinase

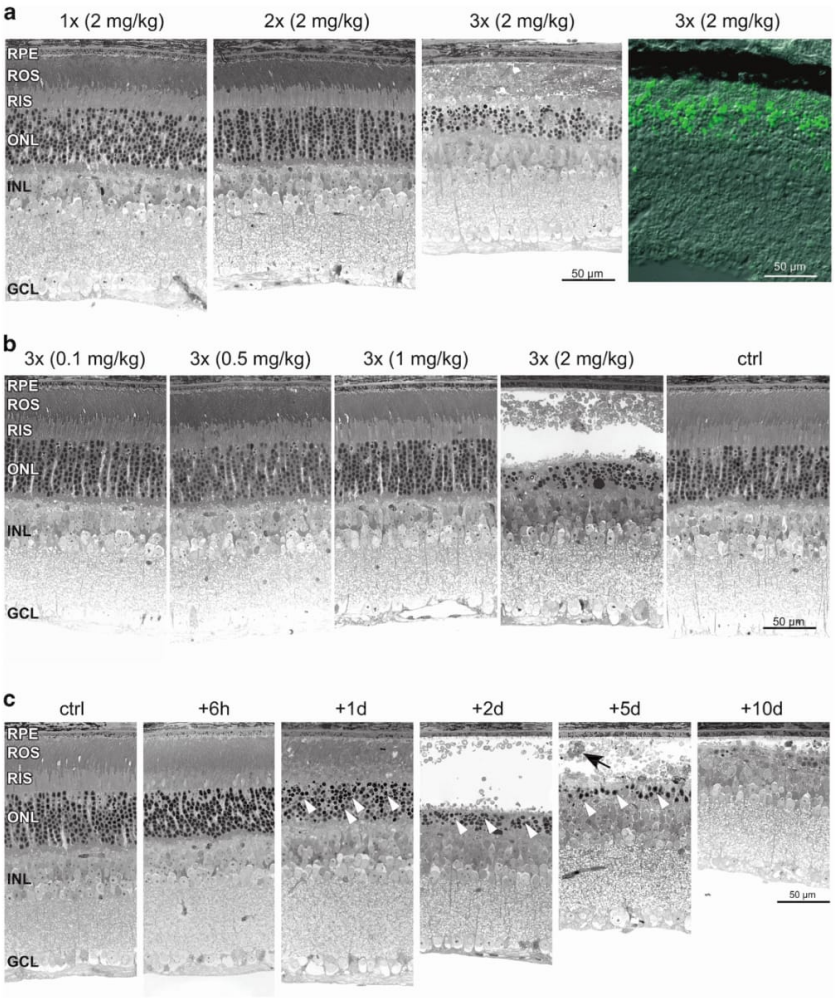

Figure 1 Digoxin-induced retinal degeneration. (**a**) Retinal morphology of mice at 2 days after the last of 1, 2 or 3 injections of 2 mg/kg digoxin as indicated. TUNEL staining (right panel) at 1 day after the last of 3 injections of 2 mg/kg digoxin. (**b**) Retinal morphology of mice at 2 days after the last of 3 injections of 0.1, 0.5, 1 or 2 mg/kg digoxin as indicated. (**c**) Retinal morphology of mice at 6 h, 1 d, 2 d, 5 d and 10 d after the last of 3 injections of 2 mg/kg digoxin as indicated. $N = 3$. Black arrow, macrophage; Ctrl, PBS-injected control mice; GCL, ganglion cell layer; INL, inner nuclear layer; ONL, outer nuclear layer; RPE, retinal pigment epithelium; ROS, rod outer segments; RIS, rod inner segments; Scale bars, 50 μm; white arrowheads: pyknotic nuclei

AMP-activated catalytic subunit alpha 1 (AMPK) and may thus affect energy levels in cells.[27] In retinas of digoxin-treated mice, however, pAMPK levels remained constant with a slight decrease by 5 and 10 days after the last injection. In contrast, proteins indicating reactive gliosis and degeneration (GFAP and CASP1) were induced primarily between 2 and 10 days, and thus after the initial signaling events. A late response of CASP1 was also observed in other models of retinal degeneration.[28] As in the light damage model and during degeneration in the VPP mouse model for inherited degeneration,[28] we did not detect P10 or P20 cleaved forms of CASP1 (not shown). Levels of the p85 regulatory subunit of PI3K remained at constant levels, even though this protein is known to be involved in Na,K-ATPase signaling.[29,30] Levels of hypoxia-inducible factor 1A (HIF1A) were bi-phasic with an initial decline at 1 d, followed by an increase until 10 d post treatment. Although ERG data (Figure 4) may indicate that digoxin application resulted in a condition resembling retinal ischemia, we did not detect increased HIF1A levels shortly after treatment presumably because digoxin can inhibit HIF1A, as reported by others.[31,32] Only after clearance of digoxin, HIF1A levels may increase and reach the levels detected between 2 and 10 days. However, this bi-phasic appearance of HIF1A was not reflected by corresponding mRNA levels of HIF1 target genes suggesting that HIF1 activity was not strongly affected by digoxin (data not shown).

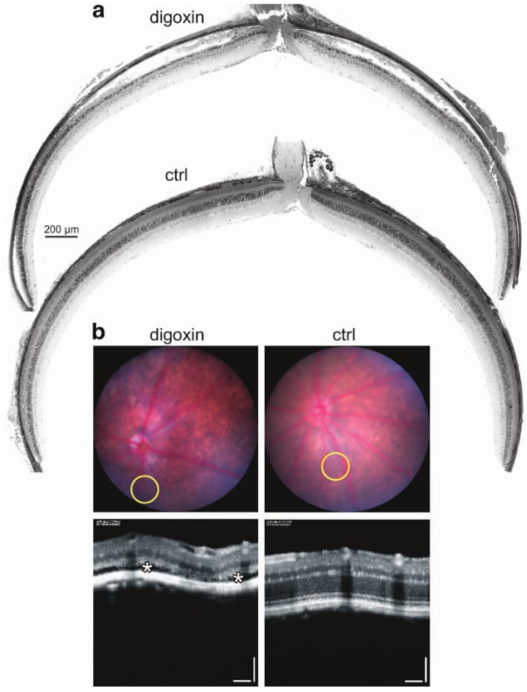

Figure 2 Geographic extent and *in vivo* imaging of digoxin-induced retinal degeneration. (**a**) Dorsoventral retinal panoramas of digoxin- (digoxin, top) or PBS-treated (ctrl, bottom) mice at 2 days after the last of 3 injections of 2 mg/kg digoxin. Scale bar, 200 μm. $N=3$. (**b**) Fundus (top) and OCT (bottom) images of digoxin (digoxin, left) and untreated (ctrl, right) mice at 9 days after the last of 3 injections of 2 mg/kg digoxin. Yellow circles indicate the position of the corresponding OCT images. White asterisks mark subretinal fluid accumulation. Scale bar, 100 μm. $N=2$

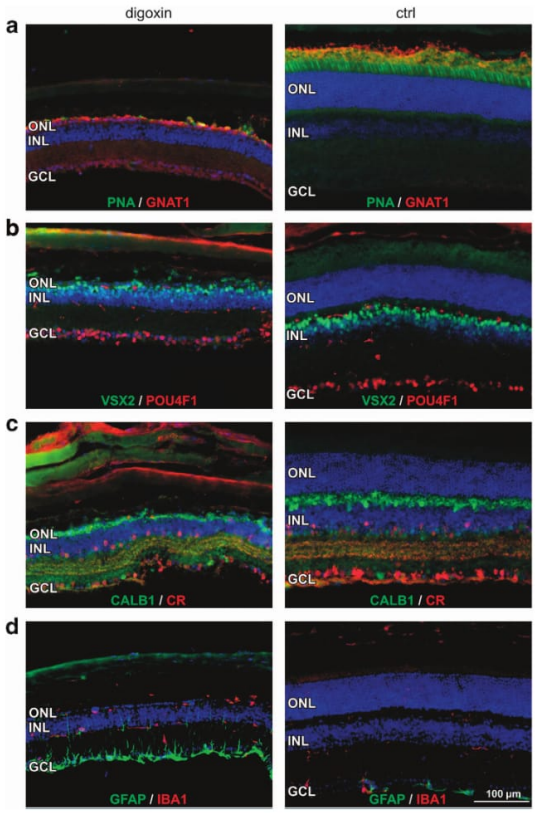

Figure 3 Localization of retinal cell markers after digoxin treatment. Retinal sections of mice at 10 days after the last of 3 injections of 2 mg/kg digoxin (left) or PBS (ctrl, right) were stained with PNA (green) and antibodies against GNAT1 (red) (**a**), VSX2 (green) and POU4F1 (red) (**b**), CALB1 (green) and CR (red) (**c**) and GFAP (green) and IBA1 (red) (**d**). Ctrl, PBS-injected control mice; GCL, ganglion cell layer; INL, inner nuclear layer; ONL, outer nuclear layer; RPE, retinal pigment epithelium; ROS, rod outer segments; RIS, rod inner segments; Scale bars, 100 μm. $N=3$

Dependency on rhodopsin. As digoxin-induced retinal degeneration might be used as a model to study degenerative processes, we tested the susceptibility of different mouse strains to degeneration. Similar to C57BL/6 mice, photoreceptors of 129S6 wild-type mice were strongly damaged 2 days after the last injection of digoxin (3 × 2 mg/kg; Figure 6a). Surprisingly, however, photoreceptors of *Rpe65*^{R91W} mice on a 129S6 genetic background were completely insensitive to digoxin treatment (Figure 6b). Similarly, photoreceptors of *Rpe65*$^{-/-}$ mice that are on a C57BL/6 background were also not damaged (Figure 6c). Common to these two mouse strains is the reduced amount (in *Rpe65*^{R91W}) or lack (in *Rpe65*$^{-/-}$) of bleachable rhodopsin caused by the low activity or complete absence, respectively, of RPE65 in the RPE.[33] Furthermore, cone photoreceptors of *Nrl*$^{-/-}$ mice did also not degenerate after digoxin application (Figure 6d). These data suggest that rhodopsin is required for digoxin-induced photoreceptor degeneration and that cones may be insensitive to digoxin cytotoxicity. Therefore, the influence on cone morphology (Figure 3) and function (Figures 4a and b) observed in C57BL/6 mice might have been indirectly caused by the degeneration of rods. Lack of digoxin sensitivity was not due to reduced expression of *Atp1a* genes in retinas of the respective strains since *Atp1a1* and *Atp1a2* were similarly expressed in all strains tested. Although the protected transgenic mice expressed *Atp1a3* at lower levels than C57BL/6 mice, expression was nevertheless similar to the susceptible mice of the 129S6 strain (Figure 6e).

As degeneration depended on rhodopsin, we tested whether increased photon absorption would accelerate the degenerative process in C57BL/6 mice. However, mice that were kept in cyclic light during treatment and during the 2-day post-treatment period (light) were damaged similarly to mice that were kept in constant darkness after the last digoxin injection (dark). The central retinal region showed similar levels of pyknotic photoreceptor nuclei and disrupted inner and outer segments whereas the peripheral retinal areas were spared independently of the light condition (Figure 6f).

Discussion

We showed that daily intraperitoneal injections of 2 mg/kg digoxin on 3 consecutive days induced severe retinal

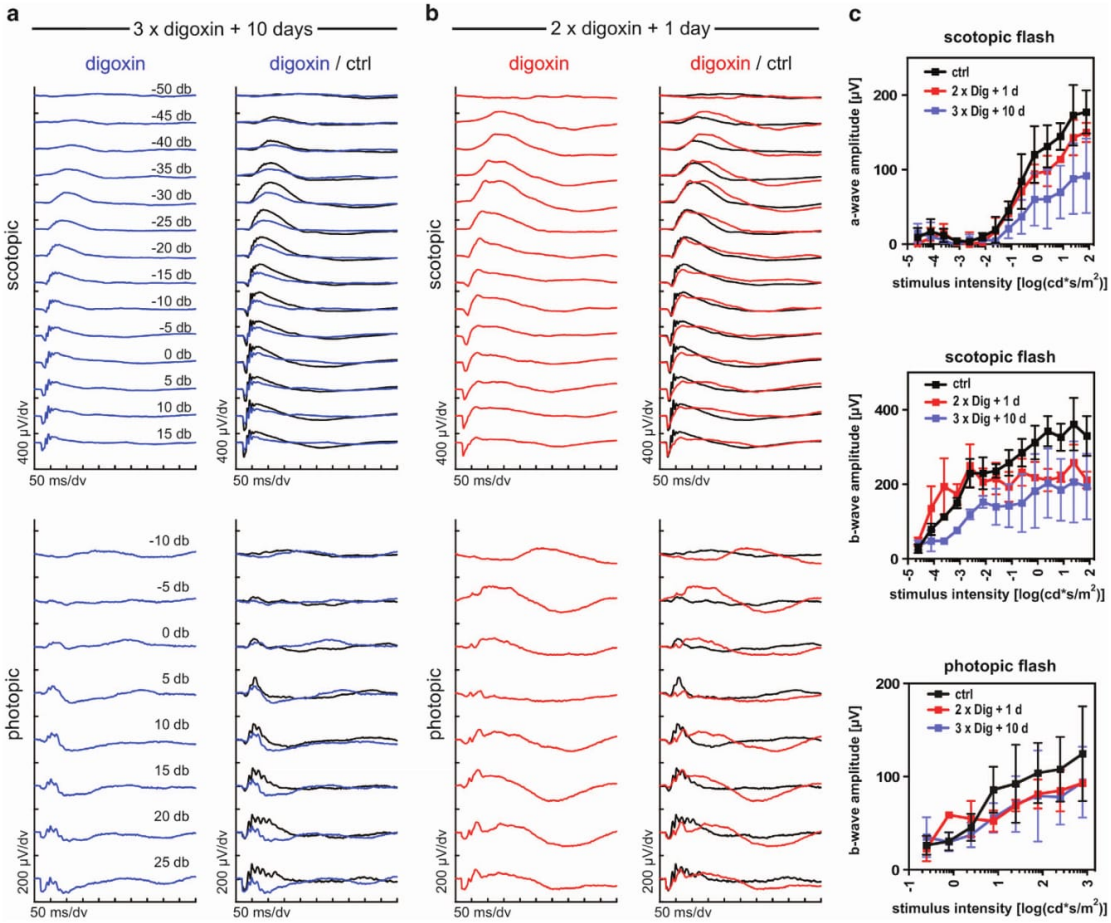

Figure 4 Retinal function after digoxin treatment. Mice received a toxic dose (three injections, 2 mg/kg each) or a subtoxic dose (two injections, 2 mg/kg each) of digoxin and were analyzed at 10 or 1 day after the last injection, as indicated. (**a**) Scotopic (top) and photopic (bottom) ERG traces were recorded from mice treated with the toxic digoxin dose (3 × digoxin, blue lines). (**b**) Scotopic (top) and photopic (bottom) ERG traces were recorded from mice treated with the subtoxic digoxin dose (2 × digoxin, red lines). ERGs were compared to mice injected twice with PBS (ctrl) and analyzed 1 day after the second injection (black lines in **a** and **b**). Shown are traces averaged from $N = 3$ mice (6 eyes). (**c**) Scotopic a- and b-wave and photopic b-wave amplitudes plotted as a function of stimulus intensity. Shown are averages ± S.D. $N = 3$ mice (6 eyes). Color scheme as in (**a** and **b**)

degeneration in wild-type mice. Degeneration was restricted to photoreceptors of the central retina, depended on the presence of rhodopsin, activated stress signaling, and induced genes involved in degeneration, inflammation and oxidative stress. The dose needed to induce retinal degeneration was 100 to 1000-fold higher than doses used to treat heart conditions in human patients. Indeed, reports indicate that patients treated with a daily dose of as little as few µg/kg digoxin may occasionally experience blurred vision, dyschromatopsia and other visual symptoms as adverse effects.[19] Whether treatment also cause some photoreceptor toxicity in patients has not been investigated as most disturbances seem reversible at the dose used in clinics.[34] In mice, however, significantly higher doses are required for an effect since polymorphisms in murine Na,K-ATPases make mice profoundly more resistant to digoxin.[20,35,36]

Digoxin was recently shown to inhibit HIF1 in the model of oxygen-induced retinopathy (OIR)[31,32] and suppressed choroidal neovascularization (CNV) in a model of laser-induced lesions.[32] Although both studies used wild-type mice, a digoxin concentration of 2 mg/kg (as used here) and repetitive intraperitoneal injections, no cytotoxic effects on photoreceptors were reported. The reason for this is unclear but may be based on the age of the mice during treatment. Both OIR studies injected digoxin between PND12 and PND17, at a time when retinal development has not yet been completed. In fact, photoreceptor function is very low at least up to PND16[37] suggesting that Na,K-ATPases may not yet be fully functional at this time. Although Yoshida *et al.*[32] also used adult mice in their model of laser-induced CNV, they analyzed treatment outcome in choroidal flat mounts focusing on neovascularization. A specific effect on photoreceptors was not investigated in their experiments.

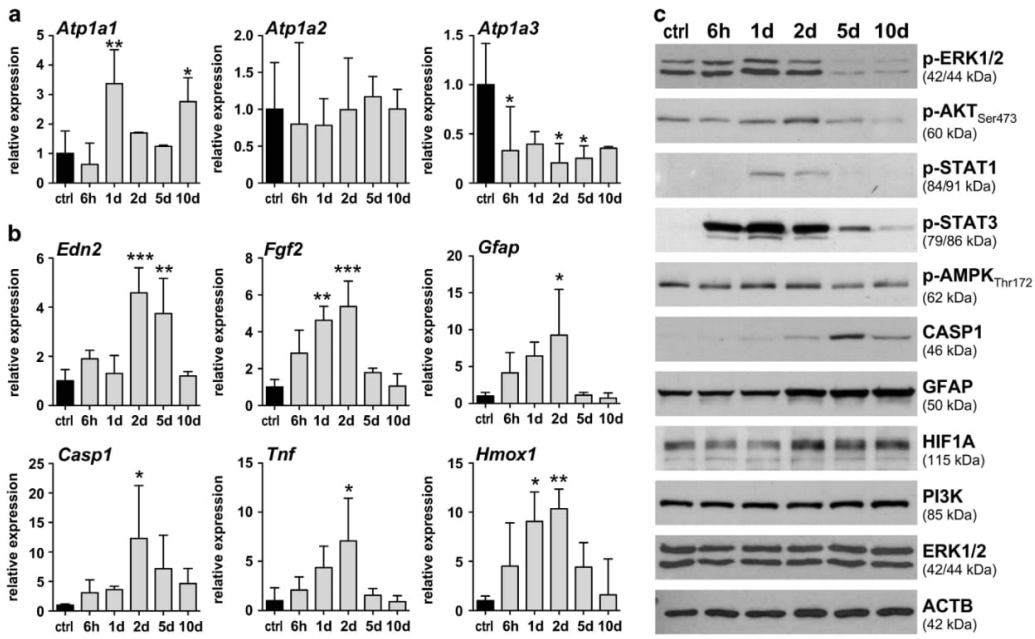

Figure 5 Retinal gene and protein expression after digoxin treatment. (**a**) Relative expression of genes encoding the alpha subunits of Na,K-ATPases. (**b**) Relative expression of genes involved in stress signaling and inflammation, as indicated. Retinal expression levels of digoxin-treated mice (gray bars) were normalized to *Actb* and expressed as fold change relatively to PBS-injected controls (ctrl, black bars, set to 1). Shown are means ± S.D. of $N=3$. *: adjusted P-value <0.05. **: adjusted P-value <0.01. ***: adjusted P-value <0.001. One-way ANOVA with Dunnett's multiple comparison test (each column compared to control). (**c**) Retinal levels of selected proteins and phospho-proteins were tested by Western blotting. All analyses were done at five time points (as indicated) after the last of 3 injections of 2 mg/kg digoxin and compared to PBS-injected controls (ctrl). $N=3$

Digoxin inhibits primarily the catalytic alpha subunits of Na,K-ATPases[14] and has a certain selectivity for α2 and α3 isoforms[7] that are also expressed in retinal cells including photoreceptors.[17,38] As Na,K-ATPases are responsible for ion homeostasis and are critical for maintaining high extracellular levels of Na^+ and high intracellular K^+,[39] inhibition of Na,K-ATPase activity by digoxin leads to an increase in Na^+ and a depletion of K^+ in the cells.[39,40] As a consequence of high intracellular Na^+, the entry-mode of the sodium/calcium exchanger (NCX) may be activated[41] potentially causing increased intracellular Ca^{2+} levels in addition.[42] Whereas a causative role of high intracellular Na^+ for the induction of cell death has not been established but may be connected to apoptosis through the regulation of cell volume,[43] Ca^{2+} has long been recognized as an important factor for the regulation of a variety of cellular processes including apoptosis.[44] Ca^{2+} may induce cell death, for example, through activation of calpains that leads to the proteolytic cleavage of intracellular substrates.[45] Importantly, calpain-mediated cell death has also been reported in models of photoreceptor degeneration.[46,47] Similarly, strong evidence suggests that depletion of intracellular K^+ is essential for the initiation of apoptosis in a variety of cells.[48] The mechanisms that contribute to cell death by K^+ depletion are not known in detail, but may include regulation of cell volume, caspase activation and changes of the membrane potential of mitochondria.[39] Loss of intracellular K^+ was directly implicated in photoreceptor degeneration in drosophila that lacked the alpha subunit of the Na,K-ATPase.[49] Thus, inhibition of Na,K-ATPases may alter intracellular ion homeostasis, which may significantly contribute to the degeneration of photoreceptor cells after digoxin application.

Increasing evidence suggests that Na,K-ATPases not only control cellular ion homeostasis but have also important functions in signal transduction[50] by interacting with endogenous cardenolides including digoxin-like substances that are found in the circulation.[51,52] Signaling may include activation of mitogen-activated protein kinases including ERK1/2,[53] activation of PI3K and AKT[29] and phosphorylation of SRC.[54] Na,K-ATPases may thus constitute a class of cell surface receptors that can influence a number of physiological processes linked to cell survival in several cell types[50] including neurons.[55] We detected slight upregulation of pERK1/2 and pAKT at 1–2 days after digoxin injection. As digoxin has a half-life of ~40 h in patients,[56] it is likely that digoxin can still signal at this time point in mice. However, as ERK1/2 and AKT are also activated by degenerative processes, we cannot discriminate between a direct digoxin-mediated effect and stress response signaling. It is interesting to note that both, pERK1/2 and pAMPK, levels drop below control levels late during the degenerative process. The reason for this is unclear but may signify the specific consequences of digoxin treatment.

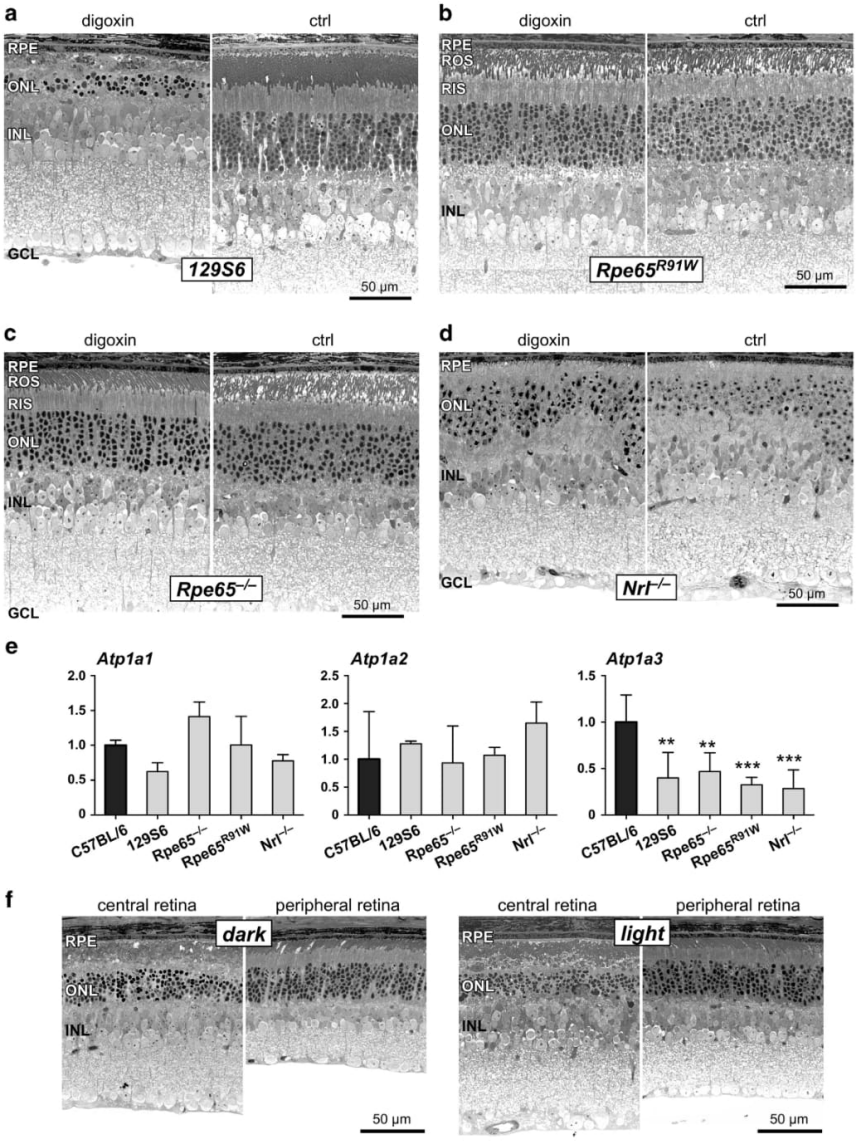

Figure 6 Dependency of digoxin-induced degeneration on rhodopsin. Retinal morphology of *129S6* wild type (**a**), *Rpe65*^{R91W} (**b**), *Rpe65*$^{-/-}$ (**c**) and *Nrl*$^{-/-}$ (**d**) mice at 2 days after the last of 3 injections of 2 mg/kg digoxin or of PBS (ctrl). $N = 3$–4 (digoxin) and $N = 2$–4 (ctrl). (**e**) Relative basal expression of *Atp1a1*, *Atp1a2* and *Atp1a3* in mice of the different strains as indicated. Expression levels were normalized to *Actb* and expressed relatively to levels in C57BL/6 mice (black bars, set to 1). Shown are means ± S.D. of $N = 3$. **: adjusted *P*-value < 0.01. ***: adjusted *P*-value < 0.001. $N = 3$. One-way ANOVA with Dunnett's multiple comparison test (each column compared to C57BL/6). (**f**) Retinal morphology of *129S6* wild type at 2 days after the last of 3 injections of 2 mg/kg digoxin. Mice were either kept in darkness after the last injection according to the standard protocol (dark) or were exposed to a regular 12 h : 12 h light–dark cycle (light, 60 lux during the light period). $N = 3$. Ctrl, PBS-injected control mice; GCL, ganglion cell layer; INL, inner nuclear layer; ONL, outer nuclear layer; RPE, retinal pigment epithelium; ROS, rod outer segments; RIS, rod inner segments; Scale bars, 50 μm

Interestingly, photoreceptor degeneration caused by digoxin resembles light-induced retinal degeneration in several points. (i) degeneration is confined to photoreceptors[57] (Figures 1 and 3); (ii) the central retina is more sensitive to damage[57] (Figure 2); (iii) similar signaling pathways are activated[58,59] (Figure 5); (iv) cones are less sensitive[60] (Figure 6); and (v) degeneration depends on rhodopsin[61,62] (Figure 6). The latter point is intriguing and not easily explained. Although hypotheses remain highly speculative, this result may indicate either an interaction of digoxin with rhodopsin inducing cytotoxicity

Table 1 Primers used for real-time PCR

Gene	Forward 5′–3′	Reverse 5′–3′	Product (bp)
Actb	CAACGGCTCCGGCATGTGC	CTCTTGCTCTGGGCCTCG	153
Atp1a1	GGTGGTGCTCTCTGCTGTAG	GACGACATCCTCCGCATTGA	161
Atp1a2	CTGTCCTTGGATGAGCTGGG	CCTGAGCTCGCTGATTGGTG	72
Atp1a3	GAACTTCACCACAGACAACC	GACCATGATGACCTTGATGC	121
Edn2	AGACCTCCTCCGAAAGCTG	CTGGCTGTAGCTGGCAAAG	64
Fgf2	TGTGTCTATCAAGGGAGTGTGTGC	ACCAACTGGAGTATTTCCGTGACCG	158
Casp1	GGCAGGAATTCTGGAGCTTCAA	GTCAGTCCTGGAAATGTGCC	138
Tnf	CCACGCTCTTCTGTCTACTGA	GGCCATAGAACTGATGAGAGG	95
Hmox1	CCGCCTTCCTGCTCAACATT	GACGAAGTGACGCCATCTGTG	99
Gfap	CCACCAAACTGGCTGATGTCTAC	TTCTCTCCAAATCCACACGAGC	240

by an unknown mechanism or an augmentation of digoxin-induced cell stress by light absorption, for example by generating all-trans-retinal as a reactive aldehyde[63] or reactive oxygen species.[64] However, digoxin-induced degeneration did not notably differ between mice that were kept in darkness or exposed to normal cycling light after digoxin treatment (Figure 6f), making the first or an alternative explanation more likely. In any case, both light exposure and digoxin application cause altered intracellular ratios of $Na^+/Ca^{2+}/K^+$ through closure of the cGMP-gated channels or inhibition of Na,K-ATPases, respectively. This leads to degenerative processes with several common features suggesting that maintenance of ion homeostasis is a crucial determinant of photoreceptor survival. Studying this model in more detail may shed light onto the regulation of ion homeostasis in connection to physiologic (signaling) and pathologic (degeneration) processes. This model may also provide an alternative to the induction of photoreceptor apoptosis by the highly toxic MNU that was used frequently to investigate cellular and molecular aspects of photoreceptor degeneration.

Material and Methods

Mice and digoxin injections. All animal experimentation was performed in accordance to the ARVO Statement for the use of animals in ophthalmic and vision research and the regulations of the veterinary authorities of Zürich. C57BL/6 (wild type; Jackson lab, Sulzfeld, Germany), 129S6 (wild type; Taconic, Ejby, Denmark), *Nrl*$^{-/-}$,[65] *Rpe65*$^{-/-}$ (ref. 66) and *Rpe65*^{R91W} (ref. 33) mice were housed in the animal facility of the University of Zürich in a 12 h : 12 h light–dark cycle with access to food and water *ad libitum*. Three mice per strain and experimental condition were used at the age of 6–10 weeks, unless indicated otherwise.

Digoxin (Sigma, Buchs, Switzerland) was dissolved at a concentration of 40 mg/mL in DMSO, followed by dilution with PBS to 2 mg/mL and stored in aliquots at − 20 °C. Immediately before use, digoxin was further diluted in PBS to 0.2 mg/ml and injected intraperitoneally at doses ranging from 0.1 mg/kg to 2 mg/kg. Injections were done once a day at 9–10 am for up to 3 consecutive days. Mice that were injected with PBS served as controls, except for Figure 2b where uninjected mice were used as controls. During digoxin treatment, mice were housed in normal cages in a 12 h : 12 h light–dark cycle (60 lux at cage level) with unrestricted access to food and water. After the last injection, mice were placed in darkness for 2 days before they were either killed or returned to the light–dark cycle until analysis. For the generation of data shown in Figure 6f (light), mice were kept in the normal light–dark cycle for the entire duration of the experiment.

Morphology. Eyes were marked nasally, enucleated, fixed in glutaraldehyde (2.5% in cacodylate buffer) over night at 4 °C, trimmed, post-fixed in 1% osmium tetroxide and embedded in Epon 812 as described.[67] Dorsoventral cross-sections of 0.5 μm were cut through the optic nerve head, stained with toluidine blue and analyzed using light microscopy (Zeiss, Axioplan, Jena, Germany). Images of higher magnifications (Figures 1 and 6) were always acquired from the central region close to the optic nerve head, except where stated otherwise.

Immunofluorescence and TUNEL staining. Eyes were marked nasally, enucleated and prepared for cryosectioning essentially as described[68] but without prior perfusion of the mice. Cryosections (12 μm) were cut in a dorsoventral orientation, blocked for 1 h with blocking solution containing 3% normal goat serum (Sigma) and 0.3% Triton X-100 (Sigma) in PBS. Sections were incubated over night at 4 °C with the following primary antibodies: PNA-FITC (1:250, L7381, Sigma), rabbit anti-GNAT1 (1:500, sc-389, Santa Cruz Biotechnology; Santa Cruz, CA, USA), mouse anti-GFAP (1:250, G3893-Clone G-A-5, Sigma), rabbit anti-IBA1 (1:500, 019-19741, Wako, Neuss, Germany), mouse anti-POU4F1 (alias BRN3A; 1:100, MAB1585, Chemicon, Temecula, CA, USA), rabbit anti-VSX2 (alias CHX10; 1:500, kindly provided by Connie Cepko, Harvard University, MA, USA), mouse anti-CR (1:1000, AB5054, Chemicon) and rabbit anti-CALB1 (1:500, AB1778, Chemicon). Sections were washed with PBS, incubated for 1 h at room temperature with appropriate secondary antibodies labeled with Cy2 or Cy3 (Jackson ImmunoResearch Laboratories, Soham, UK), counterstained with 4′,6′-diamidino-2-phenylindole (DAPI; Life Technologies, Zug, Switzerland) and analyzed using fluorescence microscopy (Zeiss).

For TUNEL staining, retinal cryosections were dried and fixed in 4% PFA solution for 10 min. After two washing steps with PBS (10 min each) a drop of 0.1% Triton X-100 in 0.1% sodium citrate was added and incubated for 5 min for tissue permeabilization. After two washing steps with PBS (5 min each) sections were tested for TUNEL-positive signals using the *in situ* cell death detection kit (Roche Diagnostics, Rotkreuz, Switzerland) according to the manufacturer's instructions. Slides were mounted with Mowiol (Sigma), sealed with nail polish solution and analyzed by fluorescence microscopy. Images were always acquired from the central region close to the optic nerve head.

RNA isolation and semi-quantitative real-time PCR. Retinas were isolated through a slit in the cornea and snap frozen in liquid nitrogen. Retinal RNA was isolated using an RNA isolation kit according to the manufacturer's instructions (RNeasy, Qiagen, Hilden, Germany) with an additional on-column DNAse treatment to digest remaining genomic DNA. Concentration of eluted RNA was measured by Nanodrop spectrophotometer (Thermo Fisher Scientific, Waltham, MA, USA) and RNA diluted to a final concentration of 50 ng/μl. cDNA was prepared from total RNA using oligo(dT) and M-MLV reverse transcriptase (Promega, Dübendorf, Switzerland). Semi-quantitative real-time PCR was performed in a LightCycler480 instrument (Roche Diagnostics) using the SYBR Green I master mix (Roche Diagnostics) and appropriate primer pairs (Table 1) designed to span large intronic regions and avoid known SNPs. Reactions were normalized to *Actb* and relative expression was calculated by the comparative threshold cycle method ($\Delta\Delta C_T$) using the LightCycler480 software.

Protein isolation and Western blot. Retinas were isolated through a slit in the cornea and homogenized by sonication in 200 μl of 100 mM Tris/HCl (pH 8,0). Homogenates were centrifuged (1000 × g; 3 min) and protein contents determined in the supernatants using Bradford reagent (Bio-Rad, Hercules, CA, USA). SDS–PAGE and Western blot analysis were performed as described[67] using the following primary antibodies: rabbit anti-pERK (1 : 1000, #9101, New England Biolabs, Herts, UK), rabbit anti-ERK (1 : 1000, #9102, New England Biolabs), rabbit

anti-pAKT$_{Ser473}$ (1:1000, #9271, Cell Signaling Technology, Danvers, MA, USA); rabbit anti-pSTAT1$_{Tyr701}$ (1:500, #9171, Cell Signaling Technology); rabbit anti-pSTAT3$_{Tyr705}$ (1:500, #913 L, Cell Signaling Technology); rabbit anti-pAMPKa1-/2$_{Thr172}$ (1:1000, sc-33524, Santa Cruz Biotechnology); rabbit anti-CASP1 (1:10 000, kindly provided by P. Vandenabeele, University of Gent, Gent, Belgium); mouse anti-GFAP (1:1000, G3893-Clone G-A-5, Sigma); rabbit anti-HIF-1 A (1:4000, NB100-479, Novus Biologicals, Cambridge, UK); rabbit anti-PI3K (1:4000, D0669, Upstate, Millipore, Darmstadt, Germany); mouse anti-ACTB (1:10,000, A5441, Sigma). Membranes were incubated with primary antibodies diluted (as indicated) in 5% non-fat blocking milk (Bio-Rad) in TBST over night at 4 °C with gentle agitation. After a 1-h incubation step with appropriate HRP-conjugated secondary antibodies, immunoreactive signals were detected using the Western lightning chemiluminescence reagent (PerkinElmer, Waltham, MA, USA). Signals were visualized using X-ray films.

Electroretinography, fundus imaging and OCT. Mice were dark adaptated over night and pupils dilated using Cyclogyl 1% (Alcon Pharmaceuticals, Fribourg, Switzerland) and Neosynephrine 5% (Ursapharm Schweiz GmbH, Roggwil, Switzerland) 20 min before recording. Mice were anesthetized by a subcutaneous injection of ketamine (85 mg/kg, Parke-Davis, Berlin, Germany) and Xylazine (4 mg/kg, Bayer AG, Leverkusen, Germany). A drop of mydriacticum dispersa (OmniVision AG, Neuhausen, Switzerland) was applied to each cornea to induce mydriasis and to keep the tissue moist. Recordings were done using flashes of 13 different light intensities ranging from − 50 db (0.000025 cd*s/m^2) to 15 db (79 cd*s/m^2) for scotopic and flashes of 8 different light intensities ranging from − 10 db (25 cd*s/m^2) to 25 db (790 cd*s/m^2) for photopic ERG as described.[69] Ten recordings were averaged per light intensity.

Fundus imaging and OCT were done essentially as described.[70] In brief, pupils of mice were dilated and mice anesthetized as describe as above. Eyes were kept moist with 2% methocel (OmniVision AG) and fundus images and OCT scans recorded using the Micron IV system (Phoenix Research Labs, Pleasanton, CA, USA).

Statistical analysis. Differences in gene expression levels were evaluated by one-way ANOVA followed by Dunnett's multiple comparison tests (GraphPad, San Diego, CA, USA) comparing all time points (Figures 5a and b) or strains (Figure 6e) to the control or C57BL/6, respectively.

Conflict of Interest

The authors declare no conflict of interest.

Acknowledgements. We thank Andrea Gubler and Cornelia Imsand for their excellent technical support and Mathias Seeliger (University of Tuebingen, Germany) for advice on ERG results. We also thank Connie Cepko and Peter Vandenabeele for kindly providing the Antibodies for VSX2 and Caspase 1. Supported by the Swiss National Science Foundation (SNF #31003A_133043), the Cattaruzza Fonds and Pro Vista foundation.

1. Klein R, Klein BE, Knudtson MD, Meuer SM, Swift M, Gangnon RE. Fifteen-year cumulative incidence of age-related macular degeneration: the Beaver Dam Eye Study. *Ophthalmology* 2007; **114**: 253–262.
2. Samardzija M, Neuhauss SCF, Joly S, Kurz-Levin M, Grimm C. Animal models for retinal degeneration. *Animal Models for Retinal Diseases* 2010; **46**: 51–79.
3. Wenzel A, Grimm C, Samardzija M, Remé CE. Molecular mechanisms of light-induced photoreceptor apoptosis and neuroprotection for retinal degeneration. *Prog Retin Eye Res* 2005; **24**: 275–306.
4. Yuge K, Nambu H, Senzaki H, Nakao I, Miki H, Uyama M *et al.* N-methyl-N-nitrosourea-induced photoreceptor apoptosis in the mouse retina. *In Vivo* 1996; **10**: 483–488.
5. Ziff OJ, Kotecha D. Digoxin: the good and the bad. *Trends Cardiovasc Med* 2016; **26**: 585–595.
6. Prassas I, Karagiannis GS, Batruch I, Dimitromanolakis A, Datti A, Diamandis EP. Digitoxin-induced cytotoxicity in cancer cells is mediated through distinct kinase and interferon signaling networks. *Mol Cancer Ther* 2011; **10**: 2083–2093.
7. Katz A, Lifshitz Y, Bab-Dinitz E, Kapri-Pardes E, Goldshleger R, Tal DM *et al.* Selectivity of digitalis glycosides for isoforms of human Na,K-ATPase. *J Biol Chem* 2010; **285**: 19582–19592.
8. Schoner W, Scheiner-Bobis G. Endogenous and exogenous cardiac glycosides and their mechanisms of action. *Am J Cardiovasc Drugs* 2007; **7**: 173–189.
9. Lawrenson JG, Kelly C, Lawrenson AL, Birch J. Acquired colour vision deficiency in patients receiving digoxin maintenance therapy. *Br J Ophthalmol* 2002; **86**: 1259–1261.
10. Kinoshita J, Iwata N, Kimotsuki T, Yasuda M. Digoxin-induced reversible dysfunction of the cone photoreceptors in monkeys. *Invest Ophthalmol Vis Sci* 2014; **55**: 881–892.
11. Morth JP, Pedersen BP, Buch-Pedersen MJ, Andersen JP, Vilsen B, Palmgren MG *et al.* A structural overview of the plasma membrane Na+,K+-ATPase and H+-ATPase ion pumps. *Nat Rev Mol Cell Biol* 2011; **12**: 60–70.
12. Geering K. FXYD proteins: new regulators of Na-K-ATPase. *Am J Physiol Renal Physiol* 2006; **290**: F241–F250.
13. Tokhtaeva E, Clifford RJ, Kaplan JH, Sachs G, Vagin O. Subunit isoform selectivity in assembly of Na,K-ATPase α-β heterodimers. *J Biol Chem* 2012; **287**: 26115–26125.
14. Kaplan JH. Biochemistry of Na,K-ATPase. *Annu Rev Biochem* 2002; **71**: 511–535.
15. Blanco G, Mercer RW. Isozymes of the Na-K-ATPase: heterogeneity in structure, diversity in function. *Am J Physiol* 1998; **275**: F633–F650.
16. Blanco G. Na,K-ATPase subunit heterogeneity as a mechanism for tissue-specific ion regulation. *Semin Nephrol* 2005; **25**: 292–303.
17. Wetzel RK, Arystarkhova E, Sweadner KJ. Cellular and subcellular specification of Na,K-ATPase alpha and beta isoforms in the postnatal development of mouse retina. *J Neurosci* 1999; **19**: 9878–9889.
18. Jimenez T, McDermott JP, Sánchez G, Blanco G. Na,K-ATPase alpha4 isoform is essential for sperm fertility. *Proc Natl Acad Sci USA* 2011; **108**: 644–649.
19. Renard D, Rubli E, Voide N, Borruat FX, Rothuizen LE. Spectrum of digoxin-induced ocular toxicity: a case report and literature review. *BMC Res Notes* 2015; **8**: 368.
20. Hinshaw SJ, Ogbeifun O, Wandu WS, Lyu C, Shi G, Li Y *et al.* Digoxin inhibits induction of experimental autoimmune uveitis in mice, but causes severe retinal degeneration. *Invest Ophthalmol Vis Sci* 2016; **57**: 1441–1447.
21. Jehle T, Wingert K, Dimitriu C, Meschede W, Lasseck J, Bach M *et al.* Quantification of ischemic damage in the rat retina: a comparative study using evoked potentials, electroretinography, and histology. *Invest Ophthalmol Vis Sci* 2008; **49**: 1056–1064.
22. Pournaras CJ, Rungger-Brändle E, Riva CE, Hardarson SH, Stefansson E. Regulation of retinal blood flow in health and disease. *Prog Retin Eye Res* 2008; **27**: 284–330.
23. Dobre D, Borer JS, Fox K, Swedberg K, Adams KF, Cleland JG *et al.* Heart rate: a prognostic factor and therapeutic target in chronic heart failure. The distinct roles of drugs with heart rate-lowering properties. *Eur J Heart Fail* 2014; **16**: 76–85.
24. Longhurst JC, Ross J. Extracardiac and coronary vascular effects of digitalis. *J Am Coll Cardiol* 1985; **5**: 99 A–105 A.
25. Li Z, Xie Z. The Na/K-ATPase/Src complex and cardiotonic steroid-activated protein kinase cascades. *Pflugers Arch* 2009; **457**: 635–644.
26. Katz A, Tal DM, Heller D, Habeck M, Ben Zeev E, Rabah B *et al.* Digoxin derivatives with selectivity for the α2β3 isoform of Na,K-ATPase potently reduce intraocular pressure. *Proc Natl Acad Sci USA* 2015; **112**: 13723–13728.
27. Wang Y, Qiu Q, Shen JJ, Li DD, Jiang XJ, Si SY *et al.* Cardiac glycosides induce autophagy in human non-small cell lung cancer cells through regulation of dual signaling pathways. *Int J Biochem Cell Biol* 2012; **44**: 1813–1824.
28. Samardzija M, Wenzel A, Thiersch M, Frigg R, Remé C, Grimm C. Caspase-1 ablation protects photoreceptors in a model of autosomal dominant retinitis pigmentosa. *Invest Ophthalmol Vis Sci* 2006; **47**: 5181–5190.
29. Liu L, Zhao X, Pierre SV, Askari A. Association of PI3K-Akt signaling pathway with digitalis-induced hypertrophy of cardiac myocytes. *Am J Physiol Cell Physiol* 2007; **293**: C1489–C1497.
30. Liu L, Ivanov AV, Gable ME, Jolivel F, Morrill GA, Askari A. Comparative properties of caveolar and noncaveolar preparations of kidney Na+/K+-ATPase. *Biochemistry* 2011; **50**: 8664–8673.
31. Xin X, Rodrigues M, Umapathi M, Kashiwabuchi F, Ma T, Babapoor-Farrokhran S *et al.* Hypoxic retinal Muller cells promote vascular permeability by HIF-1-dependent up-regulation of angiopoietin-like 4. *Proc Natl Acad Sci USA* 2013; **110**: E3425–E3434.
32. Yoshida T, Zhang H, Iwase T, Shen J, Semenza GL, Campochiaro PA. Digoxin inhibits retinal ischemia-induced HIF-1alpha expression and ocular neovascularization. *FASEB J* 2010; **24**: 1759–1767.
33. Samardzija M, von Lintig J, Tanimoto N, Oberhauser V, Thiersch M, Remé CE *et al.* R91W mutation in Rpe65 leads to milder early-onset retinal dystrophy due to the generation of low levels of 11-cis-retinal. *Hum Mol Genet* 2008; **17**: 281–292.
34. Weleber RG, Shults WT. Digoxin retinal toxicity. Clinical and electrophysiological evaluation of a cone dysfunction syndrome. *Arch Ophthalmol* 1981; **99**: 1568–1572.
35. Beheshti Zavareh R, Lau KS, Hurren R, Datti A, Ashline DJ, Gronda M *et al.* Inhibition of the sodium/potassium ATPase impairs N-glycan expression and function. *Cancer Res* 2008; **68**: 6688–6697.
36. Price EM, Lingrel JB. Structure-function relationships in the Na,K-ATPase alpha subunit: site-directed mutagenesis of glutamine-111 to arginine and asparagine-122 to aspartic acid generates a ouabain-resistant enzyme. *Biochemistry* 1988; **27**: 8400–8408.
37. Gibson R, Fletcher EL, Vingrys AJ, Zhu Y, Vessey KA, Kalloniatis M. Functional and neurochemical development in the normal and degenerating mouse retina. *J Comp Neurol* 2013; **521**: 1251–1267.
38. Maturana-Teixeira S, Braga LE, Carpi Santos R, Calaza KC, Giestal-de-Araujo E, Leão-Ferreira LR. The (Na(+)/K (+))-ATPase activity in the developing rat retina: the role of insulin-like growth factor-I (IGF-I). *Cell Mol Neurobiol* 2015; **35**: 243–254.
39. Yu SP. Na(+), K(+)-ATPase: the new face of an old player in pathogenesis and apoptotic/hybrid cell death. *Biochem Pharmacol* 2003; **66**: 1601–1609.

40. Archibald JT, White TD. Rapid reversal of internal Na+ and K+ contents of synaptosomes by ouabain. *Nature* 1974; **252**: 595–596.
41. Blaustein MP, Lederer WJ. Sodium/calcium exchange: its physiological implications. *Physiol Rev* 1999; **79**: 763–854.
42. Kamimura D, Ohtani T, Sakata Y, Mano T, Takeda Y, Tamaki S *et al.* Ca2+ entry mode of Na +/Ca2+ exchanger as a new therapeutic target for heart failure with preserved ejection fraction. *Eur Heart J* 2012; **33**: 1408–1416.
43. Bortner CD, Cidlowski JA. Uncoupling cell shrinkage from apoptosis reveals that Na+ influx is required for volume loss during programmed cell death. *J Biol Chem* 2003; **278**: 39176–39184.
44. Pinton P, Giorgi C, Siviero R, Zecchini E, Rizzuto R. Calcium and apoptosis: ER-mitochondria Ca2+ transfer in the control of apoptosis. *Oncogene* 2008; **27**: 6407–6418.
45. Storr SJ, Carragher NO, Frame MC, Parr T, Martin SG. The calpain system and cancer. *Nat Rev Cancer* 2011; **11**: 364–374.
46. Imai S, Shimazawa M, Nakanishi T, Tsuruma K, Hara H. Calpain inhibitor protects cells against light-induced retinal degeneration. *J Pharmacol Exp Ther* 2010; **335**: 645–652.
47. Sharma AK, Rohrer B. Sustained elevation of intracellular cGMP causes oxidative stress triggering calpain-mediated apoptosis in photoreceptor degeneration. *Curr Eye Res* 2007; **32**: 259–269.
48. Yu SP. Regulation and critical role of potassium homeostasis in apoptosis. *Prog Neurobiol* 2003; **70**: 363–386.
49. Luan Z, Reddig K, Li HS. Loss of Na(+)/K(+)-ATPase in Drosophila photoreceptors leads to blindness and age-dependent neurodegeneration. *Exp Neurol* 2014; **261**: 791–801.
50. Aperia A, Akkuratov EE, Fontana JM, Brismar H. Na+-K+-ATPase, a new class of plasma membrane receptors. *Am J Physiol Cell Physiol* 2016; **310**: C491–C495.
51. Bagrov AY, Shapiro JI, Fedorova OV. Endogenous cardiotonic steroids: physiology, pharmacology, and novel therapeutic targets. *Pharmacol Rev* 2009; **61**: 9–38.
52. Brar KS, Gao Y, El-Mallakh RS. Are endogenous cardenolides controlled by atrial natriuretic peptide. *Med Hypotheses* 2016; **92**: 21–25.
53. Mohammadi K, Kometiani P, Xie Z, Askari A. Role of protein kinase C in the signal pathways that link Na+/K+-ATPase to ERK1/2. *J Biol Chem* 2001; **276**: 42050–42056.
54. Haas M, Askari A, Xie Z. Involvement of Src and epidermal growth factor receptor in the signal-transducing function of Na+/K+-ATPase. *J Biol Chem* 2000; **275**: 27832–27837.
55. Sibarov DA, Bolshakov AE, Abushik PA, Krivoi II, Antonov SM. Na+,K+-ATPase functionally interacts with the plasma membrane Na+,Ca2+ exchanger to prevent Ca2+ overload and neuronal apoptosis in excitotoxic stress. *J Pharmacol Exp Ther* 2012; **343**: 596–607.
56. Chan BS, Buckley NA. Digoxin-specific antibody fragments in the treatment of digoxin toxicity. *Clin Toxicol (Phila)* 2014; **52**: 824–836.
57. Remé CE, Grimm C, Hafezi F, Marti A, Wenzel A. Apoptotic cell death in retinal degenerations. *Prog Retin Eye Res* 1998; **17**: 443–464.
58. Samardzija M, Wenzel A, Aufenberg S, Thiersch M, Remé C, Grimm C. Differential role of Jak-STAT signaling in retinal degenerations. *FASEB J* 2006; **20**: 2411–2413.
59. Joly S, Lange C, Thiersch M, Samardzija M, Grimm C. Leukemia inhibitory factor extends the lifespan of injured photoreceptors in vivo. *J Neurosci* 2008; **28**: 13765–13774.
60. Okano K, Maeda A, Chen Y, Chauhan V, Tang J, Palczewska G *et al.* Retinal cone and rod photoreceptor cells exhibit differential susceptibility to light-induced damage. *J Neurochem* 2012; **121**: 146–156.
61. Grimm C, Wenzel A, Hafezi F, Yu S, Redmond TM, Remé CE. Protection of Rpe65-deficient mice identifies rhodopsin as a mediator of light-induced retinal degeneration. *Nat Genet* 2000; **25**: 63–66.
62. Wenzel A, Grimm C, Samardzija M, Remé CE. The genetic modifier Rpe65Leu(450): effect on light damage susceptibility in c-Fos-deficient mice. *Invest Ophthalmol Vis Sci* 2003; **44**: 2798–2802.
63. Maeda T, Golczak M, Maeda A. Retinal photodamage mediated by all-trans-retinal. *Photochem Photobiol* 2012; **88**: 1309–1319.
64. Organisciak DT, Vaughan DK. Retinal light damage: mechanisms and protection. *Prog Retin Eye Res* 2010; **29**: 113–134.
65. Mears AJ, Kondo M, Swain PK, Takada Y, Bush RA, Saunders TL *et al.* Nrl is required for rod photoreceptor development. *Nat Genet* 2001; **29**: 447–452.
66. Redmond TM, Yu S, Lee E, Bok D, Hamasaki D, Chen N *et al.* Rpe65 is necessary for production of 11-cis-vitamin A in the retinal visual cycle. *Nat Genet* 1998; **20**: 344–351.
67. Heynen SR, Tanimoto N, Joly S, Seeliger MW, Samardzija M, Grimm C. Retinal degeneration modulates intracellular localization of CDC42 in photoreceptors. *Mol Vis* 2011; **17**: 2934–2946.
68. Joly S, Samardzija M, Wenzel A, Thiersch M, Grimm C. Nonessential role of beta3 and beta5 integrin subunits for efficient clearance of cellular debris after light-induced photoreceptor degeneration. *Invest Ophthalmol Vis Sci* 2009; **50**: 1423–1432.
69. Kast B, Schori C, Grimm C. Hypoxic preconditioning protects photoreceptors against light damage independently of hypoxia inducible transcription factors in rods. *Exp Eye Res* 2016; **146**: 60–71.
70. Geiger P, Barben M, Grimm C, Samardzija M. Blue light-induced retinal lesions, intraretinal vascular leakage and edema formation in the all-cone mouse retina. *Cell Death Dis* 2015; **6**: e1985.

5.2.3 A novel method combining vitreous aspiration and intravitreal AAV2/8 injection results in retina-wide transduction in mice

Romain Da Costa[1], Carsten Röger[1], Jasmin Segelken[2], **Maya Barben[3,4]**, Christian Grimm[3-5], John Neidhardt[1,6]

[1]Institute of Human Genetics, Faculty of Medicine and Health Sciences, University of Oldenburg, Oldenburg, Germany

[2]Visual Neuroscience, Faculty of Medicine and Health Sciences, University of Oldenburg, Oldenburg, Germany

[3]Lab for Retinal Cell Biology, Dept. Ophthalmology, University Hospital Zurich, University of Zurich, Switzerland

[4]Neuroscience Center Zurich (ZNZ), University of Zurich, Switzerland

[5]Zurich Center for Integrative Human Physiology (ZIHP), University of Zurich, Zurich, Switzerland

[6]Research Center Neurosensory Science, University Oldenburg, Oldenburg, Germany

Status of the manuscript:

Published in *Invest Ophthalmol Vis Sci.*, 2016 Oct 1;57(13):5326-5334. doi: 10.1167/iovs.16-19701.

Personal Contribution

Intravitreal injections, OCT/Micron IV analysis, morphology, manuscript proofreading.

Genetics

A Novel Method Combining Vitreous Aspiration and Intravitreal AAV2/8 Injection Results in Retina-Wide Transduction in Adult Mice

Romain Da Costa,[1] Carsten Röger,[1] Jasmin Segelken,[2] Maya Barben,[3,4] Christian Grimm,[3–5] and John Neidhardt[1,6]

[1]Institute of Human Genetics, Faculty of Medicine and Health Sciences, University of Oldenburg, Oldenburg, Germany
[2]Visual Neuroscience, Faculty of Medicine and Health Sciences, University of Oldenburg, Oldenburg, Germany
[3]Laboratory for Retinal Cell Biology, Department of Ophthalmology, University Hospital Zurich, Zurich, Switzerland
[4]Neuroscience Center Zurich (ZNZ), University of Zurich, Zurich, Switzerland
[5]Zurich Center for Integrative Human Physiology (ZIHP), University of Zurich, Zurich, Switzerland
[6]Research Center Neurosensory Science, University Oldenburg, Oldenburg, Germany

Correspondence: John Neidhardt, University of Oldenburg, Faculty of Medicine and Health Sciences, Institute of Human Genetics, Ammerländer Heerstrasse 114-118, 26129 Oldenburg, Germany; john.neidhardt@uni-oldenburg.de.

Submitted: April 6, 2016
Accepted: August 11, 2016

Citation: Da Costa R, Röger C, Segelken J, Barben M, Grimm C, Neidhardt J. A novel method combining vitreous aspiration and intravitreal AAV2/8 injection results in retina-wide transduction in adult mice. *Invest Ophthalmol Vis Sci.* 2016;57:5326–5334. DOI:10.1167/iovs.16-19701

Purpose. Gene therapies to treat eye disorders have been extensively studied in the past 20 years. Frequently, adeno-associated viruses were applied to the subretinal or intravitreal space of the eye to transduce retinal cells with nucleotide sequences of therapeutic potential. In this study we describe a novel intravitreal injection procedure that leads to a reproducible adeno-associated virus (AAV)2/8-mediated transduction of more than 70% of the retina.

Methods. Prior to a single intravitreal injection of a enhanced green fluorescent protien (GFP)-expressing viral suspension, we performed an aspiration of vitreous tissue from wild-type C57Bl/6J mice. One and one-half microliters of AAV2/8 suspension was injected. Funduscopy, optical coherence tomography (OCT), laser scanning microscopy of retinal flat mounts, cryosections of eye cups, and ERG recordings verified the efficacy and safety of the method.

Results. The combination of vitreous aspiration and intravitreal injection resulted in an almost complete transduction of the retina in approximately 60% of the eyes and showed transduced cells in all retinal layers. Photoreceptors and RPE cells were predominantly transduced. Eyes presented with well-preserved retinal morphology. Electroretinographic recordings suggested that the new combination of techniques did not cause significant alterations of the retinal physiology.

Conclusions. We show a novel application technique of AAV2/8 to the vitreous of mice that leads to widespread transduction of the retina. The results of this study have implications for virus-based gene therapies and basic science; for example, they might provide an approach to apply gene replacement strategies or clustered regularly interspaced short palindromic repeats (CRISPR)/Cas9 in vivo. It may further help to develop similar techniques for larger animal models or humans.

Keywords: AAV2/8, intravitreal injection, retinal degeneration, retinal dystrophy, viral vector

Mutations in more than 200 genes are known to cause retinopathies and vitreoretinopathies.[1] Despite this enormous genetic heterogeneity, ocular gene therapy has become a reality and is intensively studied in eye research.[2–4] Adeno-associated viruses (AAVs) are applied to reprogram terminally differentiated retinal cells and to ameliorate genetic conditions.[5,6] Among the AAV capsid serotypes that have been tested to transduce the different cell types of the retina, serotypes 2, 5, and 8 were found to have a broad applicability and high transduction efficiency.[7–17] In humans, AAV serotype 2 was successfully employed to treat the blinding condition of Leber's congenital amaurosis using gene augmentation therapy.[18–21] To replace the function of the mutated gene in vivo, the coding region of the *RPE65* gene was transferred to retinal pigment epithelial (RPE) cells.[22] Similar approaches have recently been successfully applied to the condition of choroideremia.[23]

Subretinal injection is a Food and Drug Administration–approved technique to mediate retinal transduction using AAV vectors and has been successfully applied to several animal models of retinal diseases. An alternative method to apply AAVs is injection into the vitreous. Intravitreal injections of naturally occurring AAVs frequently showed lower transduction efficacies compared to subretinal injections.[24–27] Nevertheless, AAV2/2 was reported to result in a widespread transduction of the retina following intravitreal injections in mice, but predominately transduced Müller and retinal ganglion cells.[28–32] Adenovirus-associated virus 2/8 was less efficient when injected into the vitreous.[29,33,34] Capsid mutants improved the transduction efficacies and/or changed the tropism of different AAV serotypes.[35–39]

Intravitreal injections would offer several advantages to the treatment of retinopathies or vitreoretinopathies. As the injected AAVs distribute via diffusion in the vitreous gel,

intravitreal injections show the potential to result in a complete and homogenous transduction of the retina. Thus, the treatment of retinal disorders would benefit from improved intravitreal injection techniques. An increase in the retinal area transduced by the AAV could result in enhanced preservation of the visual function upon treatment.

In this report, we demonstrate that aspiration of vitreous tissue prior to injecting AAV2/8 suspensions increases the probability of obtaining a widespread transduction of the retina in mice. After a single intravitreal injection, enhanced green fluorescent protein (GFP) expression was detected in all retinal layers. The method presented here provides an alternative technique to apply gene therapeutic approaches to disease models using intravitreal injection and might guide the development of improved treatment regimens for different animal models and patients suffering from inherited retinopathies or vitreoretinopathies.

Materials and Methods

Generation of Recombinant AAV Vectors

A single-stranded AAV vector (ssAAV2/8_CMV_GFP) and a self-complementary AAV vector (scAAV2/8_mCMV_GFP) were tested in this study. Both recombinant AAVs featured the GFP coding sequence encompassed within the inverted terminal repeats (ITRs) of the AAV serotype 2 and were pseudotyped with the capsid of the AAV serotype 8. The expression of GFP was controlled by either the complete cytomegalovirus (CMV) promoter in ssAAV2/8_CMV_GFP or a minimal version of this promoter lacking its upregulatory domain in scAAV2/8_mCMV_GFP. To remove the upregulatory domain in the CMV promoter, all nucleotides more than 104 base pairs upstream from the TATA box were deleted. In addition to the GFP expression cassette, the ssAAV2/8-CMV-GFP contained the β-globin intron 1 enhancing sequence and woodchuck hepatitis virus posttranscriptional regulatory element. The production and purification procedures of AAVs were extensively described by Grieger and colleagues.[40] Briefly, both AAVs were produced by polyethylenimine transfection of HEK293T cells with the helper plasmid pHGTI_Adeno1, the plasmid pLT-RC08 encoding for Rep proteins of serotype 2 and Cap proteins of serotype 8, and the AAV genome plasmid containing GFP in either a single-stranded or self-complementary manner. Viruses were extracted from the cell nuclei 48 hours post transfection through freezing–thawing cycles and dounce homogenization of the transfected cells. Cell debris was cleared by centrifugation, DNA contaminants were degraded with Benzonase (E8263; Sigma-Aldrich, Steinheim, Germany), and supernatants were further purified by ultracentrifugation on iodixanol gradient. Finally, the iodixanol buffer was exchanged with PBS and the virus suspensions were further concentrated by ultrafiltration on filter units Amicon Ultra-15 with a cutoff at 100 kDa (UFC910008; Merck Millipore, Billerica, MA, USA). Vector genomes were determined by quantitative PCR. Briefly, viral DNA was extracted from viral suspensions using the Chemagic Magnetic Separation Module I (PerkinElmer, Baesweiler, Germany) according to the manufacturer's instruction. DNA samples were diluted to 0.02 ng/μL. Quantitative PCRs using a standard curve were performed on the diluted virus-encoding plasmids. The primers and probe were designed to anneal to the GFP gene (each 5′–3′; forward primer: tgccactcaaccgaccaat, reverse primer: gggattcccacgggtgtt, FAM/TAMRA-labeled probe: aagctggtccttac tctagactcgctagggtcacgtctct). The measurements were performed in quadruplicate on ABI Prism 7900HT and the results analyzed using SDS software version 2.2.2 (Applied Biosystems, Life Technologies, Zug, Switzerland). Virus preparation of scAAV2/8 resulted in approximately 200 μL viral suspension at 2.5×10^{11} genome copies/mL (gc/mL). The viral suspension of ssAAV2/8 contained 2.5×10^{12} gc/mL.

Animals

All experimental procedures were approved by the Veterinary Authorities of Zurich and Oldenburg and were conducted in accordance with the ARVO Statement for the Use of Animals in Ophthalmic and Vision Research. All mice used in this study were on a C57/Bl6J background and were wild-type littermates. Adult mice 2 to 4 months of age were used to investigate the potential of vitreous aspiration in improving AAV transduction of the retina. Transduction efficacy was evaluated 3 to 4 months post injections. Supplementary Figure S1 provides an overview of procedures used in this study.

Vitreous Aspiration and Intravitreal Injection

Mice were first anesthetized by intraperitoneal injection of midozolam (5 mg/kg), medetomidin (0.5 mg/kg), and fentanyl (0.05 mg/kg). Pupil dilation was achieved with topical application of tropicamide 1% for 1 minute followed by application of phenylephrine 2.5% for 1 minute. Animals were kept on a heating pad at 37°C and eyes were moisturized with Lacrinorm gel (Bausch & Lomb, Zug, Switzerland). Syringes were mounted on a M3301R micromanipulator (WPI, Hertfordshire, England). To place the eye in a proper orientation and have access to the desired injection site, the eyelid was pulled toward the forehead using a surgical suture while a second one was used to attach the sclera slightly above the superior limbus and pull the eye downward in order to expose the central region of the superior sclera (Supplementary Fig. S2B). Spring scissors with a cutting edge of 2.5 mm were used to cut and remove most of the scleral tissue from the injection site (Supplementary Fig. S2C). A hole was made 2 mm posterior to the superior limbus using a sterile 30-gauge (G) needle. The needle was inserted 1.5 mm into the vitreous (Supplementary Fig. S2D). Using a surgical microscope, the position of the needles within the eye was visualized (Supplementary Fig. S2A). The needle opening was oriented toward the temporal retina facing neither the optic nerve nor the lens. Part of the vitreous was aspirated by pulling the plunger of the syringe up to a maximum of 50 μL on the graduation scale prior to removing the needle from the eye, a procedure that in the following is denoted vitreous aspiration (Supplementary Fig. S2E). Whether this procedure leads to a removal of a small portion of the vitreous or results only in a vitreous tap is a matter for further investigations. Hemorrhages on the retina were rarely observed. We excluded animals with clear retinal hemorrhages from the study, but included those that showed mild bleeding around the injection site at the sclera. Through the previously made hole, a 33-G blunt-end needle (Hamilton, Bonaduz, Switzerland) mounted onto a 5-μL glass syringe (Hamilton) was inserted 1.5 mm into the eye (Supplementary Fig. S2F). Adeno-associated virus suspension or PBS (1.5 μL) was intravitreally injected into the eye. After vitreous aspiration, 12 eyes were injected using each of the two viruses (ssAAV2/8_CMV_GFP and scAAV2/8_mCMV_GFP). In addition, 66 eyes were injected using ssAAV2/8_CMV_GFP applying two previously published techniques to inject into the vitreous but without prior vitreous aspiration. Injections were performed at 0.1 μL/s, and after the injection, the needle was left in the eye for 2 minutes in order to prevent reflux of the viral suspension. The needle and surgical sutures were gently removed from the eye and the animal was kept warm for 20 minutes prior to administration of antagonists of the

Investigative Ophthalmology & Visual Science

anesthetics (a mixture of atipamezole [0.75 mg/kg], flumazenil [0.2 mg/kg], and naloxone [0.12 mg/kg]). Detailed information about the equipment used during the procedure is provided in Supplementary Table S1.

Fundus Imaging and Optical Coherence Tomography (OCT)

Fundus photographs were taken 3 to 4 months post injections with a Micron III (Phoenix Research Labs, Pleasanton, CA, USA) system equipped with an excitation filter at 482 nm and an emission filter at 536 nm. In addition, OCT scans and corresponding retinal fundus images were taken using the Phoenix Image-Guided OCT (Phoenix Research Labs) and Micron IV, respectively. Images were captured post injection at indicated time points using Micron OCT and StreamPix 5 commercial software (Phoenix Research Labs). Animals were anesthetized with an intraperitoneal injection of ketamine (85 mg/kg) and xylazine (5 mg/kg) 20 minutes prior to fundus imaging. The distribution of the GFP signals of the central retina was measured utilizing ImageJ (http://rsb.info.nih.gov/ij/index.html; in the public domain). Briefly, photographs centered on the optic disc were used; the photographs were converted into grayscale 8-bit images, and an intensity threshold was applied to select GFP-positive areas from background signals. The number of GFP-positive pixels was counted and the percentage of positive pixels in the image was calculated. Statistical analyses were performed using Prism 7 (GraphPad Software, La Jolla, CA, USA).

Immunostaining and Morphology

After fundus imaging, animals were killed and both eyes enucleated. Eyes were fixed overnight at 4°C in a 4% paraformaldehyde in PBS solution. Retinal pigment epithelium and other retinal cell layers were prepared from the fixed eyes. The RPE cell layer was washed three times in PBS and mounted on objective trays with Fluoromount (Sigma-Aldrich). Retinae were fixed with 4% paraformaldehyde for 2 additional hours at room temperature prior to permeabilization by three consecutive incubations (10 minutes each) in a 0.5% Triton X-100 PBS solution. Unspecific antibody binding was blocked by incubation of the retinae in a 0.05% Tween 20 and 0.5% bovine serum albumin PBS solution. Samples were then incubated with primary antibodies for either 2 hours at room temperature or 16 hours at 4°C. Retinal ganglion cells (RGCs) were immunostained using a 1:100 dilution of a goat polyclonal antibody against the ganglion cell–specific transcription factor Brn3a (Sc-31984; Santa Cruz Biotechnology, Dallas, TX, USA). Blue cone outer segments were immunostained using a 1:500 dilution of a goat polyclonal antibody against S-opsin (Sc-14363, Santa Cruz Biotechnology). Alexa 568- and Alexa 647-conjugated secondary antibodies (Life Technologies) were applied for 2 hours at room temperature. Secondary antibodies were used at a working dilution of 1:200. Samples were mounted on objective trays with Fluoromount (Sigma-Aldrich). Confocal images were taken using a TCS SP8 microscope (Leica, Wetzlar, Germany). Images were processed using either the LAS AF Lite software (Leica) or Imaris v7.6.5 (Bitplane, Zurich, Switzerland).

To evaluate the retinal morphology, we performed Nissl staining. Cryosections (20 μm) were washed three times in 0.1 M phosphate buffer (PB) for 10 minutes followed by 20-minute incubation in Nissl staining solution. Cryosections were washed in water for 3 minutes. Slides were incubated in 70% acetic ethanol for 30 seconds, followed by 95% acetic ethanol for 30 seconds and isopropanol for 3 minutes. Slides were cleared in xylol for 3 minutes. Stained cryosections were embedded in Eukitt (Sigma-Aldrich).

For further morphologic analysis, eyes were enucleated and fixed in 2.5% glutaraldehyde in cacodylate buffer (pH 7.2, 0.1 M) according to the previously described procedure.[41] Nasal and temporal halves were separated by cutting through the optic nerve head and embedded in epon plastic. Semithin cross sections (0.5 μm) were counterstained with toluidine blue and analyzed by light microscopy (Axioplan; Zeiss, Jena, Germany).

Tissue Fixation and Cryosectioning

For eye cup preparations, mice were killed by cervical dislocation and eyes were enucleated and put into physiological PBS (pH 7.4) solution. Eyes were fixed in 2% paraformaldehyde (Carl Roth, Karlsruhe, Germany) for 2 to 5 minutes. Cornea, lens, and vitreous were removed and eye cups were fixed for 60 minutes in 2% paraformaldehyde in 0.1 M PB. After several washing steps in PB, eye cups were cryoprotected in PB containing 30% sucrose either overnight or for 2 hours at 4°C and embedded in cryoblock Surgipath FSC 22 Clear Compound (Leica). The central part of the eye cup was cut into 20-μm thin slices (vertical sections) on a Leica CM1860 cryotome and stored at −20°C. GFP and Enhanced green fluorescent protein and 4′,6-diamidino-2-phenylindole (DAPI) fluorescence were visualized by fluorescence microscopy (Leica DM6B) or confocal microscopy (TCS-SL Confocal Microscope, Leica).

In Vivo Electroretinography

Electroretinograms (ERGs) were recorded from anesthetized noninjected ($n = 6$) and PBS-injected ($n = 5$) wild-type mice 4 and 15 weeks after injection. Animals were dark adapted for at least 12 hours, followed by procedures performed under dim red light (>620 nm), as previously described.[42] Electroretinograms represent the recordings of averaged responses to a sequence of white full-field flashes (5 ms, band pass filtered 1–1000 Hz), ranging from 0.4 Hz (20 flashes) for low intensities to 0.066 Hz (5 flashes) for the brightest intensities (Ganzfeld ERG; Roland Consult, Brandenburg a.d. Havel, Germany). Scotopic ERGs comprised 10 light intensities, ranging from −3.5 to 1 log cds/m^2. Photopic ERGs were recorded in the presence of bright background light (25 cds/m^2) comprising five light intensities, ranging from −1 to 1 log cds/m^2. Data analysis was performed using Chart v5.5 (AD Instruments, Hastings, UK). Data were evaluated for statistical differences using 2-way analysis of variance (ANOVA) in Prism 5 (GraphPad Software, La Jolla, CA, USA).

Results

Fundus Images

The transduction efficacy of AAV2/8-GFP was evaluated from 90 intravitreal injections. Twenty-four eyes were injected with prior aspiration of the vitreous, whereas 66 eyes were injected without prior vitreous aspiration. Fundus images of the central retina were taken from all eyes. The retinal area that showed GFP expression was calculated for each image. Representative fundus photographs under bright-light illumination or applying a GFP filter are presented in Figure 1. Phosphate-buffered saline injections after vitreous aspiration served as controls, and these eyes were compared to eyes injected with GFP-expressing ssAAV2/8-GFP or scAAV2/8-GFP.

Without vitreous aspiration prior to the intravitreal injection, eyes presented with only two or three smaller GFP-positive areas, including cells around the injection site and cells in close vicinity to the retinal vasculature at the optic nerve. Occasionally, this injection technique resulted in an

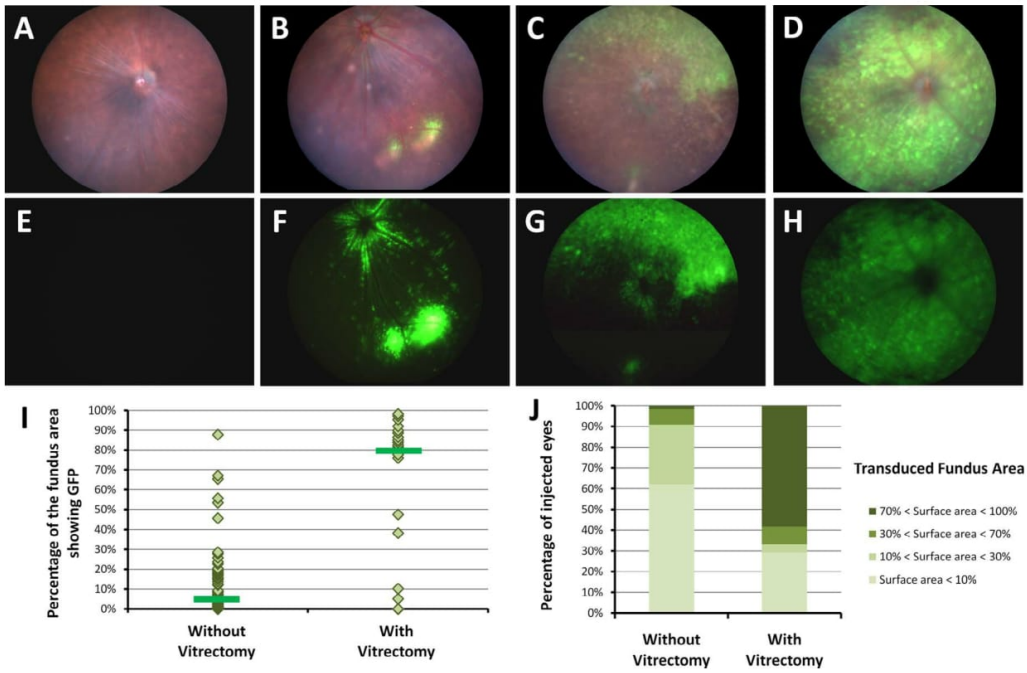

Figure 1. Fundoscopy and measurement of transduced retinal area. Fundus images of an eye that received a vitreous aspiration and intravitreal PBS injection are presented in (**A**, **E**). Representative fundus pictures of an eye intravitreally injected with ssAAV2/8_CMV_GFP without prior vitreous aspiration are shown in (**B**, **F**), with prior pressure applied around the injection site (per Chiu et al.[43]) in (**C**, **G**), and with prior vitreous aspiration in (**D**, **H**). (**A**–**D**, *upper*) show images taken under bright-light illumination. Images in (**E**, **H**) show the GFP signal only. Graph in (**I**) compares the distribution of GFP signals in eyes injected without or with prior vitreous aspiration (vitrectomy). *Horizontal bars* indicate the distributions' medians. Graph in (**J**) shows the probability of obtaining a GFP coverage above 70%, between 30% and 70%, between 10% and 30%, and below 10%.

additional GFP-positive area at the estimated site of delivery of the viral suspension (Supplementary Figs. S3C, S3D).

We attempted to improve the transduction efficacy of the standard intravitreal injections and applied a procedure to mice that was originally described by Chiu et al.[43] for rats. We inserted a 30-G needle into the vitreous and removed the needle without aspirating vitreous material from the eye. Subsequently, a gentle pressure was applied to the eye and close to the injection site prior to injecting the viral suspension.[43] As presented in Figure 1, the mechanical stress during insertion of the 30-G needle and/or the pressure applied to the eye enlarged the area covered by GFP, especially around the injection site.

These results encouraged us to develop a novel technique that robustly improves the transduction efficacies of intravitreal injections of AAV2/8. We used a 30-G needle to perform an aspiration of the vitreous prior to intravitreal injections of AAV particles. The plunger of the attached syringe was pulled to the 50-µL mark to aspirate vitreous tissue shortly before removal of the needle. In the following, this procedure is referred to as "vitreous aspiration" in mice. To verify the integrity of the retina after vitreous aspiration, we used a high-resolution operation binocular, fundoscopy with the Micron III/IV, and OCT measurements. After 2 to 4 month post injection, we did not find indications that this procedure leads to retinal alterations or detachment. Nissl stainings of cryosections suggested a well-preserved retinal morphology (Supplementary Fig. S4). Although many retinas presented without clear retinal alterations at days 1 and 3 post injection, retinas might also show detached parts that reattached after 3 to 7 days (for a representative example see Supplementary Fig. S5). Morphologic evaluation of these eyes showed well-preserved retinal structures after 14 days (Supplementary Figs. S5A, S5B). Occasionally, mice presented with detachments of large retinal areas that seemed to result in retinal remodeling as shown in Supplementary Figures S5C and S5D. Consequently, we suggest evaluating the outcome of the vitreous aspiration and intravitreal injection by funduscopy and/or OCT at day 3 post injection and considering exclusion of animals with strong retinal detachments. A more frequent side effect of the novel injection procedure was the occurrence of cataracts in approximately one-fourth of the eyes (a representative example is shown in Supplementary Fig. S4).

The GFP-positive retinal areas in eyes that received the vitreous aspiration in combination with intravitreal injection were subjectively larger compared to those with the other techniques tested (Figs. 1A–H). We quantified this observation and compared transduced retinal areas between eyes that received a vitreous aspiration and eyes intravitreally injected without prior aspiration of the vitreous (Fig. 1I). A Mann-Whitney test ($P = 0.0009$, confidence level of 99%) confirmed that the mean of the retinal area expressing GFP after transductions using the novel injection technique ($M = 55.54\%$) was significantly higher than in eyes without the vitreous aspiration ($M = 11.7\%$). Without aspiration of the vitreous, 50% of the eyes had less than 5% of the central retinal area transduced. Only 1 eye out of 66 presented with a transduction over 70%. In contrast, the majority of the eyes with vitreous aspiration (14 out of 24) showed GFP expression in more than 70% of the retinal area (Fig. 1J). The probability of obtaining a transduction over 70% of the retina is significantly increased by the novel injection technique as demonstrated by

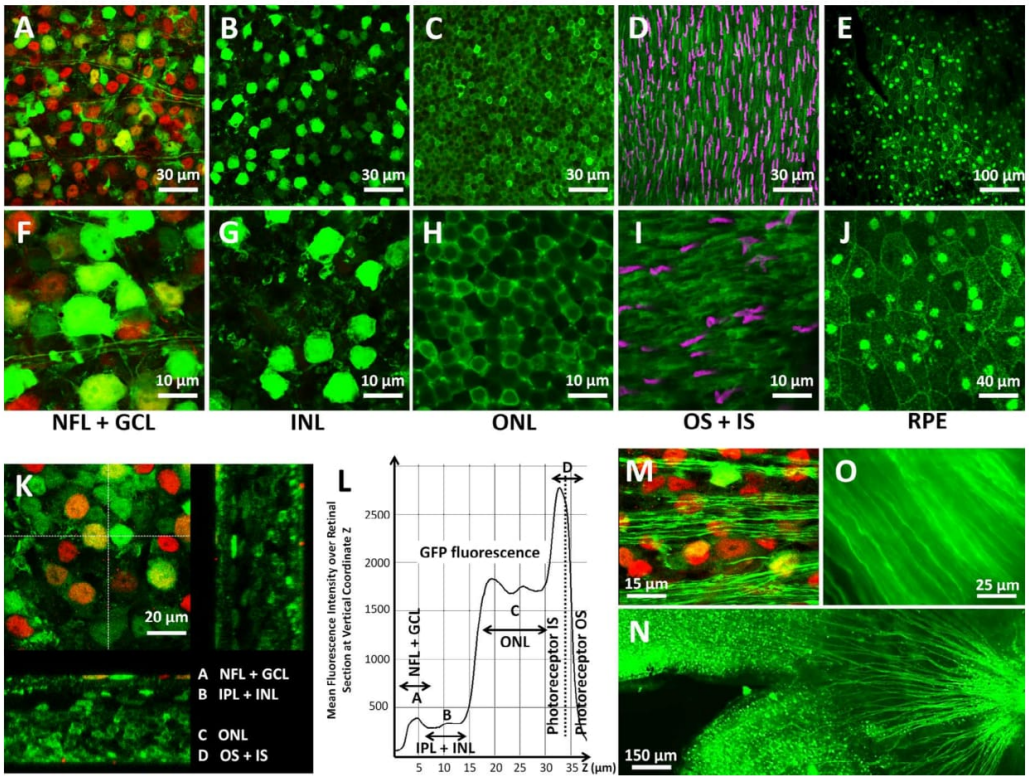

Figure 2. GFP expression within retinal layers of eyes after vitreous aspiration and intravitreal injection. Pictures were taken from a representative retina. The corresponding eye was injected with 1.5 µL ssAAV2/8_CMV_GFP at 2.5×10^{12} gc/mL. Confocal images of the GFP expression were obtained from the retinal ganglion cell and nerve fiber layer (GCL+NF [**A**, **F**]), in the inner nuclear layer (INL [**B**, **G**]), in the outer nuclear layer (ONL [**C**, **H**]), at the photoreceptor outer and inner segments (OS+IS [**D**, **I**]), and in the retinal pigment epithelium (RPE [**E**, **J**]). A scan through the entire retinal thickness showing all retinal layers transduced within the same area is presented in (**K**). A representative fluorescence profile along the retinal thickness is presented in (**L**). GFP-positive axons leaving Brn3a-positive cells were detected (**M**). Projection of the ganglion cell axons could be documented on a retinal flat mount that was poorly transduced in the central retina (**N**). The optic nerve of GFP-positive retinae showed prominent GFP-positive fibers (**O**). *Green*: GFP; *red*: Brn3a; *magenta*: S-opsin. Of note, the fundus of the presented eye is shown in Supplementary Figure S6, *upper*.

Fisher's exact test ($P < 0.0001$). Eyes with fluorescent signals exceeding 70% in the central retina were also largely transduced in the inferior, superior, nasal, and temporal retina (Supplementary Figs. 6A–E). Although not directly comparable due to different promoters and viral titers, the ssAAV2/8-GFP and scAAV2/8-GFP did not show obvious differences in the distribution of GFP signals across fundus images (Supplementary Figs. 6F–J).

GFP Expression Throughout the Retinal Layers

We asked the question whether vitreous aspiration prior to AAV2/8 injection leads to transduction of several retinal layers. Indeed, fluorescence scans documented that all retinal layers showed GFP-positive cells (Fig. 2), suggesting that the viral particles were able to penetrate throughout the retina. In the photoreceptor layer, the GFP fluorescence was approximately four times higher than in other retinal layers (Fig. 2L). Immunohistochemistry of retinal flat mounts using the RGC marker Brn3a showed costaining with GFP-positive cells, suggesting that RGCs were successfully transduced (Figs. 2A, 2F). Dendrites and axons leaving the ganglion cell body were found to be transduced (Figs. 2M, 2N) and GFP-positive axons were detected in optic nerve preparations (Fig. 2O), further confirming that the RGCs were infected by the AAV2/8-GFP viruses. Additionally, cells in the inner nuclear layer (INL), as well as the inner plexiform layer (IPL) and outer plexiform layer (OPL), were fluorescently labeled. In areas of retinal GFP expression, RPE cells were also transduced.

Two months after applying the novel injection technique, analysis of cryosections of mouse eyes confirmed that most of the photoreceptor and RPE cells were positively labeled by GFP (Fig. 3). The preparations showed weaker GFP signals in several other cell layers of the retina. As supported by confocal microscopy (Figs. 3D, 3E), the strongest signals were seen in the photoreceptor and RPE layers. These results confirm the findings shown in Figure 2.

ERG Measurements of Eyes Following Vitreous Aspiration

We aimed to evaluate whether the combination of vitreous aspiration and intravitreal injection leads to physiological alteration in the retina. Analyses of electroretinograms of eyes that received a vitreous aspiration were followed by PBS injections and compared to ERGs from untreated wild-type littermates (Supplementary Fig. S7). Electroretinograms were recorded 4 and 15 weeks after vitreous aspiration and injection.

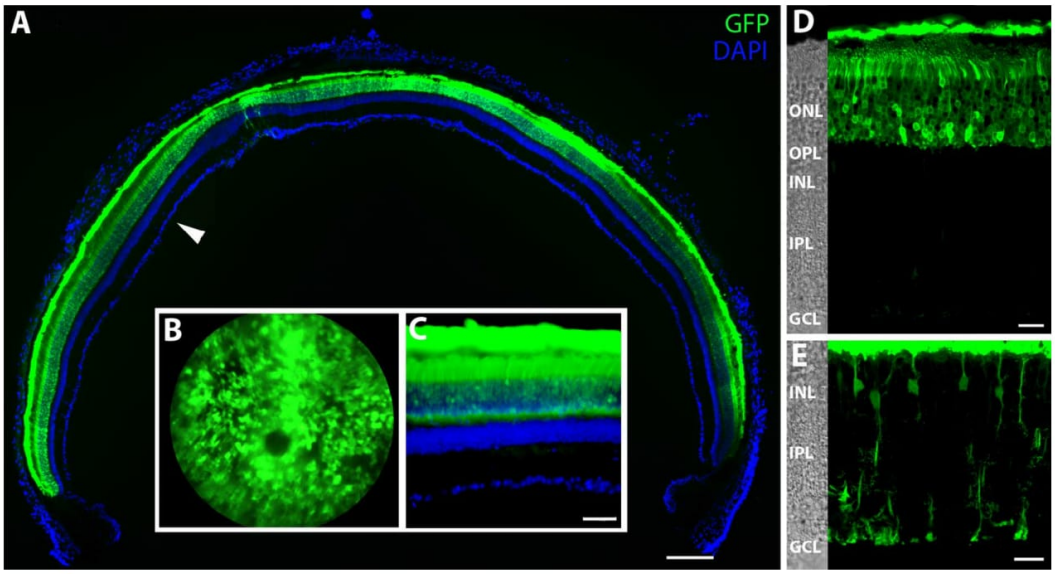

FIGURE 3. AAV8-mediated GFP immunofluorescence in the retina after vitreous aspiration and intravitreal injection into the mouse eye. The cryosection (**A**) and fundus image (**B**) illustrate the retina-wide GFP expression. *Scale bar*: 200 μm. An enlargement of the fluorescence signals of the area marked by an *arrowhead* is shown in (**C**). Confocal images are shown in (**D**, **E**). As expected for AAV2/8, mostly RPE and photoreceptors were transduced, whereas other cell layers show less GFP expression. *Scale bar*: 50 μm. ONL, outer nuclear layer; OPL, outer plexiform layer; INL, inner nuclear layer; IPL, inner plexiform layer; GCL, ganglion cell layer.

The novel injection procedure did not cause striking differences in physiological properties of the retina. Only at 4 weeks after injection, the highest-intensity flash of the scotopic a-wave showed a significant alteration, an observation that was lost after an additional 11 weeks (Supplementary Fig. S3). All other measurements showed no significant alteration at all light intensities and time points. Thus, the ERG measurements support that few or no physiological differences were induced to the retina applying the novel injection procedure described herein.

In conclusion, we developed a novel technique to apply AAVs intravitreally, which increases the probability of transducing the central and peripheral retina to above 70%. Furthermore, the technique allows the transduction of all retinal layers from the ganglion cell layer (GCL) to RPE.

DISCUSSION

Adeno-associated virus–mediated basic science applications and gene therapies to treat retinal/vitreoretinal disorders would benefit from increased transduction efficacies of viral particles across the retina. Herein, we show that intravitreal AAV2/8 administration had the potential to transduce the entire retina when a single injection was combined with vitreous aspiration.

Since previously published intravitreal injection procedures using AAV2/8 less efficiently transduced retinal cells than AAV2/2 and mainly targeted retinal ganglion and Müller glia cells, subretinal administration was more commonly applied for AAV2/8.[29,33,34] Nevertheless, recent studies have drawn attention to disadvantages of subretinal injections. Electroretinogram measurements performed on mice 3 months post injection revealed that the amplitude of both a- and b-waves was significantly decreased compared to that in fellow control eyes. The decrease was persistent after 12 months. In contrast, ERGs of eyes injected in an intravitreal manner were not affected.[34] Structural changes that explain the reduced ERG amplitudes have been characterized in retinal detachment models.[44] Upon detachment of retinal photoreceptors from the RPE, cone and rod outer segments were shortened. Opsins no longer specifically localized to the outer segments but were detected in the inner segments of photoreceptor cells. Most retinal cell types were shown to undergo remodeling after retinal detachment. In addition, connectivity within the retina was also affected. Neurite projections of both ON and OFF bipolar cells no longer located to their target layers.[45] Although our analysis only occasionally indicates such strong retinal alterations after the combination of vitreous aspiration and intravitreal injections, we cannot completely exclude that the new injection technique described herein leads to a peripheral retinal detachment. Future experiments will help to evaluate this possibility. The majority of eyes showed a well-preserved retinal morphology several weeks after the application of the novel technique. Electroretinogram measurements suggested that the new method does not lead to a persistent reduction of functional properties in the retina and thus supported the notion that frequent retinal remodeling due to the vitreous aspiration was unlikely (Supplementary Fig. S7). It will be a matter for future investigations to further optimize the combination of vitreous aspiration and injection to largely avoid side effects.

Intravitreal injection typically would not require retinal detachment and thus is considered to preserve retinal structures. Avoiding shear forces and increased pressure (e.g., due to subretinal injections) might be relevant to retinae affected with dystrophies and structural alterations. Nevertheless, preclinical trials for the treatment of Leber's congenital amaurosis (LCA) successfully improved visual function in animal models treated via subretinal injection.[2] So far, two cell types have been efficiently targeted by AAVs delivered into the vitreal space: RGCs and Müller cells.[25,35,36] Dalkara et al.[46] identified the inner limiting membrane (ILM) as a major barrier to the diffusion of AAV into the outer retina. The ILM is rich in

Investigative Ophthalmology & Visual Science

polysaccharides and proteins, such as laminin, that may bind to the AAV capsids, hence preventing their diffusion toward the outer retina.[47,48] Retinal ganglion cells and Müller cells, which are in contact with the ILM, were more efficiently transduced with intravitreal injections of AAV2/8. Using pronase as adjuvant during intravitreal injection of AAVs improved transduction efficacy of the outer retina by degrading laminins of the ILM. However, the safety of pronase applications to patients is uncertain. These studies encouraged us to try a different procedure that aimed at improving transduction efficacies via a mechanical aspiration of the vitreous during the surgical intervention.

Since the naturally occurring AAV2/8 and other serotypes showed limited capacity in transducing photoreceptors from the vitreal space in mice,[46] several studies have successfully modified the AAV capsid proteins in order to change tropism and/or improve transduction efficacy.[37–39] The AAV capsid variant AAV7m8 showed the capacity to perform panretinal transduction of photoreceptors from the vitreous. Thus, our study complements the development of capsid mutants toward panretinal transduction of all retinal layers with naturally occurring AAV2/8. Future studies will show whether the combination of our technique and efficient capsid mutants will further improve the transduction efficacy of AAVs. We speculate that such combinations of gene therapeutic approaches may help to correct gene defects in preclinical animal models. Furthermore, basic science approaches to modify functions of cells within the retina (e.g., clustered regularly interspaced short palindromic repeats [CRISPR]/Cas9 applications) or alterations of retinal properties (e.g., using growth factors applied to the vitreous) might benefit from the novel technique.

The reason for the increase in transduction efficacies as observed with the new injection technique is not fully understood. We hypothesize that vitreous aspiration removes three obstacles that influence transduction efficacy after intravitreal injection. First, the vitreous applies strong pressure to viral suspensions placed intravitreally and forces the suspensions to exit the eye through the injection site. Vitreous aspiration favors the interaction of viral particles with the retinal tissues and improves the diffusion of the particles toward the outer retina. Second, the ILM, previously shown to bind viral particles, may be destabilized by vitreous aspiration.[46,47] Pores may be created in the ILM, allowing viral particles to diffuse through the retina. Third, it has been shown that the vitreous contains neutralizing antibodies acting against AAV capsids.[49] Therefore, aspiration of the vitreous might prevent or reduce antibody-mediated neutralization of AAV vectors. A schematic drawing illustrating improved diffusion of the viral particles into the retina after vitreous aspiration is shown in Figure 4.

Although vitreous aspiration performed here differs from vitrectomy in clinical settings, a combination of vitrectomy and/or ILM peeling might enhance the therapeutic effect of AAV-based gene therapies in larger animal model or even in patients. Vitrectomy is frequently performed in patients suffering from prominent vitreous floaters, vitreous hemorrhage, and diabetic retinopathy.[50] Inner limiting membrane peeling in combination with vitrectomy has also been established for epiretinal membrane and macular hole surgery.[51–53] Due to anatomic differences, the combination of vitrectomy and ILM peeling as performed in humans is not applicable to the mouse eye. Studies in larger animal models are required in order to test the potential of vitrectomy/vitreous aspiration and/or ILM peeling in improving AAV transduction in patients receiving ocular gene therapy. Interspecies differences need to be considered. Another vitrectomy technique, based on those applied to patients, has already been tested in rats and showed an improved

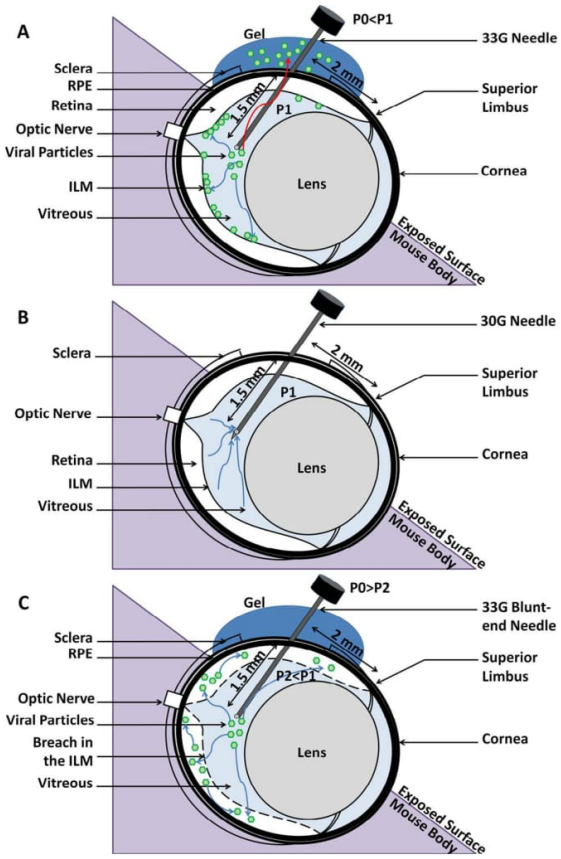

Figure 4. Schematic model of the diffusion of AAV particles in eyes after vitreous aspiration and intravitreal injection. In (**A**), AAV particles either reflux from the vitreous (*red arrow*) due to the intravitreal pressure (P1) or bind to the ILM, therefore preventing the transduction of the outer retina. The vitreous aspiration depicted in (**B**) reduces the intravitreal pressure to P2, which is now lower than the outside pressure P0, preventing the reflux of virus particles and supporting the distribution of the virus within the vitreous. In our model shown in (**C**), vitreous aspiration creates pores in the ILM, allowing free diffusion of AAV particles to the outer retina.

transduction of Müller cells using adenoviral vectors.[24] In contrast, posterior vitrectomy and posterior hyaloid membrane peeling, in combination with transductions using capsid mutant AAV2 particles, recently were applied to a canine model but failed to increase GFP signals in the retina.[54] Boyd et al.[54] observed an inflammatory response possibly against the GFP transgene and a reduced level of GFP-positive cells following vitrectomy. As our vitreous aspiration is different from vitrectomy in larger animal models and humans, it is difficult to compare these studies directly. Our procedure might be best described as a vitreous aspiration or vitreous tap that did not result in the removal of a significant portion of the vitreous.

In conclusion, we describe a novel vitreous aspiration and intravitreal injection technique that leads to widespread AAV transduction of the mouse retina. The technique is suitable for testing on AAV-based ocular gene therapies and basic science questions in mouse models and may help to develop improved intravitreal injection techniques to treat large animal models

and patients suffering from retinopathies or vitreoretinopathies.

Acknowledgments

The authors thank Ulrike Janssen-Bienhold, Wolfgang Berger, and Marijana Samardzija for helpful discussions. We thank Esther Glaus for her participation in cloning the AAV vectors. We thank Yvan Arsenjevic and Josefine Juttner for advice and training in techniques of retinal injections. We thank Cornel Fraefel for the opportunity to use his ultracentrifuge and thank the center for microscopy and image analysis (ZMB) of the University of Zürich for its support.

Supported by the Swiss National Foundation (31003A_141014 to JN; 31003A_149311 to MB and CG), the Velux Foundation (to JN), the University of Oldenburg (to JN), and Deutsche Forschungsgemeinschaft (DFG) (GRK 1885/1 to JS).

Disclosure: **R. Da Costa**, None; **C. Röger**, None; **J. Segelken**, None; **M. Barben**, None; **C. Grimm**, None; **J. Neidhardt**, None

References

1. Berger W, Kloeckener-Gruissem B, Neidhardt J. The molecular basis of human retinal and vitreoretinal diseases. *Prog Retin Eye Res*. 2010;29:335–375.
2. Boye SE, Boye SL, Lewin AS, Hauswirth WW. A comprehensive review of retinal gene therapy. *Mol Ther*. 2013;21:509–519.
3. Colella P, Cotugno G, Auricchio A. Ocular gene therapy: current progress and future prospects. *Trends Mol Med*. 2009; 15:23–31.
4. Sahel JA, Roska B. Gene therapy for blindness. *Annu Rev Neurosci*. 2013;36:467–488.
5. McClements ME, MacLaren RE. Gene therapy for retinal disease. *Transl Res*. 2013;161:241–254.
6. Mingozzi F, High KA. Therapeutic in vivo gene transfer for genetic disease using AAV: progress and challenges. *Nat Rev Genet*. 2011;12:341–355.
7. Allocca M, Mussolino C, Garcia-Hoyos M, et al. Novel adeno-associated virus serotypes efficiently transduce murine photoreceptors. *J Virol*. 2007;81:11372–11380.
8. Lebherz C, Maguire A, Tang W, Bennett J, Wilson JM. Novel AAV serotypes for improved ocular gene transfer. *J Gene Med*. 2008;10:375–382.
9. Tan MH, Smith AJ, Pawlyk B, et al. Gene therapy for retinitis pigmentosa and Leber congenital amaurosis caused by defects in AIPL1: effective rescue of mouse models of partial and complete Aipl1 deficiency using AAV2/2 and AAV2/8 vectors. *Hum Mol Genet*. 2009;18:2099–2114.
10. Zou J, Luo L, Shen Z, et al. Whirlin replacement restores the formation of the USH2 protein complex in whirlin knockout photoreceptors. *Invest Ophthalmol Vis Sci*. 2011;52:2343–2351.
11. Seo S, Mullins RF, Dumitrescu AV, et al. Subretinal gene therapy of mice with Bardet-Biedl syndrome type 1. *Invest Ophthalmol Vis Sci*. 2013;54:6118–6132.
12. Birke MT, Lipo E, Adhi M, Birke K, Kumar-Singh R. AAV-mediated expression of human PRELP inhibits complement activation, choroidal neovascularization and deposition of membrane attack complex in mice. *Gene Ther*. 2014;21:507–513.
13. Koilkonda R, Yu H, Talla V, et al. LHON gene therapy vector prevents visual loss and optic neuropathy induced by G11778A mutant mitochondrial DNA: biodistribution and toxicology profile. *Invest Ophthalmol Vis Sci*. 2014;55: 7739–7753.
14. Choi VW, Bigelow CE, McGee TL, et al. AAV-mediated RLBP1 gene therapy improves the rate of dark adaptation in Rlbp1 knockout mice. *Mol Ther Methods Clin Dev*. 2015;2:15022.
15. Ou J, Vijayasarathy C, Ziccardi L, et al. Synaptic pathology and therapeutic repair in adult retinoschisis mouse by AAV-RS1 transfer. *J Clin Invest*. 2015;125:2891–2903.
16. Palfi A, Chadderton N, O'Reilly M, et al. Efficient gene delivery to photoreceptors using AAV2/rh10 and rescue of the Rho$^{-/-}$ mouse. *Mol Ther Methods Clin Dev*. 2015;2:15016.
17. Xiong W, MacColl Garfinkel AE, Li Y, Benowitz LI, Cepko CL. NRF2 promotes neuronal survival in neurodegeneration and acute nerve damage. *J Clin Invest*. 2015;125:1433–1445.
18. Bainbridge JW, Smith AJ, Barker SS, et al. Effect of gene therapy on visual function in Leber's congenital amaurosis. *N Engl J Med*. 2008;358:2231–2239.
19. Cideciyan AV, Aleman TS, Boye SL, et al. Human gene therapy for RPE65 isomerase deficiency activates the retinoid cycle of vision but with slow rod kinetics. *Proc Natl Acad Sci U S A*. 2008;105:15112–15117.
20. Hauswirth WW, Aleman TS, Kaushal S, et al. Treatment of leber congenital amaurosis due to RPE65 mutations by ocular subretinal injection of adeno-associated virus gene vector: short-term results of a phase I trial. *Hum Gene Ther*. 2008;19: 979–990.
21. Maguire AM, Simonelli F, Pierce EA, et al. Safety and efficacy of gene transfer for Leber's congenital amaurosis. *N Engl J Med*. 2008;358:2240–2248.
22. Cideciyan AV. Leber congenital amaurosis due to RPE65 mutations and its treatment with gene therapy. *Prog Retin Eye Res*. 2010;29:398–427.
23. MacLaren RE, Groppe M, Barnard AR, et al. Retinal gene therapy in patients with choroideremia: initial findings from a phase 1/2 clinical trial. *Lancet*. 2014;383:1129–1137.
24. Sakamoto T, Ueno H, Goto Y, Oshima Y, Ishibashi T, Inomata H. A vitrectomy improves the transfection efficiency of adenoviral vector-mediated gene transfer to Muller cells. *Gene Ther*. 1998;5:1088–1097.
25. Martin KR, Klein RL, Quigley HA. Gene delivery to the eye using adeno-associated viral vectors. *Methods*. 2002;28:267–275.
26. Acland GM, Aguirre GD, Bennett J, et al. Long-term restoration of rod and cone vision by single dose rAAV-mediated gene transfer to the retina in a canine model of childhood blindness. *Mol Ther*. 2005;12:1072–1082.
27. Natkunarajah M, Trittibach P, McIntosh J, et al. Assessment of ocular transduction using single-stranded and self-complementary recombinant adeno-associated virus serotype 2/8. *Gene Ther*. 2008;15:463–467.
28. Pang JJ, Lauramore A, Deng WT, et al. Comparative analysis of in vivo and in vitro AAV vector transduction in the neonatal mouse retina: effects of serotype and site of administration. *Vision Res*. 2008;48:377–385.
29. Hellstrom M, Ruitenberg MJ, Pollett MA, et al. Cellular tropism and transduction properties of seven adeno-associated viral vector serotypes in adult retina after intravitreal injection. *Gene Ther*. 2009;16:521–532.
30. Pechan P, Rubin H, Lukason M, et al. Novel anti-VEGF chimeric molecules delivered by AAV vectors for inhibition of retinal neovascularization. *Gene Ther*. 2009;16:10–16.
31. Prentice HM, Biswal MR, Dorey CK, Blanks JC. Hypoxia-regulated retinal glial cell-specific promoter for potential gene therapy in disease. *Invest Ophthalmol Vis Sci*. 2011;52:8562–8570.
32. Chadderton N, Palfi A, Millington-Ward S, et al. Intravitreal delivery of AAV-NDI1 provides functional benefit in a murine model of Leber hereditary optic neuropathy. *Eur J Hum Genet*. 2013;21:62–68.
33. Park TK, Wu Z, Kjellstrom S, et al. Intravitreal delivery of AAV8 retinoschisin results in cell type-specific gene expression and retinal rescue in the Rs1-KO mouse. *Gene Ther*. 2009;16:916–926.

34. Igarashi T, Miyake K, Asakawa N, Miyake N, Shimada T, Takahashi H. Direct comparison of administration routes for AAV8-mediated ocular gene therapy. *Curr Eye Res*. 2013;38: 569–577.
35. Petrs-Silva H, Dinculescu A, Li Q, et al. High-efficiency transduction of the mouse retina by tyrosine-mutant AAV serotype vectors. *Mol Ther*. 2009;17:463–471.
36. Dalkara D, Kolstad KD, Guerin KI, et al. AAV mediated GDNF secretion from retinal glia slows down retinal degeneration in a rat model of retinitis pigmentosa. *Mol Ther*. 2011;19:1602–1608.
37. Ku CA, Chiodo VA, Boye SL, et al. Gene therapy using self-complementary Y733F capsid mutant AAV2/8 restores vision in a model of early onset Leber congenital amaurosis. *Hum Mol Genet*. 2011;20:4569–4581.
38. Dalkara D, Byrne LC, Klimczak RR, et al. In vivo-directed evolution of a new adeno-associated virus for therapeutic outer retinal gene delivery from the vitreous. *Sci Transl Med*. 2013; 5:189ra176.
39. Kay CN, Ryals RC, Aslanidi GV, et al. Targeting photoreceptors via intravitreal delivery using novel, capsid-mutated AAV vectors. *PLoS One*. 2013;8:e62097.
40. Grieger JC, Choi VW, Samulski RJ. Production and characterization of adeno-associated viral vectors. *Nat Protoc*. 2006;1: 1412–1428.
41. Heynen SR, Tanimoto N, Joly S, Seeliger MW, Samardzija M, Grimm C. Retinal degeneration modulates intracellular localization of CDC42 in photoreceptors. *Mol Vis*. 2011;17:2934–2946.
42. Kranz K, Dorgau B, Pottek M, et al. Expression of Pannexin1 in the outer plexiform layer of the mouse retina and physiological impact of its knockout. *J Comp Neurol*. 2013;521:1119–1135.
43. Chiu K, Chang RC, So KF. Intravitreous injection for establishing ocular diseases model. *J Vis Exp*. 2007;8:313.
44. Fisher SK, Lewis GP, Linberg KA, Verardo MR. Cellular remodeling in mammalian retina: results from studies of experimental retinal detachment. *Prog Retin Eye Res*. 2005; 24:395–431.
45. Sakai T, Tsuneoka H, Lewis GP, Fisher SK. Remodelling of retinal on- and off-bipolar cells following experimental retinal detachment. *Clin Experiment Ophthalmol*. 2014;42:480–485.
46. Dalkara D, Kolstad KD, Caporale N, et al. Inner limiting membrane barriers to AAV-mediated retinal transduction from the vitreous. *Mol Ther*. 2009;17:2096–2102.
47. Akache B, Grimm D, Pandey K, Yant SR, Xu H, Kay MA. The 37/67-kilodalton laminin receptor is a receptor for adeno-associated virus serotypes 8 2, 3, and 9. *J Virol*. 2006;80:9831–9836.
48. Mbazima V, Dias BD, Omar A, Jovanovic K, Weiss SFT. Interactions between PrPc and other ligands with the 37-kDa/67-kDa laminin receptor. *Front Biosci (Landmark Ed)*. 2010;15:1150–1163.
49. Kotterman MA, Yin L, Strazzeri JM, Flannery JG, Merigan WH, Schaffer DV. Antibody neutralization poses a barrier to intravitreal adeno-associated viral vector gene delivery to non-human primates. *Gene Ther*. 2015;22:116–126.
50. Gupta V, Arevalo JF. Surgical management of diabetic retinopathy. *Middle East Afr J Ophthalmol*. 2013;20:283–292.
51. Bahadir M, Ertan A, Mertoglu O. Visual acuity comparison of vitrectomy with and without internal limiting membrane removal in the treatment of diabetic macular edema. *Int Ophthalmol*. 2005;26:3–8.
52. Da Mata AP, Burk SE, Foster RE, et al. Long-term follow-up of indocyanine green-assisted peeling of the retinal internal limiting membrane during vitrectomy surgery for idiopathic macular hole repair. *Ophthalmology*. 2004;111:2246–2253.
53. Ikuno Y, Sayanagi K, Ohji M, et al. Vitrectomy and internal limiting membrane peeling for myopic foveoschisis. *Am J Ophthalmol*. 2004;137:719–724.
54. Boyd RF, Boye SL, Conlon TJ, et al. Reduced retinal transduction and enhanced transgene-directed immunogenicity with intravitreal delivery of rAAV following posterior vitrectomy in dogs. *Gene Ther*. 2016;23:548–556.

5.2.4 The consequences of hypomorphic RPE65 for rod and cone photoreceptors (book chapter)

Marijana Samardzija[1], **Maya Barben[1,2]**, Philipp Geiger[1] and Chrisitan Grimm[1,2,3]

[1]Lab for Retinal Cell Biology, Dept. Ophthalmology, University Hospital Zurich, University of Zurich, Switzerland

[2]Neuroscience Center Zurich (ZNZ), University of Zurich, Switzerland

[3]Zurich Center for Integrative Human Physiology (ZIHP), University of Zurich, Switzerland

Status of the manuscript:

Published in *Adv Exp Med Biol., 2016;854:341-6. doi: 10.1007/978-3-319-17121-0_45.*

Personal Contribution

Manuscript editing and proofreading.

Chapter 45
The Consequences of Hypomorphic RPE65 for Rod and Cone Photoreceptors

Marijana Samardzija, Maya Barben, Philipp Geiger and Christian Grimm

Abstract RPE65 is essential for both rod- and cone-mediated vision. So far, more than 120 disease-associated mutations have been identified in the human *RPE65* gene. Differential clinical manifestations suggested that some patients suffer from null mutations while others retain residual RPE65 activity and some useful vision. To understand the mechanism of retinal degeneration or dysfunction caused by such hypomorphic RPE65 alleles, we generated an $Rpe65^{R91W}$ knock-in mouse (*R91W*) that expresses a mutant RPE65 protein with reduced function. Data obtained suggested that the *R91W* mouse is highly suitable to study the impact of RPE65 insufficiency on rod pathophysiology. To study the impact on cones, we combined the *R91W* with the $Nrl^{-/-}$ mouse that develops an all-cone retina. Here we summarize the consequences of hypomorphic RPE65 function (reduced 11-*cis*-retinal synthesis) for rod and cone pathophysiology.

Keywords RPE65 · Retina · Photoreceptors · Cones · Nrl · Dystrophy · Blindness · Degeneration · Mouse model · R91W

45.1 Introduction

Retinal pigment epithelial protein RPE65 is essential for the regeneration of 11-*cis*-retinal—the chromophore of both cone and rod visual pigments. Photoisomerisation of 11-*cis*-retinal results in the dissociation of all-*trans*-retinal from the opsin molecule. The restoration of light sensitivity of the bleached opsin requires regeneration

M. Samardzija (✉) · M. Barben · P. Geiger · C. Grimm
Laboratory for Retinal Cell Biology, Department of Ophthalmology,
University of Zurich, Wagistr. 14, 8952 Schlieren, Switzerland
e-mail: marijana.samardzija@usz.uzh.ch

M. Barben
e-mail: maya.barben@uzh.ch

P. Geiger
e-mail: philipp.geiger@bluewin.ch

C. Grimm
e-mail: cgrimm@opht.uzh.ch

C. Bowes Rickman et al. (eds.), *Retinal Degenerative Diseases,* Advances in Experimental Medicine and Biology 854, DOI 10.1007/978-3-319-17121-0_45

of 11-*cis*-retinal through an enzymatic pathway termed the visual cycle. RPE65 acts in this cycle as an isomerohydrolase catalyzing the hydrolysis of all-*trans*-retinol and subsequently the isomerization into 11-*cis*-retinol (Jin et al. 2005; Moiseyev et al. 2005; Redmond et al. 2005). Mutations in *RPE65* lead to autosomal recessive dystrophies ranging from Leber congenital amaurosis to Retinitis Pigmentosa (Marlhens et al. 1997; Morimura et al. 1998). Recently, however, a dominant-acting mutation was also reported in RPE65 patients (Bowne et al. 2011). Based on the clinical picture some mutations are null, while some are hypomorphic and allow partial RPE65 activity leading to reduced but detectable vision in affected patients. Mouse models exist to mimic both situations in patients, with *Rpe65*$^{-/-}$ (Redmond et al. 1998) and *rd12* (Pang et al. 2005) mice being null mutants, and *R91W* (Samardzija et al. 2008) mice (see below) representing a group of patients with a milder phenotype and remnant visual function. Here we discuss the consequences of the hypomorphic RPE65^{R91W} protein for rod and cone function, and retinal pathology in general.

45.2 R91W

Patients with an amino acid substitution at position 91 (R91W) in the *RPE65* gene have useful cone-mediated vision in the first decade of life (El Matri et al. 2006) suggesting partial activity of the mutant RPE65^{R91W} protein. To understand the retinal pathophysiology caused by the mutant RPE65 protein, we generated and analyzed the *R91W* knock-in mouse (Samardzija et al. 2008). Consistent to the assumed diminished enzymatic activity of mutant RPE65^{R91W} in patients, the *R91W* mice exhibit very low chromophore levels—accounting for less than 10% of wild-type levels. The low chromophore content is a direct result of the mutant RPE65^{R91W} protein which (a) has severely reduced enzymatic activity, (b) is mislocalized and (c) is expressed at much lower levels than *wt* (Takahashi et al. 2006; Samardzija et al. 2008). It was previously shown that reduction of RPE65 protein levels directly influences rhodopsin regeneration kinetics; i.e. less RPE65 means that less 11-*cis*-retinal can be synthetized in a given period (Wenzel et al. 2003). All of these factors lead to the severely impaired synthesis of 11-*cis*-retinol resulting in minute amounts of 11-*cis*-retinal chromophore and accumulation of retinyl ester substrate in the retinal pigment epithelium of *R91W* mice (Samardzija et al. 2008). Maximal 11-*cis*-retinal amount recovered after 24 h dark-adaptation in *R91W* mice corresponded to 6% of *wt* levels (Samardzija et al. 2008). Even after prolonged dark-adaptation—adult mice were placed for days in darkness—rhodopsin levels were still below 10% of normal. Only mice that were born and kept for 24 weeks in complete darkness had rhodopsin levels 94.2 ± 11.8 pmol per eye, which is 20% of normal levels (unpublished data).

Figure 45.1a, b shows retinal morphology of wild-type and *R91W* mice. The *R91W* mutation causes slow but progressive retinal degeneration, which is characterized by the initial rapid loss of cones that is followed by a slow rod photo-

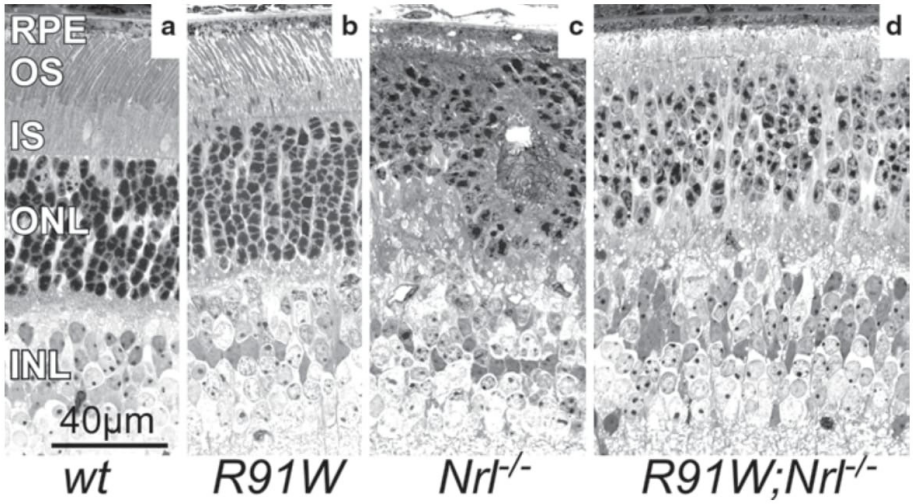

Fig. 45.1 Morphological consequences of hypomorphic RPE65 on rods and cones. *R91W* mice show reduced numbers of cone photoreceptor nuclei and a pronounced disorganization of rod outer segments already at 4 weeks of age. The functional all-cone retinas of 6 week-old *R91W;Nrl*$^{-/-}$ mice have a normal layering and better preserved cone outer segments than age-matched single mutant *Nrl*$^{-/-}$ mice

receptor death (Samardzija et al. 2008, 2009). Dark-adapted electroretinography (ERG) responses were almost undetectable but strong light-adapted responses initially suggested better preservation of the cone function in *R91W* mice (Samardzija et al. 2008). This would have been in line with the human pathology caused by the R91W mutation: night blindness and retention of useful color vision in younger patients. However, upon closer inspection of crossbreeds between *R91W*, *Rho*$^{-/-}$ and *Gnat1*$^{-/-}$ mice, generated to specifically segregate rod- from cone-mediated function, it became evident that *R91W* mice cannot generate significant cone-driven responses (Samardzija et al. 2009). Namely, the small amount of chromophore found in the rod-dominated retina of *R91W* mice is utilized almost exclusively by rods and not by cones. Since rods outnumber cones roughly by 20:1 (Carter-Dawson and LaVail 1979) and maximal levels of chromophore regenerated never exceeds 10 %, rod photoreceptors in *R91W* mice may simply have a higher chance to acquire the scarce chromophore. Rods may thus act as 'chromophore trap' preventing 11-*cis*-retinal delivery to cones. Cone opsin mislocalization in *R91W*, a known consequence of chromophore insufficiency (Rohrer et al. 2005), further supports such conclusion (Samardzija et al. 2009). The final proof that under limiting conditions the chromophore ends up in rods rather than in cones came from *R91W;Gnat1*$^{-/-}$ double mutant mice. *Gnat1*$^{-/-}$ mice have a morphologically normal retina but lack rod transducin alpha and therefore have non-functional rods (Calvert et al. 2000). The lack of any photopic and scotopic responses in *R91W*;*Gnat1*$^{-/-}$ mice suggests that their cones have no access to the chromophore and that the function detected in single mutant *R91W* mice indeed originated from rods. This was further confirmed

in *R91W*;*Gnat1*$^{-/-}$;*Rho*$^{-/-}$ triple mutant mice in which a clear ERG response was recorded that could only have been generated by cones. Obviously, physical removal of the rod opsin eliminated the chromophore trap allowing 11-*cis*-retinal to reach cones and restore cone function in *R91W*;*Gnat1*$^{-/-}$;*Rho*$^{-/-}$ mice.

Considering that the rod-cone ratio in the human macula is distinctive from the rest of the retina, the results obtained in *R91W* mice most likely phenocopy the situation in the peripheral retina of patients suffering from hypomorphic RPE65. As the mice lack a cone-rich macular region we decided to analyze the consequences of the *R91W* mutation by using the all-cone *Nrl*$^{-/-}$ mouse (Mears et al. 2001).

45.3 R91W;Nrl$^{-/-}$

The lack of neural retina leucine zipper (NRL) transcription factor during mouse retinal development drives all photoreceptor progenitors towards a cone cell fate (Mears et al. 2001). Functionally, rod-like behavior is suppressed and a super-normal light-adapted ERG is detected in *Nrl*$^{-/-}$ mice. The *Nrl*$^{-/-}$ retina is populated by a surplus of S-cones while M-cones seem to retain normal number. However, retinal morphology of *Nrl*$^{-/-}$ mice is dysmorphic and characterized by formation of rosette-like structures within the cone photoreceptor layer (Fig. 45.1c). Cone photoreceptors in *Nrl*$^{-/-}$ mice degenerate with time and rosettes are lost in older mice. We and others reported normal photoreceptor layering in *Rpe65*$^{-/-}$;*Nrl*$^{-/-}$, which, along with other evidence, suggested that rosettes may arise from normal levels of chromophore supplied by wild-type RPE65 (Wenzel et al. 2007; Feathers et al. 2008; Kunchithapautham et al. 2009). As *Rpe65*$^{-/-}$;*Nrl*$^{-/-}$ mice lack cone function, they cannot be used to test treatment options to prevent cone loss on a functional level. To reduce chromophore supply to the cones and to generate a mouse model to study the effects of the hypomorphic R91W mutation in an all-cone environment, which should represent the situation found in the macular region of patients suffering from this mutation, we crossbred *R91W* and *Nrl*$^{-/-}$ mice. Owing to reduced (3 % of wt) but detectable levels of chromophore, the resulting *R91W;Nrl*$^{-/-}$ double mutant mouse had a normally layered retinal structure without rosettes (Fig. 45.1d) and preserved retinal function (Samardzija et al. 2014). It is interesting to note that the all-cone retina of *R91W;Nrl*$^{-/-}$ mice is relatively stable with only very slow degeneration despite the severely reduced chromophore levels (Samardzija et al. 2014). Under similar—low chromophore—conditions, cone opsin is mislocalized and cones degenerate rapidly in the rod-dominated retina of *R91W* and even faster in retinas of *Rpe65*$^{-/-}$ mice that lack the chromophore (Samardzija et al. 2009). Previous studies suggested the importance of the chromophore for proper cone opsin trafficking and that cone opsin mislocalization detected in synaptic terminals in both *R91W* and *Rpe65*$^{-/-}$ mice can be corrected by different means of chromophore supplemetation (Rohrer et al. 2005; Znoiko et al. 2005; Fan et al. 2006; Zhang et al. 2008; Kunchithapautham et al. 2009; Samardzija et al. 2009; Kostic et al. 2011). The lack of cone opsin mislocalization in *R91W;Nrl*$^{-/-}$ suggested that the minute

amounts of chromophore in *R91W;Nrl*$^{-/-}$ are sufficient for proper cone opsin trafficking thereby stabilizing cone cells. Indeed, qualitative comparison of retinal degeneration in *Rpe65*$^{-/-}$*;Nrl*$^{-/-}$ (Wenzel et al. 2007; Kunchithapautham et al. 2009) and *R91W;Nrl*$^{-/-}$ (Samardzija et al. 2014) suggests better preservation of the all-cone retina in the latter. Yet, it is unclear why in the absence of chromophore cones die rapidly in rod-dominant retinas (*Rpe65*$^{-/-}$) but survive much longer in all-cone retinas (*Rpe65*$^{-/-}$*;Nrl*$^{-/-}$).

45.4 Concluding Remarks

Human vision largely depends on cones and the incidence of cone degenerative diseases such as age-related macular degeneration is expected to rise in the near future. The understanding of cone physiology and pathophysiology is urgently needed to develop therapeutic approaches for the preservation of cone-mediated vision in patients. *R91W* knock-in mice mimic many aspects of the human pathology caused by RPE65 insufficiency, complementing the *Rpe65* knock-out mouse model. While *R91W* mice are representative for the situation in the retinal periphery, *R91W;Nrl*$^{-/-}$ mice mimic more closely the situation in the central, cone-rich retina of human patients suffering from hypomorphic RPE65 function. *R91W;Nrl*$^{-/-}$ mice not only allow the investigation of the consequences of disease causing cone-specific mutations in an organized all-cone environment, but their preserved retinal function and retinal morphology should also improve the qualitative and quantitative outcomes of experiments aiming at rescuing cones on a functional level. The mice might especially be suited for neuroprotective studies, gene therapy approaches and above all, for cone cell transplantation experiments to rescue cone vision.

References

Bowne SJ, Humphries MM, Sullivan LS et al (2011) A dominant mutation in RPE65 identified by whole-exome sequencing causes retinitis pigmentosa with choroidal involvement. Eur J Hum Genet 19:1074–1081

Calvert PD, Krasnoperova NV, Lyubarsky AL et al (2000) Phototransduction in transgenic mice after targeted deletion of the rod transducin alpha -subunit. Proc Natl Acad Sci U S A 97:13913–13918

Carter-Dawson LD, LaVail MM (1979) Rods and cones in the mouse retina. I. Structural analysis using light and electron microscopy. J Comp Neurol 188:245–262

El Matri L, Ambresin A, Schorderet DF et al (2006) Phenotype of three consanguineous Tunisian families with early-onset retinal degeneration caused by an R91W homozygous mutation in the RPE65 gene. Graefes Arch Clin Exp Ophthalmol 244:1104–1112

Fan J, Wu BX, Sarna T et al (2006) 9-cis Retinal increased in retina of RPE65 knockout mice with decrease in coat pigmentationt. Photochem Photobiol 82:1461–1467

Feathers KL, Lyubarsky AL, Khan NW et al (2008) Nrl-knockout mice deficient in Rpe65 fail to synthesize 11-cis retinal and cone outer segments. Invest Ophthalmol Vis Sci 49:1126–1135

Jin M, Li S, Moghrabi WN et al (2005) Rpe65 is the retinoid isomerase in bovine retinal pigment epithelium. Cell 122:449–459

Kostic C, Crippa SV, Pignat V et al (2011) Gene therapy regenerates protein expression in cone photoreceptors in Rpe65(R91W/R91W) mice. PLoS ONE 6:e16588

Kunchithapautham K, Coughlin B, Crouch RK et al (2009) Cone outer segment morphology and cone function in the Rpe65-/- Nrl-/- mouse retina are amenable to retinoid replacement. Invest Ophthalmol Vis Sci 50:4858–4864

Marlhens F, Bareil C, Griffoin JM et al (1997) Mutations in RPE65 cause Leber's congenital amaurosis. Nat Genet 17:139–141

Mears AJ, Kondo M, Swain PK et al (2001) Nrl is required for rod photoreceptor development. Nat Genet 29:447–452

Moiseyev G, Chen Y, Takahashi Y et al (2005) RPE65 is the isomerohydrolase in the retinoid visual cycle. Proc Natl Acad Sci U S A 102:12413–12418

Morimura H, Fishman GA, Grover SA et al (1998) Mutations in the RPE65 gene in patients with autosomal recessive retinitis pigmentosa or leber congenital amaurosis. Proc Natl Acad Sci U S A 95:3088–3093

Pang JJ, Chang B, Hawes NL et al (2005) Retinal degeneration 12 (rd12): a new, spontaneously arising mouse model for human Leber congenital amaurosis (LCA). Mol Vis 11:152–162

Redmond TM, Yu S, Lee E et al (1998) Rpe65 is necessary for production of 11-cis-vitamin A in the retinal visual cycle. Nat Genet 20:344–351

Redmond TM, Poliakov E, Yu S et al (2005) Mutation of key residues of RPE65 abolishes its enzymatic role as isomerohydrolase in the visual cycle. Proc Natl Acad Sci U S A 102:13658–13663

Rohrer B, Lohr HR, Humphries P et al (2005) Cone opsin mislocalization in Rpe65-/- Mice: a defect that can be corrected by 11-cis retinal. Invest Ophthalmol Vis Sci 46:3876–3882

Samardzija M, von Lintig J, Tanimoto N et al (2008) R91W mutation in Rpe65 leads to milder early-onset retinal dystrophy due to the generation of low levels of 11-cis-retinal. Hum Mol Genet 17:281–292

Samardzija M, Tanimoto N, Kostic C et al (2009) In conditions of limited chromophore supply rods entrap 11-cis-retinal leading to loss of cone function and cell death. Hum Mol Genet 18:1266–1275

Samardzija M, Caprara C, Heynen SR et al (2014) A mouse model for studying cone photoreceptor pathologies. Invest Ophthalmol Vis Sci

Takahashi Y, Chen Y, Moiseyev G et al (2006) Two point mutations of RPE65 from patients with retinal dystrophies decrease the stability of RPE65 protein and abolish its isomerohydrolase activity. J Biol Chem 281:21820–21826

Wenzel A, Grimm C, Samardzija M et al (2003) The genetic modifier Rpe65Leu(450): effect on light damage susceptibility in c-Fos-deficient mice. Invest Ophthalmol Vis Sci 44:2798–2802

Wenzel A, von Lintig J, Oberhauser V et al (2007) RPE65 is essential for the function of cone photoreceptors in NRL-deficient mice. Invest Ophthalmol Vis Sci 48:534–542

Zhang H, Fan J, Li S et al (2008) Trafficking of membrane-associated proteins to cone photoreceptor outer segments requires the chromophore 11-cis-retinal. J Neurosci 28:4008–4014

Znoiko SL, Rohrer B, Lu K et al (2005) Downregulation of cone-specific gene expression and degeneration of cone photoreceptors in the Rpe65-/- mouse at early ages. Invest Ophthalmol Vis Sci 46:1473–1479

5.3 Curriculum Vitae

Name	**Maya Barben**
Address	Im Sträler 42, 8047 Zürich
Mobile	+41 79 516 96 64
Mail	Maya.Barben@uzh.ch
Date of Birth	February 23th, 1989
Place of Birth	Affoltern a. A.
Place of Origin	Thalwil / ZH, Spiez / BE

EDUCATION

Since 11/2013 **University of Zurich, *PhD program in Neuroscience***

PhD-student under supervision of Prof. Dr. Christian Grimm,
Lab for Retinal Cell Biology, Department of Ophthalmology, USZ, UZH

2012 – 2013 **University of Zurich, Master of Science**
Neurosciences

Master thesis: *The effect of chronic inflammation on degeneration and regeneration in adult murine neurogenic regions (grade 6.0)*

2008 - 2012 **University of Zurich, Bachelor of Science**
Biology

2003 - 2007 **High School at Kantonsschule Stadelhofen,** Zurich
Specialization: modern languages / Spanish

AWARDS

Best presentation: **Day of Clinical Research Prize**
Progressive cone degeneration in a chronic hypoxia-like situation can be rescued by targeting Hif1a (16th Day of Clinical research, February 09, 2017, Zurich, Switzerland)

Best presentation: **Retina Suisse Award 2017**
The hypoxic response in cones: consequences for vision and a potential therapeutic target (Swiss Eye Research Meeting (SERM), January 26 – 27, 2017, Neuenburg, Switzerland)

Travel fellowship: **Fritz Tobler Foundation Award** to attend the XVIIth International Symposium on Retinal Degenerations 2016
Progressive cone degeneration in a chronic hypoxia-like situation can be rescued by targeting Hif1a (RD2016, Kyoto, Japan, September 19 - 24, 2016)

Best poster: **Day of Clinical Research Prize**
Cone pathophysiology under chronic hypoxia
Barben M, Schori C, Grimm C, Samardzija M (14th Day of Clinical Research, April 9, 2015, Zurich, Switzerland)

PUBLICATIONS

Hif1a inactivation rescues photoreceptor degeneration induced by a chronic hypoxia-like stress
Barben M, Ail D, Storti F, Klee K, Schori C, Samardzija M, Michalakis S, Biel M, Meneau I, Blaser F, Barthelmes D, Grimm C.
submitted

Targeting Hif1a rescues cone degeneration and prevents subretinal neovascularization in a model of chronic hypoxia
Barben M, Schori C, Samardzija M, Grimm C.
submitted

The role of hypoxia, hypoxia-inducible factor (HIF) and VEGF in retinal angiomatous proliferation
Barben M, Samardzija M, Grimm C.
(Book chapter) Adv Exp Med Biol, in press

Digoxin-induced retinal degeneration depends on rhodopsin
Landfried B, Samardzija M, **Barben M**, Schori C, Klee K, Storti F, Grimm C.
Cell Death Dis., 2017 Mar 16;8(3):e2670. doi: 10.1038/cddis.2017.94.

A novel method combining vitreous aspiration and intravitreal AAV2/8 injection results in retina-wide transduction in mice
Da Costa R, Röger C, Segelken J, **Barben M**, Grimm C, Neidhardt J.
Invest Ophthalmol Vis Sci., 2016 Oct 1;57(13):5326-5334. doi: 10.1167/iovs.16-19701.

Blue light-induced retinal lesions, intraretinal vascular leakage and edema formation in the all-cone mouse retina.
Geiger P, **Barben M**, Grimm C, Samardzija M.
Cell Death Dis. 2015 Nov 19;6:e1985. doi: 10.1038/cddis.2015.333.

The Consequences of Hypomorphic RPE65 for Rod and Cone Photoreceptors.
Samardzija M, **Barben M**, Geiger P, Grimm C.
(Book chapter) Adv Exp Med Biol. 2016;854:341-6. doi: 10.1007/978-3-319-17121-0_45.

ORAL PRESENTATIONS

Progressive cone degeneration in a chronic hypoxia-like situation can be rescued by targeting Hif1a
(16th Day of Clinical research, February 09, 2017, Zurich, Switzerland)

The hypoxic response in cones: consequences for vision and a potential therapeutic target
(Swiss Eye Research Meeting (SERM), January 26 – 27, 2017, Neuenburg, Switzerland)

The effects of chronic hypoxia on cone pathophysiology
(Swiss Eye Research Meeting (SERM), January 22 – 23, 2015, Neuenburg, Switzerland)

POSTER PRESENTATIONS

Progressive cone degeneration in a chronic hypoxia-like situation can be rescued by targeting Hif1a
Barben M, Schori C, Samardzija M, Grimm C.
13th Symposium of the Zurich Center for Integrative Human Physiology (ZIHP), September 01, 2017, Zurich, Switzerland

Progressive cone degeneration in a chronic hypoxia-like situation can be rescued by targeting Hif1a
Barben M, Schori C, Samardzija M, Grimm C.
XVIIth International Symposium on Retinal Degenerations (RD2016), September 19 - 24, 2016, Kyoto, Japan

The effects of a chronic hypoxia-like response on cone photoreceptors
Barben M, Schori C, Grimm C, Samardzija M.
ZNZ PhD retreat, April 28 - 30, 2016, Valens, Switzerland

The effects of a chronic hypoxia-like response on cone photoreceptors
Barben M, Schori C, Grimm C, Samardzija M.
11th Symposium of the Zurich Center for Integrative Human Physiology (ZIHP), August 21, 2015, Zurich, Switzerland

A chronic hypoxia-like response leads to cone degeneration
Barben M, Schori C, Grimm C, Samardzija M.
Annual Meeting of the Association for Research in Vision and Ophthalmology (ARVO), May 03 - 07, 2015, Denver, United States

Cone pathophysiology under chronic hypoxia
Barben M, Schori C, Grimm C, Samardzija M.
14th Day of Clinical Research, April 9, 2015, Zurich, Switzerland

5.4 Acknowledgements

First, I would like to thank Prof. Dr. Christian Grimm for giving me the opportunity to conduct my PhD in his lab. Thank you for your continuous support, your scientific inputs, your time and your confidence – it is a privilege having you as a boss. Additionally, I am very grateful for the possibility to attend national and international conferences in the US / Japan, both in terms of scientific and cultural interests.

My greatest appreciations and special thanks go to PD Dr. Marijana Samardzija for her excellent supervision – I could not imagine a better mentor. Thank you for the opportunity to work on the all-cone projects, for investing a lot of time and answering my numerous questions, for your advice and infinite support. Additionally, thank you for helping me to improve my laboratory techniques and my scientific thinking – and my badminton skills.

Furthermore, I would like to express my gratitude to the other members of my PhD committee, Prof. Dr. Melanie Greter and Prof. Dr. Stephan Neuhauss, for the feedback and advices at the yearly meetings. I am also very thankful to our collaborators PD Dr. Stylianos Michalakis (Munich Center for Integrated Protein Science at the Dept. Pharmacy, Ludwig-Maximilians-Universität München, Munich, Germany), Sanford L. Boye (Dept. of Ophthalmology, University of Florida, Gainesville, USA) and Dr. Isabelle Meneau (Augenbank, Dept. Ophthalmology, University Hospital Zürich, Zurich, Switzerland) for their involvement in our projects.

I also wish to thank current and previous members of the Lab for Retinal Cell Biology, especially Christian Schori, Katrin Klee, Dr. Federica Storti, Vyara Todorova, Ana Bordonhos, Cornelia Imsand, Andrea Gubler, Colin Leikauf, Britta Landfried, Christel Beck and Sarah Nötzli for support, discussions and spending good times together. During the last years in this lab I learned a lot but I also enjoyed it a lot – the best combination I could imagine. Thank you.

Last but not least, I would like to thank my friends, my wonderful family and Manu – your support is beyond measure.